The Role of Hypertensive Vascular Disease in Brain Aging and Neurodegeneration

by

Cyrus A. Raji

BS, BA, University of Pittsburgh, 2004

Submitted to the Graduate Faculty of

The University of Pittsburgh School of Medicine in partial fulfillment

of the requirements for the degree of

Doctor of Philosophy

University of Pittsburgh

2009

UNIVERSITY OF PITTSBURGH

SCHOOL OF MEDICINE

This thesis was presented

by

Cyrus A. Raji

It was defended on

May 04, 2009

and approved by

James T. Becker, PhD, Professor, Psychiatry, Neurology, Psychology

Oscar L. Lopez, MD, Professor, Neurology

Geoffrey Murdoch, MD, PhD, Professor, Neuropathology

Clayton A. Wiley, MD, PhD, Professor, Neuropathology

Major Advisor: William E. Klunk, MD, PhD, Professor, Psychiatry

The Role of Vascular Disease in Brain Aging and Neurodegeneration

Cyrus Raji, B.S./B.A.

University of Pittsburgh, 2009

Brain aging, the phenomenon by which the passage of chronological time is associated with reduced brain volume, is important because it is regarded as a key component of increased dementia risk. The main purpose of this thesis is to present a model and supporting data that enhances knowledge of the underlying processes that drive brain aging and dementia risk. This has been done using structural and functional MRI scans from the Cardiovascular Health Study-Cognition Study (CHS-CS), a longitudinal community cohort study of elderly individuals that possesses extensive clinical and neuropsychological data. The model defended in this dissertation states that the relationship between older age and lower gray matter volume is not strictly a function of the passage of chronological time. Rather, older age is correlated with vascular diseases that themselves are a driving force behind brain aging. Most importantly, the three entities of aging, vascular disease, and neurodegeneration overlap in key strategic areas of the brain. Thus, a large factor behind dementia risk is that there are common brain areas that serve as sites of synergy by which age, vascular disease, and neurodegeneration can summate and thus amplify the risk for cognitive impairment and dementia.

Using a whole brain method for analyzing structural MRI scans, we have found that the age and vascular disease, as reflected by white matter hyperintense lesions (WMHL) jointly affect areas of the brain known to be targeted by age and neurodegeneration and that they interact in these key strategic brain regions. Finally, results from perfusion MRI imaging will be

reported showing that hypertension as the main predictor of lower regional cerebral blood flow. Taken together, these data will be interpreted to support the following model: structural and functional changes in an aging brain are modulated by hypertensive vascular disease. Additionally, the damage exerted by neurodegenerative processes on the brain is also modified by vascular disease. Finally, there are common strategic anatomical sites in which this synergy occurs and they include areas with important cognitive functions such as the hippocampus, cingulate gyrus, and precuneus.

This model has several broad implications. First, it suggests that age related brain atrophy and perhaps even neurodegenerative atrophy itself can be reduced in magnitude if underlying vascular diseases are either prevented or better managed. Second, such a reduction in brain aging may lower risk for dementia by providing additional brain reserve. Third, key strategic brain regions provide a basis for further study and therapeutic targets.

TABLE OF CONTENTS

LIST OF TABLES

LIST OF FIGURES

EQUATIONS

PREFACE

My PhD years were some of the most satisfying and enjoyable of my life and there are many people to thank for this. My family has been consistently supportive of my academic endeavors and the time it often requires of me. They have been there with me through good times and bad and loved me just the same. I am forever in their debt. Dr. James Becker and Dr. Oscar Lopez have been outstanding mentors in guiding me through the different exercises of become a competent investigator from critical thinking to experimental design, grant writing, manuscript composition, and presentations. They were exemplary in their instruction, patience, and integrity. The rest of my committee, Drs. Klunk, Wiley, and Murdoch are also to be commended in their excellent guidance. Dr. Klunk taught me the value of perseverance in any scientific endeavor. Dr. Wiley imparted me with an appreciation of having a vision in the building of an academic career. Dr. Murdoch showed me that without an understanding of basic pathology, the full value of neuroimaging research cannot be fully utilized. Dr. Carolyn Meltzer introduced me to neuroimaging research over 6 years ago and I am very grateful for her support and encouragement. I would also like to thank all of my close friends who served as good examples of trust, camaraderie, and affection. The ultimate joy of medical research for me is to create knowledge that could aid many more persons than I could ever see as a solo clinician. This opportunity alone has made the MD/PhD program a worthwhile endeavor. I hope you enjoy reading this dissertation and find the contents within useful.

1.0 INTRODUCTION

Neurodegenerative dementias are devastating syndromes in which cognitive function deteriorates to the point where an individual can no longer care for themselves, interact optimally with others, or retain personal memories. It is a common disorder among older adults, affecting 10% of those older than age 65 (1). Alzheimer's disease (AD) is the most common cause of dementia in the elderly and is projected to afflict 34 million persons worldwide by 2025 (http://www.searo.who.-int/EN/Section1174/Section1199/Section1567/Section1823_8066.htm). In the United States, it is the 7th leading cause of death, costs over $1 trillion a year, and induces immeasurable emotional suffering and burden in patient families (http://www.alz.org/national/-documents/report_alzfactsfigures2009.pdf). The only two firmly established risk factors are genetic predispositions and old age (≥65) (2-6). Vascular diseases such as hypertension (HTN) by contrast, are putative risk factors for AD but are the focus of multiple investigations due their high prevalence in the elderly. HTN also contributes to vascular dementia (VaD), the second most common form of dementia in which cerebral infarcts produce a different cognitive syndrome (7). Often, AD and VaD pathologies co-exist and overlap. Although neurodegenerative dementias encompass no less than a dozen different variants, for the purposes of this dissertation, the term dementia will refer only to AD (65% of our cases), vascular dementia (13% of cases), and cases where both pathologies may coexist (17% of cases). Understanding the relationship between brain aging and vascular disease is of particular

importance because such work can lend insight into how age confers its considerable risk for dementia on the brain. Insight into the common areas of overlap and synergy between age, vascular disease, and neurodegeneration is also desirable because it provides an idea of what brain regions need to be most carefully considered in terms of vulnerability and therapeutics.

The reduction of brain volume with age is a commonly reported phenomenon in both neuropathological and neuroimaging literature (8, 9). These frequently show a reduction in gray matter (GM) volume as age increases, with a concomitant increase in cerebrospinal fluid (CSF). The focus on gray matter is due to specific structures affected by AD and these include the hippocampal formation, posterior cingulate, and precuneus. While such structures have been shown to lose gray matter with age, the underlying nature of this relationship is not clear but is important to understand because of the role aging plays as a powerful risk factor for AD. The work presented in this doctoral dissertation had three major objectives: i) To identify markers of hypertensive vascular disease that are associated with both age and reduced gray matter in a cohort of elderly non-demented individuals ii) To test assess the interrelationships among age, WMHL, AD and its precursor stage, mild cognitive impairment (MCI) in terms of common strategic anatomical regions. iii) To assess the functional consequences of HTN using perfusion MRI. These objectives were accomplished using clinical, structural, and perfusion imaging data a large prospective community cohort, the Cardiovascular Study Cognition Study (CHS-CS). This first chapter will review pertinent literature and outline the rationale behind undertaking the stated objectives.

1.1 EVIDENCE FOR A RELATIONSHIP BETWEEN VASCULAR DISEASE AND BRAIN AGING

With the passage of chronological time from birth there are multiple deleterious alterations in the brain. These include loss of neuronal cell bodies in neocortical, hippocampal, and cerebellar areas (10, 11), shrinkage of neurons (12), and suboptimal DNA repair (13). These underlying processes generally manifest as a reduction in brain volume, measured by actual tissue loss in the parenchyma or increased CSF in the cerebral sulci and ventricles. Brain parenchyma usually shrinks 0.12% per annum in persons aged 24-46 and this number increases to 0.35% per annum in individuals between age 59-79 (8). In particular, gray matter volume decline is 4 times that of total parenchyma (gray plus white matter) shrinkage – 0.90% versus 0.20% (14). Age related brain volume loss provides a powerful explanation for why aging is such a substantial risk factor for dementia: with advanced age is less brain volume and thus less reserve against a future neurodegenerative process. Aging, however, is not a unitary condition and many processes can mediate and/or moderate the relationship between age and reduced brain volume. Such factors would have to be associated with age and have a mechanism for reducing brain volume. Those that will be discussed here are hypertension and its common end organ outcome in the brain: small vessel ischemic disease, as indexed by white matter hyperintense lesions (WMHL).

In discussing HTN, I will focus on the most common form: essential hypertension and HTN will refer only to this form for the remainder of this document. HTN is a chronic disease of vasculature characterized by a sustained increase in systolic blood pressure (SBP) over diastolic blood pressure (DBP) of 140/90 mm hg (15). Hypertensive disease can over time exert end organ damage including left-ventricular hypertrophy in the heart, microalbuminuria in the kidney, and small vessel ischemic disease in the brain (16). This damage can subsequently cause

catastrophic events such as myocardial infarction, renal failure, and stroke. Age is a powerful predictor for HTN such that the percent of persons with the condition increases from 5% among those individuals aged 18-29 to 45% for those aged 50-59 to 65% in those 80+ year olds (17). HTN is therefore one of the most common medical afflictions among the elderly population.

Radiological studies have shown that HTN can affect brain integrity beyond watershed and subcortical regions. Such work shows that HTN is correlated with gray matter volume loss and abnormal cognition in non-demented individuals. A voxel level analysis of 76 men and 58 women (mean age of 60) showed that elevated blood pressure (SBP) predicts lower brain volumes in the supplementary motor area and adjacent superior frontal gyrus, the anterior cingulate cortex, and middle temporal gyrus in the male group. In that same group of subjects there were also deficits in executive function and working memory with higher SBP (18). An earlier structural MRI study of 18 cognitively normal elderly hypertensive males with an (mean age of 69) and 17 age-equivalent male normotensives showed smaller left hemisphere brain volumes and larger CSF volumes in the lateral ventricles (19).

A study of 529 participants grouped by age (18-46 and 47-83) showed that both young and older hypertensive subjects had reduced cognitive function as assessed by multiple examinations with the Wechsler Adult Intelligence Scale. The older group had a higher magnitude of blood pressure related cognitive decline (β = -.09 vs. β = -.05 for younger) controlling for age, education, occupation, gender, alcohol consumption, cigarettes/day, psychotropic medication, body mass index, and major depressive disorder (20). HTN can modify age related gray matter volume loss and this was illustrated in a structural MRI study of 27 “young old” (age 56-69) and “old-old” (age 70-84) HTN subjects and 20 age-equivalent normotensive controls (21). The study demonstrated an interaction between age and HTN in

temporal and occipital CSF and the old-old HTN group had smaller volumes of thalamic nuclei and larger volumes of CSF in the cerebellum and temporal lobes compared to the young-old group. Taken together, these studies suggest that HTN can modify age-related gray matter volume loss and cognitive decline in non-demented persons. Specifically HTN moderates, or strengthens, the relationship between aging and declines in gray matter. Consequently, one would expect that for a given age an individual brain with HTN would look "older" than another brain without HTN.

There are several mechanisms by which HTN can induce neuronal cell loss or size reduction. One prominent mechanism is hypoperfusion secondary to vascular remodeling, which involves a series of degenerative microvascular changes including atherosclerosis, arteriosclerosis, smooth muscle hypertrophy, thickening of the tunica intima, and narrowing of the vessel lumen (22). Vascular remodeling often results from the increased wall stress induced by chronically elevated mean arterial pressure and leads to cerebral hypoperfusion, focal ischemia, perivascular edema, compromise of the blood-brain barrier, cortical deafferentation, and temporary loss of brainstem/spinal reflexes (cerebral diaschesis) (23). Because vascular remodeling can lead to decreased regional cerebral blood flow (rCBF), compromised neuronal metabolism, and subsequently reductions in the size and number of neurons, this appears as gray matter volume loss.

HTN can also lead to reduced GM volume by causing cerebral microbleeds. Cerebral microbleeds are small hemosiderin deposits visible on T2 weighted magnetic resonance imaging and are seen more often in patients with lacunar infarcts, intracerebral hemorrhage, and WMHL than in those with cardio/atheroembolic infarcts (24). They are thought to be connected to small

vessel vascular damage, actual small hemorrhages, and microaneurysms – all of which result from HTN effects on the brain (25).

Ischemic damage to the brain is perhaps the strongest mediator through which HTN causes volume reductions in gray matter. WMHL (also known as white matter hyperintensities, small vessel ischemic disease, or "leukoariosis") are a well characterized biomarker of such damage and their main etiology is HTN (26-29). They typically manifest as areas of bilateral, diffuse, or patch-like areas of reduced density on computed tomographic scans or regions of higher intensity on T2 MRI (30, 31). Though first believed to be part of normal aging they were quickly found to be associated with HTN (32-34).

Several factors support hypertensive vascular disease as a main cause of WMHL. First, cerebral white matter is located in the border zones of superficial and deep vascular territories, making it vulnerable to transient drops in regional cerebral blood flow (rCBF) (31) that can be seen with ischemia in the setting of long standing HTN. Second, arteriosclerosis and white matter pallor have been demonstrated in areas corresponding to radiologically identified white matter hyperintensities (34). Third, WMHL are correlated with stroke and the progression of lacunar infarcts – both of which are tightly linked to chronic HTN (35-38). Fourth, WM components, namely oligodendrocytes and myelin, are highly sensitive to ischemia (39) and age-related arteriolar tortuousity requires higher perfusion pressure for irrigation of WM. This increases vascular resistance, promotes ischemia, and leads to subsequent tissue damage. Finally, there is increased oxygen extraction in areas of WMHL, an indication that more oxygen is being consumed than is delivered by the circulation and an indicator of hemoydynamic compromise (40) and higher risk for ischemia and infarction –both of which are promoted by HTN

The link between WMHL and HTN related ischemia can be further refined by examining the morphology of these lesions. WMHL can be morphologically grouped into 3 categories: caps and halos, punctuate lesions, and confluent lesions. Caps and halos are not lesions in a strict sense and often outline the cerebral ventricles in a symmetrical manner. The causes of these types of WMHL are non-vascular and include local redistribution of interstitial water flow, a loose network of myelinated fibers, and ependymitis granularis or disruption of the ependymal layer (31, 41, 42). The neuropathological substrates of the caps and halos are disruption of the ependymal lining which results in CSF accumulation in the periventricular white matter. These findings also include a thin rim of subependymal gliosis and a wider band of white matter with reduced myelin staining around the lateral ventricles (23). Cap and halo WMHL do not have any associated arteriolar changes histopathologically and are thus not believed to have any vascular etiologies or clinical significance (43, 44).

Punctate WMHL are thought to arise from impaired diffusion of nutrients through thickened blood vessel walls secondary to atherosclerosis, mechanical damage to the surrounding tissue from by a water hammer effect of pulsating arterioles with HTH, or both (45, 46). Punctate WMHL are most commonly associated with dilated perivascular spaces and do not represent lacunar infarcts (47).

Confluent WMHL are caused by ischemia of white matter arterioles usually smaller than 150 μm; by contrast, occlusion of arterioles larger than 400 μm usually results in lacunar infarcts. Confluent WMHLs are thought to result from: i) ischemia followed by reactive glial changes that the border between ischemic and health tissue ii) demyelination within that area, and finally, iii) gliosis (48, 49). Chronic ischemia can result from vascular remodeling and vessel wall damage that is common in HTN. While some have suggested that anti-hypertensive

drugs cause confluent WMHL through alterations in perfusion pressure, the lack of white matter changes in patients with dilated cardiomyopathy would argue against this (42).

Given the link between HTN and WMHL, it is likely that WMHL reflects the effects of HTN on reducing brain volume in the elderly. That is, WMHL represent the end organ effect of HTN on the aging brain. Consequently, age related changes in the brain can be secondary to hypertensive vascular disease. The next section will examine evidence that vascular disease, namely HTN and WMHL, and MCI are linked.

1.2 EVIDENCE FOR A RELATIONSHIP BETWEEN VASCULAR DISEASE AND MILD COGNITIVE IMPAIRMENT

Because the slow progressive nature of dementia implies the existence of prodromal state, MCI refers to a transition state that confers higher risk of converting from normal aging to dementia because in many cases it represents early neurodegenerative changes in the brain (50, 51). Risk factors for MCI can therefore be potentially used as predictors for conversion to a future dementia. For the purposes of this dissertation, dementia is conceived as a behavioral proxy for advanced neurodegeneration and MCI is regarded as a series of subtle cognitive deficits that reflect comparatively mild or moderate neurodegeneration. While considerations of amnestic versus non-amnestic manifestations of MCI are important, they warrant separate study and are thus beyond the scope of this dissertation. This section will review evidence that vascular risk factors, namely HTN and its end organ damage effect WMHL, contribute to the development of MCI and further progression to dementia.

1.2.1 HTN and MCI

Midlife HTN is a significant predictor of subsequent cognitive deterioration (52-55). Cognitive functioning is negatively correlated with the BP values measured 12 to 14 years prior (52) and midlife SBP is associated with poor cognition later in life (56). Such studies suggest that HTN is related to MCI and may even be a risk factor for the condition because of the predictive power blood pressure has on worsening cognitive function later in life.

The link between HTN and MCI was suggested in one of the largest autopsy studies of MCI from the Religious Orders Study (57) in which 180 subjects, 37 of whom had MCI, were evaluated for the presence of vascular neuropathology. In the MCI group, 37% had cerebral infarctions, a significant risk factor of this being HTN. A prospective community cohort study with 334 MCI cases found HTN to be predictive of increased incidence of MCI (hazard ratio = 1.40, $p = .02$, adjusting for age and sex) (58). These findings were verified by work from the Italian Longitudinal Study on Aging showing that 33% of 113 cases of incident MCI went on to develop VAD, suggesting a vascular and most likely hypertensive component in their risk (59). A Chinese case control study of 423 MCI subjects compared to 925 controls showed that hypertension doubles the risk of having MCI (OR 1.97, 95% CI 1.44 – 2.69) (60). In an Indian community cohort study of 960 subjects, 15% of which had MCI, hypertension was also identified as a putative risk factor regardless of the subtype (61). Within the CHS-CS, outcomes of chronic HTN such as MRI-identified infarcts are associated with increased risk for MCI (OR = 1.4, 95% CI 1.12-1.82) (62). Finally, a longitudinal study found an OR of 1.2 (95% CI 0.7-2.2) for SBP $\geq$ 160 versus < 140 mm Hg for risk of developing Mayo Clinic defined criteria for MCI in 1449 persons (62% women) age $\geq$ 65 years with an average follow up of 21 years (54).

Pharmacological reduction of BP reduces HTN associated cognitive impairment. A prospective observational study of 6,206 persons with HTN and an average age of 66 assessed the effectiveness of the antihypertensive drug losartan on development of cognitive impairment (63). Following 1 year of treatment, systolic/diastolic BP fell from its baseline level of 158.1/90.3 mmHg to 137.3/80.6 mmHg. The proportion of patients in this study with mild/severe cognitive impairment was reduced from 30.3%/39.7% at baseline to 28.1%/37.1%, a statistically significant alteration ($p < .05$). This observation was also reflected in the Study on Cognition and Prognosis in the Elderly trial of 4937 hypertensives (age range: 70-89) undergoing double blind treatment with candesartan or placebo (64). While not formally evaluated for MCI, almost half of these HTN subjects had MCI range Mini-Mental State Exam (MMSE) scores (24-28, n = 2070). In the group with lower MMSE scores, treatment with candesartan reduced the extent of cognitive decline over a 3-5 year period (mean difference 0.49 MMSE points, 95% confidence interval 0.02 to 0.97, $p = .04$). To the extent that HTN treatment can attenuate vascular remodeling of blood vessls in the brain, this can explain why such treatment can be useful for blunting cognitive decline. While some may assert that anti-HTN treatment in the elderly is deleterious because it could drop perfusion pressures, thus leading to syncope and other adverse event, recent data suggests that this is not the case. The HYVET study in Europe employed aggressive blood pressure lower medication treatment with a combined indapamide/perindopril regimen in 358 persons over age 80 and compared outcomes at 2 years to the age matched placebo group of 448 (65). The active treatment group had a 30% reduction in risk of fatal or non-fatal stroke, 39% reduction in death from stroke and 21% reduction in death from any cause. Most important, there were fewer adverse events reported in the treatment group compared to

placebo (p = .001). Having reviewed how HTN and MCI are linked, I will now overview what is known about the WMHL and MCI.

1.2.2 WMHL and MCI

There are multiple works supporting a link between MCI and WMHL. A prospective cohort study of 156 MCI and 67 healthy subjects followed for a mean of 6 years showed WMHL to be a significant predictor of conversion to MCI (adjusted hazard ratio [HR], 3.30; 95% confidence interval [CI], 1.33-8.17; p = .01) (66). Another prospective study found that confluent periventricular hyperintensities were related to an increased risk of AD within three years among individuals with MCI (HR = 1.59, 95 % CI: 1.24 - 2.05, $p < 0.001$), even after controlling for age, education and treatment with donepezil or vitamin E (67). A combined MRI/EEG study of 94 MCI subjects found a statistically significant correlation between WMHL induced damage to long range (capsular) and short range (medial and perisylvian) cholinergic tracts and abnormalities on the delta and theta power bands (68). This study suggests that in the setting of MCI, comorbid vascular disease can exert damage to white matter tracts that are important in cognitive function.

Combined, the studies reviewed in this section suggest that HTN and its end organ CNS marker, WMHL, may promote MCI which is itself a high risk state for future dementia. Thus, I have so far examined evidence supporting the concept that age related gray matter volume loss is moderated by HTN then end organ brain effects of which are WMHL. The following section will review the relationship between HTN, WMHL and dementia, with an emphasis on AD.

1.3 EVIDENCE FOR THE RELATIONSHP BETWEEN VASCULAR DISEASE AND DEMENTIA

Environmental, personal, and genetic factors including age, family history of dementia, head trauma, cerebrovascular disease, have one of two copies of apolipoprotein E 4 (APOE-4) allele (4, 69-77) increase the risk to develop clinical dementia. In the context the present research, the relationship between HTN and dementia is especially important. Much about the synergistic mechanisms between these two processes is unknown but this section will review current knowledge.

1.3.1 Hypertension effects on cognition

The main basis for hypothesizing a link between HTN and dementia are the number of studies suggesting that HTN induces cognitive impairment. It is important to note that studies which examined the effects of HTN on cognition usually do not differentiate cases with MCI or dementia from those that have small changes in formal cognitive measures. The most common type of association tested has been between high SBP and lower scores on tests of neuropsychological function in cross-sectional investigations of non-demented elderly. A UK study of 598 healthy elderly individuals age 70+ found an inverse correlation between high SBP and lower MMSE scores, controlling for intelligence quotient (78). A study of 1339 persons aged range 69-95 years evaluated whether or not DBP was associated with having an MMSE score of less than 24. A 10 mm Hg increase in DBP corresponded to a 29% increase in risk for having an MMSE < 24 (79). Another study of 13840 participants (age range: 45-69) showed

persons with BP of ≥160/95 mm Hg performed worse on the digit symbol substitution test and had poorer word fluency, controlling for ethnicity and occupation (80). A Swedish study of 999 men aged 69-75 with BP measured found that each 1 standard deviation increase in DBP translated to an OR = 1.45 (95% CI 1.20-1.75) for lowest quintile of MMSE scores. This study controlled for stroke, body mass index (BMI), cholesterol levels, serum glucose, and anti-HTN medications (53). A community based investigation examined performance of 107 untreated hypertensives and 116 normotensive individuals aged 70-89 years and their performance on 8 domain specific neuropsychological tests. The HTN group (BP 160-169/90-99 mm Hg) performed more poorly on 3/8 of these tests with slower speed of completion being the main reason for impaired performance (81). A study of 158 community dwelling volunteers (age range 60-91) found that higher SBP predicted lower scores on both the MMSE and the Cambridge Cognitive Examination, controlling for plasma homocysteine levels. In the Cardiovascular Health Study, a study of 5888 persons (≥65 years) showed that for every 1 standard deviation increase in SBP (22 mm Hg), MMSE decline by 0.96 points every year for 7 years (82).

The severity of HTN may determine the subsequent effect on cognition. This was illustrated by of 500 men, mean age = 68, who were evaluated on a 5-test neuropsychological battery. Performance on this battery was worse in the more severe HTN group (≥180/110 mm Hg) than the less severe HTN group (140-159/90-99 mm Hg) (83). Additionally, lower education status may exacerbate the effect of HTN on cognitive function. This was reflected in a study of 278 British African Caribbean people age 55-75; those with HTN and lower educational status (no college) had lower composite scores from 11 domain specific neuropsychological

tests, including those for episodic memory and executive function (84). The relationship between HTN and lower executive function was also observed in a study of 70 persons age 65+ showing that SPB ≥ 145 mm Hg is related to deficits in executive function. Those findings held despite controlling for ethnicity, alcohol use, drug use, BMI, and total cholesterol (85). It is important to note, though, that selective survival may remove the most severely hypertensive individuals from an elderly population. Consequently, any study of hypertension and vascular disease on brain structure and function may underestimate the extent of damage these conditions can impact on the brain. This is because persons with the most severe forms of these vascular diseases may die before they can reach advanced enough aged to be studied.

In addition to the cross sectional studies cited above, considerable longitudinal evidence also exists linking HTN to reduced cognition. Such studies typically correlate mid-life BP with cognition later in life, often with a 10-30 year intervening time period. This approach is taken because it is believed to better reflect the cumulative effects of HTN than BP measurements taken later in life. The Framingham Heart Study, for example, found an inverse relationship between SBP and composite neuropsychological test scores obtained 20 year later in a cohort of 1702 individuals (age range: 55-88 years) controlling for stroke, smoking, alcohol consumption, and occupation (86). A study of 392 men aged 68-79 with SBP measured between 43-53 found that higher SBP (≥ 140 mm Hg) was related to poorer performance on MMSE and domain specific neuropsychological tests over 10 years, controlling for stroke (87). The same research group found that in 717 white males, SBP measured at age 45 was negatively correlated with measures of verbal learning and memory function obtained 30 years later, controlling for stroke, depression, and use of anti-HTN drugs (88). The same Swedish cohort of 999 discussed earlier

also examined BP obtained at age 50 with MMSE at age 70 and found that DBP was the strongest predictor of cognitive decline over that 20 year time period (53).

1.3.2 HTN and Dementia Risk

Multiple epidemiological studies support a link between HTN and dementia. The Honolulu-Asia Aging Study found in 3703 Japanese-American men (mean age = 65, BP obtained between age 45-68) that un-medicated HTN conferred a higher risk for Possible and Probable AD by NINCDS-ADRA criteria (89) than those on treatment, controlling for stroke, APOE4, heart disease, and alcohol use (90). A Finnish study of 1449 persons (age ≥ 65, 21 year follow up) found an OR for Possible and Probable AD of 2.0 (95% CI: 1.1-7.2) if midlife SBP was ≥ 160 mm Hg and 1.7 (95% CI: 0.8-3.6) if midlife DBP was ≥ 95 mm Hg (91). That study controlled for BMI, stroke, myocardial infarction, smoking, and alcohol use. A Chinese study of 602 individuals (age ≥ 65), with SBP and DBP measured 15 years prior, found that HTN (defined as ≥160/95 mm Hg) predicted higher risk of DSM-IV defined AD (OR = 2.0; 95% CI: 1.1-3.5) controlling for smoking and alcohol intake (92). In Japan, a study of 1773 persons (73% women, age ≥ 60 with BP recorded 20 years prior) found that high SBP was related to DSM-IV defined VaD (OR per 10 mm Hg 1.33; 95% CI: 1.14-1.56) but not AD (93). Finally, a study of 8845 persons (mean age 69 with midlife HTN defined at age 42) found that HTN (defined either by use of medication or BP ≥ 140/90 mm Hg) increased risk for all cause dementia (OR = 1.24; 95% CI: 1.04-1.48) (94).

A connection between HTN and dementia can also be inferred from work showing that anti-HTN drugs lower risk for developing the syndrome. One study of 2418 subjects (age ≥ 60) was a randomized clinical trial with subjects receiving placebo versus nitrendipine or enalapril.

The outcome was development of AD, VaD, or mixed after 2 year follow up with entry DBP as a covariate. It was found that the anti-HTN medications reduced dementia risk by 50% (3.8 versus 7.7 per 1000, p = .05) (95). An extension of this study in 2902 treated subjects and placebo controls involved perindopril or plus indapamide with a median follow up of 3.9 years. The clinical outcomes were identical to the prior study and covariates included BMI, APOE4, alcohol, smoking, and MMSE (96). It was found that the anti-HTN medication reduced dementia risk, specifically AD< by 55% (3.4 versus 7.4 per 1000 person-years).

1.3.3 Neuropathological Basis for HTN Promotion of Dementia

The most frequent explanation for the effect of HTN on modifying dementia risk, especially vascular dementia, is HTN increases the risk of stroke due to large vessel cerebrovascular disease (CVD) (97, 98). This has the effect of reducing brain reserve capacity due to tissue loss, thus leading to an "earlier" clinical expression of a degenerative process, with the resulting increase in disease prevalence (99-101). Ischemic vascular lesions can cause the clinical expression of AD with fewer AD lesions (75, 102). Amyloid beta peptide (Aβ) can cause cerebrovascular dysfunction (103, 104) by constricting blood vessels and attenuating the vasodilatation produced by the endothelium-dependent vasodilator acetylcholine (16, 104-106). This phenomenon may be exacerbated if HTN-related kidney dysfunction reduces the efficiency with which Aβ is cleared from the body (107). HTN, through deleterious effects on brain vasculature, appears to have the potential to mediate an additive effect with AD neurodegeneration to result in greater clinical severity of dementia at an earlier time.

Additional evidence linking HTN with dementia, particularly AD, can be found in examining common neuropathological processes in both conditions. These processes typically

converge on the vasculature. Present in both HTN and AD are basement lamina thickening and collagen accumulation, hyalinosis, fibrinoid necrosis, and the presence of lobar and intracerebral hemorrhages (108-110). Characteristic in HTN and present in AD are WMHL, lacunar infarcts, microbleeds, large cerebral infarcts, and intima thickening in the blood vessels (23). Cerebral amyloid angiopathy, neurofibrillary tangles, and amyloid plaques, while characteristic of AD, are less commonly seen in HTN. Additionally, while endothelial degeneration is present in AD it is less so in HTN (23). The link between AD and HTN can also be inferred from one particular study linking anti-hypertensive medication with attenuation of amyloid pathology. The study involved screening 55 clinically prescribed anti-HTN drugs based on their anti-beta amyloid activity in cortico-hippocampal neurons based on cultures from the Tg2576 AD mouse model (111). Of these candidates it was found that one, valsartan, attenuated the oligomerization of amyloid peptides into neurotoxic oligomeric peptides. Additionally, valsartan improved spatial learning in the actual animals even when delivered at a dose that is twice less the level used to treat HTN in humans. This study suggests that since anti-HTN drugs may have AD-modifying activity, HTN and AD may share common pathogenic mechanisms.

1.3.4 HTN and Neuroimaging

Structural MRI studies have shown that elevated systolic pressures in untreated hypertensive, but cognitively normal subjects (mean age 61.3 years) correlate with decreased GM volumes in superior frontal, anterior cingulate, and middle temporal gyri (18). GM volume is associated with memory and executive function tests, and untreated midlife HTN is associated with decreased hippocampal volume 30 years later (112).

Positron emission tomography (PET) studies conducted in middle-aged cognitively normal subjects with HTN show a pattern of reduced rCBF (113, 114). Cognitively normal hypertensive subjects had less activation when engaged in memory tasks than normotensives in the middle posterior watershed area, parietal lobes, and thalamus. Functional MRI studies have shown a negative correlation between activation in the anterior cingulate gyrus, insula, thalamus, and periaqueductal gray matter and measures of BP when cognitively normal subjects with HTN performed the Stroop test (115). A more extensive discussion of HTN effects on perfusion will be discussed in Chapter 8.

All of these studies suggest that HTN can alter brain structure and function beyond the expected cerebral regions localized at the end lenticulostriate perforant arteries (116). These limbic and paralimbic areas are critical for higher cognitive functions, and are also targeted by AD pathology (117, 118). Other studies suggest that the prefrontal cortex GM volume can be affected by HTN even when blood pressure is under pharmacological control (116). In rhesus monkeys, executive functions are reduced when HTN is artificially induced (119). These neuroimaging studies therefore hint at the existence of key strategic brain regions that may be jointly affected by aging, hypertensive vascular disease and neurodegenerative pathology such as that seen with AD.

1.3.5 WMHL and Cognition

Multiple studies suggest that WMHL may modify risk for cognitive impairment and decline. Gunning-Dixon and Raz compared the associations of visual ratings of WMHL on CT or MRI to cognition, as assessed by neuropsychological tests, across 16 different studies (120). The combined associations between WMHL and global functioning ($.22 \pm .19$, $p < .001$) and speed

(.22 ± .13, $p < .001$) were statistically significant. Nine of the studies found that WMHL were associated with deficits in executive function (.31 ± .26, $p < .01$) and 6 found WMHL were correlated with delayed memory performance (.20 ± .10, $p < .01$). Eleven studies found a smaller, but statistically significant, negative correlation between WMHL and immediate recall (.12 ± .16, $p < .05$). Most important, however, was the finding that age did not influence the relationship between WMHL and cognitive index (all Fisher's z-scores < 0.1) and choice of imaging study (CT versus MRI) did not affect the relationships. Additionally, the location of the WMHL (deep versus periventricular) did not affect the correlations with cognitive function. This review suggests that higher burden of WMHL on the brain are related to suboptimal cognition regardless of age and imaging modality. The influence of WMHL on cognition was confirmed by a CHS study of 3301 individuals, each with a visual grading of WMHL on a 10 point (0-9) scale found a progressive decline in the Modified Mini-Mental State Exam score (3MSE) in both men and women (36).

1.3.6 WMHL and Dementia

WMHL have also been shown to modify cognition in those with dementia. This was illustrated in a study of 88-nondemented controls and 68 persons with clinically adjudicated AD. An interaction was found between periventricular WMHL and AD clinical status on global cognition, suggesting that the cognitive effects of WMHL can vary as a function of co-morbid dementia (121). Another study of 115 persons with dementia found that those with higher WMHL burden had even lower scores on tests of episodic and working memory compared to

demented persons free of such lesions (122). With VaD, WMHL predicts lower scores on tests of executive function, episodic memory, and global function (48).

WMHL have also been independently linked to increased dementia risk. Progression to non-AD dementia in 152 MCI subjects was predicted by both deep (HR = 5.7; 95% CI: 1.2 – 26.7) and periventricular WMHL (HR = 6.5; 95% CI: 1.4 – 29.8) (123). WMHL predict conversion from MCI to VAD and mixed dementia over a 3.8 year time period (HR = 1.14; 95% CI: 1.06-1.24) (124). However, other work has suggested that WMHL can accelerate conversion to AD. Progression to Probable AD from MCI within 3 years was predicted by the presence WMHL (HR = 1.59; 95% CI: 1.24 – 2.45, $p < .001$) (67).

In assessing the importance of WMHL for dementia risk is it important to recognize the difficulty in separating "pure" VaD and "pure" AD, especially in very old (> 85 years) populations. In the CHS-CS, for example, it was found that there was considerable overlap between NINCDS-ARDA AD criteria and VaD as determined by modified State of California Alzheimer's Disease Diagnostic and Treatment Centers criteria in identifying incident dementia in 3,375 participants followed for 5.7 years (125). This overlap is also mirrored by neuropathology studies identifying prevent co-existence of both vascular and AD neuropathology, hence the concept of mixed dementia (126).

1.4 CONTEXT OF RESEARCH OBJECTIVES

In this chapter, I have reviewed pertinent literature regarding the role of hypertensive vascular disease in raising risk for cognitive impairment and dementia. In doing this, I have also reviewed the link between hypertensive vascular disease and normal cognitive functions. I specifically

highlight the role of HTN and its end organ marker of brain damage, WMHL because they represent well described relationships between age, vascular disease, and dementia risk. The main concept I present in this dissertation consists of several parts. First, that the effect of age on the brain is moderated by the presence of WMHL, which in turn reflects the long term effects of HTN on the brain. The implication of this concept is that it is not the mere passage of chronological time by itself that reduces brain volume but the underlying vascular pathologies, namely HTN, which themselves are more commonly observed in the elderly. If one draws this concept further, it also suggests that if vascular disease were prevented or attenuated that brains would not appear "older" for a given chronological year. This was illustrated in an autopsy case of the world's oldest woman who died at 115. Despite her advanced chronological age and being born weighing only 1600 g, her brain at autopsy showed no signs of atherosclerosis, myelin pallor, amyloid plaques, atrophy and her Braak Stage was 2 (127). Not surprisingly, her cognitive scores – last obtained when she was 113 - were above those of adults age 60-75. What makes this one particular case intriguing is that is suggests that while brain volume and cognition do decline with age they do not necessarily always have to and vascular disease could be one determinant of such an outcome. Second, the gray matter volume loss (GMVL) - the imaging marker I use to infer underlying brain atrophy – is associated with WMHL in brain regions that are also responsible for cognitive function. The significance of this concept is that it provides neuroanatomical specificity by with one can understand how hypertensive vascular disease can have potentially deleterious consequences on cognition. Third, GMVL that is associated with WMHL overlap with areas of the brain that are targeted by neurodegenerative processes, namely those affected by MCI and dementia. The key implication of this concept is that it defines a common neuroanatomical framework for how age, vascular and neurodegenerative pathologies

may overlap by identifying strategic areas targeted by all three processes. Whereas the first three concepts focus on the relationships between age, vascular disease, neurodegeneration, and brain structure the fourth deals with the relationship between vascular disease and perfusion. Specifically, hypertensive disease is associated with perfusion deficits in the brain effects areas of cognitive relevance, such as the hippocampus. This fourth concept is important because it entails using a fairly new imaging modality to provide a lens through which one can understand the mechanistic basis for how vascular disease can induce GMVL.

1.4.1 Concept of Strategic Brain Areas and Key Strategic Regions

To summarize, hypertensive vascular disease can overlap with and modify brain aging and neurodegeneration in key strategic regions. The concept of such regions was suggested by Mesulam (128) who divided the brain into the following functional areas: limbic areas that include the substantia innominata and hippocampus; paralimbic areas that include the temporal pole, insula, orbital frontal cortex, and parahippocampal gyrus; heteromodal association areas which include the precuneus, and unimodal regions such as the primary motor and sensory cortices. Many of the brain regions I hypothesize to be jointly affected by age, hypertensive vascular disease, and neurodegeneration in this dissertation are encompassed in limbic, paralimbic, and heteromodal association areas. Using the functional areas of Mesulam as a general guide, one can represent strategic (with respect to cognitive function and thus dementia risk) and non-strategic regions of the brain in Figure 1, taken from the publication of Zekry and colleagues (129). This figure summarizes the concept that there are vital strategic areas of the brain with respect to cognitive functions, including memory and executive function. Factors that induce atrophy in these areas such as age, vascular disease, and neurodegeneration could

therefore be expected to raise risk for dementia. This dissertation will extend this concept by adding that these brain areas can also act as sites of synergy whereby brain atrophy associated with age may potentially add to that of hypertensive vascular disease and co-morbid neurodegeneration, thus considerably amplifying the risk for dementia. Thus, the strategic areas outlined in dark can be conceived as sites of multiple "hits" from age, HTN, and neurodegeneration. From these strategic areas, I will specifically focus on what I refer to as key strategic brain regions: orbital frontal cortex, anterior cingulate gyrus, the posterior cingulate gyrus, the precuneus, hippocampal formation, thalamus, caudate, putamen, globus pallidus, and basal forebrain.

All of these 10 key strategic brain regions are relevant because they are known to be involved in higher order cognitive functions (128) but each has its own relevance to vascular and or neurodegenerative pathology that makes it eligible for emphasis. The orbital frontal cortex plays an important role in executive function, a cognitive domain that is often affected early in the course of AD and with hypertensive vascular disease (116, 130). Additionally, the orbital frontal cortex has been shown to have high levels of amyloid in the setting of AD (131). The anterior cingulate gyrus is also a key region that I highlight because it has reduced metabolic output with aging (132), loss of perfusion and volume with hypertensive vascular disease (133), and is also affected by the amyloid pathology of AD (134). In addition, the anterior cingulate gyrus also contributes to executive function, especially attention (135). The posterior cingulate gyrus and precuneus are highlighted because these regions are involved in some of the earliest pathological changes in AD (136-138) and are important association cortices involved in cognitive function (128, 139). The hippocampal formation, which I define here as inclusive of the hippocampus and parahippocampal gyrus, is perhaps the most frequently implicated brain

regions in the pathology of neurodegeneration – particularly AD and its neurofibrillary tangle pathology (117, 140, 141). The hippocampus also has well defined roles in memory and learning (142-145). The inclusion of the caudate, putamen, globus pallidus, and thalamus in the list of key regions is for two reasons. First, all of these regions are well known to be affected by vascular disease in terms of having a higher proportion of lacunar infarcts and strokes (146). This is due to the delicate lenticulostriate artery distribution that is especially vulnerable to damage secondary to chronically elevated mean arterial pressure (33, 147). The second reason for including the regions is because they are implicated in frontal-subcortical networks that help serve executive functions (148-150). The basal forebrain, particularly the substantia innominata which is defined as GM inferior to the anterior commissure, is included because of it is a key site of cholinergic production in the brain (151). This is important because part of AD pathology involves the loss of this production which is also known to contribute to cognitive symptoms (152, 153). The orbital frontal cortex, anterior cingulate gyrus, the posterior cingulate gyrus, the precuneus, hippocampal formation, thalamus, caudate, putamen, globus pallidus, and basal forebrain therefore represent the most important key strategic brain regions within the strategic areas of Figure 1 because damage to any of them for any one or multiple reasons incurs the most severe consequences in terms of cognitive decline and risk for dementia. Areas that would therefore not be included are primary visual, motor, and sensory areas and the cerebellum. This dissertation will also present data asserting the notion that hypertensive vascular disease adversely affects cerebral perfusion in key strategic brain areas.

The data presented here were investigated using subjects drawn from a population based community cohort, Cardiovascular Health Study Cognition Study, and MRI modalities that allow for analysis of brain structure and function. This, combined with extensive clinical data on each

subject, allowed for more detailed investigations than in many of the studies reviewed. The study subjects utilized are also draw from the community, thus minimizing the referral biases of specialty clinics and more accurately representing the structural and functional changes that are likely to be observed in a general elderly population. The following chapter will review the general methods used in the CHS-CS.

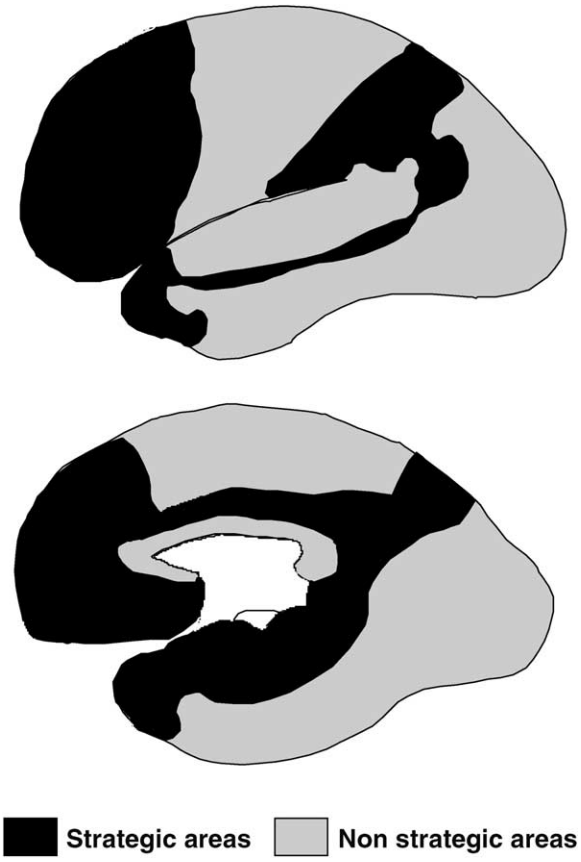

Figure 1: Conceptual Model of Strategic Brain Areas in black versus non-strategic areas in gray. The strategic areas represent brain regions that are likely to bet the subject of multiple "hits" from aging, hypertensive vascular disease, and neurodegeneration. These areas include regions such as the orbital frontal cortex, hippocampus, posterior cingulate gyrus, and precuneus.

2.0 BACKGROUND AND DESCRIPTION OF METHODS

Having identified the research objectives of interest, three components are needed to achieve them. First, I require a group of human subjects that has extensive information on their state of vascular disease, WMHL, and dementia diagnoses. Such a sample should ideally be drawn from the community to most broadly represent the vascular, MCI, and dementia being investigated and thus avoid the referral bias of specialty clinics. This is achieved in the work discussed by use of participants in CHS-CS, the description of which will occupy the first section of this chapter. Second, imaging methods are needed to provide detailed structural and functional information on the brains of these participants. This methodological requirement is accomplished by employing advanced 3-D volumetric structural MRI (SPGR) and a relatively new technique for perfusion imaging, arterial spin labeled (ASL) MRI. Third, computational imaging analyses are necessary to provide whole-brain information on the regionally specific effects of age, hypertensive vascular disease, and neurodegenerative states (MCI and dementia) on brain structure and function. This is achieved using the Statistical Parametric Mapping (SPM, v. 2; SPM2) software and its extension, Voxel Based Morphometry (VBM, v. 2; VBM2). Description of these methods will be done in the third and final section of this chapter.

2.1 THE CARDIOVASCULAR HEALTH STUDY COGNITION STUDY (CHS-CS)

The CHS-CS is derived from the larger multi-site CHS. The CHS is a population-based, longitudinal study of coronary heart disease and stroke in person age 65 and older (154). Its recruitment is based on Medicare eligibility lists in: Forsyth County, North Carolina; Sacramento County, California; Washington County, Maryland; and Pittsburgh, Pennsylvania. By drawing participants from the community, CHS avoids the referral biases that often plague studies of subjects from specialty clinics. The study was initiated in 1989 and began with a total of 5888 subjects. Extensive physical and laboratory evaluations were performed at baseline to identify the presence and severity of such vascular diseases as HTN. Periodic follow up examinations (1-3 years) further ascertained the severity of hypertensive vascular disease. This section will overview the composition of the CHS-CS arm, including information on cognitive diagnoses, and definition of HTN and WMHL.

2.1.1 Description of the CHS-CS

In 1997/99, dementia was diagnosed in 3,602 CHS participants as part of the CHS-CS (155, 156). All participants completed an informed consent and Institutional Review Board approvals were received at all sites. A separate DNA consent was obtained for genetic studies. The CHS-CS participants were included in the study based on completion of brain MRI (MRI at time 1 or MRI 1) and 3MSE in 1992/94. These subjects were further screened using neuropsychological data obtained at the clinical visit closest to MRI 1 to identify those at increased risk for dementia. A participant was regarded to be at high risk for dementia if he or she had: i) previously scored less than 80 or had a decrease of 5 or more points on 3MSE completed at previous exams ii) a

prior Telephone Interview for Cognitive Status (TICS) (157) score <28 iii) an Informant Questionnaire on Cognitive decline in the Elderly (IQCode) (158) score > 3.6, iv) incident stroke v) medical records indicating dementia diagnosis by their primary care physician (PCP) vi) or current residence in a nursing home.

For those agreeing to revisit the clinic or receive an in-home visit the following neuropsychological tests were administered: the Digit Symbol Substitution test (DSST), the America version of the National Reading test, the Benton Visual Retention test (BVRT), Raven's Colored Progressive Matrices, the California Verbal Learning Test (CVLT), the Rey-Osterreith figure, Immediate and Delayed Recall, modified Boston naming test, Verbal fluency test, Block design (modified from the revised Wechsler Adult Intelligence Scale), Stroop test, Trail Making, Trails A and B, Digit Spans, and the Baddeley and Papagno Divided Attention Task (155, 159). Domain specific neuropsychological tests were then transformed into age and education (college versus no college) adjusted t-scores for the following cognitive functions: executive function, motor function, language, processing speed, and visual-constructional/visual-spatial functions (159). The mean of these 5 t-scores are referred to as a composite cognitive score (CCS) and will later be used for correlations between cognitive function and brain structure in Chapter 5. For persons who declined the full neuropsychological battery, TICS, IQCode, 3MSE, DSST, and BVRT, were still available from the multiple follow up visits during the course of the CHS-CS. Neuropsychological test results were considered abnormal (>1.5 standard deviations below individuals of comparable age and educational level) based on normative data collected from a sample of 250 unimpaired subjects in Pittsburgh.

Additional information available to the CHS-consensus committee were activities of daily living, instrumental activities of daily living, physical function measures (gain, speed,

balance, grip strength, etc), known medications, and documentation of all hospitalized medical events such as stroke, myocardial infarctions, etc. that had transpired. Psychiatric information was obtained with the Center for Epidemiologic Studies–Depression Scale 10-item version (160) and the Neuropsychiatric Inventory (161).

A neurological exam for each subject included a brief mental status examination, cranial nerve testing, motor tone, abnormal movements, strength, deep tendon reflexes, release signs, plantar response and clonus, cerebellar testing, primary sensory testing, gait, postural stability, the Unified Parkinson's Disease Rating Scale (162) and the Hachinski Ischemic Scale (159, 163). All of these data were compiled into packets that were then later reviewed by a consensus panel of neurologists, psychiatrists, and neuropsychologists for the purposes of classifying each subject.

2.1.2 Classification of MCI in the CHS-CS

While delineating between MCI subtype effects on brain structure and function is beyond the score of this dissertation, a description of how MCI was identified in the CHS-CS is included for completeness. A minimum of 5 neuropsychological measures, encompassing 3 cognitive domains, one of which must be memory, had to be done for an MCI evaluation to be complete. MCI was identified as either amnestic type (AT) or multiple cognitive deficits (MCD). Persons with MCI-AT had impairments in delayed verbal or nonverbal recall that had to represent a decline from a previous level of comparatively higher function as detected with standard CHS neuropsychological evaluations. This diagnosis did not exclude individuals with mild defects on IADLs. To be classified with MCI-MCD, a subject needed to have had deterioration in at least 1 cognitive domain (not including memory), or 1 abnormal test result in at least 2 other domains,

without sufficiently severe cognitive function impairment for classification of dementia, or loss of instrumental activities of daily living to constitute dementia. As with the MCI-AT diagnosis, these deficits had to represent a decline from a previous level of higher function.

The certainty of MCI diagnosis was represented by the categories probable (greater certainty) and possible (lesser certainty). Participants were classified as having probable MCI if they met the following criteria: i) participants or their families reported cognitive problems and ii) there were no neurological, psychiatric, or systemic illnesses that could explain their presence of cognitive deficits. To be identified with possible MCI, two considerations were: i) neither participants nor their families reported cognitive problems ii) there were neurological, psychiatric, or systemic illnesses that might explain the presence of cognitive deficits.

It is important to note that I conceive of MCI as a behavioral and cognitive proxy for a relatively earlier or less advanced level of neurodegeneration compared to dementia. Referral clinic studies have provided evidence to support this notion (164) but the particular population under study here is drawn from the community. Thus, multiple potential causes of MCI could be at work in including systemic disease (i.e. cancer), polypharmacy, and psychiatric conditions such as major depressive disorder. While my ability to study MCI subjects representing early neurodegeneration may have been aided by selecting those with Probable MCI, this would have resulted in a large (> 25%) reduction in sample size. Concurrently, there is still a non-trivial likelihood that subject with Possible MCI may still have early neurodegenerative changes. Thus, to maximize statistical power and to avoid potentially excluding anyone with early neurodegenerative changes I used both Probable and Possible MCI subjects in my analyses. In doing so, I fully acknowledge that this makes the interpretation of the data potentially more

challenging but this is a tradeoff that I have judged to be acceptable. This same logic applies with the use of possible dementia subjects in all of my analyses.

2.1.3 Classification of Dementia in the CHS-CS

AD was classified as Probable or Possible using NINCDS-ARDA criteria (89). Briefly, this diagnosis of dementia was based on deficits in two or more cognitive domains severe enough to hinder ADLs in the context of a history of normal intellectual function before the onset of cognitive symptoms. An abnormal domain was present when at least two tests of the same domain were below standard cutoffs. This clinical diagnosis of dementia has been successfully used over the last two decades, and it has shown 98% sensitivity and 88% specificity for AD in the context of a referral based clinic (165). The diagnosis of dementia was independent of the MRI findings, although the MRI was used to exclude other pathologies. The diagnostic certainty was grouped into Probable versus Possible with the main difference being that Possible AD concedes that other pathologies (vascular, tumor, psychiatric) could be accounting for the dementia syndrome whereas with Probable AD this confound is less likely.

VaD classification was done in two steps. First, the consensus committee provided a diagnosis based on the clinical evidence: non-VaD, VaD, or mixed (VaD with AD, or other cause of dementia). This was done using only the clinical and neuropsychological data available but not the MRI. In a second step, the adjudication committee applied a set of diagnostic criteria to classify VaD: DSM-IV, State of California Alzheimer's Disease Diagnostic and Treatment Centers ADDTC, and National Institute of Neurological Disorders and Stroke-Association Internationale pour la Recherche et l'Enseignement en Neurosciences NINDS-AIREN and this step involved input from MRI scans (7). In this dissertation, vascular dementia will be defined

using ADDTC criteria. This is preferred over other criteria because it allows for a subject to have both a secondary AD diagnosis whereas other standards require exclusion of AD in order for VaD to be diagnosed. Given the intimate associations between AD and vascular pathology in the brain, it was therefore felt that the ADDTC criteria best captured subjects with both pathologies – a group that would be undesirable to exclude. As with AD, the diagnostic certainty of ADDTC defined VaD is classified as either Probable or Possible.

2.1.4 Identification of HTN and WMHL in the CHS-CS

HTN in CHS-CS subjects is considered present when: i) they are diagnosed by their physicians as having HTN ii) are placed on antihypertensive treatment or iii) have SBP $\geq$ 140 or DBP $\geq$ 90 mm Hg in two separate measurements.

Small vessel vascular disease, a reflection of HTN end-organ damage to the brain, was indexed by measurements of WMHL using standard CHS criteria of visual white matter grade (WMG) done by experienced neuroradiologists at MRI I and MRI II (166). These criteria estimated total extent of subcortical and periventricular WM signal hyperintensities on axial spin-density images. These hyperintensities were graded by successive increase from none to nominally detectable (grades 0 and 1) to involvement of almost all WM (grade 9). Excellent intrareader agreement (96.9%) has been found with the WMG scale (167). Examples of different WMG visual manifestations can be seen in Figure 2 from Longstreth et al (36). Large infarcts on MRI were judged as an area of abnormal signal change of greater than 3 mm in diameter (168).

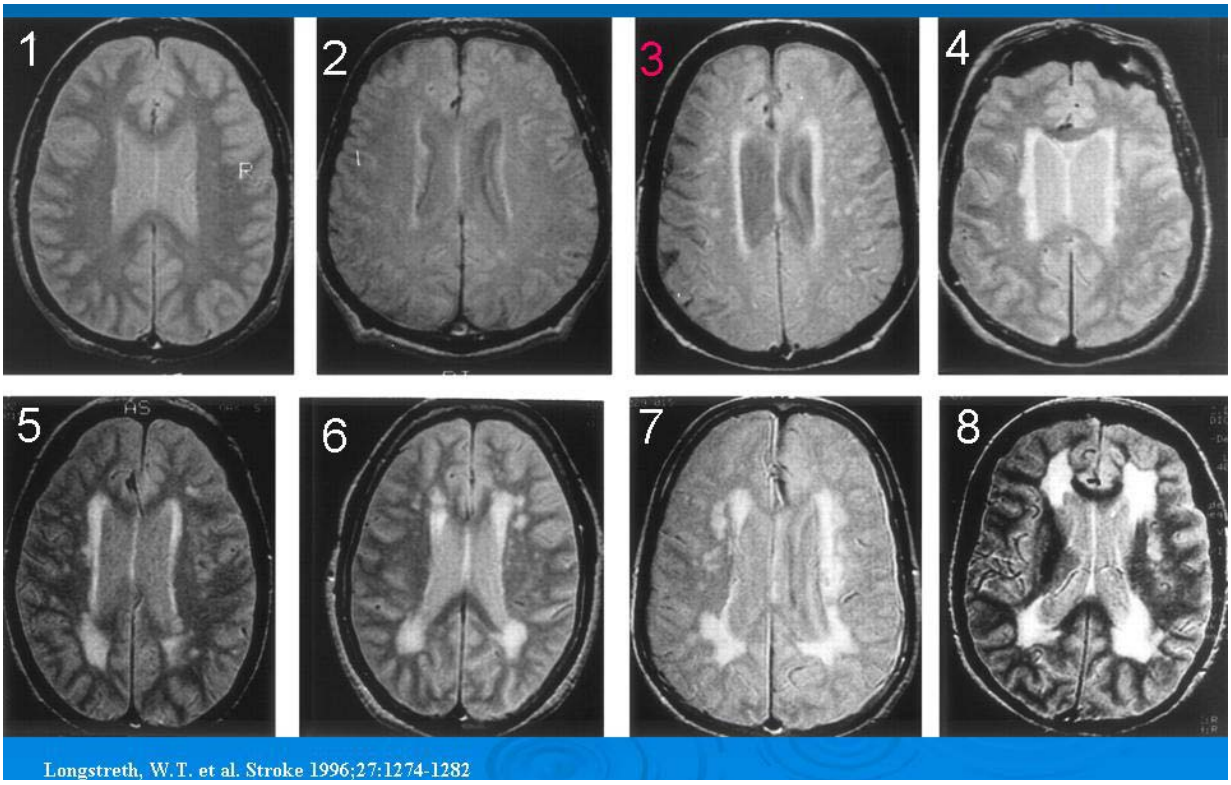

Figure 2: Classification of WMHL using CHS WMG scale on either proton density or T2 weighted MRI. The numbers in each box are the corresponding rating from the CHS WMG scale. WGM of 3 is when subcortical WMHL are visible and a WMG of 9 involves all WM (not shown). Confluent WMHL are first appreciable at grade 5.

2.2 IMAGING MODALITIES USED IN CHS-CS

2.2.1 Basic Concepts in Magnetic Resonance Imaging

MRI is an imaging technique that produces computerized images of tissue hydrogen using magnetic fields (169). This process is done in a scanner that surrounds the human body with electromagnets super cooled by liquid helium and generating a magnetic field that is, at minimal field strengths, 60,000 time as powerful as the magnetic field of the Earth. This field in turn

substantially affects the body tissue protons, the nuclei of hydrogen atoms. Protons typically wobble, or precess at a specific rate or frequency and this is known as the Lamor frequency, the equation of which is:

Equation 1: $\omega = \gamma B$

Where ω is the angular frequency and *B* represents the magnitude of the external magnetic field applied to the organ or tissue of interest (170). The north/south axis of each proton is typically represented by a magnetic moment, and these moments usually point in random directions as the protons precess (see Figure 3). Inside an MRI scanner, these proton magnetic moments align in the direction of the field's poles (Figure 4). Even in alignment, however, the protons still precess at a specific frequency and the magnitude of this frequency increases in relation to the strength of the magnetic field, as per the Lamor equation.

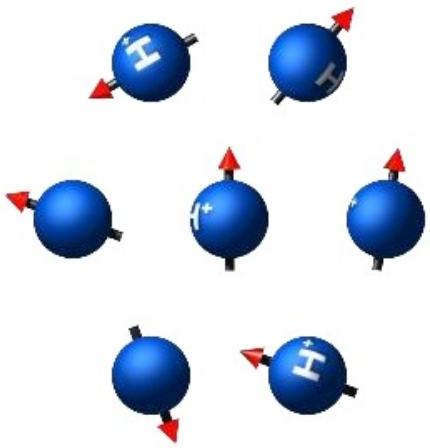

Figure 3: Magnetic moments of protons at rest, with no external magnetic field applied. At rest, all of the protons point in random directions. Figure from www.e-mri.org .

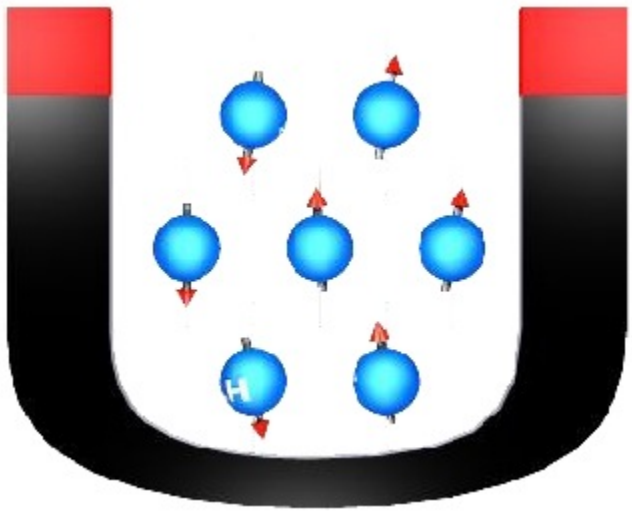

Figure 4: Within a large external magnetic field (called B0, represented by the magnet), nuclear spins align with the external field. Some of the spins align with the field (parallel, up arrows) and some align against the field (anti-parallel, down arrows). Figure from www.e-mri.org .

When the MRI scanner subsequently excites these protons with a radiofrequency (RF) pulse timed to the same frequency of precession, it knocks the protons out of alignment and within several milliseconds they spiral back into their original configurations, producing a faint electrical signal of their own that is then detected by a computer. The computer then processes this signal into an image by creating a grid of tiny boxes, called voxels, in three dimensions (x,y,z). A voxel is therefore a 3-D pixel.

The process of creating an MRI can therefore be summarized in three basic steps (169). First, the magnetic field is varied in the z direction to define a plane of interest in, for example, the brain. Within this plane, protons precess at a given frequency and are knocked out of alignment by the RF pulse tuned to the frequency of precession. Second, before the protons can realign themselves, other magnetic coils in the MRI scanner briefly vary the magnetic strength in the y axis. This causes protons to precess at different rates in the entire imaging plane. Detecting

these differences over hundreds of RF pulse and signal detection cycles, the computer locates voxels in the y-direction. Third, the MRI scanner coils vary the magnetic field from left to right in the x direction, causing protons to resonate at different frequencies as they realign themselves. Having now located each voxel in the x, y, and z directions, the computer assigns each voxel a coordinate on a computer screen. The signal intensity, or brightness of the spot, varies as a function of the number of protons and the magnetic properties of the tissue. Consequently, GM will have different properties and appearance on the image than WM or CSF. This tissue contrast forms the basis of readable MRI images and makes subsequent computational analysis possible. By varying the delay between the RF pulse and the refocusing pulse, distinct magnetic properties of the tissues examined can be emphasizes and these tissue can subsequently appear different upon visual examination. This is the basis of the different visual appearance of T1-weighted MR images in which CSF is dark versus T2 weighted sequences in which CSF shows as bright. The number of slices acquired during a scan also determines the extent to which detailed volumetric analyses can be done.

To understand basic concepts in MRI, it is also necessary to briefly review the different classes of pulse sequences to better understand the neuroimaging techniques used in the CHS-CS. Spin echo pulse sequences are a type of MRI in which tissue is exposed to a 90° RF excitation pulse then 180° RF refocusing pulse to obtain an MR signal. T1-weighted conventional spin-echo is used for acquiring anatomic images in moderate time periods and at high resolution whereas T2-spin echo images are rarely acquired with this technique due to long scan times (171). Gradient echo pulse sequences use a gradient to generate an RF echo, rather than a 180° refocusing pulse, as is the case in spin-echo sequences. Gradient-echo sequences

consequently allow faster imaging than spin-echo sequences and are frequently used in fast 3D imaging.

The spoiled gradient echo (SPGR) pulse sequence is a type of gradient echo pulse sequence used by General Electric (GE) medical systems for 3-D volumetric sequences (169). Whereas a typical T1 weighted image of the brain only has 52 slices, 3-D T1 SPGR has 124 slices acquired. This allows for whole brain coverage of all GM structures, subcortical nuclei, and WM tracts. This 3-D volumetric acquisition also allows for superior delineation between different brain tissues such as at GM-WM borders and GM-CSF boundaries, a feature that will become very important in subsequent discussions about MRI image segmentation.

2.2.2 Details of 3-D Volumetric Imaging Acquisition in CHS-CS

While structural imaging methods in the CHS have been previously described (168) they are briefly reviewed here. All MRI data were acquired at the University of Pittsburgh Medical Center MR Research Center using a 1.5 T GE Signa scanner (GE Medical Systems, Milwaukee, WI, LX Version). A 3D volumetric spoiled gradient recalled acquisition (SPGR) sequence was obtained for the whole brain (TE/TR = 5/25, flip angle = 40°, NEX = 1, slice thickness = 1.5 mm/0 mm interslice gap) set parallel to the AC-PC line with an in-plane acquisition matrix of 256x256 image elements, 250 x 250 mm field of view and an in-plane voxel size of 0.98 x 0.98 mm. All images produced from the scanner were in Digital Imaging and Communications in Medicine (DICOM), the standard default file format for handling, storing, printing, and transmitting information in medical imaging (169). The DICOM format is written such that every image slice is generated as a separate file, resulting in 124 separate files per one scan acquisition. To simplify the number of files involved for subsequent image analysis the DICOM

images are compiled into the Analyze image file format (http://mayoresearch.mayo.edu/mayo/research/robb_lab/analyze.cfm). This reduces 124 files to two files: a header file (.hdr) and an image file (.img). The .img file contains numbers conveying information about the image such as image intensities or in the case of perfusion images, blood flow values. The .hdr file contains information about the .img file, such as the volume represented by each number in the image (voxel size) and the number of voxels in the x, y and z directions. Analyze format images are the default file type used for all computational image analyses in this dissertation.

2.2.3 Basic Concepts of Perfusion MRI imaging ASL

The main purpose of perfusion MRI is to generate an image contrast that provides information on regional cerebral blood flow (rCBF), a key physiological metric of brain function. In evaluating the relative merit of a perfusion MRI method for both clinical and research use, it should be: i) Totally non-invasive and thus completely safe of use in elderly patients ii) Provides information on brain physiology that is known to be altered early in the course of neurodegeneration iii) can detect rCBF changes known to occur in the setting of hypertensive vascular disease. ASL perfusion MRI has the ability to fulfill both criteria.

ASL MRI works through the application of radiofrequency pulses to magnetically label water proton spins in blood flowing through the carotid arteries (172, 173). These labeled spins exchange with unlabeled spins in brain tissue to yield a quantifiable map of regional cerebral blood flow with no requirement for radiolabled or contrast agents. Practically, this is achieved by subtracting a labeled plane from an unlabeled plane (Figure 5), yielding a signal change on the order of 2-8%, higher than the 1% signal change seen with fMRI (174). Another advantage over

fMRI is that ASL provides actual units of rCBF, making it a fully quantitative type of neuroimaging. This makes ASL MRI an attractive choice for perfusion imaging in elderly persons, whom have been shown to be a higher risk for such adverse contrast reactions as nephropathies, hypotension, and nephrogenic systemic fibrosis (175-177). Perfusion imaging with ASL has been validated against quantitative perfusion techniques such as O^{15} PET (178). ASL MRI has also been utilized in research studies of AD and other dementias to show that perfusion abnormalities occur very early in the course of neurodegeneration (179-182). This makes ASL MRI compelling for studying dementia because it can detect perfusion alterations that are subtly altered early in the disorder. Because ASL MRI images rCBF it is also a sound imaging method for detecting perfusion alterations secondary to hypertensive vascular disease (183).

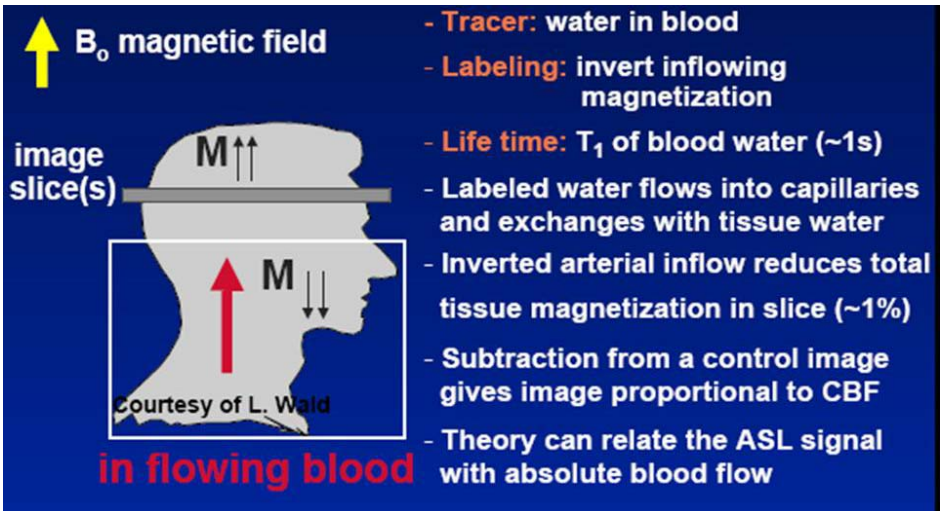

Figure 5: Summary of ASL Perfusion MR imaging.

ASL perfusion MRI can be typically applied in two forms: pulsed ASL (PASL) and continuous ASL (CASL). With PASL, an imaging slice of blood is labeled upstream of the region of interest by a short RF pulse, typically delivered to the base of the carotid and vertebral arteries. Signal acquisition is then carried out after a delay of typically 1-2 seconds. The

difference in signal the labeled and unlabeled imaging slices reflect the amount of labeled blood arriving in the volume of interest during the delay, and this allows for subsequent calculations of rCBF (184, 185). A major drawback to PASL is the limited lifespan of the endogenous tracer, since the magnetization of the labeled blood bolus returns to equilibrium after about 1-2 seconds. This can limit detailed perfusion MRI of structures which might not be reach reached by the tracer in time such as the inferior temporal lobe and the hippocampus.

With CASL, an adiabatic inversion pulse is applied to the blood upstream of the slice using a continuous radiofrequency associated with a gradient applied in the direction of flow. Consequently, the signal of the labeled slice of interest will reach steady state and rCBF is calculated by comparing with the signal from the same, unlabeled slice. The main strength of this method is that it allows for greater whole brain coverage, including in the hippocampus and inferior temporal lobes (184, 185). Its main drawback is the amount of RF energy delivered, and this has led to the development of sequences with pseudo-continuous labeling or the use of two coils: one for labeling, with a reduced signal intensity centered on the carotids, and one for signal reception (186). With both PASL and CASL, it is imperative that blood can flow unhindered through the main arteries such as the carotids because this enables the subsequent endogenous labeling and rCBF calculations. Consequently, carotid stenosis can result in labeled blood flowing through collateral vessels to have a delayed arrival time in the brain tissue that results in an underestimation of the CBF. This underestimation is worse in patients with severe carotid stenosis (172).

2.2.4 Details of Perfusion ASL MRI Acquisition in CHS-CS

All MRI data were acquired using the same 1.5 T GE Signa system (Milwaukee, WI, LX Version) as was used for the structural MRI scans and this was achieved in 187 CHS-CS subjects. Of these 187 scans, 74 were analyzed for the purposes of this dissertation. The rest were excluded from the analysis for the following reasons: a) history of clinical stroke or carotid stenosis as assessed with standard CHS criteria (187) b) radiological or clinical evidence of structural brain lesions (e.g. tumors, trauma, or surgery), c) history of head trauma or encephalitis d) no consumption of caffeine within 8 hours prior to exam, e) inability to process images using semi-automated tools, f) placement of the labeling place was not orthogonal to both carotid arteries and/or the difference between left and right carotid arterial mean velocities exceeded 20% of the mean, leading to acquisition of perfusion data in only half of the brain g) excessive patient motion as evidenced in structural images, or h) excessive image artifact (e.g., secondary to hair oil or dental implant).

Multi-slice continuous ASL was done using ramp-sampled echo-planar imaging to acquire 19 contiguous axial slices (64x64 matrix, 20 cm FOV, 5 mm slice thickness, 0 spacing, 21 ms echo time (i.e., minimum full), 76 kHz effective receiver bandwidth, 1 s acquisition time, 700 ms transit delay, 90° flip angle). The alternating single adiabatic inversion label and double adiabatic inversion control pulses were developed to cover the entire cerebrum and repeated 50 times for signal averaging the pairs of acquisitions. All perfusion images were registered to a common stereotactic space in the Standard Single Subject Montreal Neurological Institute template using a fully deformable registration method (188). This was done to atrophy correct the perfusion images, thus reducing the likelihood that any analyzed hypoperfusion patterns were secondary to cerebral volume loss (189).

2.2.5 Summary of Imaging Modalities used in CHS-CS

The imaging methods employed in the CHS-CS provide complementary information on brain structure and function. An axial section from both an SPGR MRI and a perfusion ASL scan are displayed in figure 6. Having outlined the subjects and imaging modalities used for this work, I will now review the image analyses techniques used.

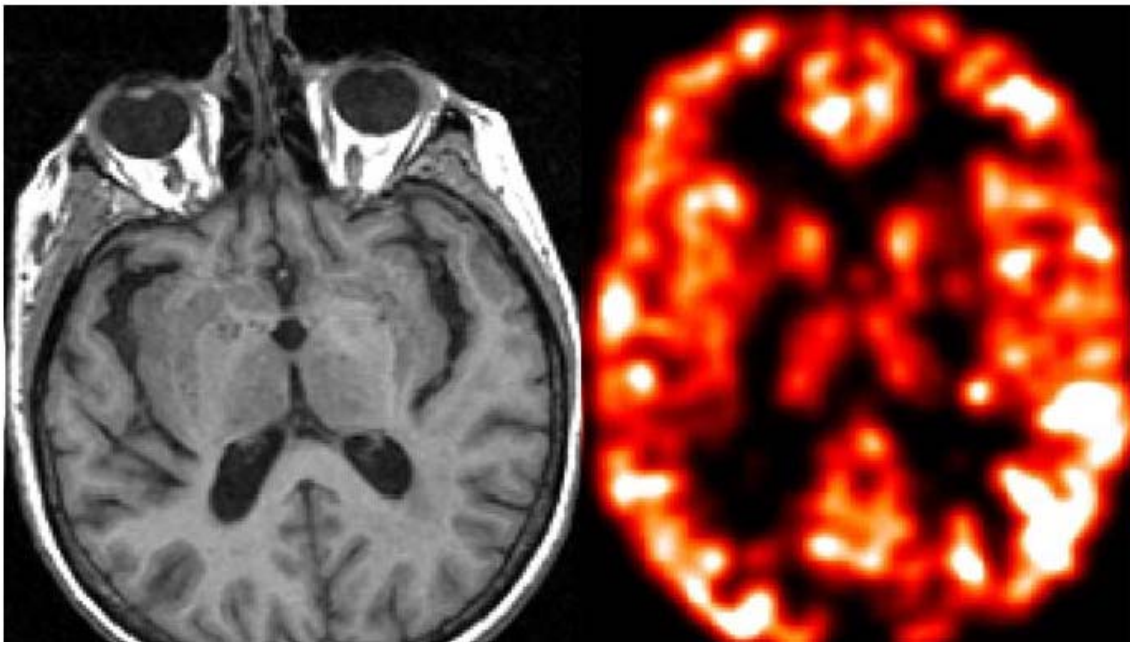

Figure 6: This figure shows two axial MRI images from the same CHS-CS control subject, taken at the level of the thalamus. On the right is a 3-D volumetric SPGR which provides information on brain structure. On the left is an ASL MRI image in a hot iron (hotter = more blood flow, range: 0-100 mL blood/g tissue/minute) scale that provides a map of rCBF.

2.3 METHOD OF STASTICIAL IMAGE PROCESSING AND ANALYSIS

Having identified subjects with extensive information on their state of vascular disease, cognitive status, and other factors and having obtained structural and functional imaging on this group, I now require a method for analyzing this data in a systematic way. This framework is provided by statistical parametric mapping (SPM) and this section will focus on analysis of structural images, with perfusion MRI processing reserving its own methods section in Chapter 8. SPM is a method for applying linear (parametric statistics) to the analysis of MRI images at a voxel-by-voxel level. This can be done in both a univariate (one independent or predictor variable and one dependent or response variable) or a multivariate fashion (one independent variable, multiple confounding variables or covariates, and one dependent variable). The general linear model (GLM) is summarized in the following equation:

Equation 2: $y = mx + b$

In its simplest univariate form, y is the variable I want to predict (GM for example), m is the slope of a straight line, x is the predictor variable (age for example), and b is the y intercept of the straight line. This equation can be subsequently expanded into a multivariate model represented by Equation 2:

Equation 3: $y = m1x1 + m2x2 + b1 + b2 + e$

This equation has the same variable I seek to predict (GM) but now has additional terms. The term m1 refers to the slope of x1 (age from Equation 1) and m2 is the slope of line 2 corresponds to a second variable in this case one that could be confounding the relationship between age and GM. This variable is x2 which in this example is gender. The intercepts for each line is are represented by b1 and b2 and e is the error term for the equation. Equation 2 therefore represents a multiple regression model. If one wants to test an interaction, that is if the

effect of age on gray matter varies as a function of gender, one would multiply the age and gender terms (age by gender interaction). Statistically, this is how one tests moderation, whether or not one variable alters the strength of a relationship between two others. In statistically testing mediation, one seeks to determine if the effect of x on y may in fact be accounted for by another variable. SPM is consequently nothing more than the application of these different statistical concepts at a voxel level, in this case in structural and perfusion MRI scans. To do this, though, all scans have to first be processed for statistical analysis. This is done using VBM, which is described in the next section.

2.3.1 Introduction to Voxel Based Morphometry

The basic principles of VBM are displayed in Figure 7 and VBM itself is fully described in previously published work (190). First, all MRI scans were processed using Smallest Univalue Assimilating Nucleus (SUSAN) from the FMRI Software Library (FSL; http://www.fmrib.ox.ac.uk/fsl/) for 3-D non-linear noise reduction, which improves the resolution of an MR image by only averaging a voxel with local voxels which have similar signal intensity. Second, I invoked the Brain Extraction Tool (BET) from FSL to automatically strip the scull and scalp from the images (http://www.fmrib.ox.ac.uk/analysis/research/bet/) and this has been shown to improve the quality of subsequent segmentation (191). Third, Voxel Based Morphometry (VBM2) (http://dbm.neuro.uni-jena.de/vbm/vbm2-for-spm2/) was utilized in Statistical Parametric Mapping (SPM2) (http://www.fil.ion.ucl.ac.uk/spm/) running in MATLAB v 7.0 (The MathWorks, Natick, MA, USA) to normalize all images use a 12-parameter affine transformation and non-linear registration with 16 iterations to spatially normalize and scale the

individual magnetic resonance images to the custom Pittsburgh Elderly Template of 419 brains (69 ± 7.5 years) (192).

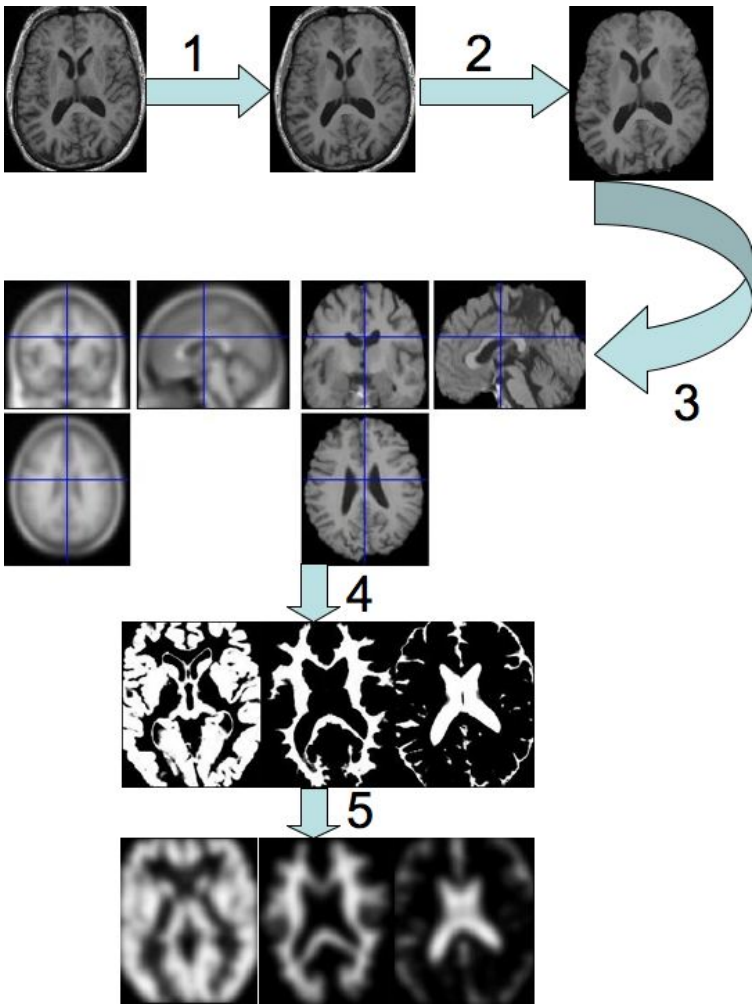

Figure 7: Outline of VBM. See text for details.

During this step, images were visually inspected to ensure that no registration errors occurred. The Pittsburgh Elderly Template was selected due to it large sample size representing the most likely variations in healthy aging that could be observe in the population. Fourth, SPGR images were segmented into grey matter (GM), white matter (WM), and cerebrospinal fluid (CSF) based on registered spatial priors from our template. A hidden Markov random field threshold of 0.3 was used in the segmentation step to remove isolated voxels of one tissue type that are unlikely to reside in that particular tissue. Additionally, volumes for each tissue type

were calculated by multiplying all voxels by the inverse of the Jacobian determinant of their spatial transformation matrix to correct for any changes in the size of the individual voxels during the normalization step and this process is known as modulation in VBM. The volumes of GM, WM, and CSF obtained from this were summed to compute total intracranial volume (TIV), a measure of head size. Fifth, modulated, normalized, segmented images were smoothed using a 10 mm isotropic Gaussian kernel (full width at half maximum) to increase statistical power and preparation for parametric statistical analysis. The use of a 10 mm smoothing filter in particular is also recommended to minimize confounding results that could occur due to normalization errors (193). The use of modulation and the hidden Markov random field allows for full volumetric information of SPGR images to be obtained and ensures a more accurate segmentation process. Because of this, the version of VBM used in this study is known as optimized VBM and has also been described previously (194), with main modifications in our method being i) prior image processing with SUSAN and BET ii) use of a general elderly template instead of a study specific template iii) application of the hidden Markov random field. The VBM pipeline used in CHS-CS is described in Table 1.

Table 1: VBM protocol steps with associated software.

Step	Software
3-D Non-linear Noise Reduction	SUSAN http://www.fmrib.ox.ac.uk/fsl/ Smallest Univalue Segment Assimilating Nucleus
Skull/Scalp Removal	BET http://www.fmrib.ox.ac.uk/analysis/research/bet/ Brain Extraction Tool 2
Normalization to Pittsburgh Elderly	SPM2 http://www.fil.ion.ucl.ac.uk/spm/

Template (419 subjects, 69 ± 7.5 years)	Statistical Parametric Mapping 2
Gray Matter Segmentation with Hidden Markov Random Field Threshold of 0.3	VBM2 http://dbm.neuro.uni-jena.de/vbm/ Voxel Based Morphometry 2
Modulation by Inverse Jacobian Determinant to obtain tissue volumes.	VBM2
Smooth with 3-D 10 mm Gaussian Filter	SPM2
Statistical Analysis of GM images	VBM2/SPM2

While VBM methods have advantages relative to studies that focus on a restricted number of regions of interest, there are some important limitations to the technique. Registration errors can occur during spatial normalization due to the increased variability encountered with atrophic brains; such errors depend greatly on template selection. We addressed this problem by using a custom template of 419 normal elderly brains (69 ± 7.5 years) (192) for the normalization step, which can produce more biologically plausible inter-group comparisons than the use of a "standard" template image (195). I did not use separate templates for the controls and AD subjects because this can result in an overestimation of GM volume loss by over 300% and a misclassification of the location of volume loss (196). I further minimize the effects of any registration errors by using a GM mask derived from the Pittsburgh Elderly Brain template to restrict the statistical search space to gray matter voxels. The use of a large smoothing kernel (10 mm) also reduces the probability that the volumetric differences found are due to registration error (193). Thus, while I cannot completely rule out registration errors in the data, I have taken multiple precautions at different levels of the analysis to minimize these confounds.

It has been suggested that the unified segmentation method of SPM5 (197) provides better normalization results than SPM2. However, a recent paper from that same group shows that in fact the quality of normalization is the same between SPM2 and SPM5 using mathematical formulas to describe surface overlap, volume similarity, and distance measures (198). Thus, I have no compelling reason to use SPM5 normalization, an additional drawback of which is that it uses an iterative approach to minimize the use of customized templates. While this may work well for smaller studies of normal subjects it may also fail in cases of age related brain atrophy (http://www.fil.ion.ucl.ac.uk/-spm/software/spm5/SPM5_new_features.pdf; SPM5 graphical user interface). Thus, I do not use SPM5 for my analysis of this data that consists of elderly or atrophied brains. The same paper also suggests that the newest SPM image processing toolbox, the Diffeomorphic Anatomical Registration Through Exponentiated Lie algebra or DARTEL offers superior spatial normalization (http://www.fil.ion.ucl.ac.uk-/~john/misc/dartel_guide.pdf). There are three reasons I do not use DARTEL. First, it requires that images be down sampled from 1 mm to 1.5 mm resolution, which may obscure important volumetric results in smaller structures such as the hippocampus. Second, the fundamental approach of DARTEL requires that all brains be warped to custom templates of the subjects being studied and the disadvantages of this have already been discussed above and investigated in prior work (196). Third, "In practice though, because DARTEL uses a constant velocity framework, it means that the further it has to deform something, the less accurate are the resulting warps." (John Ashburner, SPMlistserv, 01/26/2009). In other words, because DARTEL uses an iterative approach for normalization (warps) there is a greater the probability that it may overmatch fine cortical anatomical details, leading to normalization results that could underestimate the actual extent of tissue loss.

2.3.2 Statistical Concepts of Mediation and Moderation

Mediation and moderation are two statistical concepts with relevance for the present work. This separate section defines them so that it is clear that when such language is used it refers to specific statistical ideas and not other concepts.

Mediation is the process by which the Main Effect of an independent variable on a dependent variable is completely accounted for by a third mediator variable does not have a direct statistical test as is the case with moderation. However there are several criteria (http://davidakenny.net/cm/mediate.htm#WIM) that can be used to guide whether or not mediation is occurring. They are:

Step 1: Show that the candidate mediator is correlated with the dependent variable. This can be done using a simple bivariate Pearson correlation coefficient *r*.

Step 2: Show that the independent variable is correlated with the candidate mediator variable, which can also be established using a bivariate correlation.

Step 3: Show that the candidate mediator variable reduces the effect size of the independent variable when both are included in a multiple regression model that predicts the dependent variable. For complete mediation, the effect size of the independent variable should go to zero when the candidate mediator variable is included in the model. For partial mediation, the independent variable effect size does not have to go to zero but it should be reduced to the extent where it is no longer statistically significant in predicting the dependent variable.

An example of mediation is shown in the following diagram in Figure 8. Part a is a conceptual model of partial mediation in which the relationship between the X and Y variables is in fact accounted for in part but not fully by the variable Z. The black arrow reflects the correlation between X and Y. The blue arrow shows the correlation between the X and Z variables and the red arrow shows that the candidate mediator variable is associated with the outcome variable Y. Part b replaces this model with the ideal posited by this dissertation: that the association of age and GM may be accounted for in part by WMHL. This is identical to saying that WMHL partially mediate the association between age and GM.

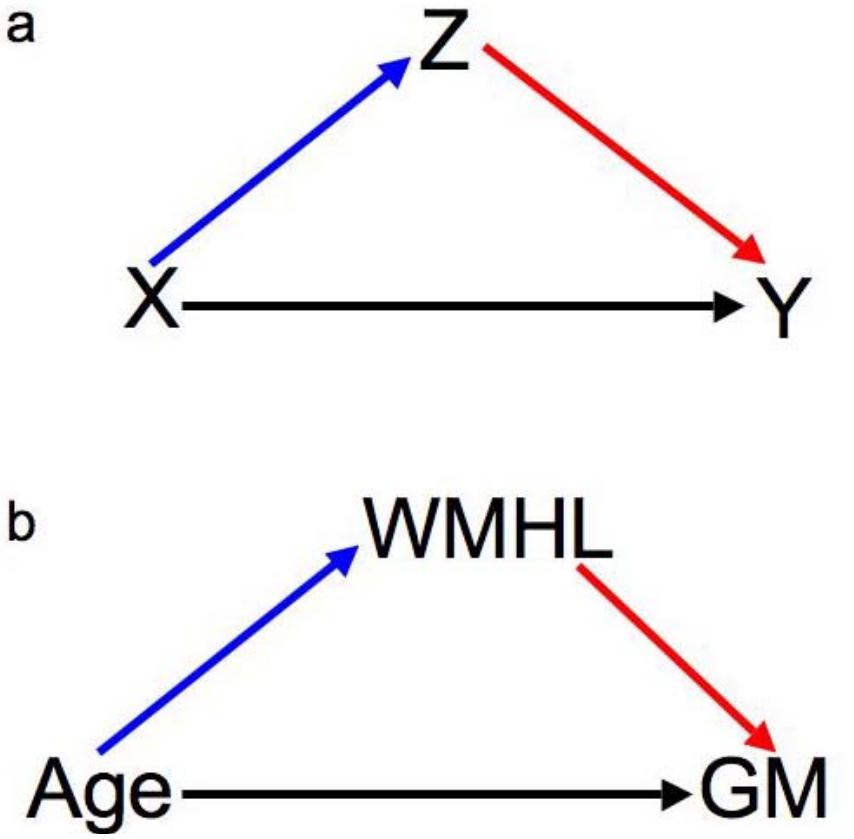

Figure 8: This figure has two parts. Part a depicts a partial mediation in which changed in variable X are correlated with changes in variable Y (black arrow) and changes in X are also correlated with changes in variable Z (blue arrow). The red arrow shows that changes in Z also correlated in those in Y, thus showing a partial mediation. Where complete mediation to exist, the black arrow would vanish once Z is entered into

the model. Part b replicates the partial mediation model of part a, with actual variables of interest: age, WMHL, and GM. In this case of mediation, changes in age are associated with those in GM; specifically, as age increases, GM goes down in volume (black arrow). Concurrently, as age increases WMHL also increase in magnitude (blue arrow) and such lesions are themselves inversely associated with GM (red arrow). Thus, one can conclude in this case that the inverse association of age on GM is partially mediated by WMHL. With complete mediation, the black arrow between age and GM would no longer exist once WMHL are entered into the model.

Moderation in statistics is defined in terms of an interaction. Interactions assess if the Main Effect of an independent variable on a dependent variable varies as a function of a third variable. If this is the case, it is an example of moderation (199). Another way of defining moderation is that the Main Effect of a certain variable, such as age and its relationship with GM, varies as a function of gender. Thus, gender would be said to moderate the Main Effect of age on gray matter volume. With respect to this work, moderation can be hypothesized in terms of WMHL strengthening the association between age and GM. This is depicted in Figure 9. Figure 9 shows a red arrow drawn from WMHL to the black arrow linking age to GM. What this means is that WMHL is strengthening the association between age and GM, thus moderating it. Another way of expressing this relationship is that the main effect of age in those with WMHL will be stronger than in those without such lesions. A practical consequence of moderation in this case would therefore be that persons with WMHL would have "older" looking brains in terms of having a higher magnitude of age associated GMVL.

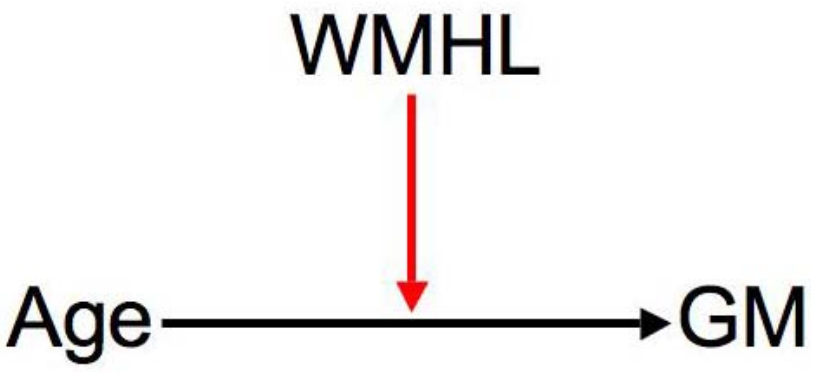

Figure 9: This figure depicts moderation of the inverse association of age and GM (black arrow) by WMHL (red arrow). Specifically, the red arrow means that in persons with WMHL, the magnitude of the age association is higher than in those without.

2.3.3 Statistical Modeling in SPM

For the purposes of structural MRI analyses, I analyze only GM voxels. Whether nor not a voxel is classified as GM or not is determined in VBM by how likely those voxel intensity values match those in the Pittsburgh Elderly Brain template. Therefore, a voxel was only analyzed statistically if it displayed a GM value greater than corresponding WM and CSF values. To additionally protect against inclusion of WM or CSF voxels in my statistical analyses, I also applied an absolute voxel intensity threshold of 0.1 (range 0 – 1) according to standard VBM guidelines (http://dbm.neuro.uni-jena.de/vbm/vbm2-for-spm2/) so that any voxel below that value is automatically excluded from the analysis. This measure is to especially exclude those voxels that are WM or CSF but may be mistakenly classified as GM voxels due to their locations at GM-WM or GM-CSF borders.

I conducted statistical analysis in SPM by applying the general linear model on a voxel-by-voxel level in the subjects MRIs of the specific groups I examined (controls, MCI, dementia, etc). The main model I use in SPM multiple regression, which allows the specification of one dependent variable (GM) and multiple independent variables. So, for example, one could assess the relationship between age and GM while controlling for such potential confounders as gender, race, and education. In doing this, an investigator can determine whether or not increasing age predicts a decrease in gray matter (an inverse association or negative correlation) or if higher age is associated with larger tissue volumes (a positive relationship). Such associations of the independent variable with the dependent variable are called Main Effects. Thus, if higher age is positively or negatively associated with GM volume that is the Main Effect of age on GM. In SPM, building statistical models is achieved through the construction of a design matrix. An example of a multiple regression design matrix is seen in Figure 10. This figure shows the independent or predictor variables in an SPM multiple regression model. The context of this model it is possible to test, for instance, if age is associated with GM while controlling for the potentially confounding influences of head size (TIV), gender, or race.

When a design matrix is constructed, the Main Effects of each independent variable on GM are specifically determined using contrast modeling. Contrast modeling entails the specification of contrast vector weights. Thus, if I wanted to assess the Main Effect of age on GM in the Figure 10 design matrix I would code a contrast vector weight of -1 (testing for an inverse relationship) and I would code the covariates as 0 so as to control for their confounding effects. Were I to be interested in a positive relationship between age and GM the contrast vector weight would be 1.

Figure 10: Four columns model the Main Effects of age, total intra-cranial volume (TIV), gender, and race on gray matter, all independent variables. Values for each variable are represented by a grayscale color scheme (ex. 0s are white, 1s are gray in group columns and continuous variables are varying shades of white, gray and black in the age and TIV columns). Each row corresponds to a smoothed modulated normalized segmented gray matter MRI, GM being the dependent variable.

Statistical interactions can also be evaluated within the SPM framework. A specific example of an interaction or moderation that could be tested in SPM is to assess if the Main Effect of age on GM varies as a function of whether or not an individual has AD. Such an interaction may hypothesize, for instance, that age has a stronger Main Effect in persons with AD. In the SPM design matrix, this would be represented with the following design matrix in Figure 11, which shows specific columns for an age by group interaction with control and AD subjects. If one wanted to therefore test whether or not an Age by AD interaction is predictive of lower GM volume a -1 contrast vector weight would be coded for that column in the design matrix. In other words, this would allow for a test of whether or not age moderates or in this case strengthens the inverse association between AD and GM volume. Continuous variable are

centered around their overall means (overall mean – continuous variable) to reduce confounding due to multicollinearity – a problem in statistics in which correlation between independent variables leads to faulty statistical output from a multiple regression model.

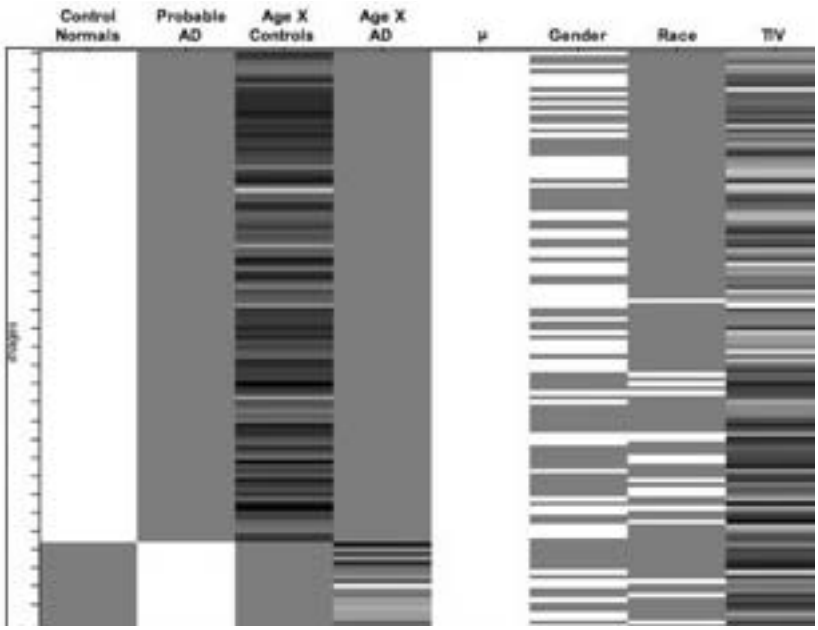

Figure 11: Interaction analysis design matrix with separate columns for the two groups (controls and AD) and their respective interaction terms with age. Interaction terms are calculated by multiplying the two independent variables that are hypothesized to interact in columns 3 and 4. Remaining columns model the effects of gender, race, and TIV as nuisance covariates. The column marked μ models the mean data across all subjects.

Mediation cannot be evaluated directly in SPM but will be tested in several ways. First, it will be formally evaluated using total GM volume obtained from VBM as the dependent variable in multiple regression models using Statistical Package for Social Science (SPSS, SPSS Inc, Chicago, IL.). Within SPM itself, a candidate mediator variable will then be added to a model with the independent variable. If the independent variable is no longer statistically significant when the candidate mediator variable is added, this will interpreted as evidence for complete mediation. Should the Main Effect of the independent variable remain statistically significant but

is attenuated on visual exam using the overlay of the r-images that include and exclude the candidate mediator variable, then this will be taken as evidence to support partial mediation. Mediation analyses will only be referred to if they are statistically significant and full all criteria for either partial or complete mediation. The reader should therefore assume that no mediation effects are seen unless they are specifically described.

A third type of statistical analysis that I will be conducting in SPM is what is called a conjunction analysis (200). A conjunction is a statistical test for determining whether two independent variables have Main Effects in the same brain areas. This kind of analysis therefore allow me to identify, for example, if age and WMHL both exert Main Effects in the hippocampus or any other brain region encompassed by the scan. Conjunction analyses will be very important in subsequent chapters and multiple results will be presented regarding them. As with mediation, the reader should assume no conjunctions unless they are described.

2.3.4 Statistical Thresholds in SPM

A statistical threshold is typically a cutoff value by which results are deemed as statistically significant. A common challenge in defining statistical thresholds, however, is the problem of multiple comparisons, a common dilemma in statistics that is especially pertinent to SPM analyses of brain images. The problem of multiple comparisons states that a statistically significant result can be obtained by sheer virtue of conducting large numbers of statistical tests simultaneously. Thus, if an MRI volume contains 10 million GM vowels and one conducts separate univariate tests at each voxel with SPM, then a p-value of .05 would mean .05 * 10 million = 500,000 false-positive voxels due to chance alone. The multiple comparisons problem can therefore amount to almost a half a liter of false positive (type I error) volume per MRI scan.

An early approach to correcting for multiple comparisons was the Family Wise Error correction, which functioned as a Bonferroni style (p-value/number of tests) correction using Gaussian Random Field Theory (201). This method, however, was regarded as being too stringent – thus increasing the risk of false negatives (type II error). Newer approaches consequently emerged and the most successful one in neuroimaging has been the innovation of the False Discovery Rate (FDR) (202). Rather than control chance of any false positives as is the case with random field theory, FDR controls the expected proportion of false positives among statistically significant voxels. FDR thresholds are therefore determined from the p-value distribution the actual data set and consequently adapts to the amount of signal within that data; this makes FDR more sensitive signal than other methods that correct for multiple comparisons. If there are truly no statistically significant results in an analysis, FDR achieves similar results to random field theory thus minimizing type I error (203). The most common FDR threshold applied in SPM is the FDR = .05 ($p < .05$) that means that no more than 5% of the statistically significant voxels in an image cluster are the result of type I error. For all structural image analyses presented here, this is the method used. Correction for multiple comparisons of perfusion images will be discussed in Chapter 8.

Finally, another type of threshold in SPM is the extent threshold (k). This threshold refers to how many contiguous (bordering or adjacent voxels) need to pass a statistical threshold for the entire cluster to be statistically significant. The extent threshold is typically signified in terms of the number of voxels. Thus, if I establish an extent threshold of 10 voxels ($k = 10$) this means that 10 continuous voxels must exceed statistical threshold in order for the overall cluster to be regarded as significant. For the majority of structural statistical analyses, the extent threshold is 100 for Main Effects, 100 for conjunction, and 30 for interactions. For perfusion analysis the

extent threshold is 30 for all analyses. As there are no published guidelines for what extent thresholds to use, my choice of how large to make these thresholds is largely arbitrary.

2.3.5 Statistical Output in SPM

Statistical output in SPM is represented both visually and quantitatively. The most common statistical output of SPM is the t-statistic, which can be obtained from most type of parametric statistical analyses including multiple regressions. In SPM, each cluster of statistically significant voxels has individual voxel level t-values that represent the highest effect sizes. These are called peak maxima and have an associated FDR-corrected p-value, all of which are reported in default SPM output tables (200). Visually, t-statistics generated by converting them into brain images that are then projected onto a template brain. This allows for subsequent anatomical localization of Main Effects. The most common template brain used for this purpose is the Standard Single Subject Montreal Neurological Institute brain (204). Such rendering can be done either in volume/surface rendered images or in orthogonal sections (sagittal, coronal, and axial) and these will be also referred to as section renderings. With respect to section renderings, t-values can be converted to a more intuitive measure of statistical effect size: the point biserial correlation (205) or correlation coefficient *r*. The formula used to achieve this in SPM is shown below:

Equation 4: $r = \text{sign}(t)/\text{sqrt}((df/t^2) + 1)$

Where t = the t-statistic in an individual voxel and df = the degrees of freedom in the multiple regression model. Because the *r*-value is calculated using a *t*-value obtained form a multiple regression model, it is a partial correlation (r^p). Thus, if I were correlating age to GM

while controlling for gender, the correlation from that analysis is a partial correlation because it is the correlation between age and GM that accounts for the correlation between gender and GM. Because *r* values can only range between -1 and 1, they represent a more intuitive measure of effect size than the *t*-statistic which can take on a wide array of values (206). For this reason, all section renderings presented in this dissertation will be done using the *r*-value. The only exception to this will be Main Effects that are masked for other Main Effects as r-images cannot be produced in such a manner using SPM. Volume rendering will be done with the t-statistic as that is default and only option for doing so in SPM. Additionally, volume rendering of all structural results will be done using the Standard Single Subject MNI template.

2.3.6 Anatomical Localization in SPM Analyses

A key component in SPM output is defining anatomical locations of statistically significant voxels. This is commonly done by identifying the peak maxima in a given cluster, those voxels with the highest effect sizes, and mapping their locations onto a stereotactic grid. The standard stereotactic space used in neuroimaging is the Montreal Neurological Institute (MNI) space. Thus, the purpose of normalization in VBM was to warp all subject scans into the spatial system of the Pittsburgh Elderly Brain Template which itself had been constructed in MNI space. Thus, a coordinate system of (x = -10, y = -15, z = 12) would correspond to the same anatomical location in each subject. For MNI space, an atlas called the Automated Anatomical Labeling (AAL) atlas was constructed to define the locations of brain areas (207) using MNI spatial coordinates and the AAL toolbox for SPM (http://www.cyceron.fr/freeware/). The AAL atlas is shown in Figure 12 (top row) and its overlay onto the Standard Single Subject MNI template (bottom row). For display purposes only, I overlay all section rendered results onto

orthogonal sections of this image (204) and this is done using the *MRIcron* image viewer software (208). With very large clusters (k > 50,000 voxels) considerably more local maxima will be listed than for smaller clusters in all SPM statistical output tables.

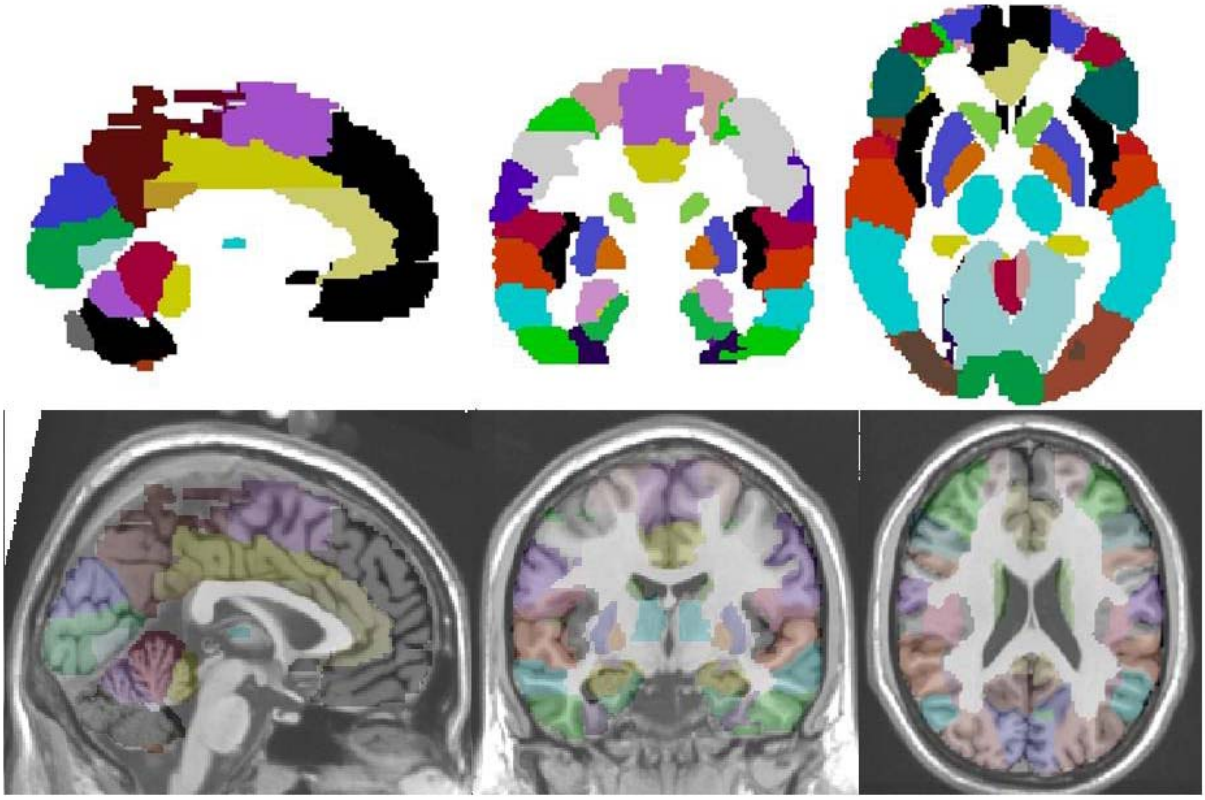

Figure 12: The top row shows color coded brain regions defined by the AAL. The bottom row depicts the overlay of this atlas onto the Standard Single Subject MNI template.

There has been much debate regarding how appropriate it is to overlay group data onto single subject images. Overlaying group results onto a single subject brain may deceptively imply that the resolution of the data is higher than in reality and this debate has mainly been carried out with respect to non-quantitative functional MRI activation studies (209). Such studies typically use small numbers of subjects (n = 10-30) and attempt to make statements regarding brain function in relatively focal brain areas in which case precise anatomical localization takes

on added importance. I present my work on the Standard Single Subject MNI template because to use an average template for an overlay would be less precise due to inter-subject morphological variability blurring anatomical landmarks. Consequently, the Standard Single Subject MNI template serves as a useful high resolution visual guide one can use to understand the general anatomical location of Main Effects. Another reason for using the Standard Single Subject MNI template for overlay purposes is that it enhances comparability with the number of studies has have used the template for this purpose (210-212). Thus, projecting our results onto the Standard Single Subject MNI template is methodologically consistent with other studies of elderly brains. Indeed, were every study to use their own average templates for overlaying results it would quickly lead to confusion in visual comparisons of such data due to lack of consistency in the basic display. Ideally, different standard high resolution templates would exist for various demographic and age groups and would be the standard of visualizing neuroimaging results but consensus regarding this has not been reached in the field (209).

That stated, it is important to understand that the Standard Single Subject MNI template serves only as a guide for general visualization of the anatomical locations targeted by Main Effects of such variables as age and WMHL. It is not meant to provide absolutely precise anatomical localization but rather is meant to support a general description of such anatomical locations. The same caveat applies to the use of the AAL, which itself was defined from the Standard Single Subject MNI template. Additionally, caution should be taken with inferring the resolution of the data I present from that of the template – they are not the same. Ultimately, the final resolution of the data that will be presented is limited by the size of my smoothing filter (10 mm) but in general neuroanatomical regions of interest defined on MRI tend to be quite large and thus have low anatomical resolution compared to what is obtainable with microscopic

neuropathological methods. Thus, optimally precise resolution of neuroanatomy is neither the goal nor the capability of the methods I use. My methods for neuroanatomical localization and display, however, are sufficient enough to determine and illustrate if gross structures represented by key strategic brain regions (hippocampal formation, precuneus, etc.) are affected by variables of interest.

2.3.7 Emphasis on Key Strategic Brain Regions in SPM Output

SPM provides whole brain analysis of GM and the main advantage of this aspect of the program is that it avoids the bias of region-of-interest studies. Because of this, for every analysis done I provide a table that documents the stereotactic coordinates of the strongest statistical results in a cluster volume, the actually size in cubic mm of the cluster volume, the t-score from the multiple regression and it's more parametric counterpart, the z-score, the correlation effects size and the voxel level p-value. This table is very important in any analysis because it quantitatively compliments the visual information provided in the volume and section renderings. As such, it is presented in an unabridged form but there are certain markers that will aide the reader in its interpretation. First, all regions reported in an SPM output table are rank ordered from the most negative correlation effect size (largest absolute value of the partial correlation coefficient) to the smallest. This provides the reader with an understanding of which of a potentially large number of brain regions most strongly show the statistical relationship being tested.

In addition to rank ordering the regions, the reader will find that several regions are in bold. These are 10 key strategic brain regions, a subset of the key strategic brain areas highlighted in black in Figure 1. To reiterate, the key strategic brain regions that will be in bold in all SPM output tables are orbital frontal cortex, the anterior cingulate gyrus, the posterior

cingulate gyrus, the precuneus, hippocampal formation (hippocampus and parahippocampal gyrus), thalamus, caudate, putamen, globus pallidus, and basal forebrain. However, they will be highlighted in the context of a rank order of statistical main effects so that the reader understands how strongly these areas are affected in the context of other brain regions.

3.0 WHITE MATTER HYPERINTENSE LESIONS ARE PREDICTED BY AGE AND BLOOD PRESSURE IN THE CARDIOVASCULAR HEALTH STUDY COGNITION STUDY

3.1 INTRODUCTION

Having established the context and methods for the work in this dissertation, I now begin with presenting data pertinent to the model in Figure 1. To reiterate: I will first show in this chapter that WMHL are vascular in nature and are also associated with aging. In the next chapter I will provide results to support a main hypothesis: that the Main Effects of age on GM vary as a function of WMHL and that this moderation takes place in brain areas relevant to cognitive function such as the hippocampus and cingulate gyrus. In Chapter 5, I will show a conjunction between WMHL and cognitive function as assessed with domain specific CHS-CS neuropsychological tests in key strategic brain regions. In Chapters 6 and 7, I will examine conjunctions and interactions of WMHL with MCI and dementia respectively. In Chapter 8, I will present results regarding the relationship between hypertension, a key predictor of WMHL, and rCBF abnormalities key strategic brain areas. Finally, I will conclude in Chapter 9 with an overall discussion of the results of this dissertation and avenues for future investigation. This chapter, however, will seek to relate the main predictors of WMHL in the CHS-CS cohort. My specific hypothesis is that age and blood pressure, a quantitative measure used for HTN

diagnosis, are the main predictors of these lesions. Chapter 1 established that age and HTN are key predictors of WMHL using studies reviewed from the literature. The purpose of this chapter is to therefore establish that this is also the case in those CHS-CS subjects whom were scanned with structural MRI. This is important because if WMHL are to be used as a proxy measure for long term HTN damage to the brain, it is imperative that HTN is actually identified in this sample as a main predictor of WMHL.

3.2 MATERIALS AND METHODS

The subjects used for this study are drawn from the CHS-CS as described in Chapter 2. In all, 456 subjects were scanned with 3-D volumetric SPGR MRI from 1997-1999. From this group, relevant demographic variables, WMG, and blood pressure values were available for 410 participants. For the purposes of establishing the predictive value of age and HTN on WMHL, only controls were examined (n = 302). Including dementia classification as a predictor variable of WMHL would not be logical as WMHL often precede the onset of dementia. Thus, dementia and MCI subjects were not included in the analysis. From the group of 302 control subjects, clinical data on all of them, including blood pressures in the year of structure MRI were available for 284 subjects. The demographics of the subjects analyzed are provided in Table 2. The average systolic and diastolic blood pressures were below hypertensive range and majority of the subjects studied were female, educated, and Caucasian.

Table 2: Demographic Variables of the 284 Control Subjects Analyzed

Variable	Mean, Standard Deviation, Range, Percent
Age	77.92 ± 3.58 (70-89)
WMG	2.28 ± 1.39 (0-8)
Systolic Blood Pressure	132.36 ± 19.22 (87-197)
Diastolic Blood Pressure	68.05 ± 10.84 (30-104)
Gender (M/F)	40% M (112)/60% F (172)
Education (Beyond 12^{th} Grade/12^{th} Grade)	65% (184)/ 35% (100)
Race (Caucasian/African American)	82% (234)/18% (51)

Multiple regression analysis was performed using SPSS. CHS WMG values were used as the dependent variable. Independent variables were age, gender, education, race, systolic blood pressure at MRI2 (averaged from two visits over that same year), and diastolic blood pressure (also averaged).

3.3 RESULTS

The results of the multiple regression are displayed in Table 3.

Table 3: This table shows independent variable and their correlation with WMHL, the dependent variable, from a multiple regression model in SPSS. The first column lists the independent variables in the model. The next three columns provide information t, p, and partial correlation coefficient values.

Independent Variable	t-value	p-value	Partial Correlation Value (r^p)
Age	3.63	< **.001**	.21
Diastolic_Blood_Pressure	4.28	< **.001**	.25
Systolic_Blood_Pressure	-.95	.34	-.06
Gender	1.19	.24	.07
Race	-1.08	.28	-.07
Education	.41	.69	.02

As is evident in Table 3, variables that were positively correlated with WMHL as defined by CHS WMG are age ($t(277) = 3.63$, $r^p = .21$, $p < .001$) and diastolic blood pressure ($t(277) = 4.28$, $r^p = .25$, $p < .001$). Age accounts for over 4% of the variance in WMG (Figure 13) and DBP accounts for over 6% of the variance in WMG ($p < .001$) as shown in Figure 14. DBP is therefore the most strongly correlated with of WMHL in the CHS-CS cohort scanned in 1997-1999.

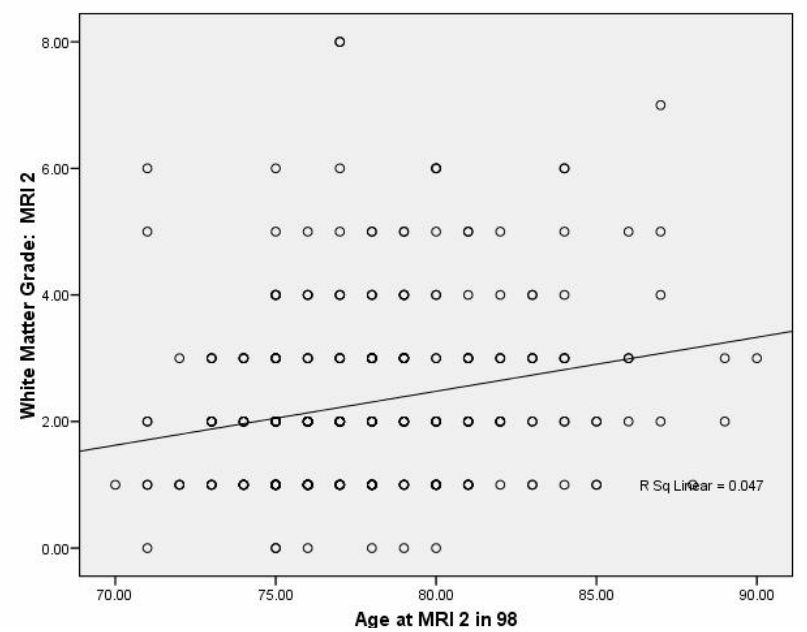

Figure 13: Scatter plot of age at MRI 2 and its correlation with WMG. Age accounts for 4.4% of the variance in WMG.

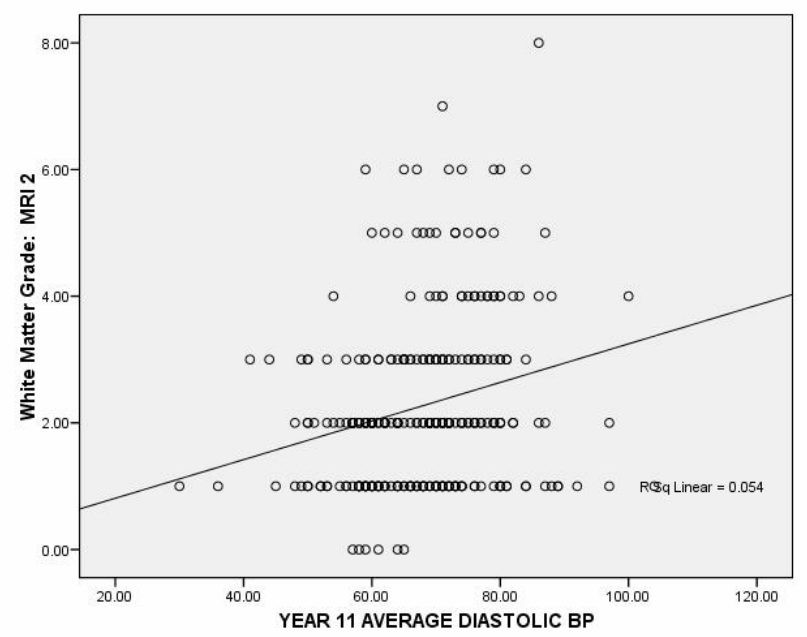

Figure 14: Predictive power of diastolic blood pressure on CHS WMG. DBP accounts for 6.3% of the variance in WMG.

The main outcome of these results is to establish that in the CHS-CS cohort that was scanned in 1997-1999, older age and higher blood pressure are positively correlated with WMHL. No other variable entered, including presence of MCI or dementia, served as statistically significant predictors of WMHL. Thus, in constructing a model on the complex relationships between hypertensive vascular disease, brain aging, neurodegeneration, and cognition, the data presented in this chapter establishes the following paths in Figure 15:

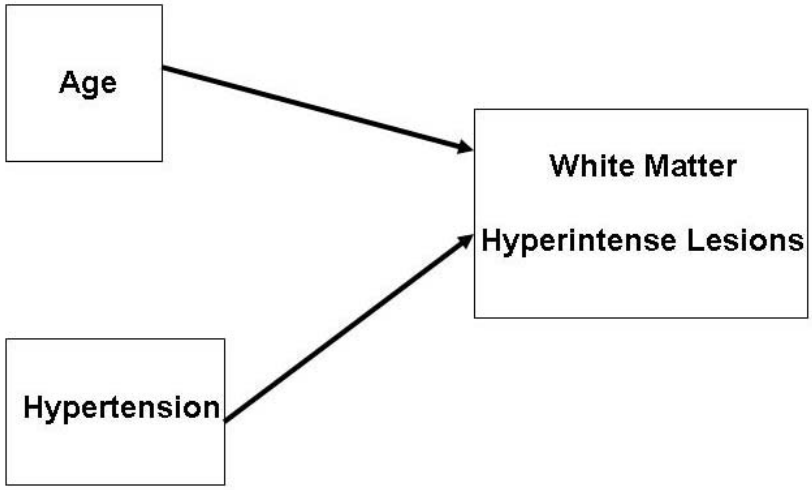

Figure 15: This figure summarizes the main findings of this chapter in terms of building a model towards understanding how hypertensive vascular disease related to aging and neurodegeneration in the brain. This figure in particular shows that age and hypertension are positively correlated with a greater magnitude of white matter hyperintense lesions in the brain.

Having established that age and hypertension are correlated with WMHL, I will next describe both the conjunction and the interaction between age and WMHL in gray matter in the next chapter.

4.0 CONJUNCTION AND INTERACTION BETWEEN WMHL AND AGE IN GRAY MATTER OF COGNITIVELY NORMAL ELDERLY PERSONS

4.1 INTRODUCTION

The main hypothesis that will be tested in this chapter is that the Main Effect of age on GM overlaps with WMHL and varies as a function of such lesions. This question is important to examine because of the risk for dementia that older age confers. It is not well understood, though, how this risk is applied but it is my assertion that it is not only the passage of chronological time itself that reduces GM volume in the brain; rather the presence of age-correlated vascular disease, expressed as WMHL, that induces atrophy. This chapter will present evidence to support this hypothesis.

4.2 MATERIALS AND METHODS

This analysis was done in all 302 cognitively normal subjects scanned with structural SPGR MRI. I included all controls, including those who progressed to MCI or dementia. My main reason for doing so was to maximize the sample size, and thus statistical power since this optimizes detection of interactions (206). To confirm that conversion would not confound my analyses, I investigated for any statistically significant Main Effects of either MCI or dementia

conversion on GM in three steps. The first was to perform a partial correlation of MCI conversion status to GM in 235 CHS-CS subjects (169 controls who stayed cognitively normal 5 years after MRI2 and 66 controls who converted to MCI) controlling for the metric of head size, TIV. The relationship between MCI conversion and GM was again test in a multiple regression model in SPSS that had total GM volume as the dependent variable and TIV, MCI conversion, age, gender, race, MRI infarcts and education as independent variables. Finally, the Main Effect of MCI conversion was assessed at the voxel level in SPM2 using TIV as the sole covariate with a standard FDR threshold. This process was repeated for controls whom remained normal and dementia converters (n = 56). Table 4 shows the demographic and vascular variables of controls subjects whom remained normal 5 years after their MRI scans in 1997-1999 versus those control who progressed to MCI. No statistically significant differences are noted ($p < .05$).

Table 4: Demographic and vascular characteristics of controls that remained normal versus MCI converters.

Variable	**Controls who Remained Controls (n = 169)**	**MCI Converters (n = 66)**	**χ^2 or t-value/ p-value***
Age	77.57 ± 3.62	78.06 ± 3.44	-.95, .34
Gender	73/96	23/43	1.37, .31
Race	139/30	54/12	.01, .54
Education (Beyond Grade 12/Grade 12)	108/61	43/23	.03, .49
MRI Infarcts (N/Y)	129/40	48/17	.16, .41
WMG	2.18 ± 1.32	2.46 ± 1.63	-1.38, .69

* df = 234

The demographic and vascular variables of persons who progressed to dementia versus controls who did not convert are shown in Table 5. Persons who converted to dementia were more likely to be older and female ($p < .05$) than stable controls.

Table 5: Demographic and vascular characteristics of controls that remained normal versus dementia converters.

Variable	**Controls who Remained Controls**	**Dementia Converters**	**χ^2 or t-value/ p-value***
Age	77.57 ± 3.62	79.0 ± 3.78	-2.54, **.01**
Gender (M/F)	73/96	14/50	5.13, **.03**
Race	139/30	45/9	.03, .86
Education (Beyond 12th Grade/12th Grade)	108/61	31/23	.74, .39
MRI Infarcts (N/Y)	129/40	35/19	2.79, .07
WMG	2.18 ± 1.32	2.43 ± 1.39	-1.38, .69

*df = 223

Having established that conversion to MCI and dementia did not affect my outcome measures, I assessed the Main Effects of age and WMHL on GM volume. Covariates in the model were gender, race, education, and MRI identified infarcts. Masked Main Effects were produced for age by visualizing only those voxels in which there was an age Main Effect and not a WMHL Main Effect using a mask threshold of $p < .05$. The same procedure was done to show only those voxels that has a WMHL Main Effect and not an age Main Effect. Figure 16 shows the SPM design matrix used for the evaluation of the independent Main Effects of age and

WMHL (labeled as wmg2 in the design matrix) on GM volume. This design matrix is also the same used for assessing the conjunction of age and WMHL Main Effects.

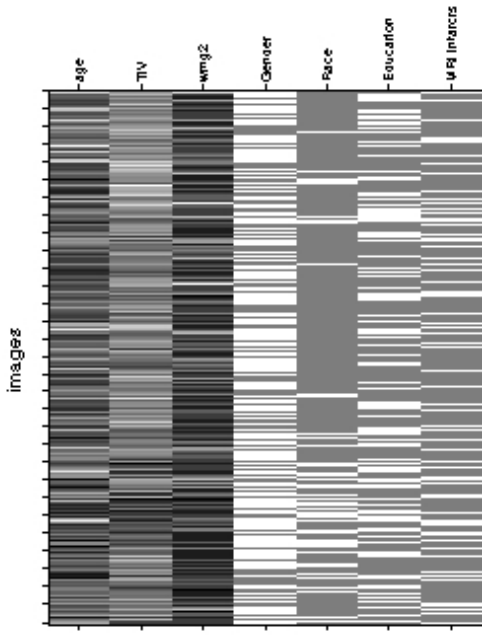

Figure 16: SPM Design Matrix for Age-WMHL conjunction analysis.

To determine whether or not age Main Effects on GMVL are moderated by WMHL, an interaction between age and WMG was coded in SPM by multiplying the centered (variable – overall mean) variables. This interaction is depicted in the SPM design matrix in Figure 17.

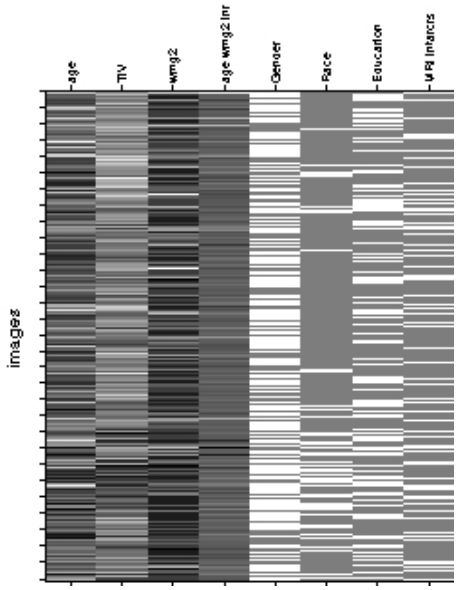

Figure 17: SPM design matrix showing the interaction between age and WMHL in the 4th column from the right. The interaction column is produced by centering age and wmg2 values around their overall means and then multiplying the two centered variables by each other.

To summarize the methods applied in this chapter, a combination of SPSS and SPM multiple regression models were applied to verify that conversion to MCI and dementia exert no Main Effects on GM at MRI2. Table 6 shows the demographic characteristics for the 302 controls in which the conjunction and interaction between age and WMG were assessed.

Table 6: Demographics of CHS-CS Controls from MRI2 (n = 302).

Variable	**Mean, Standard Deviation, Range, Percent**
Age	77.96 ± 3.63 (70-90)
WMG	2.30 ± 1.43 (0-8)
MRI Infarcts (N/Y)	74% (223)/26% (79)
Gender (M/F)	40% (120 M)/60% (182 F)
Education (Beyond 12^{th} Grade/12^{th} Grade)	63% (191)/37% (111)
Race (Caucasian/African American)	83% (250)/17% (52)

4.3 RESULTS

4.3.1 MCI and Dementia Conversion Main Effects on Gray Matter

The was no correlation between MCI conversion and total GM volume, controlling for TIV $r(232) = -.04$, $p = .57$. The multiple regression model with additional covariates also failed to reveal any relationship between MCI conversion and total GM volume ($t(227) = -.14$, $r^p = -.01$, $p = .89$), though age and TIV were statistically significant predictors as shown in Table 7.

Table 7: This table shows the SPSS output of a multiple regression model, with total GM volume in mL as the dependent variable, showing no statistically significant relationship between MCI conversion after 5 years and total GM volume.

Independent Variable	t-value	p-value	Partial Correlation Value (r^p)*
Age	-4.15	< **.001**	-.27
MCI Conversion	-.14	.89	-.01
Gender	-.36	.72	-.02
Education	-1.88	.06	-.12
Race	-1.58	.16	-.11
MRI Infarcts	-1.07	.29	-.07
TIV	19.53	< **.001**	.79

* df = 227

Additionally, there was no correlation between MCI and GM at the voxel level in SPM, controlling for TIV. Thus, there were no focal effects of MCI conversion on GM that could be detected.

In examining conversion to dementia, there was no correlation between dementia conversion and total GM volume, controlling for TIV $r(222) = -.06$, $p = .35$. This was confirmed in a multiple regression model with additional covariates ($t(215) = -.10$, $r^p = -.01$, $p = .92$).

Table 8: This table shows the SPSS output of a multiple regression model showing no statistically significant relationship between dementia conversion after 5 years and total GM volume.

Independent Variable	t-value	p-value	Partial Correlation Value (r^p)*
Age	-4.75	< **.001**	-.31
Dementia Conversion	-.11	.92	-.01
Gender	-.36	.71	-.03
Education	-2.12	**.04**	-.14
Race	-1.08	.28	-.07
MRI Infarcts	-.97	.34	-.07
TIV	19.75	< **.001**	.81

* df = 215

As was seen with MCI conversion, there was no Main Effect of dementia conversion on GM volume in SPM. Having established that MCI/dementia conversion do not influence gray matter either on a whole volume or voxel level, I will now present the results showing the separate Main Effects of age and WMG before presenting results pertaining to their conjunction and interaction.

4.3.2 Main Effect of Age on GM

The Main Effects of age on GM are shown on Figure 18, projected onto a volume rendered Standard Single Subjects MNI template (P_{FDR} = .05, k = 100). This figure conveys how substantially widespread age-related gray matter volume loss (GMVL), or atrophy, is. There is age associated reduction in GM in the frontal lobe, motor cortex, temporal lobe, medial temporal lobe, parietal cortex and cerebellum controlled for WMHL, gender, race, education, and MRI identified infarcts. Hotter colors denote a stronger Main Effect in those voxels. These can be seen in the right frontal lobe, cerebellum, and mesial temporal lobe. A positive correlation was tested to see if higher age is associated with larger GM volumes in any areas of the brain. No such regions were found even when uncorrected p-value thresholds (.0001, .01, and .1) were applied.

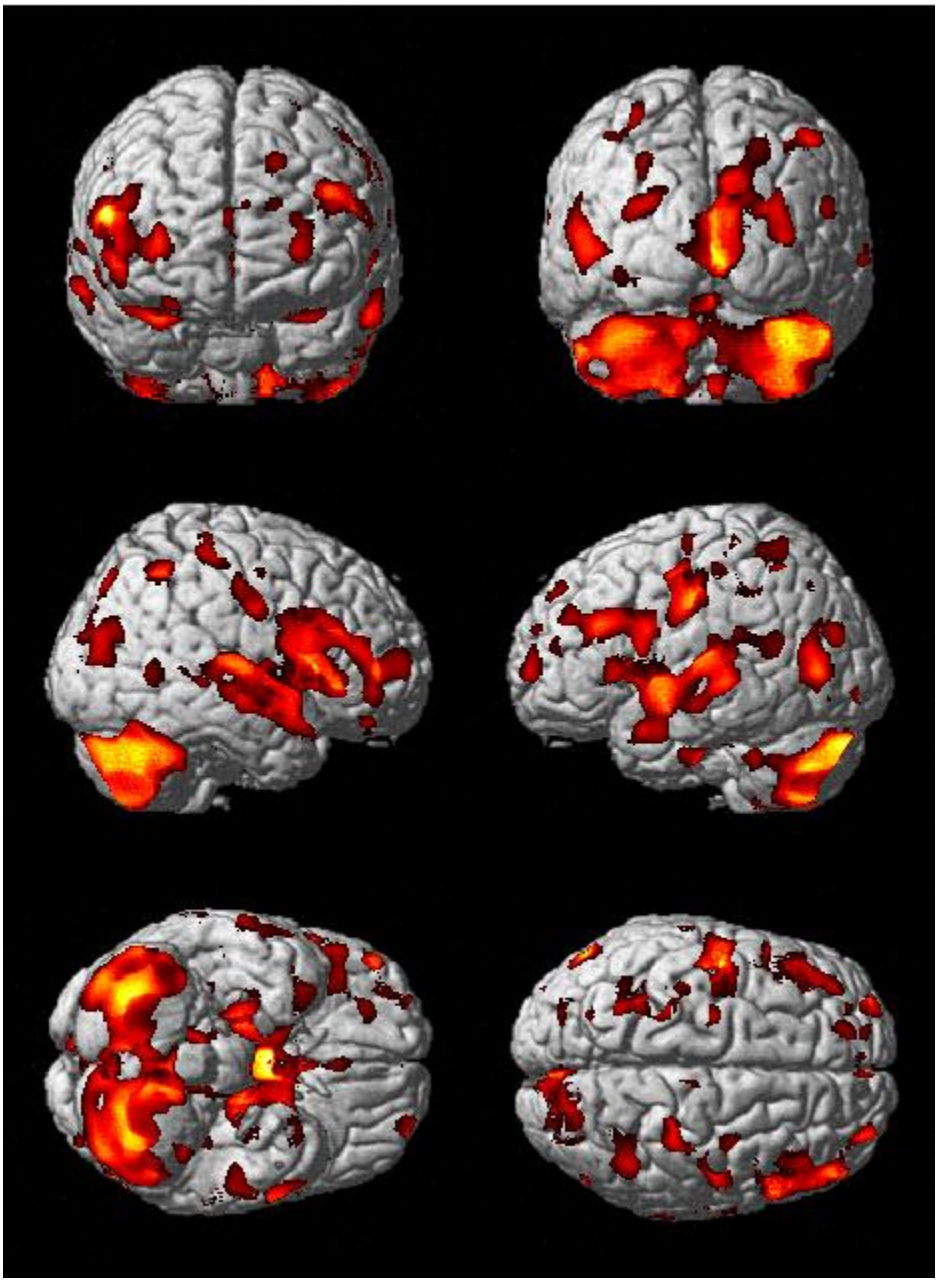

Figure 18: Volume rendered projection of age associated GM volume loss on the Standard Single Subjects MNI template. In the first column, the middle rendering portrays Main Effects in the right hemisphere and the second column these effects are shown in the left hemisphere.

Figure 19 shows these same Main Effects projected onto orthogonal sections of the Standard Single Subject MNI template. In panel 1, the Main Effect of age is clearly visible in

both hippocampi (double headed arrow). This age related hippocampal volume loss is localized to the anterior hippocampus on the left (Panel 2) and the anterior and posterior hippocampus on the right (panel 3). Panel 4 shows age related GMVL in the posterior cingulate (red arrow) and the anterior cingulate (blue arrow). The precuneus is also reduced in volume with increasing age (Panel 5, black arrow, right hemisphere). Additionally, both caudate nuclei are observed to be lower in GM volume with older age (Panel 6, red arrows). Partial correlation coefficient values on the above color scale range from 0 to .30 and were rendered on *MRIcron* using the classic overlay option with red colors corresponding to higher values. Correlation effect sizes and corresponding spatial coordinates fro the regions shown here are listed in Table 9.

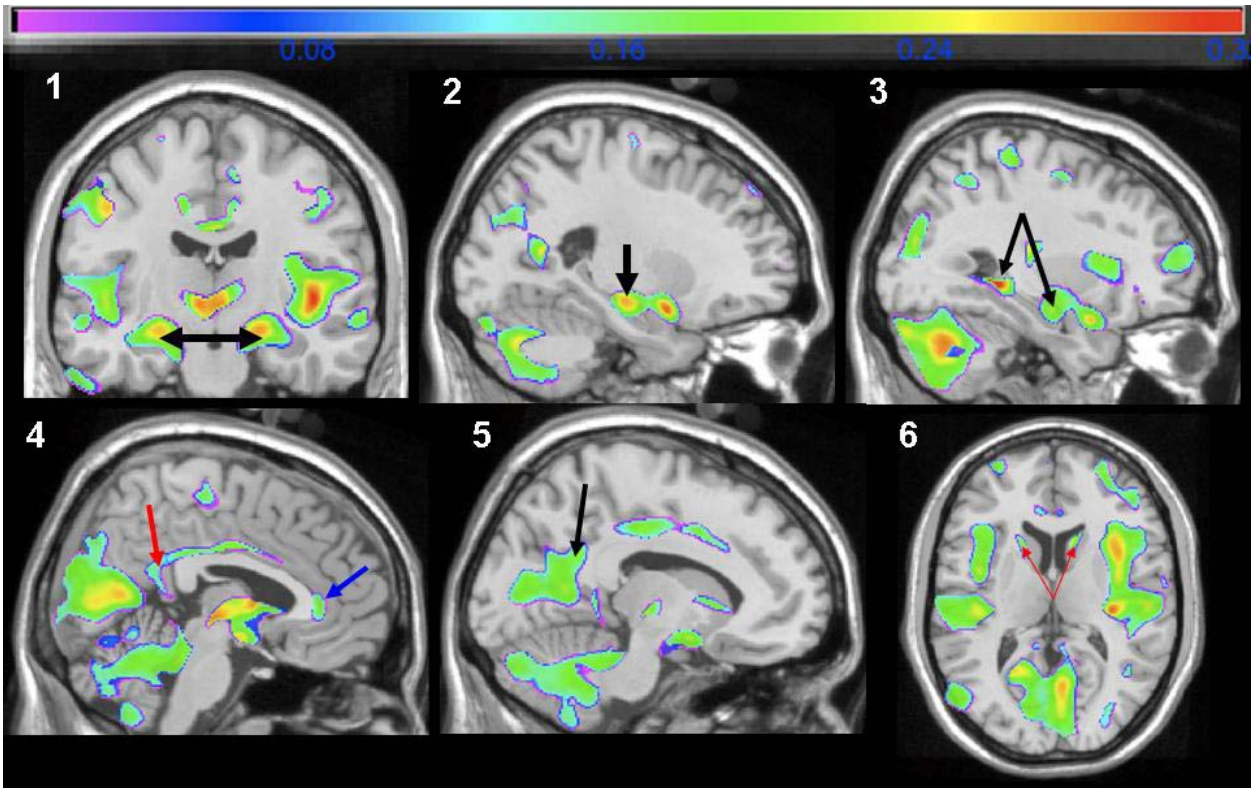

Figure 19: Age related GMVL projected onto orthogonal sections of the Standard Single Subject MNI template ($P_{FDR} = .05$, $k = 100$). Areas that show lower volume with increasing age include such key strategic brain areas as the hippocampus, parahippocampal gyrus, posterior cingulate, and caudate.

Table 9 shows the contents of an SPM statistical output table that include the anatomical location of those voxels with the largest partial correlation effect sizes (r^p values) and these are collectively referred to as peak maxima. They can be conceived as locations in which the Main Effect of age is strongest. The table is rank ordered in descending direction with the largest absolute partial correlation values on top. If multiple peak maxima were listed for a given cluster volume the value of that cluster volume is written only once, with blank boxes denoting that same volume until a new on is written. If any peak maxima was located in any one of the 10 key strategic brain areas or their subdivisions (i.e. inferior (inf), superior (sup), anterior (ant), posterior (post)), then they are highlighted in bold. To reiterate, the key strategic brain regions are: orbital frontal cortex, the anterior cingulate gyrus, the posterior cingulate gyrus, the precuneus, hippocampal formation (hippocampus and parahippocampal gyrus), thalamus, caudate, putamen, globus pallidus, and basal forebrain. Sixteen of the peak maxima were located in key strategic brain regions with the strongest age Main Effect being in one of these areas, the right posterior parahippocampal gyrus.

Table 9: This table provides the location and quantitative information on brain regions with strongest Age Main Effect. Key strategic brain regions are highlighted in black.

Structure	**Peak MNI Coordinates (x, y, z)**	**Cluster Volume (mm^3)**	**t/z scores**	**r^p value**	**P_{FDR}**
R_Post_Parahippocampal	33, -41, -4	696	6.49/6.27	-.35	< .001
R_Fusiform	33, -49, -3		3.85/3.80	-.22	.004

R_Mid_Hippocampus	19, -21, -11	188122	5.34/5.21	-.30	.001
R_Sup_Temporal	46, -13, -3		5.25/5.12	-.29	.001
R_Crus1_Cerebellum	26, -65, -35		5.11/4.99	-.29	.001
R_Insula	37, -22, 10		5.08/4.97	-.28	.001
L_Sup_Temporal_Pole	-24, 5, -19		5.05/4.94	-.28	.001
L_Caudate	-14, 21, 3		4.96/4.85	-.28	.001
R_Caudate	11, 18, 5		4.72/4.63	-.28	.001
L_Mid_Hippocampus	-18, -19, -15		4.72/4.63	-.28	.001
R_Inf_Frontal_Operculum	41, 11, 7		4.66/4.57	-.26	.001
R_Calcarine	9, -66, 7		4.61/4.53	-.26	.001
L_Sup_Temporal	-43, 0, -7		4.56/4.48	-.26	.001
R_Sup_Temporal_Pole	31, 10, -24		4.52/4.44	-.25	.001
L_Ant_Hippocampus	-21, -15, -17		4.52/4.44	-.25	.001
L_Calcarine	-19, -56, 7		4.42/4.34	-.25	.001
R_Inferior_Frontal_Operculum	57, 18, 20		4.34/4.26	-.25	.001
L_Thalamus	-7, -12, 0		3.48/3.46	-.20	.005
R_Thalamus	8, -12, 0		3.82/3.80	-.22	.007
L_Amygdala	-23, -2, -14		2.96/2.94	-.17	.02
R_Amygdala	20, 1, 14		2.65/2.63	-.15	.03
L_Mid_Cingulate	-12, -27, 37	1827	4.72/4.63	-.27	.001
L_Post_Hippocampus	-35, -35, -6	216	4.07/4.01	-.23	.001
L_Inf_Frontal_Trigone	-44, 26, 26	5900	3.83/3.78	-.22	.004
R_Postcentral	47, -8, 33	1346	4.02/3.96	-.23	.003

R_Precentral	41, -16, 42		3.28/3.25	-.19	.01
L_Mid_Temporal	-60, 6, -23	1111	3.67/3.63	-.21	.005
L_Postcentral	-27, -36, 60	1892	3.65/3.60	-.21	.006
L_Inf_Parietal	-37, -43, 40		3.54/3.50	-.20	.007
L_Sup_Parietal	-29, -45, 59		3.14/3.11	-.18	.01
R_Inf_Parietal	46, -53, 53	1445	3.64/3.60	-.21	.006
R_Angular	27, -58, 46		2.46/2.45	-.14	.04
L_Mid_Occipital	-50, -72, 6	3099	3.62/3.58	-.21	.006
L_Post_Cingulate	-10, -58, 28		2.81/2.79	-.16	.02
R_Post_Cingulate	5, -42, 24		2.82/2.80	-.16	.02
L_Precuneus	-9, -53, 19		2.67/2.65	-.15	.03
R_Precuneus	5, -45, 22		2.69/2.64	-.15	.03
L_Mid_Frontal	-30, 63, 6	831	3.47/3.43	-.20	.008
L_Sup_Frontal	-19, 41, 43	339	3.45/3.41	-.20	.008
R_Mid_Cingulate	13, 6, 41	415	3.42/3.38	-.20	.009
R_Mid_Temporal	46, -55, 5	372	3.23/3.20	-.19	.01
R_Ant_Cingulate	6, 35, 1	1186	3.10/3.07	-.18	.02
L_Ant_Cingulate	-4, 34, 6		2.82/2.80	-.16	.02
L_Precentral	-25, -14, 63	257	2.94/2.91	-.17	.02
R_Sup_Temporal	67, -5, 5	119	2.87/2.85	-.17	.02
R_Mid_Orbital_Frontal	27, 43, -20	281	2.85/2.83	-.16	.02
L_Sup_Parietal	-24, -68, 41	466	2.80/2.78	-.16	.03
R_Medial_Sup_Frontal	3, 60, 15	266	2.68/2.66	-.15	.03

L_Medial_Sup_Frontal	-6, 56, 24		2.49/2.47	-.14	.04
L_Inf_Occipital	-29, -78, -8	259	2.67/2.65	-.15	.03
L_Lingual	-25, -66, -8		2.51/2.50	-.14	.04

4.3.3 Main Effect of WMHL on GM

WMHL lesions had more extensive Main Effects on GM than age, affecting larger portions of the frontal, temporal and parietal lobes. Figure 20 shows the projection of the Main Effect of WMHL, as quantified by CHS WMG, on GM. These results are adjusted for age, gender, race, education, head size, and the presence of MRI identified infarcts. With higher WMG, there is lower GM volume in the areas highlighted with the hot colors. Hotter colors correspond to higher t-values obtain from the multiple regression and thus are brain areas with a stronger association between WMHL and brain atrophy. These associations are seen most impressively in the frontal lobes, particularly the orbital frontal cortex. The temporal lobes and are also exhibited lower GM volumes in relation to a higher grade of WMHL. The medial parietal and superior occipital lobes are largely spared from the Main Effects of WMHL. There were no positive correlations between WMHL and GM volume even using uncorrected p-value thresholds (.0001, .01, and .1).

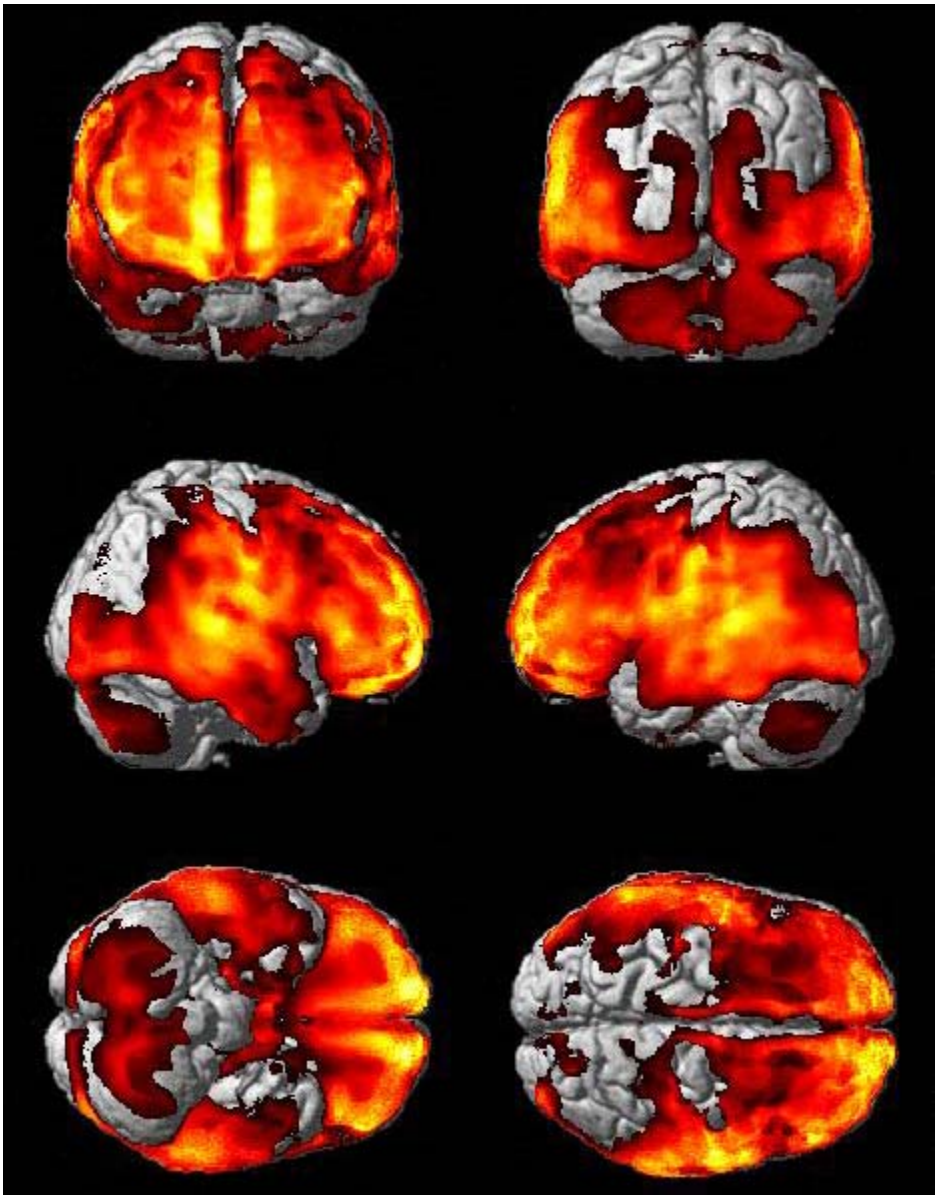

Figure 20: Main Effect of WMHL, as quantified by CHS WMG, on GM. This is a volume rendered figure with the t-values from the multiple regression model evaluating the association between WMHL and GM volume projected onto the Standard Single Subject MNI template. Hotter colors represent larger t-values and are seen in areas such as the orbital frontal cortex which show a particularly strong relationship between WMHL and GM atrophy.

Figure 21 shows the Main Effect of WMHL projected onto the Standard Single Subject MNI template, with an emphasis visually displaying key strategic brain areas that are lower in

GM volume in relation to a higher magnitude of WMHL. Panel 1 shows WMHL related gray matter volume loss in the right anterior hippocampus (arrow at r^P = -.19 at x= -21, y= 0, z = -32). Panel 2 shows that this GMVL is also seen in the middle and posterior right hippocampus (arrow point to r^p = -.21 at x = 29, y = -27, z = -9 and r^p = -.19 at x = 29, y = -33, z = -4). Panel 3 shows a similar Main Effect in the left anterior hippocampus (arrow point to r^p = -.15 at x = -21, y = -18, z = -14). Panel 4 shows that GM volume in the left precuneus is reduced with increasing WMHL burden (r^p = -.29 at x = -10, y = -31, z = 3). This same panel also shows GM atrophy in the left orbital frontal cortex (asterisk at r^p = - .31 at x = -10, y = 56, z = -40). Panel 5 shows that the GM atrophy associated with WMHL is also visible in the right precuneus (r^p = -.34 at x = 9, y = -33, z = 3). Finally, as WMHL increased in magnitude there was decreased GM volume in the thalamus as delineated by the blue box in Panel 6 (left: r^p = -.26 at x = -9, y = 4, z = -19 and right: r^p = -.28 at x = 12, y = 1, and z = -19).

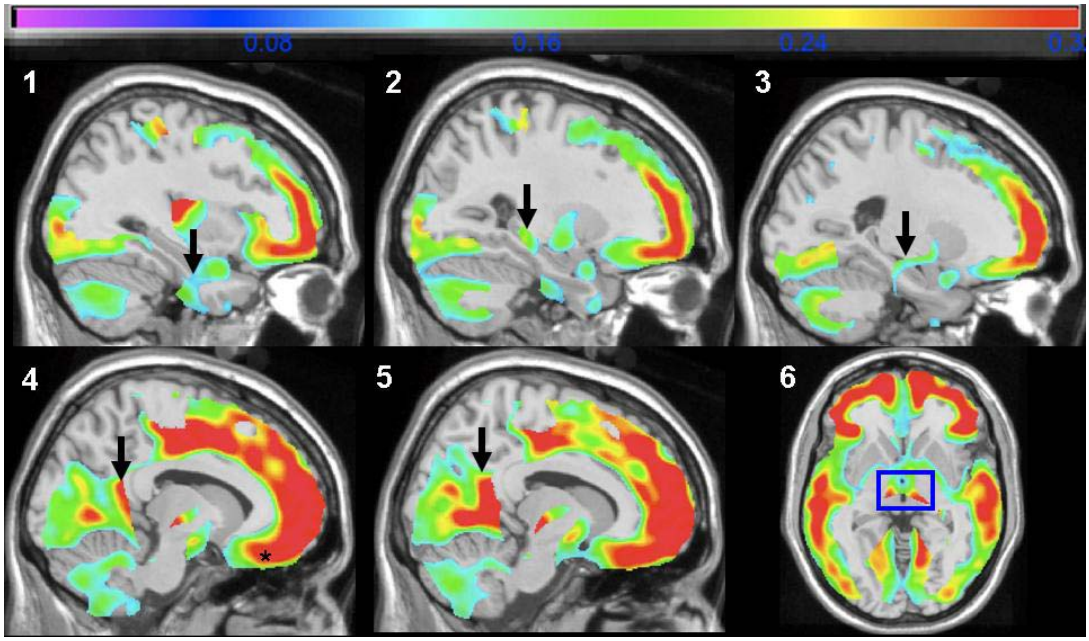

Figure 21: This figure shows the Main Effect of WMHL projected onto the Standard Single Subject MNI template, with black arrows and an asterisk identifying the key strategic brain areas. Red colors

indicate partial correlation effect sizes that are above 0.3 and the posterior cingulate, precuneus, orbital frontal cortex, and thalamus are all in that range of values.

In examining the actual effect sizes, the partial correlation coefficient values were approximately double those of the age Main Effects and were seen most impressively in the orbital frontal cortex (Table 10). Note that while key strategic brain areas were affected by WMHL as shown in Figure 21, not all of them were peak maxima of GM volume decline and are thus not included in the table. This highlights the complimentary value of both the SPM output figures and tables. All peak maxima shown in the following table were located within the same cluster volume.

Table 10: Peak GM volume declines in association with higher magnitude of WMHL.

Structure	Peak MNI Coordinates (x, y, z)	Cluster Volume (mm^3)	t/z scores	r^p value	P_{FDR}
R_Med_Orbital_Frontal	9, 66, -8	737055	8.70/8.68	-.45	< .001
L_Med_Orbital_Frontal	-12, 63, -4		8.62/8.60	-.45	< .001
L_Postcentral	-57, -13, 28		8.57/8.55	-.45	< .001
L_Mid_Temporal	-60, -37, 7		8.37/8.34	-.44	< .001
R_Supramarginal	59, -16, 23		8.36/8.33	-.44	< . 001
L_Sup_Frontal	-15, 62, 7		8.08/7.66	-.43	< .001
R_Inf_Frontal_Trigone	53, 35, 0		8.05/7.64	-.42	< .001
R_Sup_Temporal	61, -34, 8		8.03/7.63	-.42	< .001

L_Sup_Temporal	-58, -44, 13		7.96/7.57	-.42	< .001
L_Inf_Orbital_Frontal	-34, 30, -5		7.85/7.47	-.42	< .001
R_Sup_Frontal	18, 62, 11		7.66/7.31	-.41	< .001
L_Rolandic_Operculum	-56, 0 , 11		7.57/7.23	-.40	< .001
R_Medial_Sup_Frontal	15, 61, 14		7.52/7.18	-.40	< .001
L_Mid_Cingulate	-12, -12, 46		7.46/7.13	-.40	< .001
R_Rolandic_Operculum	38, -14, -19		7.32/7.01	-.39	< .001
R_Mid_Temporal	-57, -26, -11		7.31/7.00	-.39	< .001
R_Heschl	37, -24, 9		7.28/6.97	-.39	< .001
R_Supp_Motor_Area	9, -19, 56		7.24/6.93	-.39	< .001
R_Mid_Cingulate	15, -22, 46		7.23/6.93	-.39	< .001

4.3.4 Age Main Effects Masked for WMHL

To better conceptualize with areas of GM are affected only by an age main effect, a Main Effect image showing voxels that are solely associate with age and not WMHL was generated. Thus, Figure 22 shows only those voxels affected by age Main Effects and not WMHL Main Effects. In viewing this figure, one can observe that when the WMHL is masked out there are no longer any observable age Main Effects in the frontal lobes. Thus, those voxels with both an age and WMHL Main Effect were excluded from this graphic. Age Main Effects exist only in the anterior temporal lobe, parietal lobe, and cerebellum.

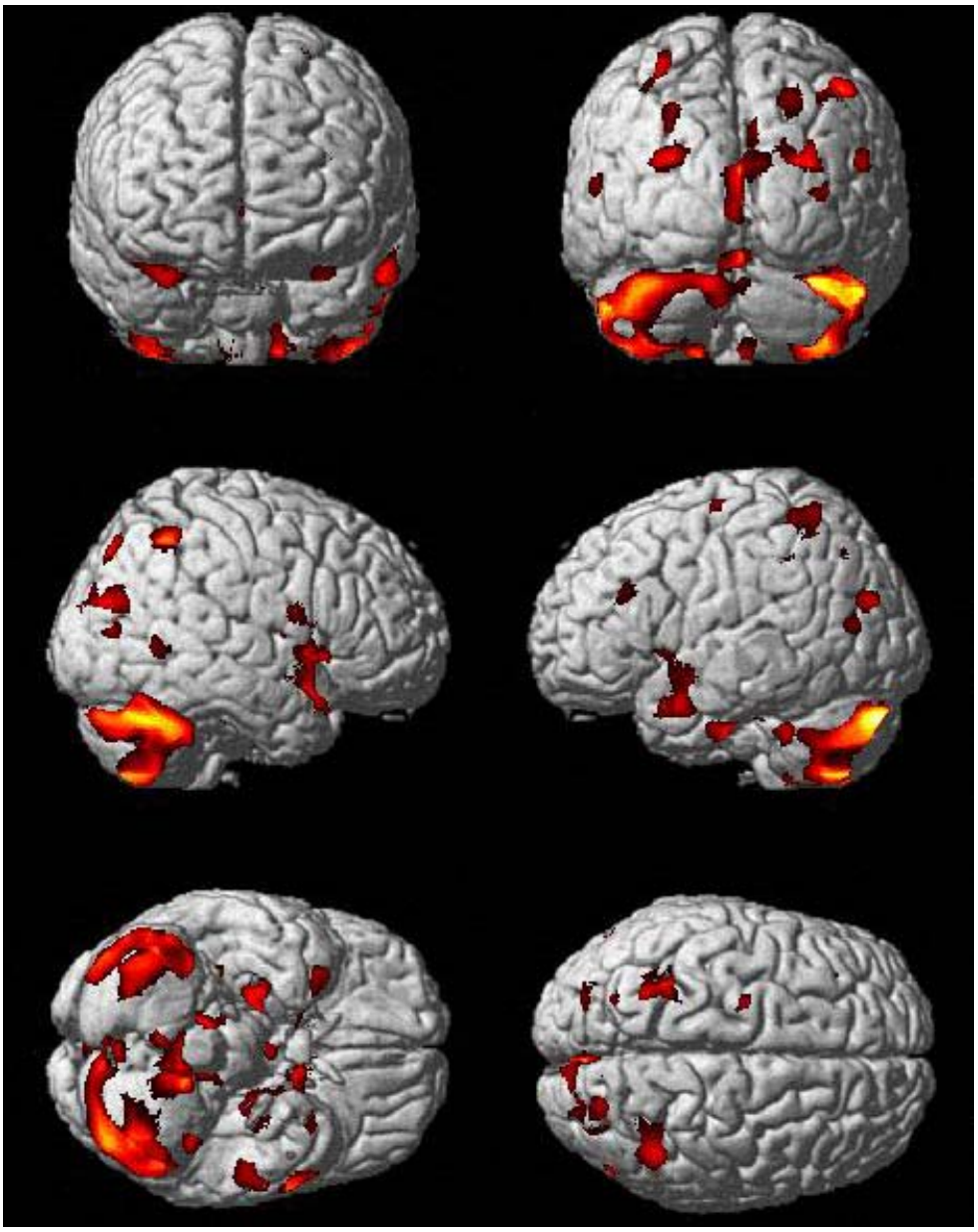

Figure 22: Age Main Effects in 302 cognitively normal CHS-CS controls projected onto the Standard Single Subject MNI template and masked for WMHL Main Effects (P_{FDR} = .05, k = 100, uncorrected p-value mask < .05).

Because masked r-images cannot be produced in SPM, I show the section rendering for the masked Main Effect of age on GM as a t-image in Figure 23. This picture shows an SPM produced t-image of age Main Effects masked for WMHL Main Effects. T-values range from 0 to 6 with hotter colors corresponding to higher values. While age Main Effects are still observed

in the caudate, anterior cingulate, and hippocampus they are absent from the posterior cingulate and precuneus because these are areas also affected by WMHL and were thus masked from the image. This image can therefore be thought of showing those voxels with "age-only" effects in the context of concurrent WMHL Main Effects.

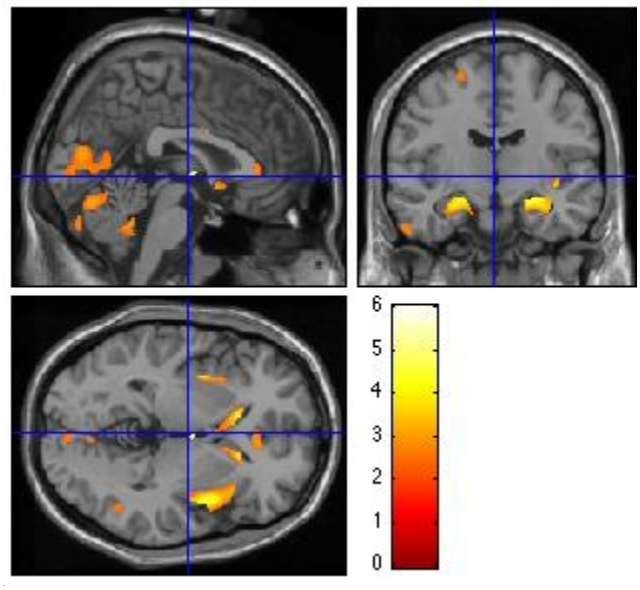

Figure 23: This figure is an SPM t-image of Age Main Effects masked for WMHL Main Effects. Even when excluding regions with GM atrophy associated with WMHL, there are this still age related atrophy in such key strategic brain regions as the anterior cingulate, caudate, and hippocampus.

Table 11 shows the peak maxima for the WMHL masked Main Effects of age on GM. The right posterior parahippocampal gyrus is still the location of the strongest age Main Effect and in all, 6 of the peak maxima are located in key strategic brain regions.

Table 11: Peak locations of age related GM volume loss masked for WMHL.

Structure	Peak MNI Coordinates (x, y, z)	Cluster Volume (mm^3)	t/z scores	r^p value	P_{FDR}
R_Post_Paraphippocampal	32, -38, -4	291	6.03/5.85	-.33	< .001
L_Caudate	-14, 21, 3	6330	4.96/4.85	-.28	.001
L_Amygdala	-23, 3, -18		4.95/4.85	-.28	.001
R_Cerebellum	37, -84, -32	17860	4.21/4.14	-.24	.002
R_Hippocampus	23, -16, -15	9889	4.81/4.71	-.27	.001
R_Inf_Frontal_Operculum	41, 11, 7		4.66/4.57	-.26	.001
R_Insula	42, 4, -3		4.48/4.41	-.25	.001
L_Crus_Cerebellum	-37, -85, -31	10664	4.73/4.64	-.27	.001
Vermis_Cerebellum	2, -72, -17		3.45/3.41	-.20	.008
R_Caudate	11, 18, 5	854	4.72/4.63	-.27	.001
L_Mid_Cingulate	-10, -29, 42	469	4.50/4.43	-.25	.001
L_Calcarine	-20, -57, 8	6386	4.39/4.31	-.25	.002
R_Lingual	6, -66, 7		4.17/4.11	-.24	.002
R_Sup_Occipital	15, -91, 20		4.17/4.10	-.24	.002
R_Mid_Occipital	31, -79, 19	913	3.79/3.74	-.22	.004
L_Mid_Temporal	-60, 6, -23	761	3.67/3.63	-.21	.005
R_Mid_Cingulate	13, -29, 41	259	3.67/3.62	-.21	.005
R_Inf_Parietal	46, -53, 53	1429	3.64/3.60	-.21	.006
R_Angular	27, -58, 46		2.46/2.45	-.14	.04

L_Inf_Parietal	-37, -43, 40	1351	3.54/3.50	-.20	.007
L_Sup_Parietal	-29, -45, 59		3.14/3.11	-.18	.007
R_Sup_Parietal	24, -78, 48	340	3.28/3.25	-.19	.01
R_Cuneus	18, -58, 22	240	3.22/3.19	-.18	.01
R_Mid_Temporal	46, -55, 4	225	3.18/3.15	-.18	.01
L_Ant_Cingulate	-10, 16, 30	254	2.87/2.85	-.17	.02
R_Ant_Cingulate	6, 35, 1	670	3.10/3.07	-.17	.02
L_Inf_Frontal_Trigone	-38, 28, 25	114	3.03/3.00	-.17	.02
L_Precentral	-24, -13, 64	155	2.39/2.91	-.17	.02

4.3.5 WMHL Main Effects Masked for Age

The Main Effect of WMHL on GM was largely unchanged even after masking out voxels that were also affected by age as shown in Figure 24. The orbital frontal cortex is still a site of strong WMHL related GM atrophy as reflected by the hotter colors but there is some lack of WMHL Main Effect in the lateral frontal lobe. Also, while WMHL associated GM volume loss is still very much observed in the temporal lobe, there is and this is some comparative absence in the lateral temporal lobe and this is attributable to concurrent age Main Effects in that area. There is also a conspicuous lack of WMHL Main Effect in the cerebellum and this is expected given the age Main Effect in that area that was masked out.

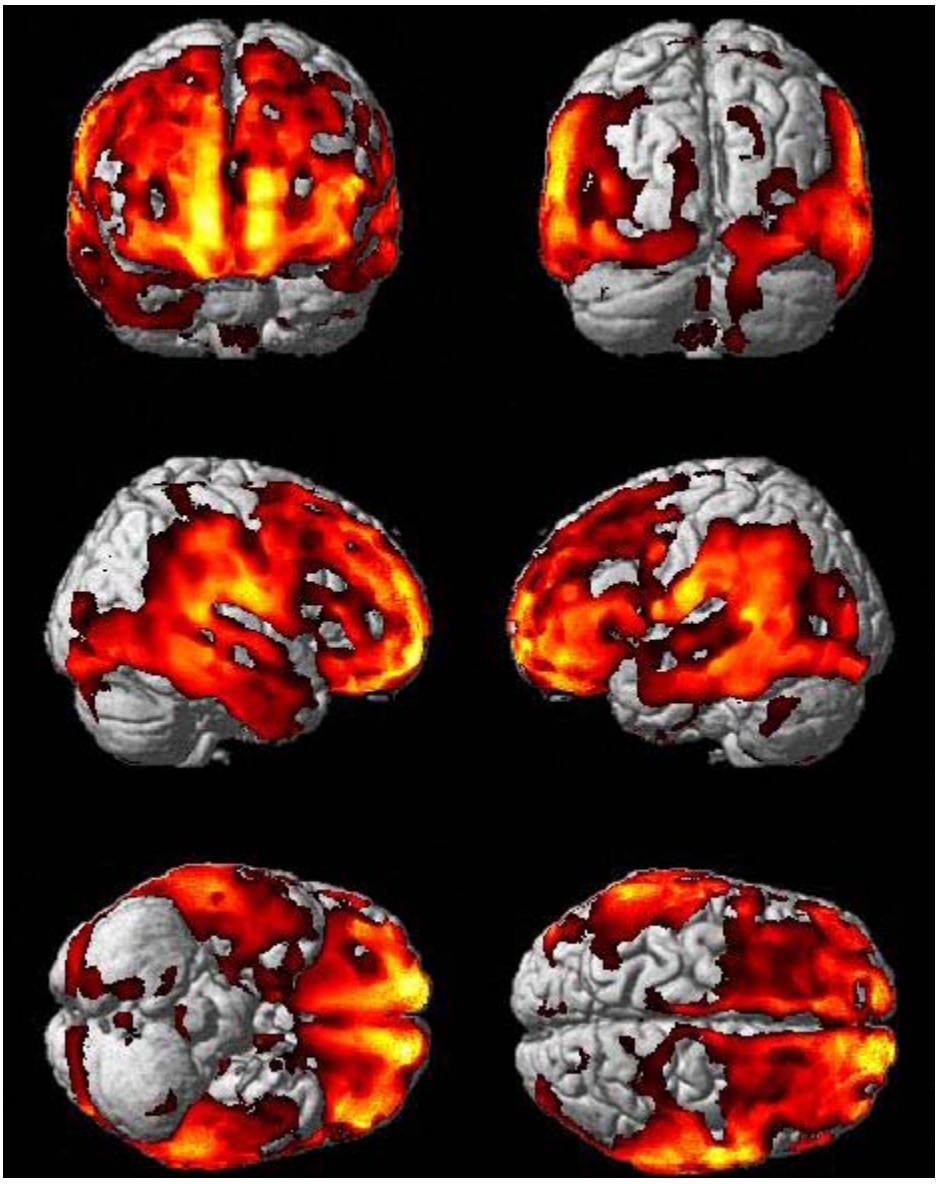

Figure 24: This figure shows the projection of WMHL effects, masked for age, onto the Standard Single Subject MNI template. Some of the frontal lobe effects of WMHL are no longer visible because of concurrent age Main Effects. This is also the case in the temporal lobes and especially evident in the cerebellum.

In examining the section rendered t-images, the age masked WMHL Main Effects still persist in key strategic brain areas such as the hippocampus, posterior cingulate, and anterior cingulate gyrus as is seen in Figure 25. Part a shows that the Main Effects of WMHL persist in

the middle portion of the right hippocampus (crosshairs) even after masking out the Main Effect of age (P_{FDR} = .05, k = 100). Part b shows that the Main Effect of WMHL also persist in the posterior cingulate (yellow arrow) and the anterior cingulate (green arrow) despite masking out the Main Effect of age.

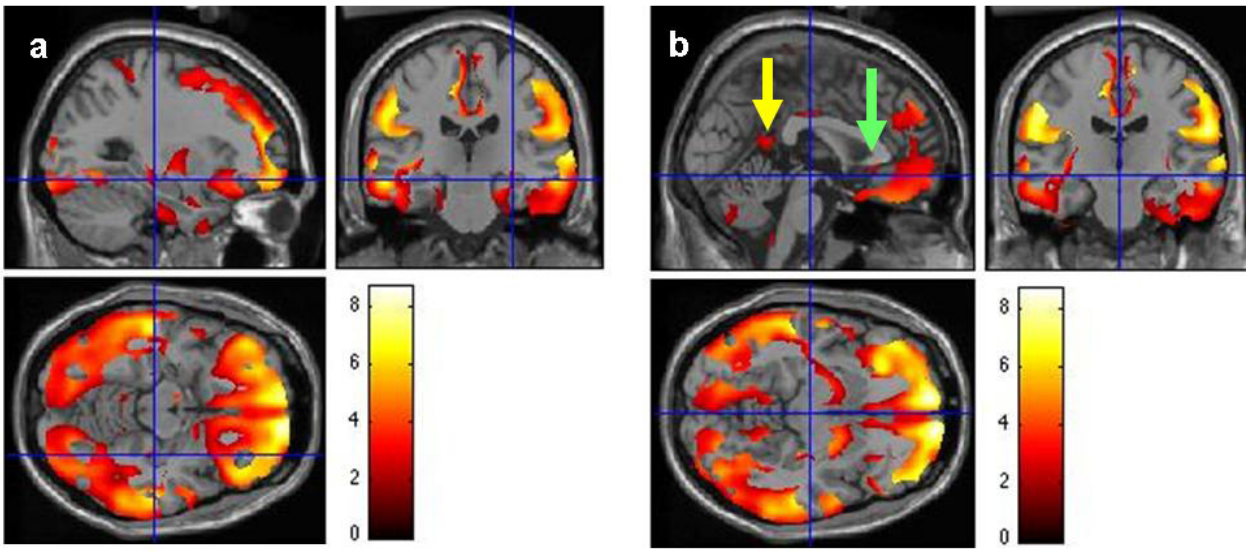

Figure 25: This figure shows the Main Effect of WMHL after masking out voxels that are also encompassed by an age Main Effect. Part a shows the presence of WMHL GM atrophy in the hippocampus and in the posterior cingulate gyrus (part b, yellow arrow) and anterior cingulate (green arrow).

In examining the peak maxima of WMHL Main Effects, it is interesting to note that the left hippocampus becomes a location of a peak maximum when the age effect is masked out (Table 12). Otherwise the majority of peak maxima of the WMHL Main Effect are unchanged, especially in the orbital frontal cortex – the left and right medial subdivision of which exhibit the strongest areas of WMHL atrophy.

Table 12: Age-masked Main Effect of WMHL presented as peak areas of statistical significance.

Structure	Peak MNI Coordinates (x, y, z)	Cluster Volume (mm^3)	t/z scores	r^p value	P_{FDR}
R_Med_Orb_Frontal	9, 66, -8	455461	8.70/8.68	-.45	< .001
L_Med_Orb_Frontal	-12, 63, -4		8.62/8.60	-.45	< .001
L_Postcentral	-57, -13, 28		8.57/8.55	-.45	< .001
L_Mid_Temporal	-60, -37, 7		8.37/8.34	-.44	< .001
R_Supramarginal	59, -16, 23		8.36/8.33	-.44	< . 001
L_Sup_Frontal	-15, 62, 7		8.08/7.66	-.43	< .001
R_Sup_Temporal	61, -34, 8		8.03/7.63	-.42	< .001
L_Sup_Temporal	-58, -44, 13		7.96/7.57	-.42	< .001
R_Inf_Frontal_Trigone	53, 38, -1		7.76/7.39	-.41	< .001
R_Sup_Frontal	18, 62, 11		7.66/7.31	-.41	< .001
L_Rolandic_Operculum	-56, 0 , 11		7.57/7.23	-.40	< .001
R_Sup_Temporal	62, -25, 5		7.55/7.21	-.40	< .001
L_Inf_Orbital_Frontal	-35, 31, -6		7.53/7.20	-.40	< .001
R_Medial_Sup_Frontal	15, 61, 14		7.52/7.18	-.40	< .001
L_Inf_Frontal_Trigone	-50, 26, 11		7.51/7.18	-.40	< .001
R_Mid_Temporal	-57, -26, -11		7.31/7.00	-.39	< .001
R_Heschl	37, -24, 9		7.28/6.97	-.39	< .001
R_Supp_Motor_Area	9, -19, 56		7.24/6.93	-.39	< .001
R_Mid_Cingulate	15, -22, 46		7.23/6.93	-.39	< .001

L_Mid_Cingulate	-12, -15, 46		7.25/6.94	-.39	< .001
L_Supramarginal	-54, -29, 34		7.18/6.88	-.39	< .001
R_Rolandic_Operculum	60, -5, 13		7.09/6.81	-.38	< .001
R_Postcentral	62, 2, 17		7.08/6.80	-.38	< .001
R_Crus_Cerebellum	13, -53, -46	308	2.13/2.13	-.12	.03
L__Crus_Cerebellum	-39, -56, -36	2404	3.02/3.00	-.17	.003
L_Parahippocampal	-21, -24, -18	229	2.86/2.84	-.16	.005
L_Hippocampus	-26, -26, -12		2.21/2.21	-.13	.02

4.3.6 Conjunction between Age and WMHL

The conjunction of age and WMHL represents voxels in the 302 brains examined that have both a Main Effect of age and of WMHL. This is represented on a volume rendered projection in Figure 26 and shows the projection of age-WMHL conjunction onto the Standard Single Subject MNI template. Age and WMHL Main Effects are jointly statistically significant in the frontal lobes, temporal lobes, mesial temporal lobe, and the inferior cerebellum.

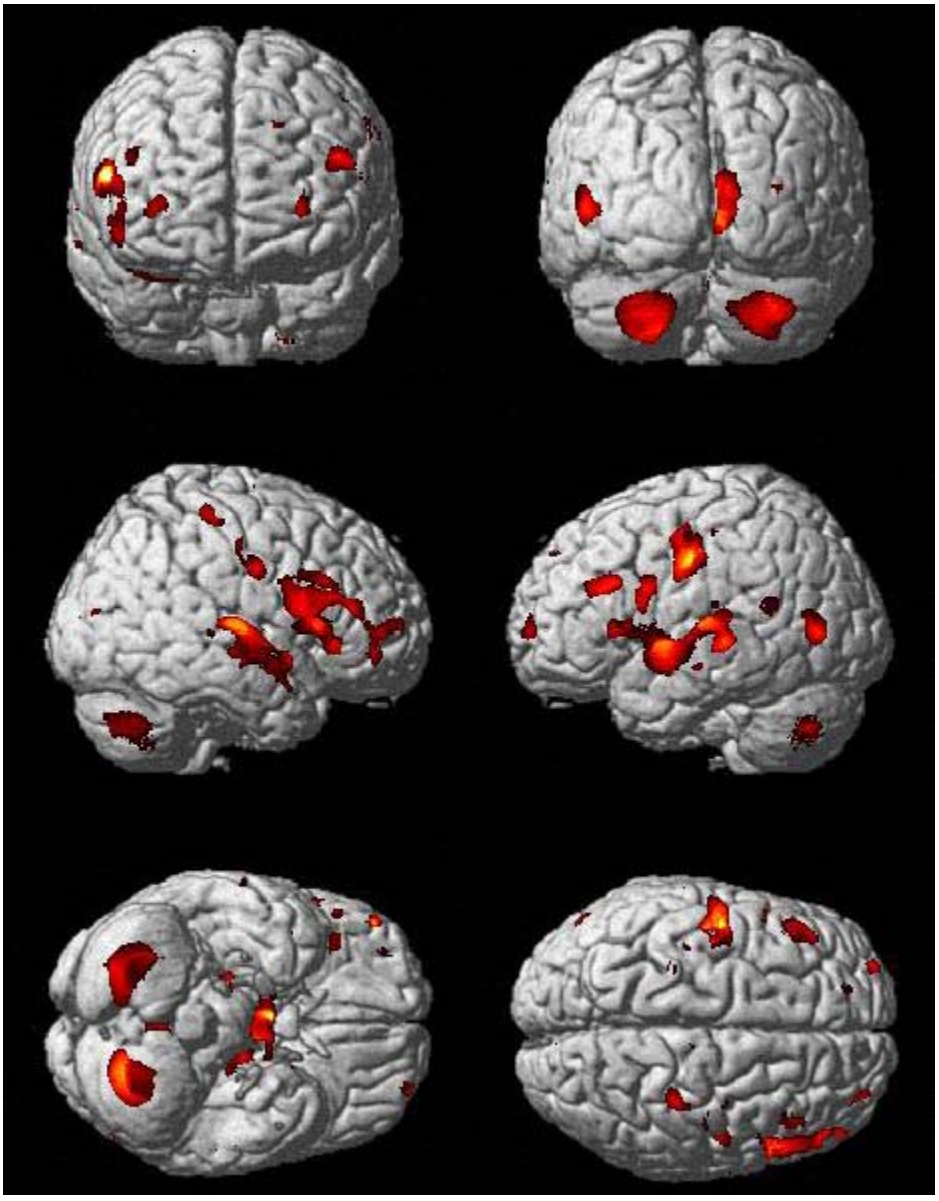

Figure 26: This displays the conjunction of age and WMHL Main Effects in all 302 control subjects.

Figure 27 shows Sectioned rendered t-images showing the conjunction between age and WMHL Main Effects key strategic brain areas. Parts a and b show that the age and WMHL Main Effects are jointly statistically significant in the left parahippocampal gyrus and right middle hippocampus respectively (crosshairs). Part c shows and age/WMHL conjunction in the right precuneus (crosshairs) and part d also shows a conjunction in the thalamus. All coordinate

locations and effect sizes for these areas can be found in table 13. T-values range from 0 to 5 with larger values corresponding to hotter colors.

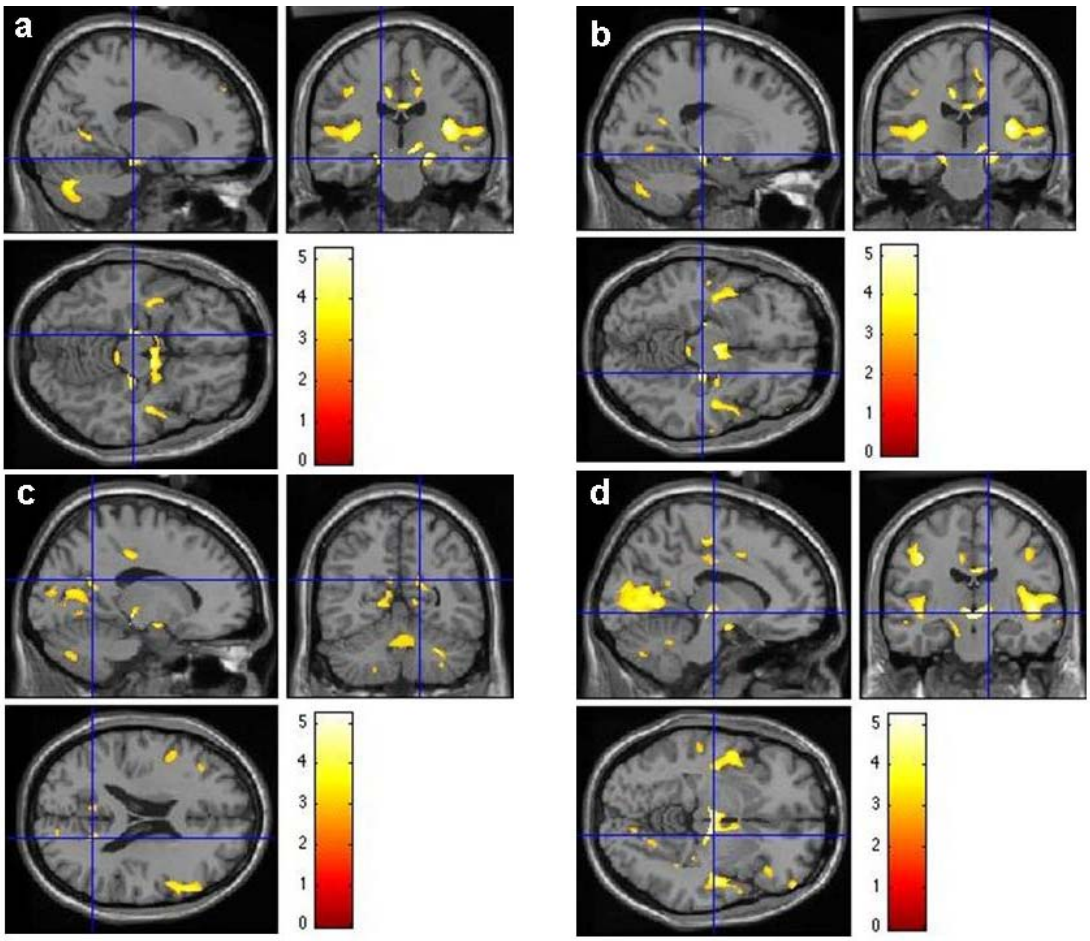

Figure 27: SPM t-images showing the conjunction between age and WMHL main effects. Key strategic brain regions affects both by age and WMHL related brain atrophy are the hippocampal formation (parts a and b; crosshairs), the precuneus (part c, crosshairs), and the thalamus (part d, crosshairs).

Table 13 shows peak local maxima that correspond to the conjunction between age and WMHL Main Effects. These areas show both a statistically significant Main Effect on GM from both age and WMHL. The top three conjunction sites with the largest effect sizes are in key strategic brain regions: the right middle hippocampus, right thalamus, and left thalamus. In all, 6 of the peak maxima were located in key strategic brain regions.

Table 13: The conjunctions between age and WMG Main Effects on GM are shown in Table 13. This table shows areas of the brain where both age and WMG are correlated with lower GM volume, controlling for head size, gender, education, race, and MRI infarcts. Key strategic brain regions are highlighted in bold.

Structure	Peak MNI Coordinates (x, y, z)	Cluster Volume (mm^3)	t/z scores	r^p value	P_{FDR}
R_Mid_Hippocampus	18, -22, -11	4120	5.25/5.13	-.29	.007
R_Thalamus	6, -17, -5	4120	4.94/4.83	-.28	.007
L_Thalamus	-3, -16, -5	4120	4.85/4.76	-.27	.007
Heschl_R	37, -22, 10	7124	5.08/4.97	-.28	.007
R_Sup_Temporal	48, -13, -2	7124	4.97/4.87	-.28	.007
R_Sup_Temporal	58, -18, 7	7124	3.92/3.87	-.22	.02
L_Postcentral	-43, -14, 40	2552	4.58/4.50	-.26	.007
L_Postcentral	-43, -10, 47	2552	3.99/3.93	-.23	.02
L_Postcentral	-60, -12, 38	2552	3.42/3.38	-.20	.03
L_Parahippocampal	-17, -21, -14	434	4.40/4.32	-.25	.009
R_Mid_Cingulate	5, -12, 29	1451	4.39/4.32	-.25	.009
L_Post_Cingulate	-4, -29, 26	1451	3.56/3.52	-.20	.03
R_Lingual	10, -64, 4	4793	4.33/4.26	-.24	.009
R_Calcarine	13, -68, 11	4793	4.20/4.14	-.24	.01
L_Crus_Cerebellum	-21, -69, -35	4277	4.16/4.10	-.24	.01
L_Heschl	-37, -28, 12	9059	4.15/4.09	-.24	.01

L_Sup_Temporal	-44, -21, 6	9059	4.08/4.02	-.23	.01
R_Inf_Frontal_Trigone	55, 20, 21	4936	4.06/4.00	-.23	.02
R_Insula	38, 24, 5	4936	3.86/3.81	-.22	.02
R_Postcentral	47, -8, 33	529	4.02/3.96	-.23	.02
R_Precentral	41, -16, 42	529	3.28/3.25	-.19	.03
L_Precentral	-44, 4, 27	915	3.91/3.85	-.22	.02
L_Inf_Frontal_Operculum	-53, 9, 19	915	3.34/3.31	-.19	.03
R_Crus_Cerebellum	31, -67, -37	3927	3.89/3.84	-.22	.02
L_Inf_Frontal_Trigone	-44, 26, 26	1069	3.83/3.78	-.22	.02
R_Precuneus	15, -55, 21	334	3.72/3.68	-.21	.02
L_Lingual	-14, -58, 3	1319	3.65/3.61	-.21	.02
L_Calcarine	-10, -76, 8	1319	3.46/3.42	-.20	.03
L_Mid_Occipital	-50, -72, 6	808	3.62/3.58	-.21	.02
L_Mid_Temporal	-51, -68, 13	808	3.15/3.12	-.18	.04
R_Supp_Motor_Area	10, -21, 54	235	3.53/3.49	-.20	.03
L_Mid_Frontal	-29, 62, 6	239	3.45/3.42	-.20	.03
R_Mid_Frontal	35, 49, 4	334	3.27/3.24	-.19	.03

4.3.7 Interaction between Age and WMHL in GM

This section will display results regarding statistical interaction, or moderation of age Main Effects on GM by WMHL. Figure 28 shows areas of the brain in which the Main Effect of age on GM varies as a function of WMHL magnitude. Specifically, this graphic shows the projection of the interaction between age and WMHL as an r^p image onto orthogonal sections of the Standard Single Subject MNI template in *MRIcron* ($P_{FDR} = .05$, k = 30). Part a shows that the Main Effect of age on GM is moderated by WMHL lesions in the right posterior hippocampus ($r^p = -.22$, x = 36, y = -28, z = -9). This interaction is also observable in part b in the mammillary bodies (red box, left: $r^p = -.21$, x = -6, y = -4, z = -15 and right: $r^p = -.22$, x = 6, y = -4, z = -15) on coronal projection. This interaction is also visible in part c which shows more impressively the moderation of age by WMHL in the anterior cingulate gyrus (left: $r^p = -.22$, x = -4, y = 27, z = 20 and right: $r^p = -.25$, x = 5, y = 25, z = 20). The interaction also extends into the middle cingulate gyrus (left: $r^p = -.25$, x = -3, y = 1, z = 33 and right: $r^p = -.26$, x = 4, y = 2, z = 33).

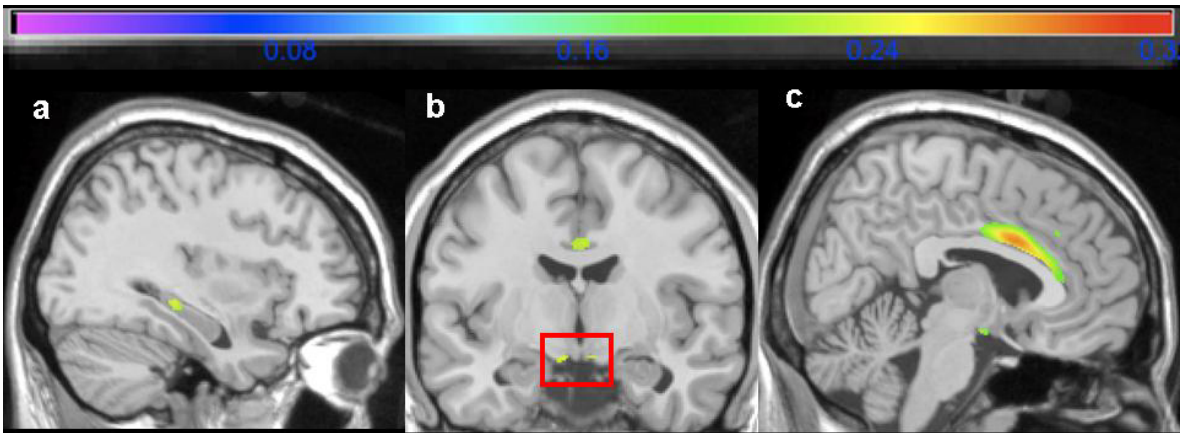

Figure 28: This figure shows areas of the brain in which the Main Effect of age on GM varies as a function of WMHL. This is seen in such key strategic brain areas as the left posterior hippocampus (part a) anterior cingulate (part c) and also in the mamillary bodies (part b, red box).

The peak local maxima of the interaction between age and WMHL are displayed in Table 14. The top three most strongly affected areas in terms of this interaction are in key strategic brain areas.

Table 14: Local Peak Maxima of the Moderation of Age Main Effects on GMVL by WMHL.

Structure	**Peak MNI Coordinates (x, y, z)**	**Cluster Volume (mm^3)**	**t/z scores**	**r^p value**	**P_{FDR}**
L_Ant_Cingulate	0, 8, 29	4242	5.24/5.12	-.29	.003
R_Ant_Cingulate	5, 26, 18	4242	4.32/4.25	-.24	.008
R_Post_Hippocampus	37, -29. -8	173	4.08/4.02	-.23	.02
L_Mid_Cingulate	-1, 30, 33	207	3.94/3.89	-.22	.02
L_Mid_Temporal	-67, -38, 4	172	3.84/3.79	-.22	.03
R_Rolandic_Operculum	41, 1, 18	33	3.79/3.75	-.22	.03
L_Inf_Temporal	-59. -36, -19	65	3.71/3.67	-.21	.03

This chapter has several main findings. First, age and WMHL both separately and jointly affect large portions of GM with particular emphases on key strategic brain regions, namely the hippocampus, precuneus, and anterior and posterior cingulate gyrus. These conclusions are based on data regarding the Main Effects of WMHL and age and their conjunction. The interaction between WMHL and age suggests that the relationship between higher age and lower GM is moderated by co-morbid WMHL which in turn reflects end organ brain damage from

hypertensive vascular disease. That that interaction took place in key strategic brain areas such as the hippocampus suggests that one mechanism by which age can confer higher risk for dementia is because vascular disease is more likely to occur in older age and thus induce brain atrophy in these areas. Thus, if vascular disease could be prevented or better controlled this may reduce risk for dementia by lower the extent of age related brain atrophy in areas relevant to cognitive function such as the hippocampus and cingulate gyrus. With respect to building the model on the relationships between vascular disease, brain aging, neurodegeneration and cognition, the contributions of this chapter to that model are shown in Figure 29.

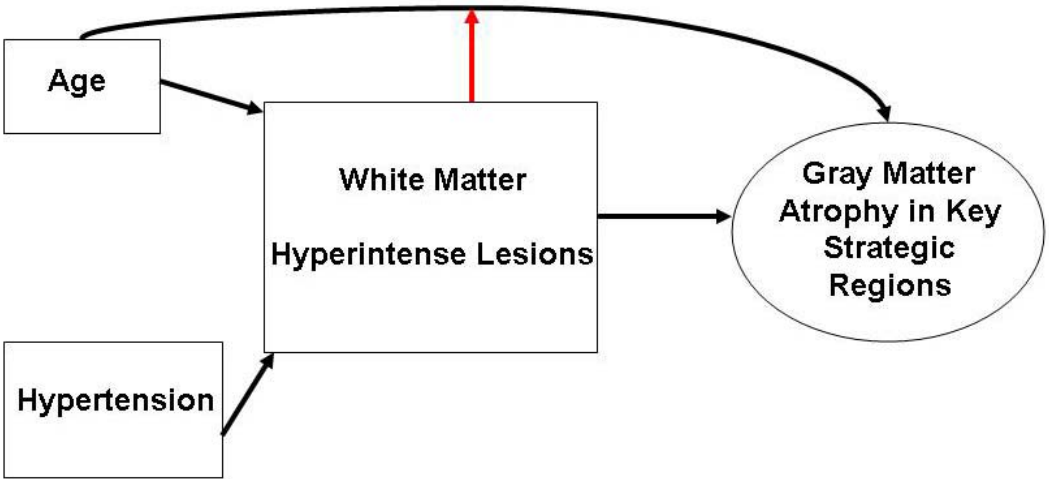

Figure 29: This figure shows the progressive construction of the overall model of this dissertation with contributions from chapter 4 added. Age and hypertension are correlated with WMHL. More WMHL are correlated with gray matter atrophy in key strategic brain regions as is older age. The conjunction between age and WMHL in terms of this atrophy is symbolized by both arrows from each of those boxes pointing to the circle that represents GM atrophy in key strategic regions. The red arrow drawn from the WMHL lesions box to the older age arrow symbolizes how these lesions moderate the relationship between age and GM volume.

This concludes the chapter detailing the Main Effects of age, WMG, their conjunction, an interaction in GM in the CHS-CS cohort of 302 controls. Having examined the Main Effect of

WMHL and it's moderation of age Main Effects on the brain, I will now present results pertaining to the relationship between WMHL and cognition.

5.0 COGNITION MAIN EFFECTS ON GRAY MATTER OVERLAP WITH THOSE FROM WHITE MATTER HYPERINTENSE LESIONS AND ARE MEDIATED BY CO-MORBID NEURODEGENERATION

5.1 INTRODUCTION

Having identified that WMHL moderate the effects of age on GM atrophy, it now becomes relevant to inquire whether or not these lesions have implications for cognitive function. The data presented in this chapter will seek to answer this question in several ways. First, I will present data showing that WMHL is a statistically significant predictor of lower scores on a composite cognitive score (CCS) of domain specific neuropsychological tests and that this is mediated by GM volume. Next, I will show SPM data pertaining to areas of the brain that are higher in volume better CCS scores and the overlap of these areas with the Main Effects of WMHL. I hypothesize that WMHL Main Effects target brain areas that are themselves correlated with improved cognitive function, such as the hippocampus. Verifying this hypothesis will provide an appropriate context for next investigating the overlap between MCI and dementia, which I use as behavioral proxies for underlying neurodegeneration, in Chapters 6-7.

5.2 MATERIALS AND METHODS

All subjects were drawn from the CHS-CS as described in Chapter 2. The metric of cognition used in these analyses was a composite cognitive score (CCS) and was derived, as described in chapter 2, from age and education adjusted t-scores from domain specific tests of executive function, motor function, language function, processing speed, and visual-spatial functions. Of the 456 subjects scanned with SPGR MRI in 1997-1999, detailed domain specific neuropsychological data and thus CCS scores were available for 350. A regression model designed to predict CCS was constructed in SPSS with WMG, gender, and race as the independent variables. This model was then re-run with GM as a proportion of total head size included as a covariate in order to determine if the Main Effect of WMHL on CCS was mediated either partially or completely by brain structure.

SPM analyses were then conducted. First, CCS correlated with GM while controlling for TIV and WMHL to yield both the unmasked and masked Main Effects of CCS to determine which areas of GM have higher volume in relation to better CCS performance and the SPM design matrix for this is seen in Figure 30. This figure shows the SPM design matrix used in examining the correlations of CCS and WMHL with GM volume. Age and education were not covariates in this model because CCS was already adjusted for them. Gender, race, and MRI infarcts were not included in the model either because neither were correlated with GM volume (gender: r^p (347) = .02, p = .73, TIV covariate); (race: r^p (347) = -.03, p = .61, TIV covariate); (MRI infarcts r^p (347) = -.09, p = .08, TIV covariate). With this model, a conjunction analysis was also performed to reveal voxels with both a CCS and WMG Main Effect. The conjunction analysis is the most important one conducted in this chapter because it shows which areas of the brain atrophy in relation to WMHL and are correlated with higher CCS. In doing this, I will

therefore show that WMHL affect brain areas that are specifically correlated with cognition in the CHS-CS. To maximize sample size and statistical power, control, MCI, and dementia subjects were included in the analysis. However, because MCI and dementia are outcomes of impaired cognition, they are highly correlated with CCS in this sample ($r(350) = -.69$, $p < .001$). To avoid multicollinearity, we therefore did not use MCI or dementia as predictor variables of CCS in this analysis.

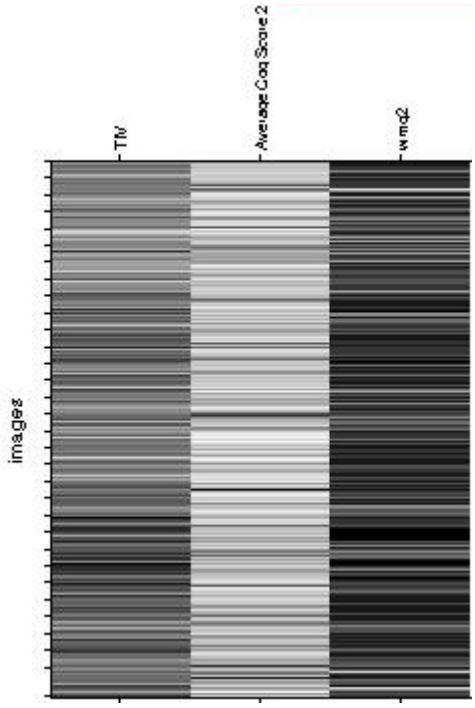

Figure 30: This figure shows the SPM design matrix used in examining the Main Effect of CCS (2nd column) and WMHL in the third column.

Table 15 shows the demographic characteristics of the subjects utilized in this analysis. There were statistically significant differences in age between normals and MCI, normals and dementia, and MCI and dementia with the demented subjects having the oldest average age. There were also demographic differences in education and race with the MCI group having the

highest percentages of African-American persons, and those with only a high school education. Demented persons had the highest burden of WMHL, statistically different from controls but not those with MCI. Finally, with respect to CCS, there was progressive worse cognitive function along the spectrum of normal, MCI, and dementia.

Table 15: Demographic characteristics of CHS-CS subjects with domain specific cognitive scores at MRI2 in 1997-1999.

Variable	Normal (n=248)	MCI (n=70)	Dementia (n=32)	T-test(t, p)/χ^2
Age	77.77 ± 3.59	79.42 ± 4.66	82.72 ± 4.85	*-2.75, **.007** ** -5.57, < **.001** *** -3.27, **.001**
Gender (F)	61% (151)	56% (39)	63% (20)	.70, .72
Education (12^{th} Grade only)	35% (86)	53% (37)	44% (14)	7.89, .**02**
Race	22% (44)	49% (23)	32% (10)	9.02, .**01**
Infarcts	27% (66)	31% (22)	41% (13)	2.99, .24
WMG	2.23 ± 1.35	2.37 ± 1.73	3.06 ± 1.79	* -.75, .46 ** -3.16, **.002** *** 1.85, .07
CCS	50.22 ± 4.98	40.71 ± 8.18	32.13 ± 9.19	* 12.04, < **.001** ** 16.75, < **.001** *** -4.28, < **.001**

- *Normal compared to MCI
- **Normal compared to dementia

- ***MCI compared to dementia

5.3 RESULTS

5.3.1 Mediation of WMHL Main Effects on CCS by Brain Structure

Table 16 shows the results of the first SPSS model in which CCS is the dependent variable and WMHL, gender, race, and MRI infarcts were the independent variables. The strongest predictors of CCS were WMHL and race.

Table 16: Predictors Composite Cognitive Score

Independent Variable	t-value	p-value	Partial Correlation Value (r^p)
WMHL	-2.62	**.009**	-.14
Gender	-.09	.93	-.01
Race	-2.68	.**008**	-.15
MRI Infarcts	-1.39	.17	-.07

To determine if the correlation between WMHL and CCS was mediated by GM volume itself, GM as a fraction of TIV was inputted into the model as an independent variable. The results of this model are shown in Table 17. When GM volume as a proportion of TIV is included in the analysis, the correlation between WMHL and CCS is no longer statistically significant. The Main Effect of WMHL on CCS is therefore partially mediated by brain

structure. This is represented by Figure 31 which shows that the manner in which WMHL affects cognition is through brain structure, which is logical given the known Main Effects that such lesions have on GM volume based on the data presented in Chapter 4.

Table 17: Predictors of Combined Cognitive Score with Mediation Effect by Brain Structure

Independent Variable	t-value	p-value	Partial Correlation Value (r^p)
WMHL	-1.52	.13	-.08
GM/TIV	2.69	**.007**	.19
Gender	-.53	.59	-.03
Race	-2.68	**.008**	-.14
MRI Infarcts	-1.51	.13	-.08

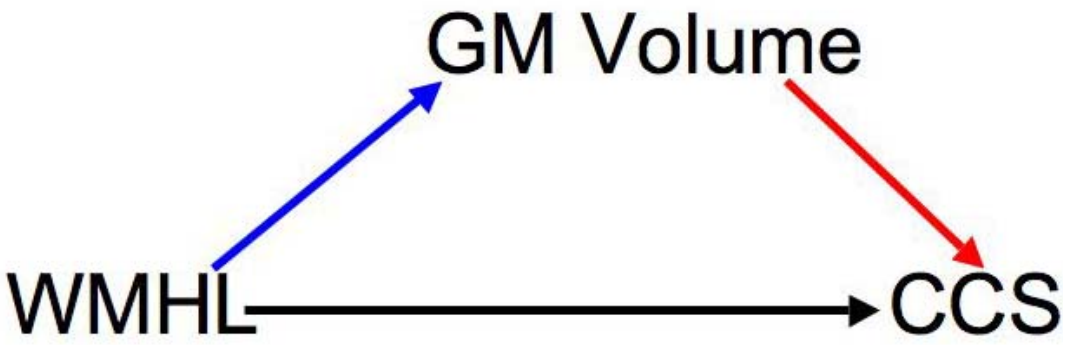

Figure 31: This figure shows how the relationship between WMHL and cognition is partially mediated by GM volume. That is, the reason that WMHL are related to cognition is through their Main Effect on GM volume. That is, WMHL induce changes in GM volume (blue arrow) and it is those alterations that themselves results in the changes in cognition. The red arrow reflects how increases in GM volume translate to increases in CCS and the red arrow shows the negative correlation between WMHL and CCS.

5.3.2 Positive Correlation between CCS and GM volume

Figure 32 shows the positive correlation between CCS and GM volume at the voxel level. It is very important to understand that in showing this figure, I do not mean to imply that increasing CCS is causing higher GM volume. Rather, what I am trying to convey in this figure is that if CCS is higher it is most likely attributable to higher GM volume in the areas highlighted.

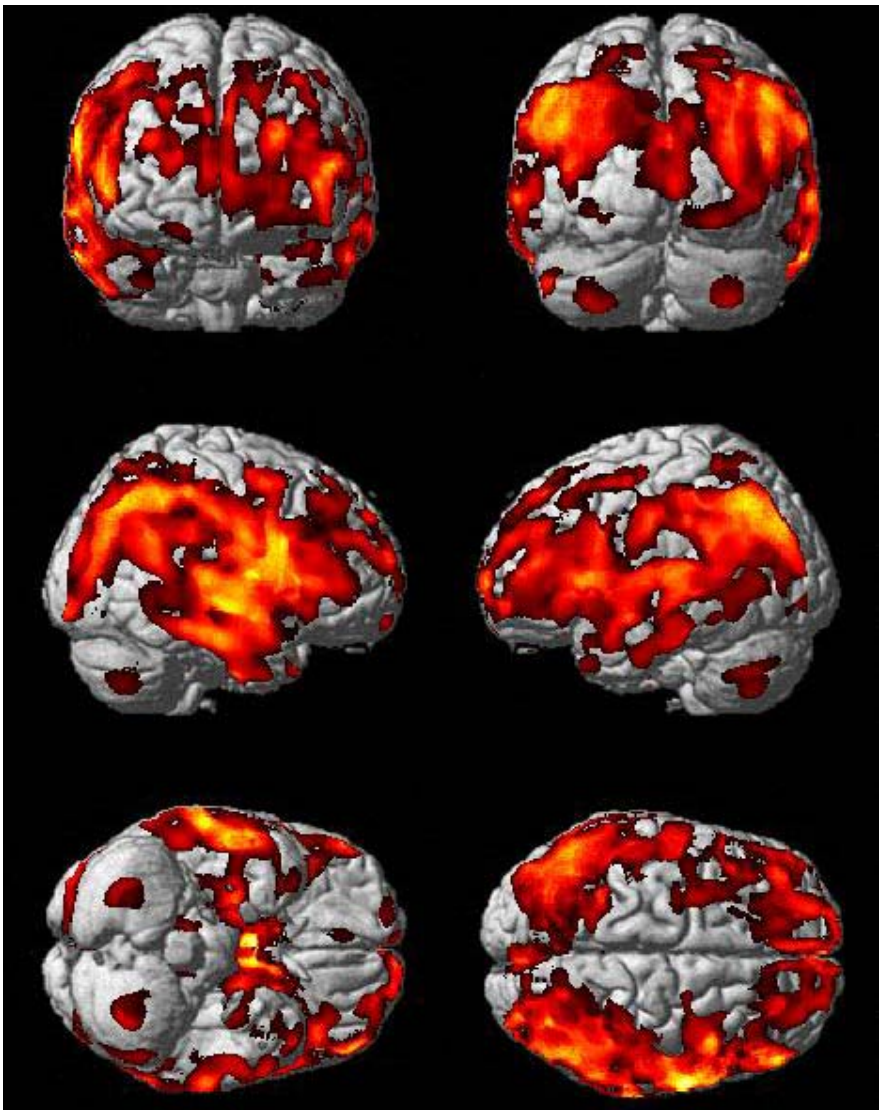

Figure 32: This figure shows the positive correlation between GM and CCS, observed in all four lobes of the cerebrum including the frontal and temporal lobes.

The section renderings of this correlation are shown in Figure 33. It shows areas of the GM that are higher in correlation with higher CCS scores, controlling for WMHL and TIV (P_{FDR} = .05, k = 100). Panel 1 shows a coronal image indicating higher GM volume in the highlighted areas translates to better scores on CCS. This is evident in both hippocampi (double headed arrows). Panel 2 shows that in the left hippocampus, this relationship is localized in the anterior hippocampus (r^p = -.17, x = -24, y = -11, z = -19). By contrast, Panel 3 shows that the right hippocampus has higher volumes throughout the extent of the hippocampus in correlation to higher CCS (posterior: r^p = -.15, x = 32, y = -33, z = -5). Panel 4 shows that the left posterior cingulate gyrus (red arrow: r^p = -.18, x = -9, y = -50, z = 24), left precuneus (black arrow: r^p = -.17, x = -9, y = -65, z = 37) and the left anterior cingulate gyrus (blue arrow) all have higher GM volume and that these larger volumes translate to a better performance on CCS. Panel 5 shows that while this relationship is also observed for the right posterior cingulate (r^p = -.19, x = 10, y = -48, z = 23) and precuneus (r^p = -.24, x = 10, y = -55, z = 20) (red box) it is not for the right anterior cingulate. Panel 6 shows that larger GM volumes in both caudate nuclei and thalami (blue box) are positively correlated to better CCS results. All remaining correlation effect sizes are provided in Table 18.

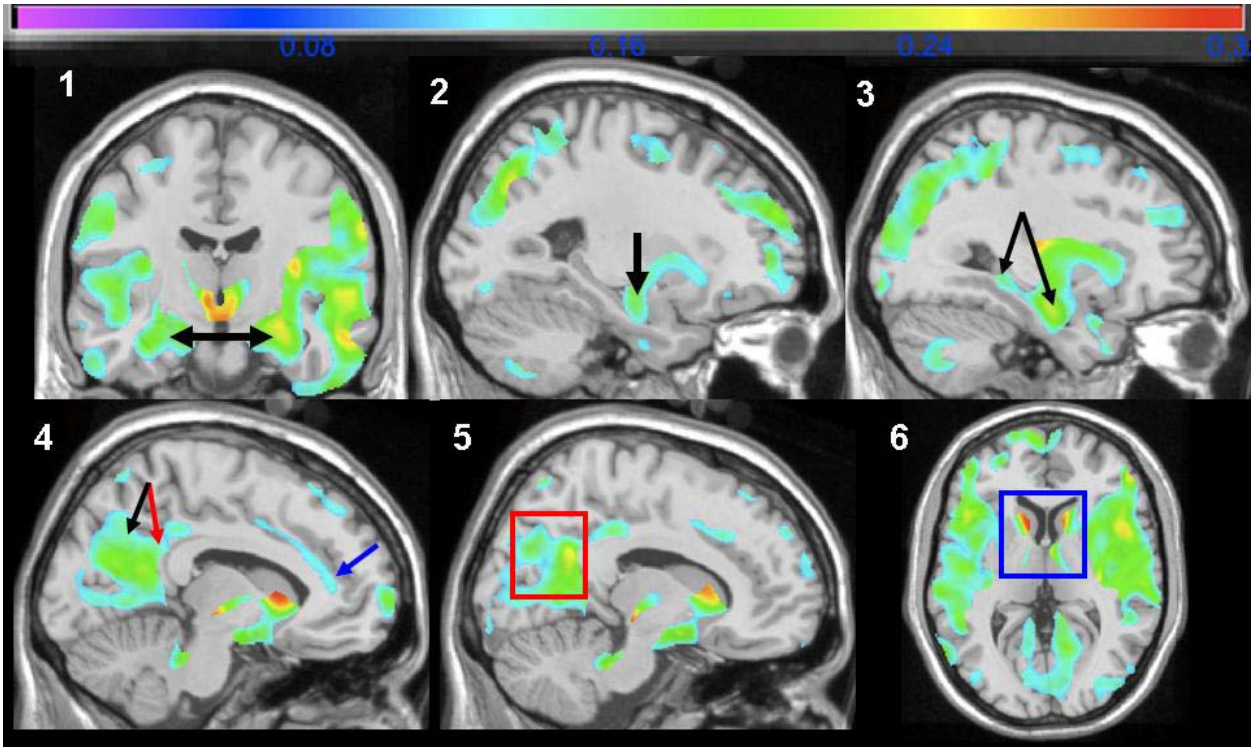

Figure 33: This figures shows areas of the GM that are higher in correlation with higher CCS scores, controlling for WMHL and TIV (P_{FDR} = .05, k = 100).

The peak maxima of CCS Main Effects are displayed in Table 17.

Table 18: Peak Maxima showing brain regions where larger GM volumes are correlated with higher CCS.

Structure	Peak MNI Coordinates (x, y, z)	Cluster Volume (mm^3)	t/z scores	r^p value	P_{FDR}
R_Postcentral	67, -6, 28	374634	6.14/5.98	.31	< .001
L_Thalamus	-10, 11, 8		6.03/5.93	.31	< .001
R_Caudate	12, 14, 7		5.77/5.63	.30	< .001
R_Inf_Temporal	64, -23, -22		5.59/5.47	.29	< .001

R_Insula	34, -15, 12		5.42/5.31	.28	< .001
R_Mid_Temporal	61, -15, -1		5.31/5.20	.27	< .001
L_Mid_Temporal	-46, -47, 16		5.29/5.19	.27	< .001
R_Rolandic_Operculum	46, -1, 11		5.23/5.13	.27	< .001
R_Angular	47, -66, 46		5.22/5.12	.27	< .001
R_Inf_Frontal_Trigone	53, 43, 3		5.13/5.03	.27	< .001
R_Inf_Frontal_Operculum	45, 10, 24		5.02/4.93	.26	< .001
R_Sup_Temporal	59, -9. 0		4.87/4.79	.25	< .001
L_Inf_Frontal_Operculum	-41, 14, 29		4.86/4.78	.25	< .001
R_Precuneus	13, -55, 27		4.82/4.74	.25	< .001
R_Ant_Hippocampus	28, -11, -15		4.81/4.73	.25	< .001
L_Sup_Occipital	-27, -70, 39		4.75/4.67	.25	< .001
L_Inf_Parietal	-32, -43, 45		4.70/4.63	.25	< .001
L_Mid_Cingulate	-12, 6, 42	1156	3.22/3.19	.17	.007
L_Ant_Cingulate	-10, 31, 24		2.83/2.82	.15	.01
L_Crus_Cerebellum	-54, -59, -42	817	3.04/3.02	.16	.01
L_Cerebellum	-31, -64, -47	1805	3.02/3.00	.16	.01
R_Mid_Cingulate	14, 22, 35	192	2.91/2.89	.15	.01
L_Mid_Occipital	-32, -92, -6	405	2.83/2.81	.15	.01
L_Fusiform	-25, -81, -9		2.69/2.68	.14	.02
R_Fusiform	28, -78, -11	101	2.34/2.35	.13	.03

5.3.3 Positive Correlation between GM Volume and CCS with WMHL Main Effects masked out

The positive correlation between GM volume and CCS is now presented having excluded any voxels statistically significant in terms of having a Main Effect of WMHL (Figure 29).

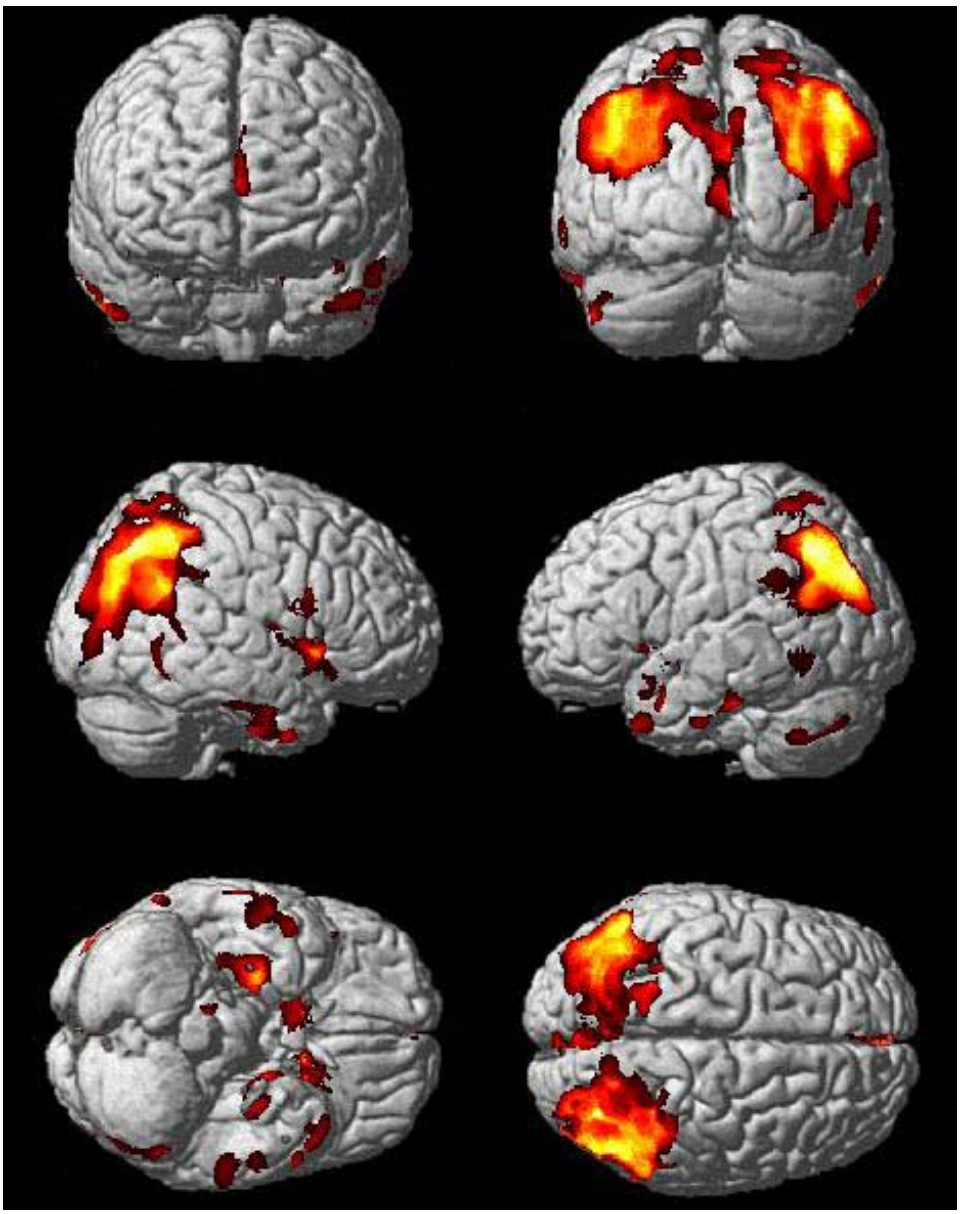

Figure 34: The positive correlation between GM volume and CCS are confined largely to the, temporal, parietal and occipital lobes when masking out the Main Effects of WMHL (P_{FDR} = .05, k = 100).

The section rendering of the positive correlation between GM volume and CCS masked for WMG are shown in Figure 35. Part a shows that even after masking, there is still an independent correlation of GM volume and CCS in the right hippocampus (crosshair). This is also the case for the left anterior hippocampus as shown in part b (crosshair). Part c reveals that both the left (crosshair), right precuneus and right anterior cingulate main affects still persist in this correlation though the posterior cingulate effect is no longer visible due to the fact that it was encompassed in the WMHL Main Effect and thus masked out. Part d show that the correlation of GM volume and CCS in the left (crosshair) in the right caudate nuclei is still present.

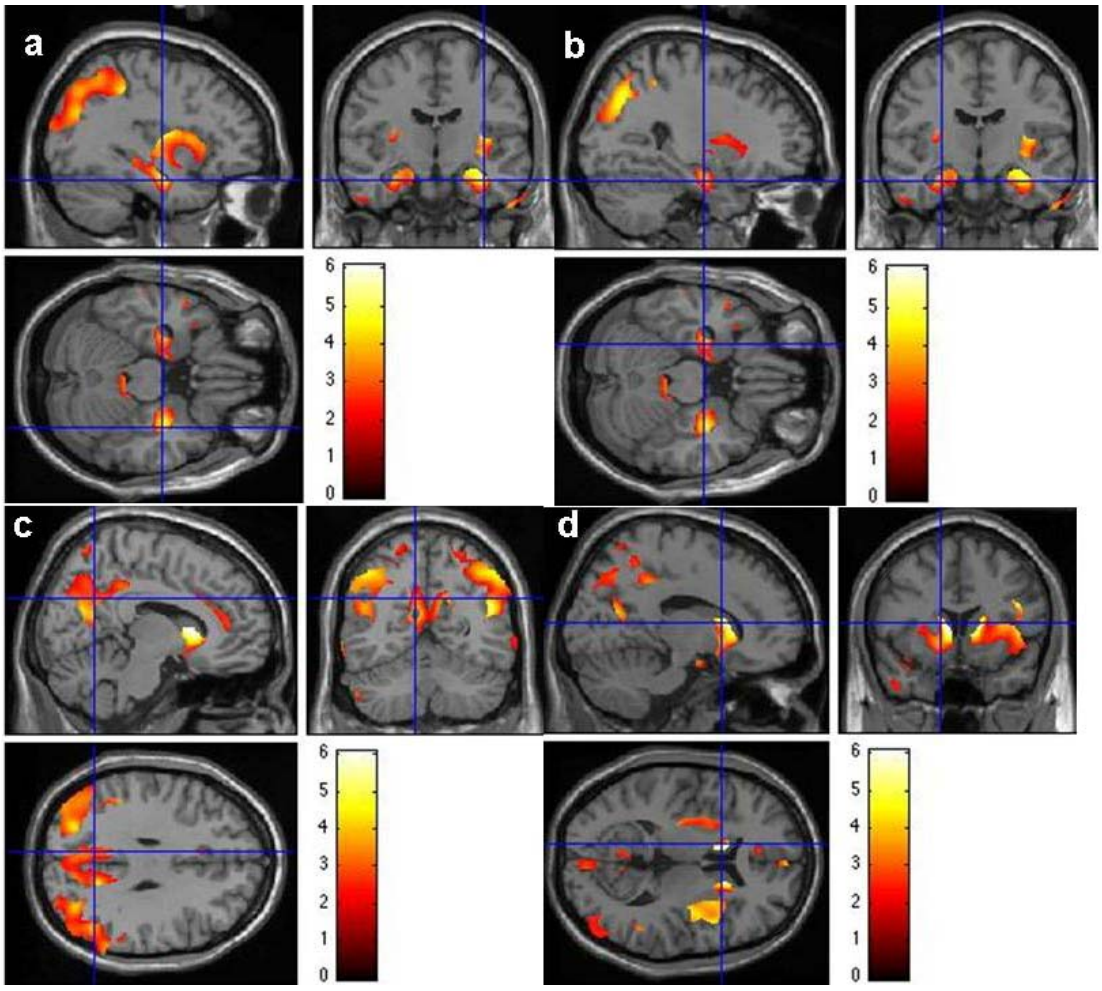

Figure 35: Section rendering in SPM of the positive correlation between GM volume and CCS after masking out the Main Effect of WMHL.

The spatial coordinates corresponding to the highest correlations between GM and CCS, masking out the WMHL Main effect, are shown in Table 19. The top two peak maxima are in the key strategic brain area of the caudate and the anterior hippocampus is the fourth largest peak maximum in terms of effect size. In all, five peak maxima are located in key strategic brain areas.

Table 19: This table shows the peak maxima in GM in association with CCS while masking out WMHL Main Effects.

Structure	Peak MNI Coordinates (x, y, z)	Cluster Volume (mm^3)	t/z scores	r^p value	P_{FDR}
L_Caudate	-10, 11, 8	8310	6.09/5.93	-.31	< .001
R_Caudate	12, 14, 7	18257	5.77/5.63	-.30	< .001
R_Inf_Frontal_Operculum	43, 11, 24		4.81/4.73	-.25	< .001
R_Ant_Hippocampus	28, -11, 15		4.81/4.73	-.25	< .001
R_Angular	46, -66, 46	31135	5.22/5.12	-.27	< .001
R_Mid_Temporal	45, -57, 22		5.15/5.05	-.27	< .001
R_Inf_Parietal	50, -53, 48		4.63/4.56	-.24	< .001
L_Mid_Temporal	-46, -48, 20	37442	5.09/5.00	-.26	< .001
R_Precuneus	14, -54, 27		4.81/4.73	-.25	< .001
L_Sup_Occipital	-27, -70, 39		4.75/4.67	-.25	< .001
R_Inf_Temporal	66, -20, -36	1022	4.69/4.62	-.24	< .001
L_Med_Sup_Frontal	-1, 62, 10	709	3.73/3.69	-.20	.002
L_Inf_Temporal	-69, -25, -25	416	2.93/2.91	-.16	.01

L_Calcarine	3, -88, 9	1195	2.83/2.81	-.15	.01
L_Lingual	-4, -80, 5		2.34/2.33	-.12	.03
L_Ant_Cingulate	-11, 33, 21	480	2.81/2.79	-.15	.02
L_Sup_Temporal_Pole	-40, 11, -20	125	2.58/2.56	-.14	.02

5.3.4 Conjunction of GM Volume/CCS Correlation and WMHL Main Effects

Voxels in which there is both a statistically significant CCS and WMHL correlations with GM are shown in Figure 36.

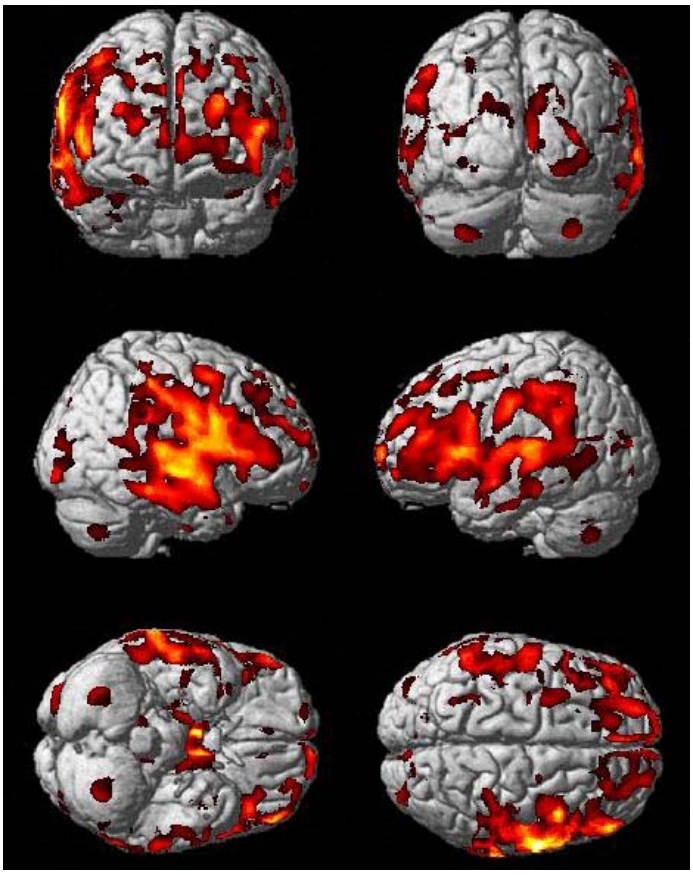

Figure 36: This figure shows the conjunction of CCS and WMHL correlations with GM volume (P_{FDR} = .05, k = 100). The conjunction is evident in the frontal, temporal (including mesial temporal), occipital lobes, and cerebellum.

Figure 37 shows the conjunction between CCS and WMHL correlations with GM volumes. Part a shows that both CCS and WMHL are jointly significant in their correlations with GM in voxels residing in the left anterior hippocampus (part a, crosshairs). Part b shows a similar conjunction in the right posterior hippocampus. Part c indicates a CCS-WMHL conjunction in the posterior cingulate gyrus, with the crosshair located on the left side. Part d shows joint CCS and WMHL Main Effects in the thalamus. This figure therefore shows that WMHL are correlations with lower GM volume in the same brain regions in which larger GM volumes translate to better performance on neuropsychological evaluations of cognition.

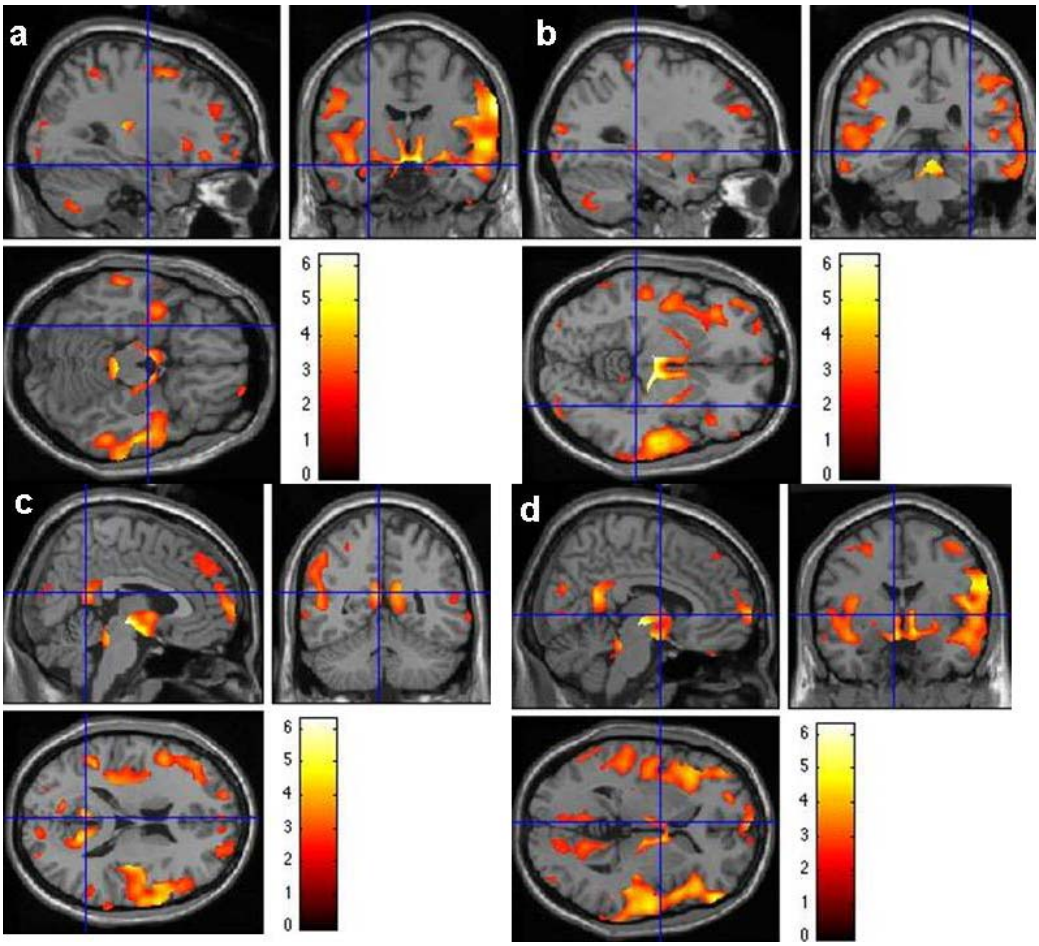

Figure 37: Section rendered SPM t-imaging showing brain areas in which both increased volumes translate to better cognitive scores and where WMHL related atrophy occurs.

The peak maxima with respect to the CCS-WMHL conjunction are visible in table 20. This conjunction includes 7 peak maxima located in key strategic brain areas.

Table 20: Peak Maxima of the Conjunction between CCS and WMHL Correlations with GM.

Structure	Peak MNI Coordinates (x, y, z)	Cluster Volume (mm^3)	t/z scores	r^p value	P_{FDR}
R_Postcentral	66, -7, 29	145310	6.12/5.96	-.31	< .001
R_Insula	34, -15, 13		5.37/5.36	-.28	< .001
R_Rolandic_Operculum	50, 8, 7		5.03/4.94	-.26	< .001
R_Inf_Frontal_Trigone	53, 42, 1		4.95/4.86	-.26	.001
R_Sup_Temporal	59, -9, 0		4.87/4.79	-.25	.001
L_Inf_Frontal_Operculum	-41, 14, 29		4.86/4.78	-.25	.001
R_Mid_Temporal	56, -18, -7		4.79/4.71	-.25	.001
R_Inf_Frontal_Operculum	49, 9, 22		4.77/4.69	-.25	.001
L_Inf_Frontal_Trigone	-47, 17, 5		4.59/4.52	-.24	.001
L_Heschl	-33, -27, 12		4.39/4.33	-.23	.002
L_Sup_Temporal	-49, -45, 18		4.38/4.31	-.23	.002
R_Inf_Frontal_Trigone	49, 22, 5		4.34/4.28	-.23	.002
R_Precentral	53, 2, 26		4.26/4.20	-.22	.002
R_Sup_Temporal	61, -23, 5		4.25/4.19	-.22	.002
L_Sup_Temporal	-50, -45, 22		4.20/4.15	-.22	.003
R_Precuneus	12, -55, 23	9084	4.69/4.61	-.24	.001

R_Calcarine	16, -62, 8		3.68/3.64	-.19	.006
L_Precuneus	-7, -52, 16	2689	4.43/4.37	-.23	.002
L_Post_Cingulate	-6, -44, 23		3.06/3.04	-.16	.02
L_Lingual	-11, -63, 2		3.04/3.01	-.16	.02
L_Sup_Frontal	-17, 41, 49	5031	4.09/4.04	-.21	.003
L_Medial_Sup_Frontal	-5, 65, 6		3.88/3.83	-.20	.005
L_Mid_Frontal	-41, 25, 46	547	3.81/3.77	-.20	.005
R_Post_Cingulate	11, -38, 31	287	3.69/3.66	-.19	.006
L_Cuneus	-13, -72, 20	2016	3.69/3.65	-.19	.006
L_Sup_Occipital	-22, -74, 25		2.88/2.86	-.15	.02
L_Inf_Temporal	-58, -9, -30	1621	2.99/2.97	-.19	-.16
L_Inf_Parietal	-30, -42, 52	390	3.52/3.48	-.19	.008
L_Sup_Parietal	-29, -58, 50		2.81/2.79	-.15	.03
R_Cuneus	12, -76, 27	1304	3.41/3.38	-.18	.01
R_Sup_Occipital	25, -73, 29		2.96/2.94	-.16	.02
L_Thalamus	-19, -24, 8	590	3.37/3.34	-.18	.01
R_Sup_Frontal	22, 54, 20	2186	3.33/3.30	-.17	.01
R_Mid_Frontal	29, 50, 24		2.98/2.96	-.16	.02
R_Med_Sup_Frontal	8, 36, 56	245	2.78/2.76	-.15	.03
R_Mid_Occipital	30, -92, 12	1659	3.26/3.23	-.17	.01
R_Inf_Occipital	32, -94, -6		3.18/3.16	-.17	.01
L_Mid_Cingulate	-12, 6, 42	317	3.22/3.19	-.17	.01
L_Ant_Cingulate	-11, 27, 28		2.78/2.77	-.15	.03

L_Mid_Temporal	-63, -53, -2	1057	3.19/3.17	-.17	.01
L_8_Cerebellum	-31, -64, -47	834	3.02/3.00	-.16	.02
R_Mid_Cingulate	11, -30, 36	114	2.99/2.97	-.16	.02
R_Angular	32, -64, 45	942	2.95/2.93	-.16	.02
R_Sup_Temporal_Pole	32, 10, -27	255	2.95/2.93	-.16	.02
R_Paraphippocampal	23, 6, -21		2.41/2.40	-.13	.04

While a conjunction existed between WMHL and CSS, there was no statistically significant interaction between the two. To summarize, domain specific tests of neuropsychological function can be combined to form a composite score that is positively correlated with brain areas that are known to be implicated in cognitive function, mainly in the temporal and parietal lobes. This relationship is present even when controlling for WMHL atrophy. Thus, WMHL have relevance for cognitive impairment because they are related to atrophy in the same brain areas in which larger GM volumes are correlated with better performance on CCS. The contribution of this chapter's results to the overall model is displayed in Figure 38.

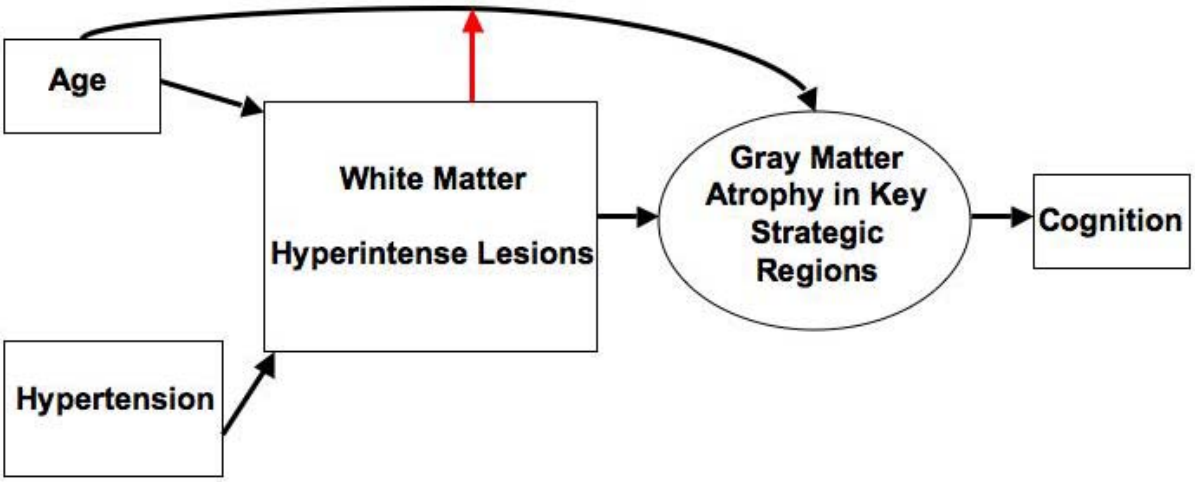

Figure 38: This figure shows the contributions of the chapter 5 results to the overall model. WMHL are correlated to impaired cognition and this is mediated mainly by alterations in the volume of key strategic brain regions

Based upon this reasoning, I next investigated the interactions and conjunctions of WMHL with MCI and dementia. The results of these analyses occupy the contents of chapters 6 and 7 with chapter 6 focused on the relationship between WMHL and MCI and chapter 7 engaged with WMHL and dementia Main Effects on GM volume.

6.0 INTERACTION BETWEEN WHITE MATTER HYPERINTENSE LESIONS AND MILD COGNITIVE IMPAIRMENT IN GRAY MATTER

6.1 INTRODUCTION

I have identified WMHL as predictors of lower GM volume in areas of the brain that are known to be affected by aging and cognitive function. Having done this, I now focus on whether or not WMHL either conjunct or interact with behavioral proxies for neurodegeneration. As I have discussed in chapter 2, MCI is commonly acknowledged as a high risk state for dementia and thus potentially represents a relatively early phase of neurodegeneration. This chapter presents data that examines the interaction between WMHL and MCI. All MCI subjects were used for this analysis regardless of whether or not they progressed after 5-years. This chapter shows MCI effects on brain structure varies as a function of WMHL and this moderation is localized in the anterior cingulate gyrus: an area relevant to vascular disease, dementia pathology, and cognitive function.

6.2 MATERIALS AND METHODS

This analysis utilized 399 CHS-CS scans from individual participants in 1997-1999. Subject demographics are detailed in Table 21. MCI subjects tended to be older, less educated and more

likely to be African-American compared to the control group ($p < .05$). The MCI group also had a higher percentage of MRI identified infarcts than the control group though this difference did not reach statistical significance ($p = .06$).

Table 21: Demographics Characteristics of Control and MCI Subjects

Variable	Normal (n=302)	MCI (n=97)	T-test(t, p)/χ^2
Age	77.96 ± 3.63	79.47 ± 4.56	-3.33, **.003**
Gender (F)	60% (182)	56% (54)	.64, .25
Education (12^{th} Grade only)	37% (111)	30% (47)	4.20, .**03**
Race	17% (52)	30% (29)	7.29, .**006**
Infarcts	26% (79)	35% (34)	2.86, .06
WMG	2.30 ± 1.43	2.49 ± 1.74	-1.08, .28

Before testing the interaction between WMHL and MCI itself, I wanted to first assess the Main Effect of WMHL in the MCI group only to see if the distribution of this atrophy differed in these subjects compared to what was observed in Chapter 4 in the controls. The SPM statistical model that was used to test this Main Effect is seen in Figure 9. This model included standard covariates such as age, gender, race, education, and MRI infarcts (design matrix not shown). I next tested the Main Effect of MCI and WMHL in all 399 subjects with standard covariates and this model is shown in Figure 39, which depicts the SPM2 design matrix used to assess the Main Effects of MCI, WMHL, and their conjunction.

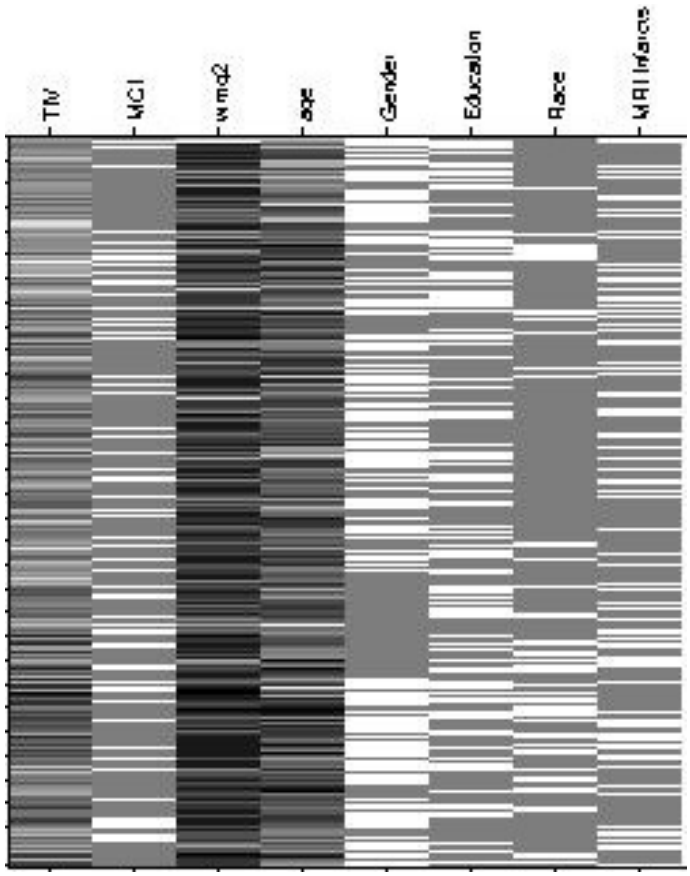

Figure 39: This SPM2 design matrix shows columns modeling the Main Effect of MCI (2nd column) and WMHL (3rd column). The remaining columns model the confounding effect of head size, age, gender, education, race, and MRI identified infarcts.

A separate statistical model was constructed to investigate the interaction between WMHL and MCI. This was done by centering the CHS WMG visual grading around its overall mean and multiplying that by the binary MCI variable. This interaction term then comprised its own column in the subsequent SPM2 design matrix shown in Figure 40. A contrast vector weight of -1 was applied to the interaction column to yield the subsequent areas of the brain that are reduced in GM volume in correlation with the interaction term. All analyses were done with an FDR threshold of 5% and an extent threshold of 30 voxels for the interaction analysis.

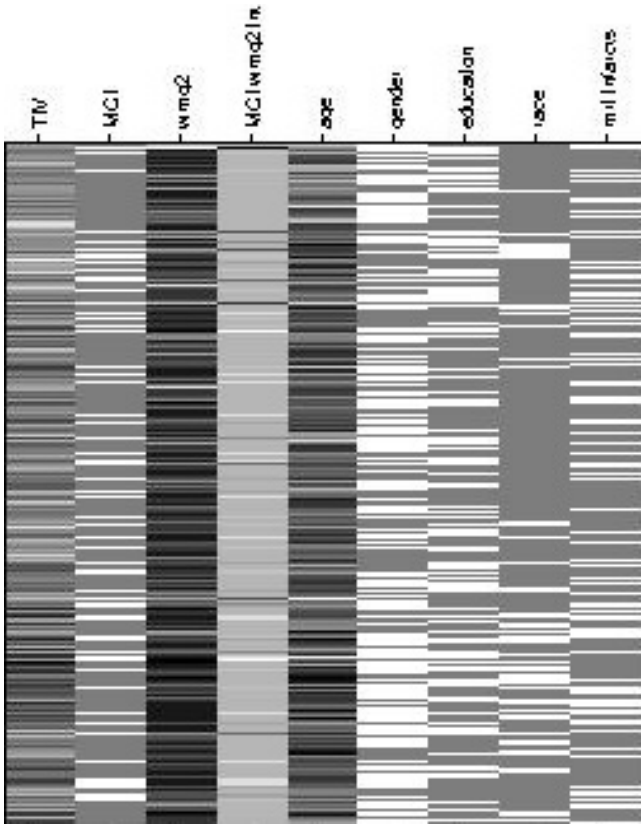

Figure 40: This design matrix is identical to that presented in Figure 33 with the sole difference being the additional interaction term in the fourth column of the design matrix.

6.3 RESULTS

In all 399 subjects, there were no independent Main Effects of MCI on GM volume. The WMHL Main Effects were identical to those described in chapter 4. For the Main Effect of WMHL in only the 97 MCI subjects, the volume rendered t-image is displayed in Figure 41. Like the Main Effects observed in Chapter 4 in the controls, the Main Effect of WMHL in the 97 MCI subjects was observed most impressively in the frontal lobes, including the orbital frontal cortex. This similarity also holds in viewing the temporal lobes in which there is atrophy in relation to

WMHL. Unlike the WMHL Main Effects in controls, however, there are fewer observable parietal lobe Main Effects in MCI group.

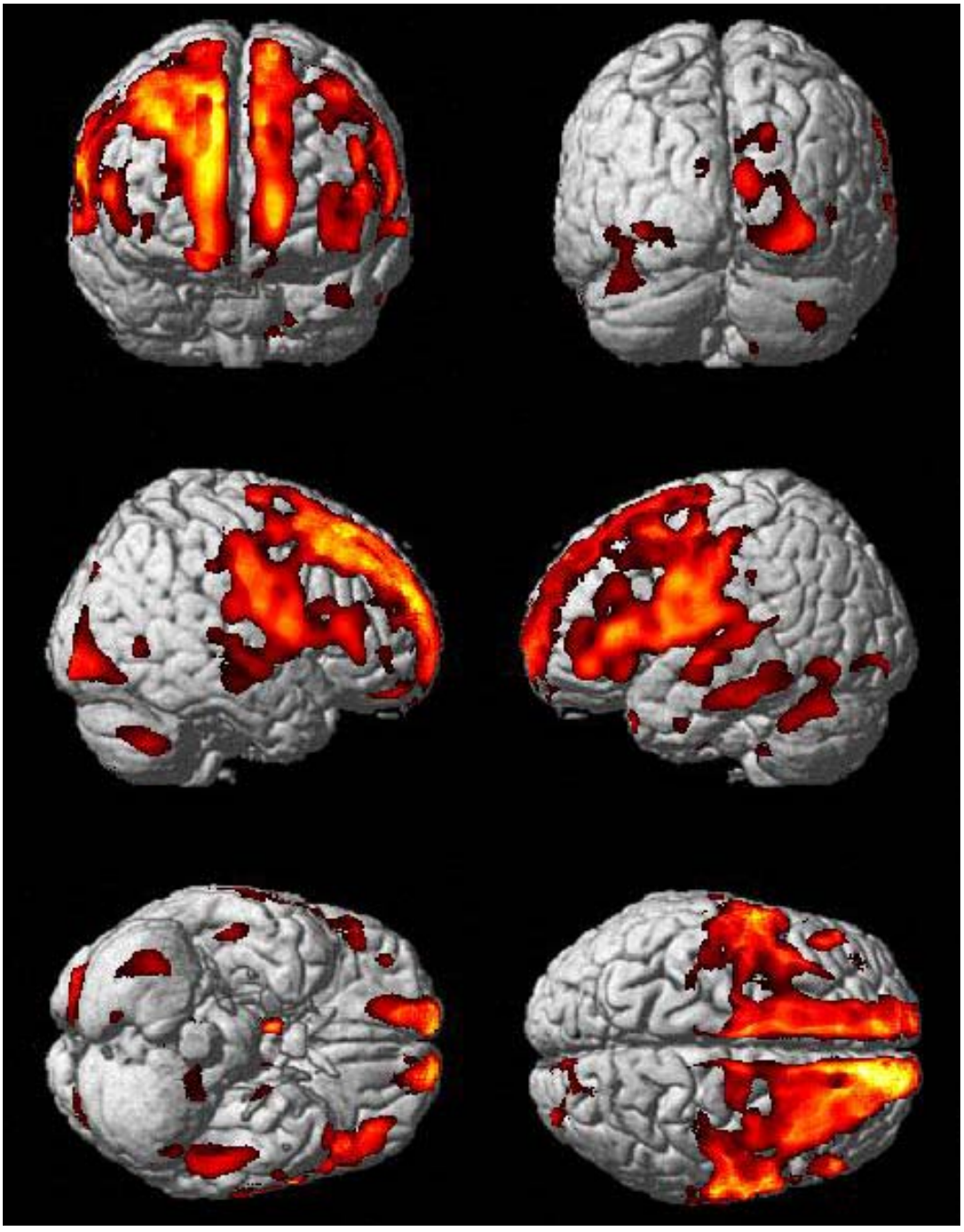

Figure 41: This figure shows the Main Effect of WMHL in 97 MCI subjects from the CHS-CS, volume rendered onto the Standard Single Subject MNI template (P_{FDR} = .05, k = 100). These Main Effects are most impressive in the paramedian frontal lobes, orbital frontal cortex, and the temporal cortices.

Figure 42 shows section renderings of the Main Effect of WMHL in only the MCI subjects. Correlation effects sizes in all regions are above .30 in magnitude. Part a highlights how impressively the frontal lobes are lower in GM volume with increased WMHL burden. Part b shows that the Main Effects of WMHL are seen in both the putamen and the thalamus. Part c shows in the center of the crosshairs how higher WMHL is associated with lower GM volumes in the right precuneus.

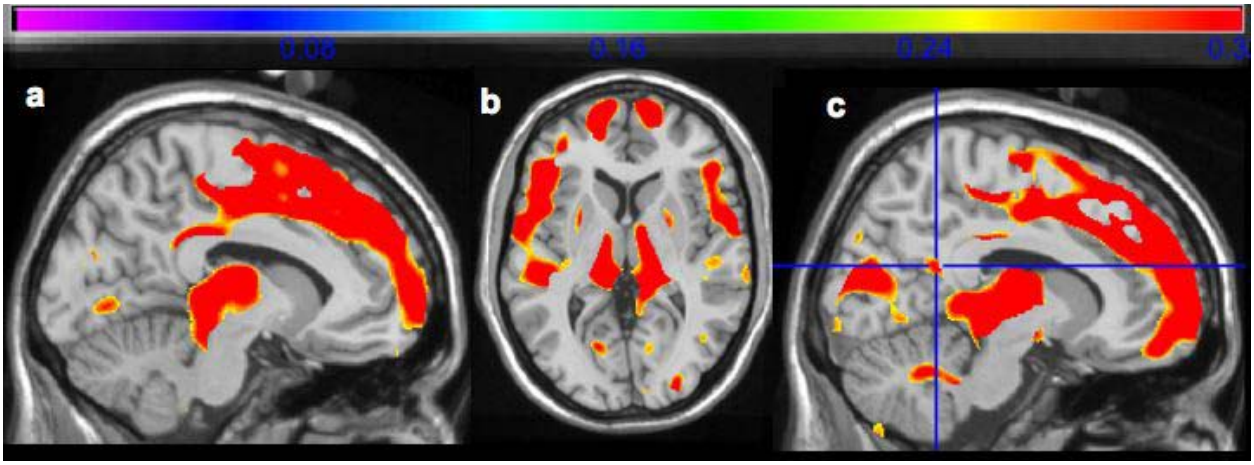

Figure 42: Main Effect of WMHL in 97 MCI subjects.

Table 22 shows the peak maxima of the WMHL Main Effect in the MCI group. Eleven sites of these peak maxima are in key strategic brain areas and are highlighted in bold.

Table 22: Peak Maxima of the WMHL Main Effect in the MCI Subjects

Structure	Peak MNI Coordinates (x, y, z)	Cluster Volume (mm^3)	t/z scores	r^p value	P_{FDR}
R_Sup_Frontal	15, 60, 21	74758	6.25/5.68	-.55	< .001
R_Med_Sup_Frontal	11, 46, 45		6.12/5.58	-.54	< .001
R_Mid_Frontal	38, 17, 47		5.36/4.98	-.49	< .001
R_Mid_Cingulate	12, 26, 39		5.27/4.90	-.49	< .001

R_Rolandic_Operculum	61, -1, 11		5.24/4.88	-.49	< .001
R_Supp_Motor_Area	9, -21, 57		5.00/4.68	-.47	< .001
R_Postcentral	39, -24, 42		4.97/4.66	-.47	< .001
R_Supramarginal	65, -20, 22		4.58/4.33	-.44	< .001
R_Sup_Orbital_Frontal	16, 51, -15		4.52/4.27	-.43	< .001
R_Mid_Orbital_Frontal	10, 67, -3		4.36/4.14	-.42	< .001
R_Inf_Frontal_Trigone	51, 28, 9		4.34/4.12	-.42	< .001
R_Sup_Temporal	65, 1, 2		4.16/3.96	-.40	< .001
L_Postcentral	-56, -8, 23	78470	5.87/5.38	-.53	< .001
L_Inf_Frontal_Trigone	-47, 28, 9		5.77/5.30	-.52	< .001
L_Precentral	-55, -2, 29		5.71/5.26	-.52	< .001
L_Paracentral_Lobule	-10, -23, 52		5.62/5.18	-.51	< .001
L_Supp_Motor_Area	-9, -10, 54		5.45/5.05	-.50	< .001
L_Sup_Frontal	-15, 61, 9		5.14/4.80	-.48	< .001
L_Roladic_Operculum	-59, 0, 10		5.01/4.69	-.47	< .001
L_Mid_Cingulum	-13, -22, 48		4.91/4.60	-.46	< .001
L_Inf_Frontal_Operculum	-16, 41, 38		4.78/4.50	-.45	< .001
L_Supp_Motor_Area	-15, -11, 64		4.61/4.35	-.44	.001
L_Mid_Orbital_Frontal	-13, 66, -1		4.57/4.32	-.44	.001
L_Post_Cingulate	-8, -35, 29		4.48/4.24	-.43	.001
L_Medial_Sup_Frontal	-11, 19, 42		4.39/4.17	-.42	.001
L_Inf_Orbital_Frontal	-39, 40, -7		4.25/4.04	-.41	.001
L_Inf_Frontal_Operculum	-50, 9, 15		4.19/4.00	-.41	.001

R_Thalamus	15, -14, 16	21825	5.57/5.14	-.51	< .001
L_Thalamus	-14, -15, 13		5.47/5.06	-.50	< .001
R_Calcarine	11, -84, 16	7747	4.55/4.30	-.43	.001
R_Inf_Occiptial	29, -95, -6		4.12/3.93	-.40	.002
L_Lingual	-14, -70, -1	2090	3.81/3.65	-.37	.004
R_Crus_Cerebellum	38, 59, -41	1802	3.73/3.59	-.37	.004
L_Inf_Temporal	-51, -27, -19	3934	3.63/3.49	-.36	.006
R_Sup_Temporal	50, -12, -9	2556	3.56/3.43	-.35	.006
R_Cuneus	19, -72, 33	1207	3.32/3.21	-.33	.01
R_Sup_Occiptial	18, -85, 37		2.90/2.83	-.29	.02
L_Crus_Cerebellum	-40, -65, -26	3520	3.28/3.18	-.33	.01
L_Inf_Occipital	-37, -67, -9	3520	3.25/3.15	-.33	.01
L_Angular	-47, -49. -33		3.16/3.07	-.32	.01
L_Putamen	-25, 4, 5	472	3.20/3.10	-.32	.01
R_Precuneus	12, -50, 21	226	3.17/3.08	-.32	.01
R_Mid_Temporal	44, -65, 1	324	3.13/3.04	-.31	.02
R_Putamen	27, 3, 9	694	3.10/3/02	-.31	.02
L_Cuneus	-8, -81, 22	105	3.00/2.92	-.30	.02
L_Supramarginal	-46, -33, 34	103	2.98/2.90	-.30	.02
R_Supramarginal	65, -32, 39	107	2.95/2.87	-.30	.02
L_Fusiform	-27, -78, -10	636	2.75/2.68	-.28	.03
R_Inf_Orbital_Frontal	39, 46, -1	244	2.85/2.78	-.29	.03
L_Mid_Tepmoral_Pole	-46, 20, -36	367	2.59/2.54	-.26	.04

L_Inf_Temporal	-58, 0, -33	140	2.70/2.64	-.28	.03

The WMHL by MCI interaction is depicted in the volume rendered t-image of Figure 43 which shows the moderation in the temporal, parietal, and frontal lobes – including orbital frontal cortex.

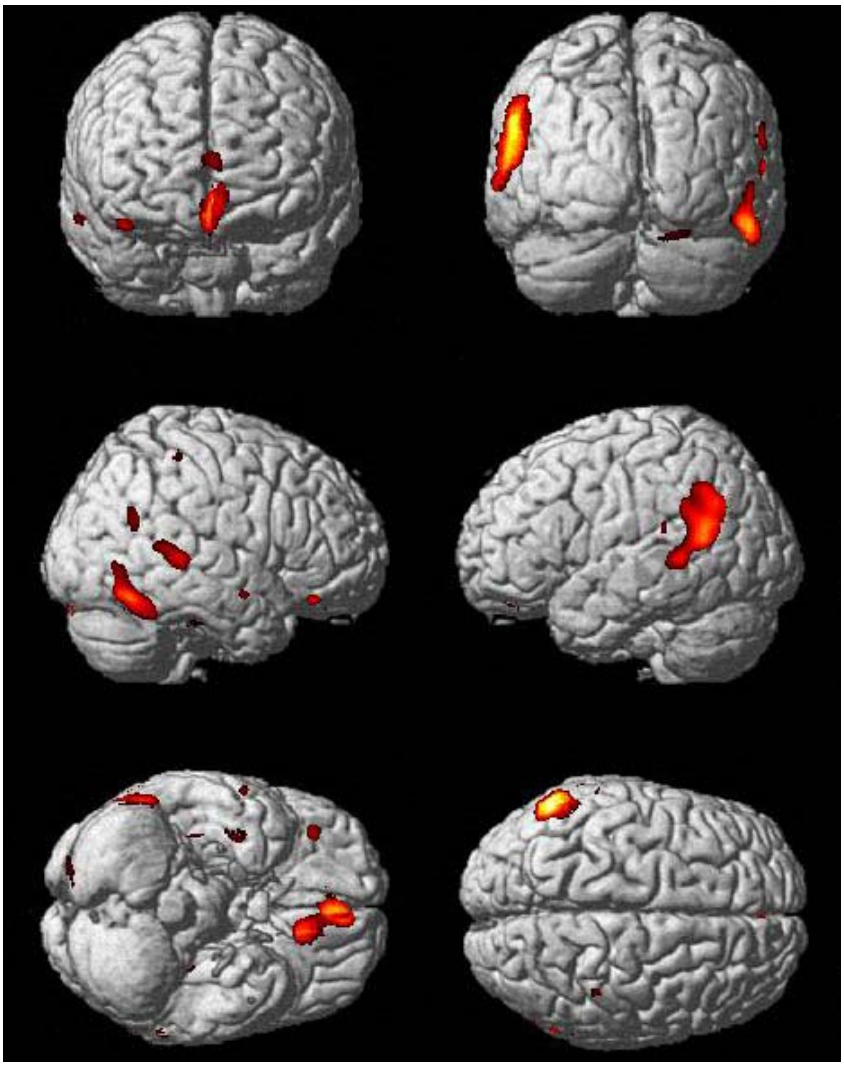

Figure 43: This figure shows the volume rendered representation of the interaction between WMHL and MCI status.

Figure 44 shows section renderings of the interaction between WMHL and MCI. Part a shows that WMHL moderates MCI in GM in the left anterior cingulate gyrus (r^p = -.18, x = -5, y

= 39, z = -6). This interaction is also observed in the right anterior cingulate gyrus in part b (r^p = -.18, x = 8, y = 43, z = 8). Finally, part c shows the interaction in the left posterior hippocampus as marked with the crosshairs (r^p = -.17, x = -30, y = -30, z = -11). There was no such interaction in the right hippocampus.

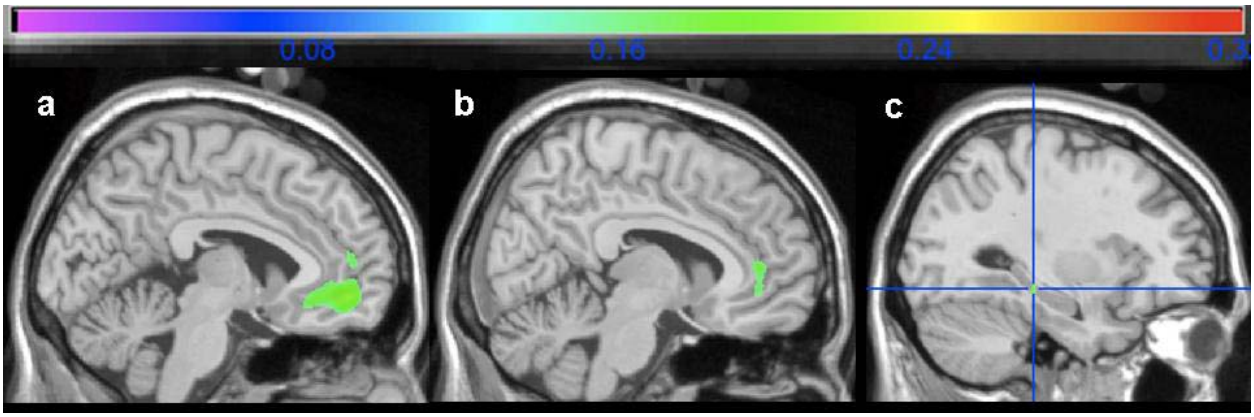

Figure 44: This figure brain areas in which WMHL moderate MCI in GM volume. All of the sites of this interaction are shown in key strategic brain areas: the left anterior cingulate gyrus in part a, right anterior cingulate gyrus in part b, and left posterior hippocampus in part c (crosshairs).

The peak local maxima of the WMHL and MCI interaction are listed in Table 23. Eight peak maxima are located in key strategic brain areas and four out of the top 5 peak maxima are located in such areas.

Table 23: Peak Maxima for the Interaction between WMHL and MCI

Structure	Peak MNI Coordinates (x, y, z)	Cluster Volume (mm^3)	t/z scores	r^p value	P_{FDR}
L_Gyrus_Rectus	-13, 30, -12	5441	5.66/5.55	-.28	.005
L_Med_Orbital_Frontal	-3, 50, -8	5441	4.46/4.41	-.22	.01
R_Med_Orbital_Frontal	13, 40, -3	5441	3.74/3.71	-.19	.02

L_Ant_Cingulate	-5, 39, -6	5441	3.70/3.67	-.18	.03
R_Ant_Cingulate	8, 43, 8	5441	3.58/3.55	-.18	.03
L_Mid_Temporal	-56, -56, 16	6258	4.83/4.76	-.24	.01
L_Angular	-55, -62, 30	6258	4.33/4.27	-.21	.01
R_Inf_Temporal	53, -61, -16	2327	4.50/4.44	-.22	.01
R_Mid_Temporal	59, -36, 4	887	3.93/3.89	-.20	.02
R_Inf_Orbital_Frontal	41, 34, -18	225	3.84/3.80	-.19	.02
R_Postcentral	41, -36, 57	38	3.48/3.45	-.17	.03
L_Post_Hippocampus	-30, -30, -11	61	3.47/3.44	-.17	.03
R_Fusiform	39, -26, -29	36	3.42/3.39	-.17	.04
L_Sup_Temporal	-62, -36, 21	57	3.30/3.30	-.17	.04
R_Rolandic_Operculum	39, -19, 17	59	3.31/3.29	-.17	.04

Because age and WMHL have been shown to interact in Chapter 4, a separate age by WMHL interaction was tested but was not found to be statistically significant. Additionally, there was no Main Effect of age in the analysis of WMHL on only the MCI subjects.

That no separate Main Effect of MCI was found on GM suggests that WMHL may mediate the effect of MCI on GM but the lack of MCI Main Effects was not noted until the SPM model was adjusted for gender, race, and education covariates. Thus, the lack of MCI Main Effects on GM is not due to mediation by co-morbid WMHL. However, there is an interaction between MCI and WMHL in GM in key strategic brain regions targeted by neurodegeneration, such as the hippocampus and this interaction is unchanged even when having MCI, WMHL and TIV as the only covariates in the analysis. This suggests that any MCI related brain atrophy, and

thus brain atrophy seen relatively early in neurodegenerative disease, may be moderated by comorbid vascular disease as reflected with WMHL. Consequently, WMHL may contribute to the pathophysiology of early neurodegeneration. The contributions of this chapter to the overall model are provided in Figure 45.

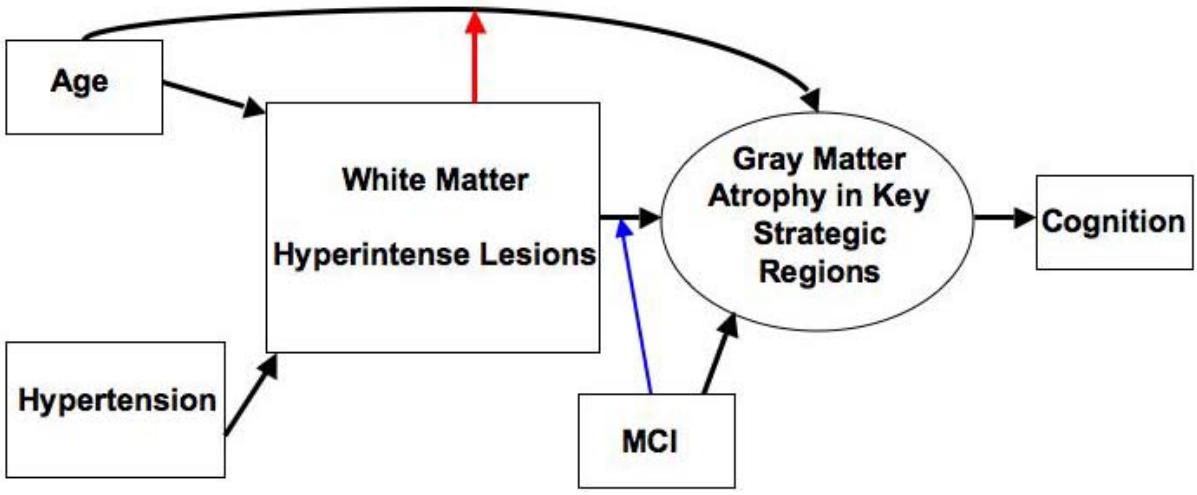

Figure 45: This figure shows the contribution of Chapter 6 data to the overall model. The blue arrow symbolizes the interaction between WMHL and MCI on gray matter volume loss. In this case, both black arrows from WMHL and MCI to the circle of gray matter atrophy in key strategic brain areas reflects not a conjunction of the two Main Effects but rather the fact that WMHL predicts lower gray matter volumes in just the MCI subjects.

To see if WMHL may contribute to the brain atrophy of a more advanced neurodegenerative process, dementia, Chapter 7 examined the relationships between WMHL and dementia status.

7.0 CONJUNCTION BETWEEN WMHL GRAY MATTER VOLUME LOSS AND DEMENTIA ASSOCIATED ATROPHY

7.1 INTRODUCTION

Having identified the interactive patterns of WMHL and MCI associated GM volume loss, I now present results of my attempts to replicate this analysis with respect to WMHL and dementia. While this may seem redundant, it is not for several important reasons. The chapter 6 results suggest that MCI related brain atrophy varies as a function of co-morbid WMHL and this was shown to occur in such key strategic brain regions as the hippocampus and anterior cingulate gyrus. This suggests that early neurodegeneration, as reflected by MCI, is moderated by co-morbid vascular disease, as indexed by WMHL. This chapter therefore seeks to establish whether or not advanced neurodegeneration is also moderated by co-existing vascular disease. I do not believe that such an interaction will be statistically significant because in a state of dementia, neurodegeneration is likely to be advanced and thus unlikely to vary as a function of co-morbid vascular disease. A conjunction analysis between WMHL and dementia was also performed to determine if hypertensive vascular disease and advanced neurodegeneration overall in key strategic brain regions.

7.2 MATERIALS AND METHODS

This study utilized 302 cognitively normal controls and 52 persons with dementia (34 Probable AD, 9 Possible AD, and 9 with ADDTC defined VaD). The controls and dementia subjects are compared in Table 22. Compared to controls, persons with dementia were older, less educated, African-American, and afflicted with more WMHL and MRI identified infarcts ($p < .05$).

Table 24: Demographic Comparisons of CHS-CS Controls and Dementia Subjects

Variable	Normal (n=302)	Dementia (n=52)	T-test(t, p)/χ^2
Age	77.96 ± 3.63	82.56 ± 4.99	-6.34, < **.001**
Gender (F)	60% (182)	65% (34)	.49, .29
Education (12^{th} Grade only)	37% (111)	54% (28)	5.43, .**02**
African American Race	17% (52)	28% (15)	3.91, .**04**
MRI Infarcts Present	26% (79)	40% (21)	4.43, .**03**
WMHL visual grading (WMG)	2.30 ± 1.43	3.21 ± 1.85	-4.03, < **.001**

Six statistical analyses were done within SPM. The first analysis assessed for dementia associated atrophy while controlling for age, gender, race, education, WMHL and MRI identified infarcts. The second analysis also tested for dementia atrophy but masked out any voxels that were part of a WMHL Main Effect. The third analysis assessed WMHL Main Effects in just the dementia subjects. The fourth statistical analysis then re-evaluated WMHL Main Effects but did

so by masking out any voxels that were also part of a dementia Main Effects. The fifth analysis tested for a conjunction between WMHL and dementia related atrophy. The sixth and final analysis tested for the interaction between WMHL and dementia Main Effects in GM.

7.2.1 Dementia Main Effects

The Main Effect of dementia is observed in Figure 46.

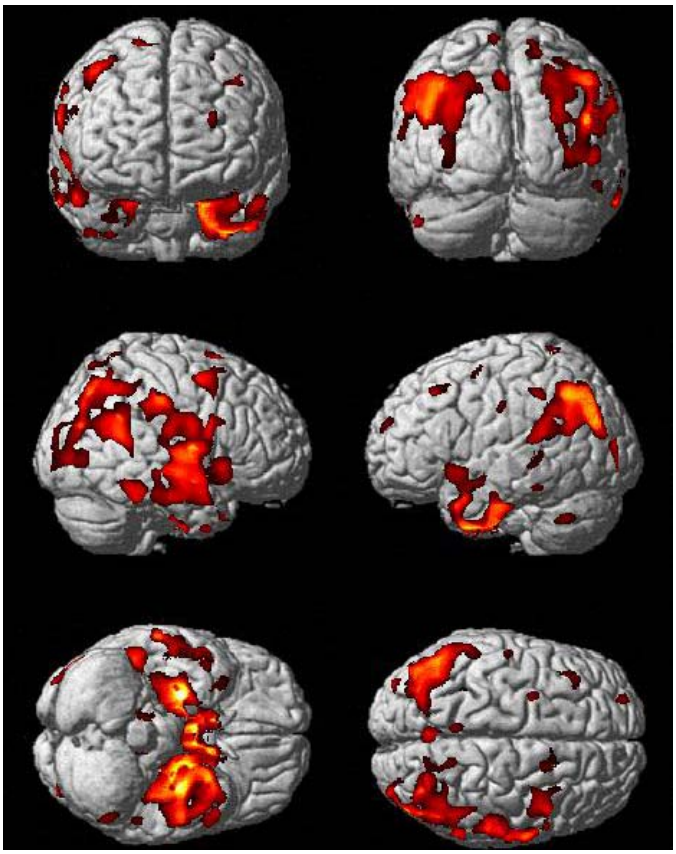

Figure 46: This figure shows the Main Effect of dementia on GM projected onto the Standard Single Subject MNI template (P_{FDR} = .05, k = 100). The distribution of these effects are seen notable in the temporal lobes, particularly the medial temporal lobes. They are also seen in the temporal-parietal junction and frontal lobes.

Figure 47 shows the section renderings of the Main Effect of dementia on gray matter. Part a shows that being demented is correlated with lower GM volumes in the left precuneus (crosshairs). Part b shows the main effect of dementia on the bilateral hippocampus. Part c shows that in the left hippocampus, this effect is localized mainly to anterior hippocampus. Part d shows that in the right hippocampus, the Main Effect of dementia spans the entire length of the hippocampus. Correlation effects sizes for each of these areas are provided in Table 25.

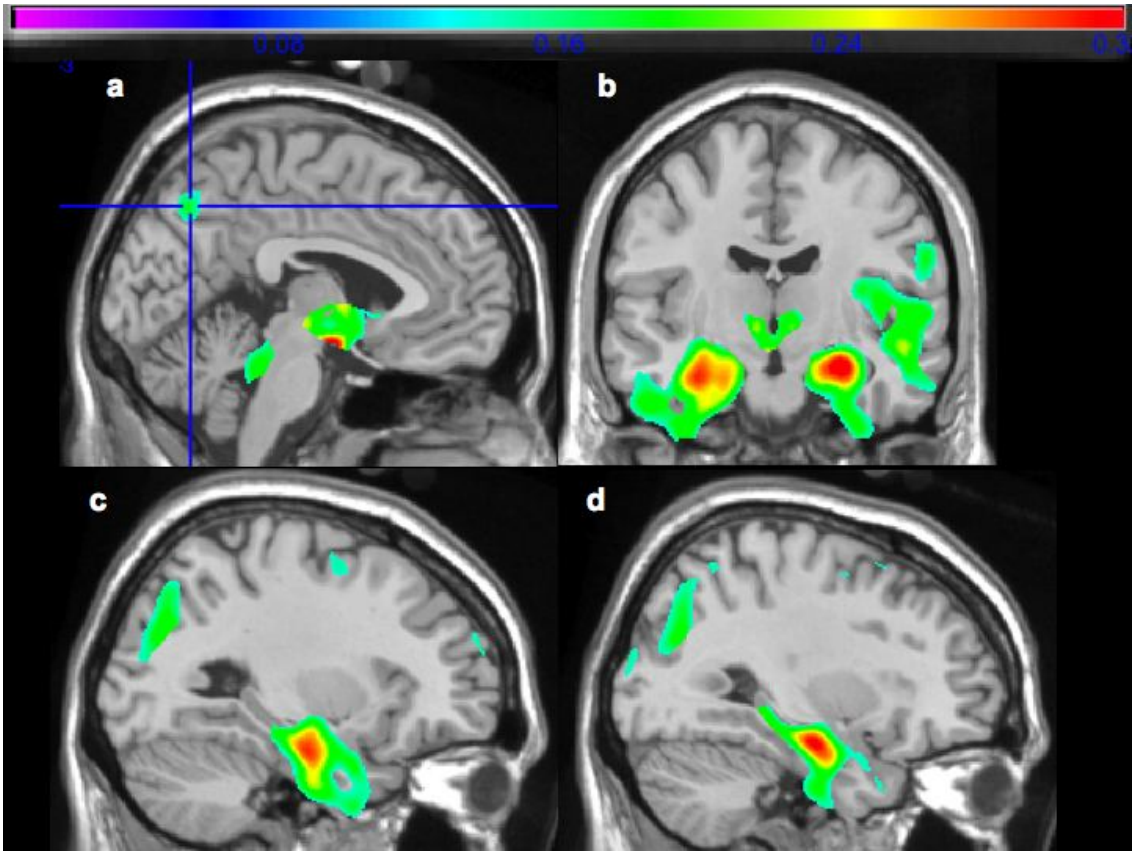

Figure 47: This figure shows dementia related atrophy projected onto the Standard Single Subject MNI template.

Peak maxima for the dementia Main Effect are displayed in Table 25. Ten of these peak maxima are in key strategic brain areas including the hippocampus, basal forebrain, and precuneus. Nine out of the top 10 largest effect sizes for the Dementia Main Effect are located in

key strategic brain areas. The precuneus itself was the site of two different peak maxima, hence the delineations of upper and lower.

Table 25: Peak areas of gray matter volume loss associated with clinical status of dementia.

Structure	Peak MNI Coordinates (x, y, z)	Cluster Volume (mm^3)	t/z scores	r^p value	P_{FDR}
R_Mammillary_Body	7, -7, -14	56024	7.46/7.18	-.37	< .001
R_Ant_Hippocampus	28, -13, -18		6.33/6.16	-.32	< .001
L_Ant_Hippocampus	-31, -15, -21		6.01/5.85	-.31	< .001
L_Caudate	-9, 13, 2		5.83/5.69	-.30	< .001
R_Caudate	10, 12, 2		5.61/5.49	-.29	< .001
L_Parahippocampal	-26, -11, -32		4.93/4.84	-.26	< .001
R_Basal_Forebrain	5, 3, -7		4.75/4.68	-.25	< .001
R_Post_Hippocampus	31, -35, -7		4.16/4.11	-.22	.002
R_Parahippocampal	35, -28, -12		4.05/4.00	-.21	.002
L_Insula	-42, 13, -9		3.88/3.84	-.20	.003
L_Inf_Temporal	-49, -14, -33		3.88/3.84	-.20	.003
L_Sup_Temporal_Pole	-35, 9, -26		3.54/3.50	-.18	.008
L_Fusiform	-26, 6, -45		3.33/3.30	-.18	.01
R_Mid_Temporal	53, -12, -11	26552	4.64/4.56	-.24	< .001
R_Sup_Temporal	58, -9, 2	26552	4.43/4.37	-.23	< .001
R_Insula	45, -7, 4	26552	4.33/4.27	-.23	.001
R_Mid_Occipital	29 -70, 30	15837	3.91/3.86	-.21	.003

R_Inf_Temporal	52, -40, -20	1916	4.09/4.04	-.22	.002
L_Mid_Occipital	-29, -73, 29	17043	4.05/4.00	-.21	.002
L_Angular	-42, -61, 44		3.85/3.81	-.20	.004
L_Mid_Temporal	-47, -48, 20		3.61/3.57	-.19	.007
R_Precentral	45, 8, 52	1761	3.61/3.57	-.19	.006
R_Mid_Frontal	33, 14, 59		2.77/2.76	-.15	.03
R_Sup_Frontal	18, 11, 69	267	3.51/3.48	-.19	.008
L_Upper_Precuneus	-6, -49, 73	181	3.41/3.38	-.18	.01
L_Sup_Frontal	-26, 59, 23	186	3.39/3.36	-.18	.01
L_Lower_Precuneus	-3, -68, 44	791	3.30/3.27	-.18	.01
L_Crus_Cerebellum	-53, -59, -38	286	3.22/3.19	-.17	.02
L_Mid_Frontal	-42, 26, 45	248	3.10/3.08	-.16	.02
L_Calcarine	-8, -48, 5	184	3.07/3.05	-.16	.02
L_Inf_Parietal	-58, -41, 43	329	3.03/3.01	-.16	.02
R_Sup_Parietal	15, -53, 70	409	2.94/2.92	-.16	.03
L_Postcentral	-55, -17, 35	147	2.86/2.85	-.15	.03

The Main Effect of dementia masked for the Main Effect of WMHL is visible on the volume rendered picture in Figure 48. Unlike the unmasked Main Effect, where some small clusters of statistically significant voxels could be seen in the frontal lobe, the masked Main Effect exhibits a classic temporal-parietal pattern of brain atrophy seen most often in AD.

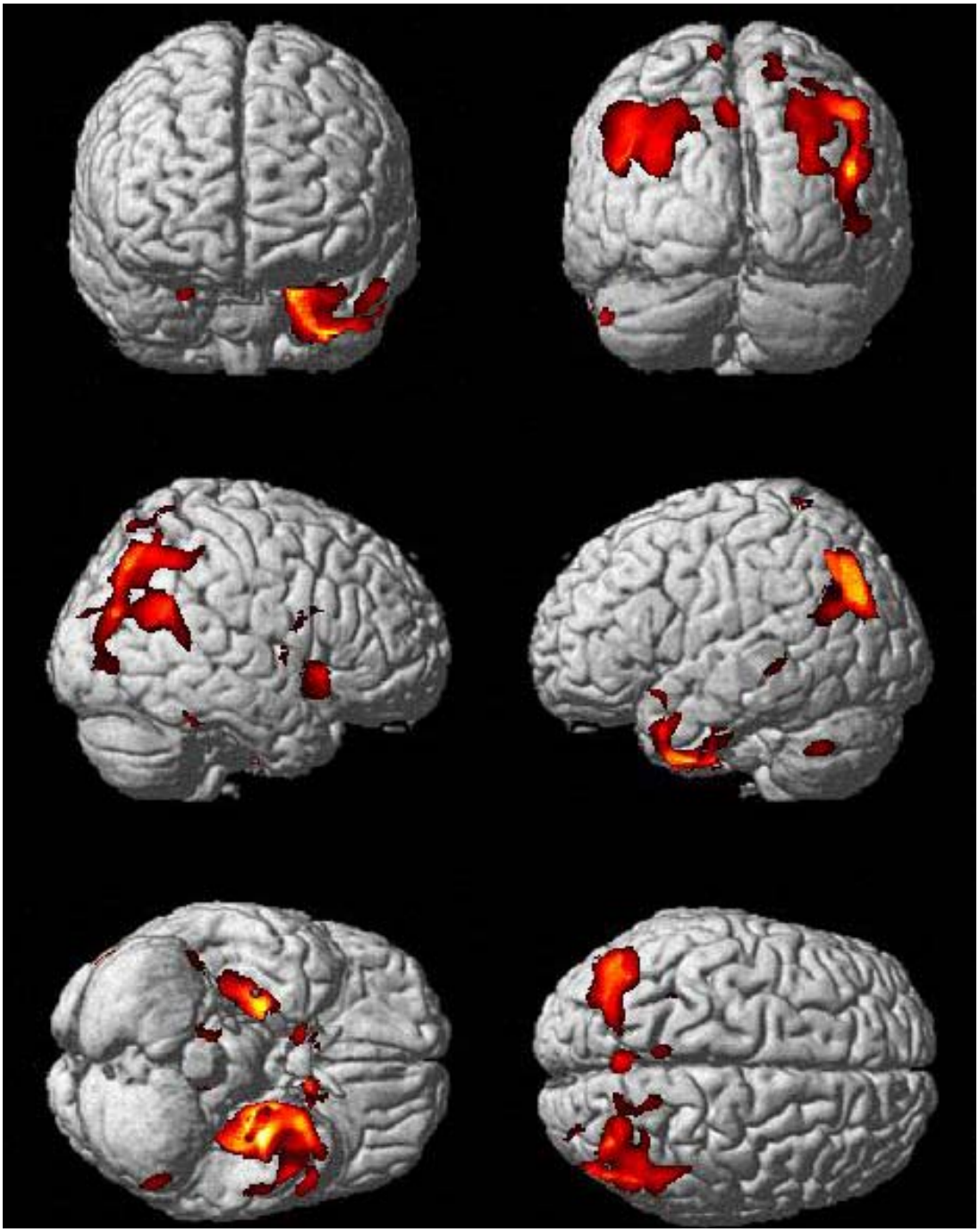

Figure 48: This figure shows the Main Effect of dementia on GM when masking out voxels that are also statistically significant for a WMHL Main Effect. The subsequent dementia main effect is representative of a typical temporal-parietal atrophy pattern seen most typical with AD in the temporal lobe, parietal lobe, and temporal-parietal junction.

Figure 49 shows the section rendering of the Main Effect of dementia atrophy masked for voxels also encompassed in a WMHL Main Effect. In viewing this, one can see that even after masking there is still dementia related atrophy in the left precuneus (part a, green arrow), caudate nuclei (part a, blue box), left anterior hippocampus (part b, crosshairs) and right anterior hippocampus (part c, cross hairs).

.

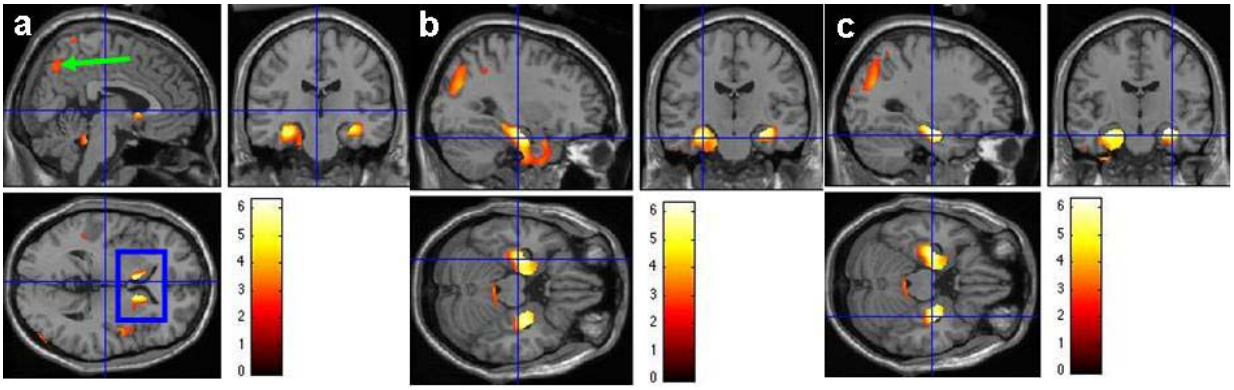

Figure 49: This figure shows the section rendered t-image of the Main Effect of dementia atrophy masked for voxels also encompassed in a WMHL Main Effect and projected onto the Standard Single Subject MNI Template. Table 26 shows the corresponding effect sizes.

Table 26 shows peak maxima of the dementia Main Effect with voxels affected by WMHL related atrophy masked out. Eight of the top ten effect sizes are in key strategic brain regions. In all, 9 of the peak maxima were located in key strategic brain regions.

Table 26: Peak Maxima of Dementia Atrophy Masked for WMHL Main Effects

Structure	Peak MNI Coordinates (x, y, z)	Cluster Volume (mm^3)	t/z scores	r^p value	P_{FDR}
R_Ant_Hippocampus	28, -13, -18	4195	6.33/6.16	-.32	< .001
R_Paraphippocampal	35, -28, -12	4195	4.05/4.00	-.21	.002

R_Post_Hippocampus	34, -36, -6	4195	3.89/3.84	-.20	.003
L_Ant_Hippocampus	-31, -15, -21	14860	6.01/5.85	-.31	< .001
L_Parahippocampal	-26, -11, -32	14860	4.93/4.84	-.26	< .001
L_Caudate	-9, 13, 2	1571	5.83/5.69	-.30	< .001
R_Caudate	10, 12, 2	1147	5.61/5.49	-.29	< .001
R_Putamen	22, 9, 0	1147	2.78/2.76	-.15	.03
R_Mid_Temporal	50, -50, 17	11662	4.41/4.35	-.23	.001
R_Sup_Temporal	48, -56, 23	11662	4.22.4.17	-.22	.001
R_Mid_Occipital	29, -70, 30	11662	3.91/3.86	-.21	.003
R_Insula	42, 14, -9	2227	4.21/4.16	-.22	.001
R_Inf_Frontal_Operculum	44, 10, 23	2227	3.15/3.13	-.17	.02
L_Mid_Occipital	-29, -73, 29	8789	4.05/4.00	-.21	.002
L_Angular	-42, -61, 45	8789	3.83/3.79	-.20	.004
L_Precuneus	-6, -9, 73	181	3.41/3.38	-.18	.01
R_Inf_Temporal	48, -42, -25	124	3.31/3.28	-.18	.01
L_Crus_Cerebellum	-53, -59, -38	286	3.22/3.19	-.17	.02
R_Sup_Parietal	15, -53, 70	402	2.94/2.92	-.16	.02
L_Inf_Parietal	-33, -50, 41	143	2.82/2.81	-.15	.03
L_Mid_Temporal	-50, -39, -1	154	2.67/2.65	-.14	.04

7.2.2 WMHL Main Effects in the Dementia Group

Figure 50 shows the Main Effect of WMHL in the 52 dementia subjects. There are lower GM volumes in relation to increasing WMHL in the frontal lobes, including the orbital frontal cortex.

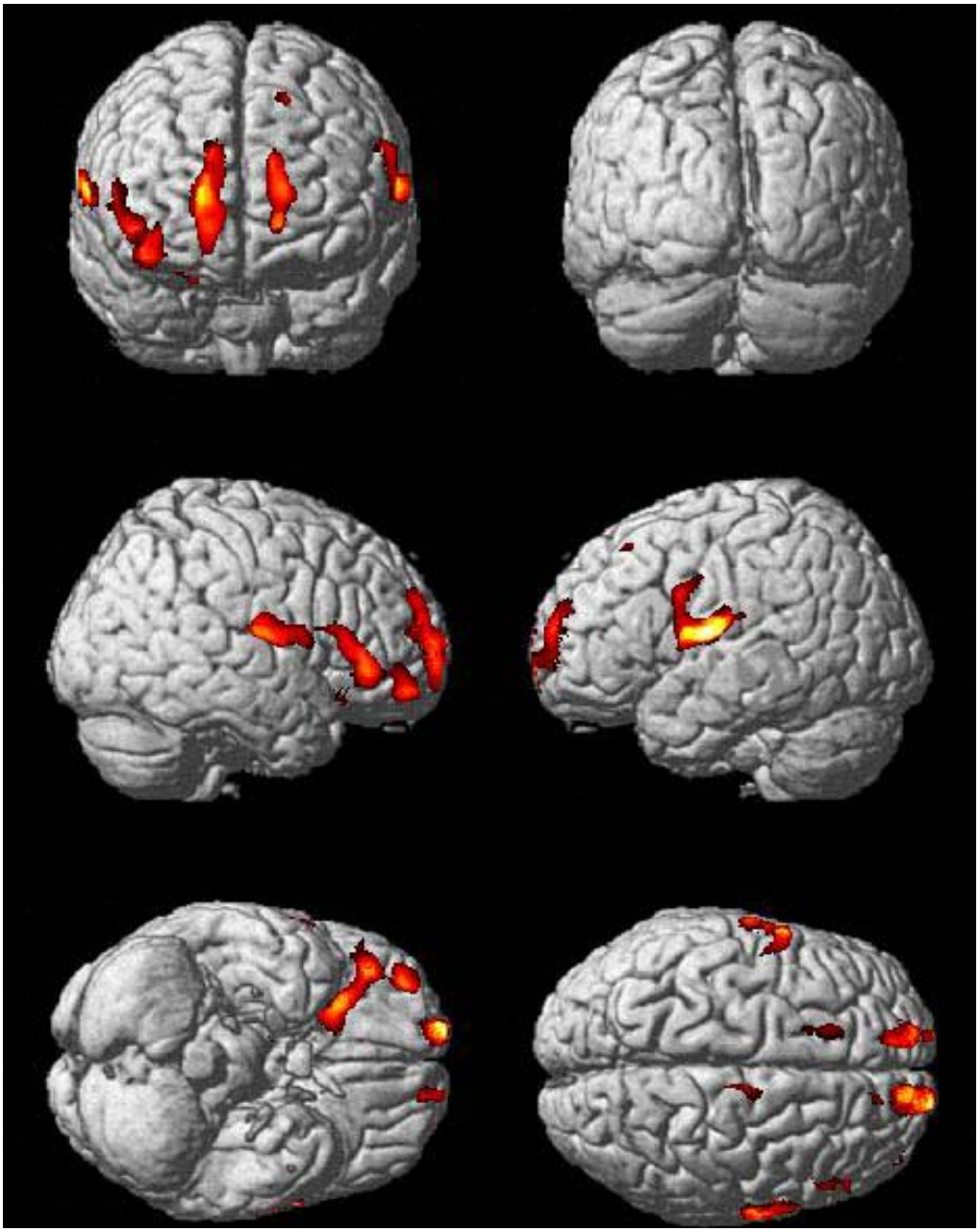

Figure 50: This figure shows the main effect of WMHL in only the dementia subjects.

Figure 51 shows the section rendered *r*-image of the Main Effect of WMHL in the dementia subjects. Part a shows that as WMHL increases in the dementia subjects, there is a decrease in GM volume in the right posterior cingulate and extending into the right precuneus (crosshairs). Part b shows a WMHL Main Effect in the right posterior hippocampus (crosshairs). Part c shows two boxes with a WMHL Main Effect. The red box is drawn around the left putamen and the blue box encompasses a WMHL Main Effect in the right thalamus.

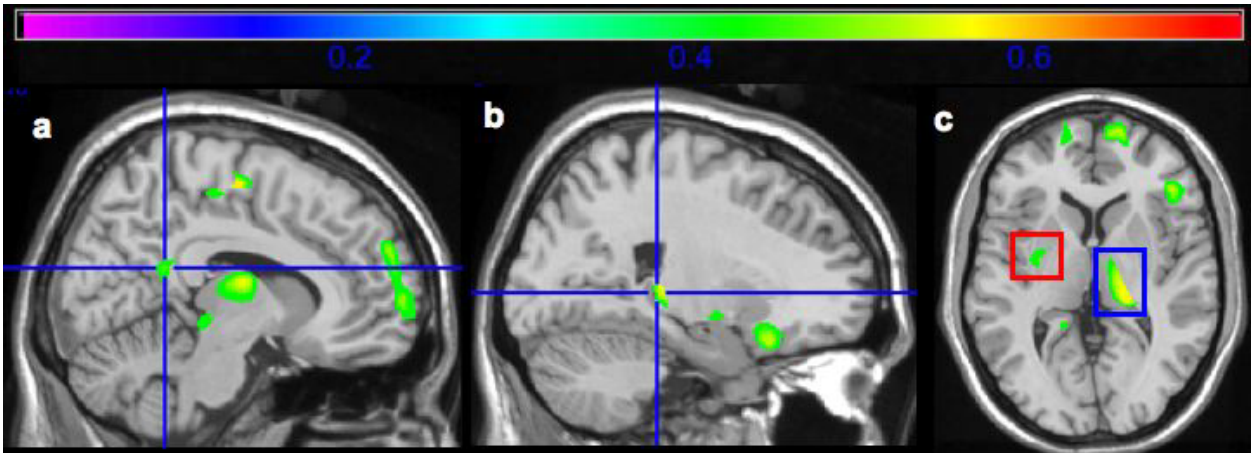

Figure 51: This figure shows the section rendered Main Effect of WMHL in the dementia subjects. WMHL are associated with atrophy in the right posterior cingulate/precuneus (part a, crosshairs), the right posterior hippocampus (part b, crosshairs), the left putamen (part c, red box) and the right thalamus (part c, blue box). Correlation effect sizes for these highlighted regions are provided in Table 27.

Table 27 displays statistical information on the peak maxima of the Main Effect of WMHL in the dementia subjects. Eight of the peak maxima were located in key strategic brain regions and are highlighted in bold.

Table 27: Peak Maxima for the WMHL Main Effect in the Dementia Group

Structure	Peak MNI Coordinates (x, y, z)	Cluster Volume (mm^3)	t/z scores	r^p value	P_{FDR}
R_Thalamus	16, -10, 16	4320	5.89/5.03	-.66	.01
L_Lingual	9, -30, -6		3.61/3.36	-.48	.03
R_Rolandic_Operculum	67, -7, 14	2165	5.45/4.74	-.63	.01
L_Rolandic_Operculum	-65, -6, 13	5016	5.27/4.62	-.62	.01
L_Precentral	-59, 5, 28		4.69/4.20	-.58	.01
R_Inf_Frontal_Trigone	44, 36, -1	6131	5.27/4.62	-.62	.01
R_Mid_Orbital_Frontal	41, 53, -14		4.76/4.25	-.58	.01
R_Insula	28, 24, -10		4.74/4.24	-.58	.01
L_Medial_Sup_Frontal	-15, 61, 12	2399	5.25/4.60	-.62	.01
L_Mid_Orbital_Frontal	-13, 62, 0		3.78/3.50	-.50	.02
L_Putamen	-25, -7, -6	1799	5.25/4.60	-.62	.01
R_Supp_Motor_Area	11, -12, 59	302	4.74/4.24	-.58	.01
R_Paracentral_Lobule	12, -28, 54		3.94/3.62	-.51	.02
R_Sup_Frontal	16, 64, 10	4332	4.63/4.16	-.57	.01
R_Sup_Orbital_Frontal	16, 67, -2		4.58/4.12	-.57	.01
R_Medial_Sup_Frontal	11, 58, 27		4.24/3.86	-.54	.01
R_Precuneus/R_Post_Cingulate	12, -49, 19	296	4.48/4.05	-.56	.01
L_Precuneus	-16, -43, 2	120	3.74/3.47	-.49	.03
R_Hippocampus	23, -32, 3	122	3.65/3.38	-.48	.03

7.2.3 WMHL Main Effects Masked for Dementia Main Effects

Figure 52 shows the Main Effect of WMHL in all 354 subjects (controls and dementia) with exclusive masking for the dementia Main Effects. Compared to the Main Effect of WMHL seen in Chapter 4, masking for dementia Main Effects results in comparatively less observable WMHL Main Effects in the temporal lobes.

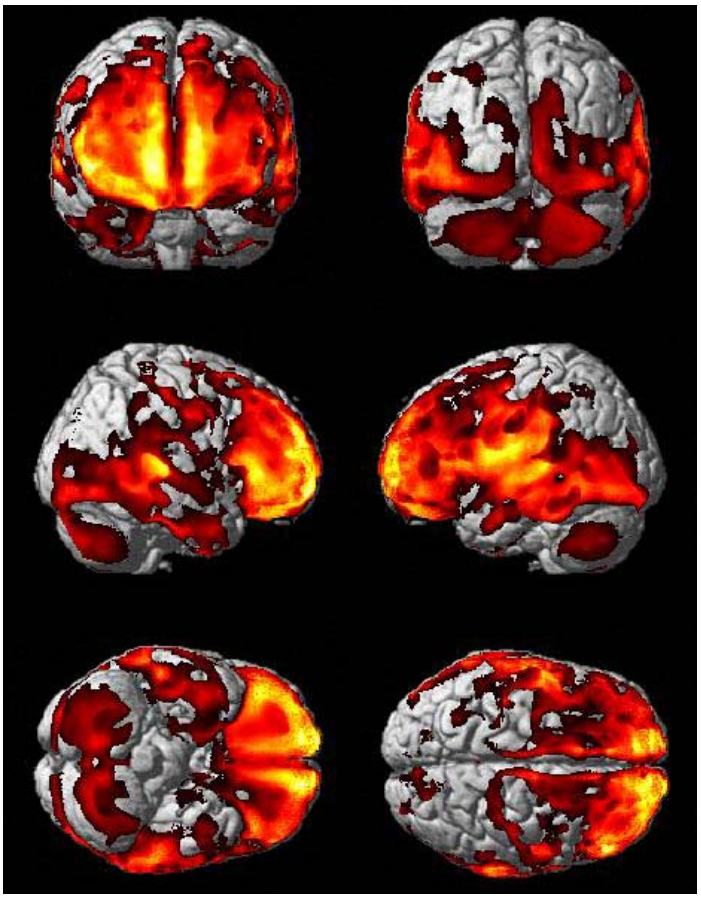

Figure 52: Main Effect of WMHL in a combined group of 302 controls and 52 demented subjects with voxels in which dementia related atrophy is statistically significant being masked out. The effect of this masking is seen mainly in the temporal lobes.

Figure 53 shows the section rendered image of WMHL related atrophy with dementia related atrophy masked out. Even when masking is applied, WMHL related atrophy is still observed in the posterior cingulate gyrus (part a, black arrow), the thalamus (part b, blue square), and the hippocampus (parts c and d, black arrows). The large effect sizes in the frontal lobes (part a) are still present as well after masking out dementia Main Effects.

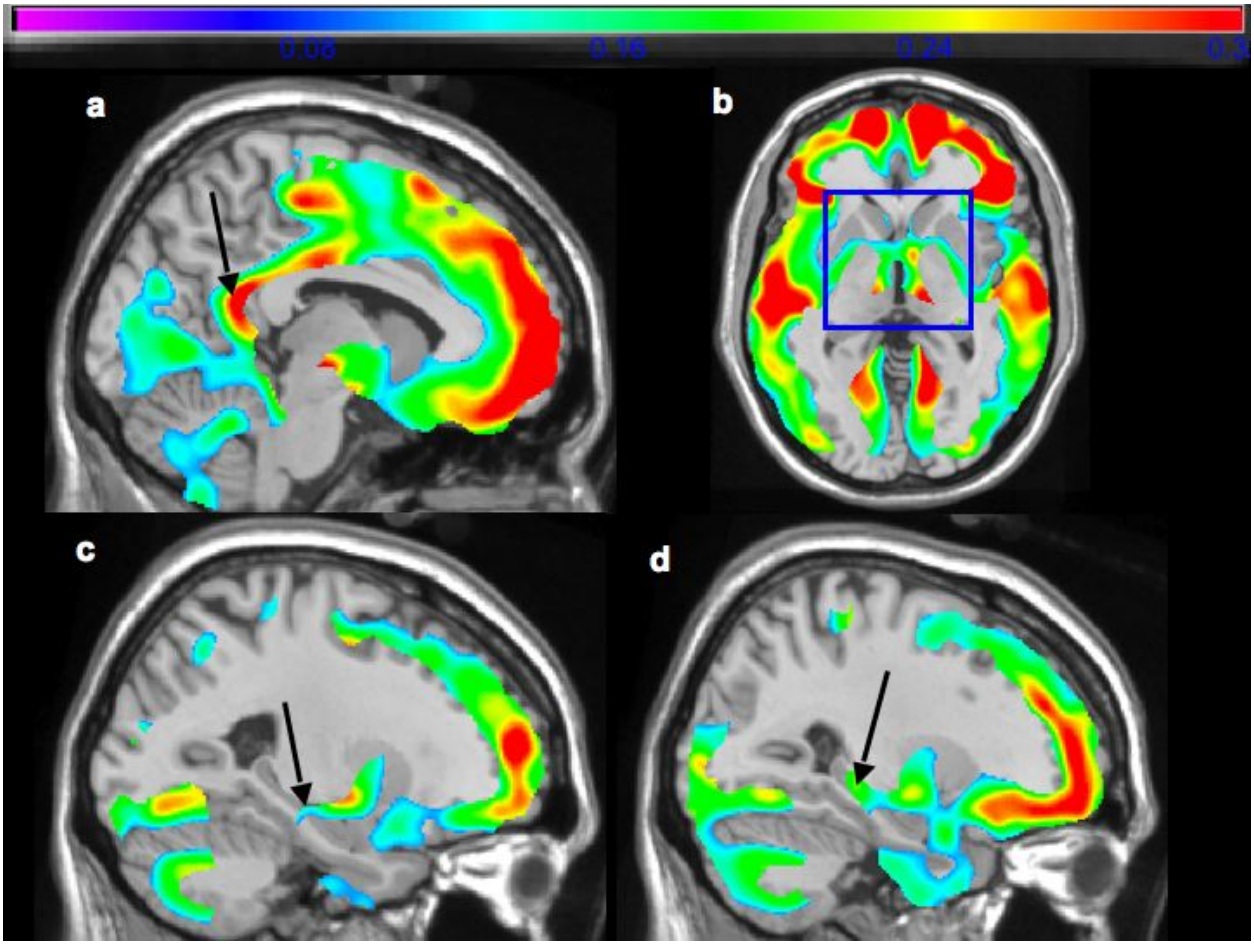

Figure 53: This figure shows the Main Effect of WMHL masked for the Main Effects of dementia. Even after masking for dementia Main Effects, a greater WMHL burden is associated with lower volumes in the posterior cingulate gyrus (part a), basal ganglia (part b, blue box), left middle hippocampus (part c, arrow), and right posterior hippocampus (part d, arrow).

Table 28 shows the peak maxima of the Main Effect of WMHL masked for dementia diagnosis. The orbital frontal cortex remains the as key strategic brain region most strongly affected by WMHL related atrophy. In all, peak maxima were located in 7 key strategic brain regions (all in bold) and these included the orbital frontal cortex, precuneus, and thalamus. The posterior cingulate gyrus was also affected by WMHL atrophy but was not a peak local maximum and is thus not listed in Table 28.

Table 28: Main Effect of WMHL on GM masked for Dementia Main Effects

Structure	Peak MNI Coordinates (x, y, z)	Cluster Volume (mm^3)	t/z scores	r^p value	P_{FDR}
L_Medial_Sup_Frontal	-15, 61, 13	501285	9.38/9.35	-.45	< .001
R_Sup_Frontal	16, 66, 2	501285	9.31/9.28	-.45	< .001
L_Mid_Orbital_Frontal	-11, 61, -2	501285	9.13/9.10	-.44	< .001
R_Inf_Frontal_Trigone	52, 34, 1	501285	9.04/9.02	-.44	< .001
R_Mid_Orbital_Frontal	10, 66, -8	501285	9.00/8.97	-.44	< .001
L_Rolandic_Operculum	-59, -1, 14	501285	8.98/8.88	-.43	< .001
L_Postcentral	-56, -13, 26	501285	8.93/8.81	-.43	< .001
R_Med_Sup_Frontal	11, 59, 27	501285	8.47/8.40	-.41	< .001
L_Mid_Cingulate	-12, -10, 46	501285	8.36/8.34	-.41	< .001
R_Supp_Motor_Area	9, -19, 57	501285	8.33/8.29	-.41	< .001
L_Inf_Frontal_Trigone	-51, 27, 11	501285	8.18/7/80	-.40	< .001
R_Precuneus	10, -50, 18	501285	7.83/7.50	-.39	< .001
L_Inf_Orbital_Frontal	-34, 29, -4	501285	7.80/7.48	-.39	< .001

L_Sup_Temporal	-39, -28, 7	501285	7.76/7.45	-.39	< .001
R_Inf_Orbital_Frontal	40, 37, -12	501285	7.73/7.42	-.38	< .001
L_Mid_Temporal	-59, -33, 6	501285	7.73/7.41	-.38	< .001
R_Sup_Temporal	66, -23, 4	501285	7.69/7.39	-.38	< .001
R_Heschl	35, -24, 14	501285	7.61/7.31	-.38	< .001
R_Thalamus	17, -21, 0	149	6.81/6.59	-.34	< .001
L_Thalamus	-17, -14, 12	141	5.64/5.51	-.29	< .001
R_Supramarginal	63, -35, 43	859	5.00/4.91	-.26	< .001
L_Sup_Parietal	-28, -60, 50	1117	3.60/3.56	-.19	.001
L_Inf_Parietal	-30, -43, 54	1117	2.32/2.31	-.12	.02

7.2.4 Conjunction between WMHL and Dementia Main Effects

The surface rendering of the conjunction between WMHL and dementia Main Effects on GM are seen in Figure 54. Dementia and WMHL co-occur in the right temporal lobe and mesial temporal lobe.

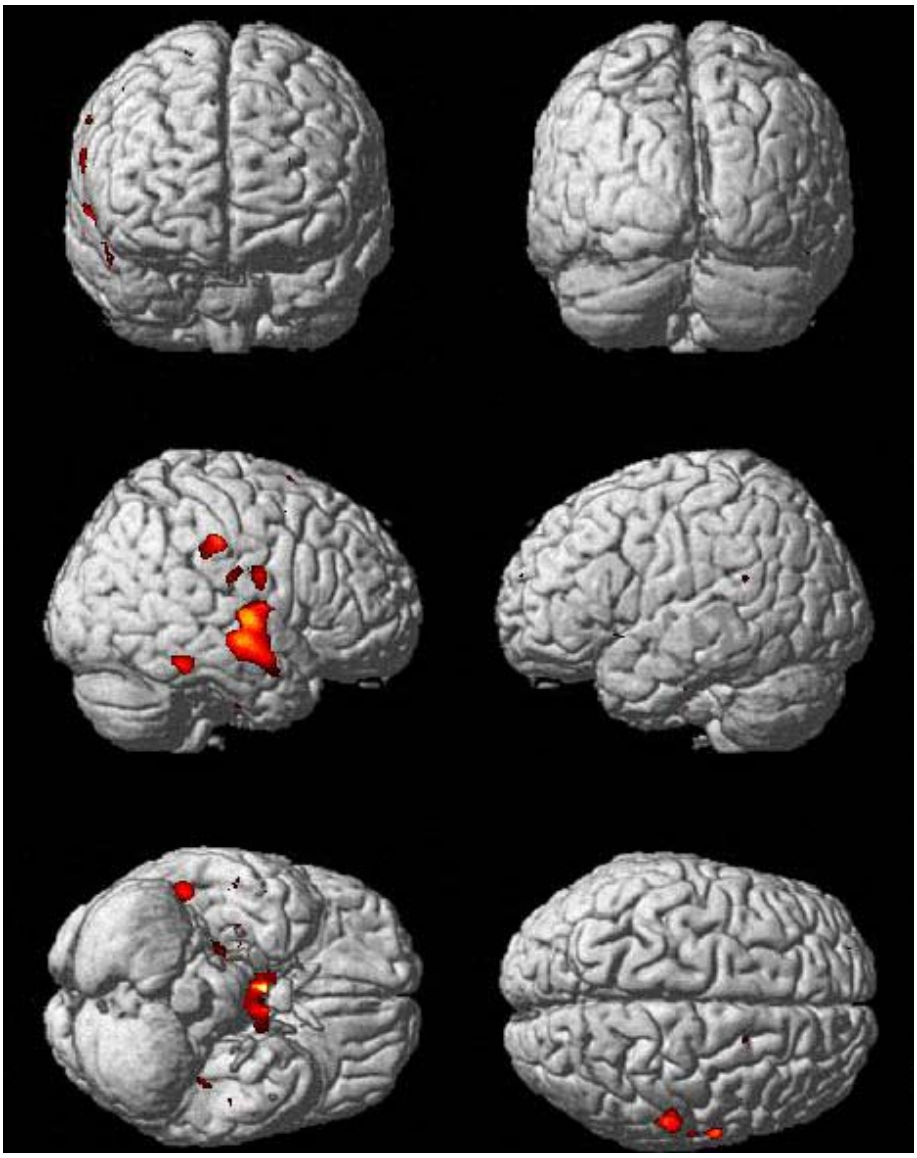

Figure 54: This figure shows that the conjunction between WMHL and dementia Main Effects in GM are seen mainly the right temporal lobe and the mesial temporal lobe.

Figure 55 shows section renderings of several conjunctions between the Main Effects of WMHL and dementia on GM. Part a shows a small conjunction between WMHL and dementia atrophy in the right middle hippocampus (crosshairs). Part b shows a conjunction in the right basal forebrain substantia innominata area (red arrow) and the thalamus (green box).

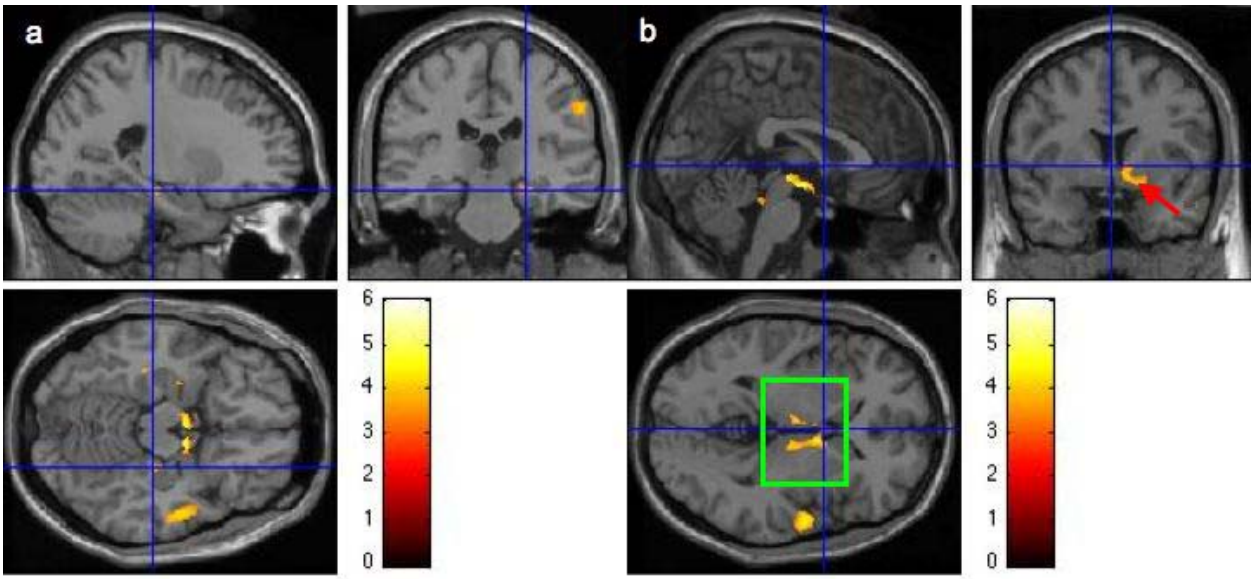

Figure 55: This figure shows section rendered t-images of the conjunctions between the Main Effects of WMHL and dementia on GM projected onto the Standard Single Subject MNI template.

Peak maxima for the conjunction between WMHL and dementia is shown in Table 29. In this case, cluster specific local maxima are listed for any clusters above 100 voxels as the overall conjunction effect is relatively focal in distribution. The top two peak maxima for the overlap between dementia and WMHL related atrophy are in the left and right anterior hippocampus respectively. The hippocampus was the only key strategic brain regions identified in this analysis. There was no interaction between WMHL and Dementia Main Effects in GM.

Table 29: Peak Maxima of the Conjunction between WMHL and Dementia Atrophy

Structure	Peak MNI Coordinates (x, y, z)	Cluster Volume (mm^3)	t/z scores	r^p value	P_{FDR}
L_Ant_Hippocampus	-27, -12, -11	3868	4.33/4.27	-.23	.01
R_Ant_Hippocampus	27, -10, -12	3868	4.02/3.97	-.21	.02
R_Amygdala	23, -7, -13	3868	3.62/3.59	-.19	.03
L_Amygdala	-17, 1, -12	3868	3.50/3.47	-.19	.04
R_Sup_Temporal	52, -9, -12	4273	4.50/4.43	-.24	.01
R_Mid_Temporal	54, -15, -9	4273	4.44/4.37	-.23	.01
R_Heschl	52, -5, 6	4273	3.93/3.89	-.21	.02
R_Rolandic_Operculum	46, -5, 11	4273	3.77/3.73	-.20	.03
R_Inf_Temporal	52, -40, -20	442	4.09/4.04	-.22	.02
R_Supramarginal	58, -25, 38	621	4.05/4.00	-.21	.02
R_Post_Hippocampus	29, -33, -6	115	3.82/3.77	-.20	.03
R_Postcentral	63, -4, 22	324	3.79/3.75	-.20	.03

This chapter had several major findings. First, the GM atrophy seen in demented CHS-CS subjects follows a pattern of temporal-parietal atrophy most appreciated when WMHL Main Effects are masked out. Second, WMHL Main Effects still target AD specific structure such as the precuneus even when the Main Effects of dementia on GM are masked out. Third, both WMHL and dementia Main Effects are jointly significant in areas relevant to AD pathology, especially the anterior hippocampus and the basal forebrain. The lack of an interaction of

dementia related brain atrophy suggests that WMHL might not play as important a role in later stage neurodgeneration than in a comparatively earlier time point, as was seen with MCI. However, the fact that WMHL are correlated in lower GM volumes even in dementia subjects, and that the areas affected include brain regions targeted by neurodegeneration, namely the hippocampus, suggests that prevention or better treatment of hypertensive vascular disease may lessen the magnitude of brain atrophy seen in dementia. The contribution of this chapter's data to the model is displayed in Figure 51.

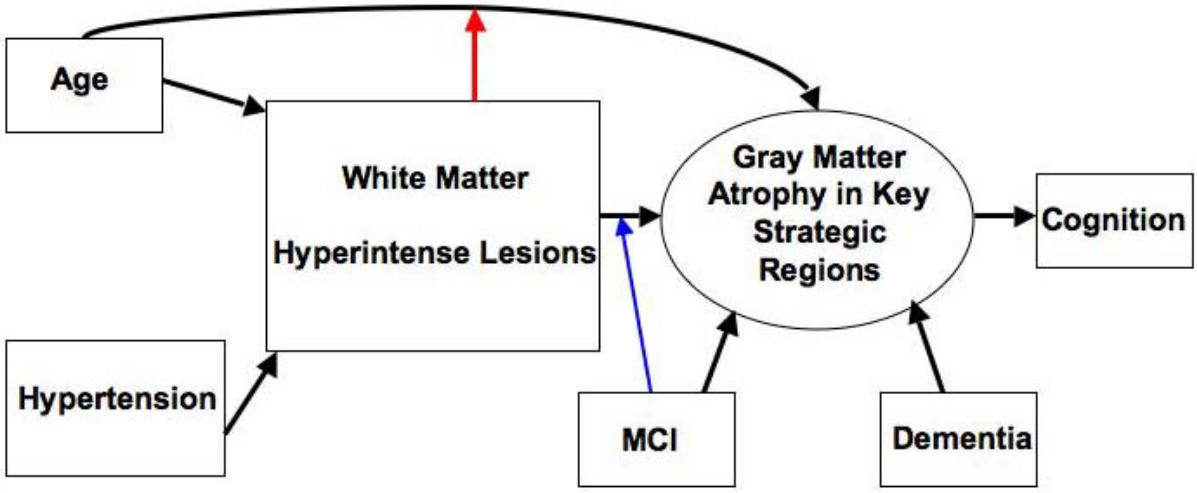

Figure 56: This figure shows the contribution to the overall model by chapter 7 data. This can be seen in the Dementia box in the far right lower corner of the figure. The arrow drawn from that box to gray matter volume loss represents both the conjunction of WMHL and dementia effects on GM, specifically the hippocampus, and the predictive power of WHML on lower gray matter volumes in only the dementia subjects.

This concludes all chapters focused on the structural aspect of vascular disease Main Effects on GMVL in the context of aging, MCI, and dementia. Chapter 8 will focus on the relationship between vascular disease and brain function, as assessed with perfusion MRI with an ASL pulse sequence. Rather than use WMHL as a proxy of vascular disease, as such measures

were not taken at the time of the perfusion MRI, the relationships examined will be between cerebral perfusion and hypertension, which was identified in Chapter 3 as a main predictor of WMHL. Other variables such as age and comorbid MCI and dementia will also be examined.

8.0 HYPERTENSION IS ASSOCIATED WITH LOWER PERFUSION IN BRAIN REGIONS RELEVANT TO NEURODEGENERATIVE DISEASE

8.1 INTRODUCTION

To this point, I have shown how vascular disease, as indexed by WMHL, is strongly associated with atrophy in key strategic brain areas. The WMHL I have used in these analyses are predicted by HTN. HTN is most commonly believed to result in WMHL through ischemic/embolic events in the brain (213, 214) and this is frequently facilitated through damage to the cerebral blood vessels itself. All of these processes have the effect of reducing regional cerebral blood flow (rCBF). Thus, a potential sequence of events by which long-standing HTN could lead to brain atrophy is damage to cerebral blood vessels leading to rCBF reductions. These reductions in rCBF can subsequently lead to ischemic changes most characteristic of WMHL that in turn have been shown to be strongly associated with gray matter volume loss. What this chapter will seek to establish is the relationship between HTN and lower rCBF as evaluated with ASL MRI. The main reason for examining HTN as opposed to WMHL is that data on HTN was available at far more time points in the CHS, including the year of ASL scan, but this was not the case for CHS scales of WMHL. Another reason for foregoing WMHL correlations with perfusion is because they may be an effect rather than a cause of lower rCBF (42, 215, 216) whereas HTN is more likely a viable etiological candidate for lower rCBF.

8.1.1 Evidence for a Relationship between HTN and Lower rCBF

A small number of neuroimaging studies suggest that long-standing HTN is associated with lower rCBF. Dai and colleagues compared ASL MRI scans between 19 hypertensive cognitively normal individuals with HTN for an average of 30 years from CHS-CS and 22 normotensive counterparts (217). Using voxel-level analyses, they found that the HTN group had lower rCBF compared to the non-HTN group in such key strategic brain regions as the anterior cingulate gyrus, left posterior cingulate, with extension into the medial precuneus, and left middle hippocampus. A longitudinal 7 year study of 14 cognitively normal persons with HTN and 14 age-matched control used biannual O^{15} –water PET scans to show decreased rCBF in the middle and inferior prefrontal cortex, anterior cingulate gyrus, and occipital-temporal cortices in the HTN group (218). PET imaging studies conducted in middle-aged cognitively normal subjects with HTN showed a pattern of reduced resting rCBF (113, 114), as well as less activation in the thalamus when engaged in memory tasks than normotensives. Another study showed is also decreased metabolism in the striatum and thalamus in HTN (219, 220). These studies suggest that HTN, either short term or long standing, is associated with perfusion reductions in key strategic brain regions. The work presented in this chapter will extend this field by examining that question in 74 control, MCI, and demented subjects scanned in the CHS-CS with ASL MRI. Most importantly, the analyses presented in this chapter will extend my thesis by showing that HTN, which is the underlying vascular disease that targets brain structure, also adversely affects brain function – specifically cerebral perfusion. If this assertion is verified with the data analyzed it will suggest an important mechanism by which HTN can lead to atrophy in key strategic regions of the brain.

8.1.2 ASL Imaging Evidence of Lower rCBF in MCI and Dementia.

Several ASL imaging studies suggest that clinical syndromes associated with neurodegeneration such as MCI and dementia are linked to lower rCBF. Dai and colleagues compared the extent of rCBF reductions in MCI (n = 19) and AD (n = 15) compared to cognitively normal controls (n = 19). Both MCI and AD subjects had lower rCBF in the posterior cingulate gyrus that extended into the medial precuneus (221). MCI subjects had a statistically significant *increase* in rCBF, or hyperperfusion, in left hippocampal, right amygdala, right head of the caudate nucleus, ventral putamen, and globus pallidus compared to controls. The majority of these subjects were right handed. AD subjects had lower rCBF compared to MCI and control subjects in the left inferior parietal, left lateral frontal, left superior temporal, and left orbital frontal cortices. Persons with AD had increased rCBF compared to controls only in the right anterior cingulate gyrus.

The hippocampal hyperperfusion findings from the Dai study were also observed in a study of 22 AD subjects compared to 16 controls, albeit these findings were not statistically significant (182). This same study found lower rCBF in bilateral precuneus, parietal association cortex and the left inferior temporal lobe in the AD subjects. An ASL study of 20 persons with AD, 18 with MCI and 23 cognitively normal subjects showed that persons with AD had lower rCBF in right inferior parietal lobe extending into the bilateral posterior cingulate gyri and left and right middle frontal gyri (181). This study, however, did not reveal any statistically significant differences between the MCI group and the control and AD groups. Finally, a study of 18 AD subjects and 11 age-matched controls showed statistically significant perfusion declines in temporal, parietal, frontal, and posterior cingulate cortices (179). Mini-Mental State

Examination in the AD subjects correlated most strongly with posterior parietal and posterior cingulate decreases but not temporal decreases. These studies suggest that the perfusion alterations can be observed in MCI and dementia, making it the most logical covariate in examining the Main Effects of HTN on cerebral perfusion using ASL MRI with my analyses since I will be examining rCBF in controls, MCI, and dementia subjects. The next section will overview the specific methods for subject selection ASL MRI image processing, including missing data analysis, and SPM statistical modeling.

8.2 METHODS

Basic methods for subject selection and ASL image processing have also been described extensively elsewhere (217, 221) but are briefly discussed here, with additional methods of missing data analysis included. In all, 74 subjects were available for analysis and had both ASL and SPGR imaging acquired in 2002/2003: 30 with HTN and 44 without. Subject demographics are outlined in Table 30 and include distribution of the 30 control normals, 21 MCI, and 23 dementia subjects. There were no statistically significant differences between non-HTN and HTN persons in terms of age, gender, education, distribution of control, MCI, and dementia subjects or any of the other variables examined.

Table 30: This table shows the demographic characteristics of non-HTN versus HTN subjects in the CHS-CS

Variable	Non-HTN (n = 44)	HTN (n = 30)	T-test(t, p)/χ^2
Age	82.9 ± 3.47	83.2 ± 3.68	-.34, .74
Gender (F)	52% (23)	57% (17)	.20, .80
Education (12^{th} Grade only)	34% (15)	37% (11)	.05, 1.0
Race	18% (8)	36% (11)	3.19, .07
Infarcts at MRI2	18% (8)	17% (5)	.02, 1.0
WMG at MRI2 (1997-1999)	2.21 ± 1.49	2.63 ± 1.41	-1.17, .25
Controls/MCI/Dementia	36%(16)/ 32%(14)/32%(14)	46.7%(14)/ 23.3%(7)/30%(9)	.93, .63

8.2.1 ASL MRI Image Processing

ASL image processing involves a series of steps designed to obtain perfusion values in GM. First, each ASL MRI scan was coregistered (with no reslicing) to its corresponding SPGR scan in its native (not normalized) space in SPM2. Second, manual tracing was done in MATLAB to remove the skull from the ASL scan but not from the SPGR. After using the phase-contrast derived flow velocities to exclude persons with a greater than 20% difference in blood flow velocities between both carotid arteries, rCBF was calculated using a modified Buxton kinetic model (222). Next, a fully deformable method for registration method (223) was used to

normalize both ASL and SPGR scans to the Standard Single Subject MNI template. The fully deformable method uses a higher dimensional algorithm than that used with SPM2 (224, 225). Consequently, a higher resolution template is needed for normalization than is the case with the Pittsburgh Elderly Brain template. Since the Standard Single Subject MNI template is the highest resolution image available for such a purpose and most widely available to researchers, this was the image employed for registration purposes. As part of the fully deformable registration method, a 6 mm smoothing filter was applied. This smaller smoothing filter was chosen due to i) The higher dimension normalization algorithm used ii) It corresponds roughly to the cross sectional dimensions of the hippocampus and thus increases the sensitivity for hippocampal findings in the relatively small number of 74 subjects examined in this chapter.

8.2.2 Missing Data and ASL MRI Image Analysis

Missing data in ASL MRI can occur because the signal of the endogenous tracer may degrade before it reaches certain areas of the brain such as the inferior temporal lobes (226). Such issues are not typically addressed in the literature (174) but warrant consideration. Thus, missing data was accounted for in ASL image analysis using the following steps. First, gray matter from the Standard Single Subject MNI template was segmented in SPM2 and used as a mask to define missing voxels in ASL MRI data. The Standard Single Subject MNI template was used because it was the template utilized for normalization and only GM from this template was used because ASL perfusion provides information on GM perfusion. This mask, segmented in SPM2, is shown in Figure 57.

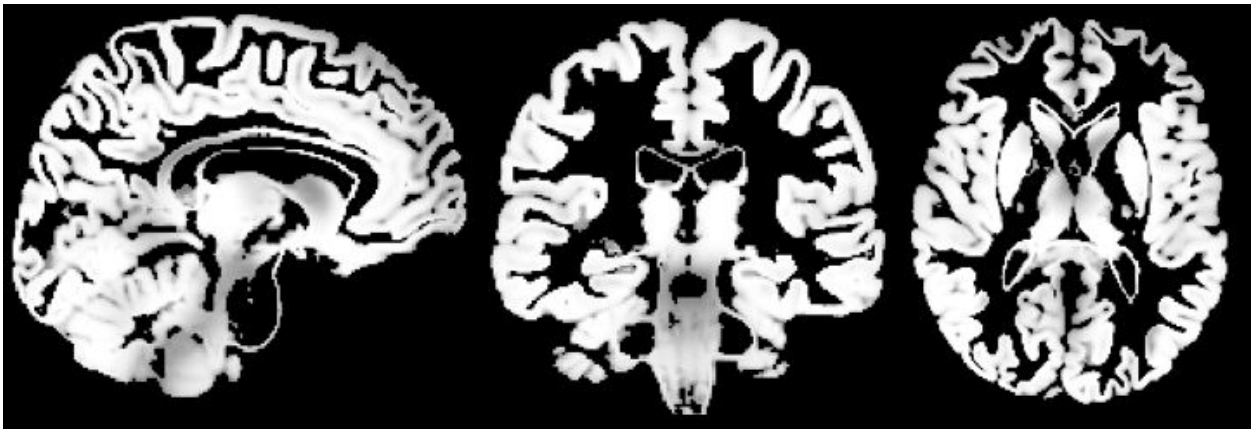

Figure 57: This figure shows the GM mask used for missing ASL MRI data analysis. The mask is segmented GM from the Standard Single Subject MNI template.

The main criterion for defining whether or not a perfusion voxel was missing was to examine all 74 ASL images: If greater than 10% of these images lacked a voxel in the above GM mask, that voxel was considered to be missing data. From this data a mask was created of missing ASL perfusion voxels that could then be used in SPM analyses as an exclusive mask (i.e. voxels in those brain areas with missing perfusion voxels would be excluded from the analysis. This mask is shown as an overlay onto the Standard Single Subject MNI template in Figure 58. The regions with missing data are the cerebellum, periventricular areas, GM/WM border, and the inferior temporal lobe. However, key strategic brain regions such as the hippocampus, posterior cingulate, and precuneus have intact data. Thus, this assures me that ASL MRI can be reliably employed in the statistical models I am about to describe.

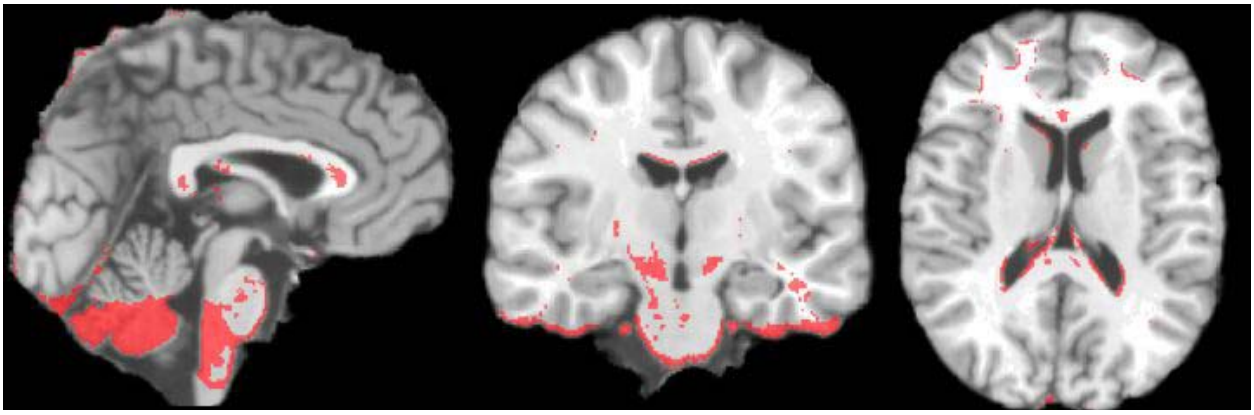

Figure 58: This figure shows areas of missing perfusion data at the voxel level in greater than 10% of the 74 subjects scanned with ASL MRI projected as a red color map onto the Standard Single Subject MNI template. The sagittal view shows how much missing data is observed in inferior cerebellum but not in the frontal lobes, posterior cingulate gyrus or precuneus. The coronal view shows missing perfusion data in the inferior temporal lobes but not in the hippocampus. Finally, the axial view shows missing voxels in the GM/WM border and periventricular areas.

8.2.3 Statistical Models in SPM for Analysis of HTN Effect on rCBF

The analysis was done in three ways. The first was to correlate a binary categorical diagnosis of HTN with rCBF while controlling for MCI and dementia. The second was to correlate systolic and diastolic blood pressures separately with rCBF while also adjusting for MCI and dementia. The systolic and diastolic blood pressures were taken from baseline study entry in 1989, because blood pressure taken the furthest before the scan is more likely to reflect the long term burden of HTN in the brain as opposed to a value taken during the year of scan.

Separate tests of the Main Effects of age, gender, race, Cystatin C - marker of glomerular function, education, MRI infarcts, WMHL, interleukin 6, heart disease (as defined by medical history of myocardial infarction or congestive heart failure), serum creatinine, left cardiac ventricular mass as assessed on echocardiogram, serum beta amyloid (both 40 and 42 amino acid

lengths), intima-media thickness, systolic blood pressure from year of ASL MRI scan, diastolic blood pressure form year of ASL scan, and APOE4. All of these variables were gathered using standard CHS methods (36, 37, 62, 154-156, 168, 227). Each variable was entered as a variable in a multiple regression model with MCI/dementia classification as the only other covariate. If no Main Effect could be seen with an uncorrected threshold of $p < .001$ (FDR = 15%) then that variable was not used as a covariate in the statistical analysis of HTN and blood pressure effects on the brain. None of the listed variables had a Main Effect on perfusion, even when the classification of MCI/dementia was removed as a covariate and the analyses were re-run as simple bivariate correlations with rCBF. Consequently, none of them were included as covariates in the analysis of HTN and baseline SBP and DBP Main Effects. Thus, the statistical analyses done were to separately identify the Main Effects of HTN, baseline SBP, and baseline DBP all controlling for MCI and dementia. All of these analyses were done as multiple regressions in SPM2 as previously described.

Correcting for multiple comparisons was done using an FDR threshold set at a comparatively liberal threshold of 15%, meaning if a map has cluster of 30 statistically significant voxels (the extent threshold used), approximately 26 of them are valid and not false positives. This was done mainly because the sample size of the ASL images used was relatively low compared to what was used for structural analyses. Thus, as a compromise between being sensitive to statistically significant statistical effects, an FDR of $p = .15$ was adopted for ASL analyses. This approach was done based upon prior published literature in which an uncorrected threshold was used for voxel based ASL MRI analyses in AD (182). Results are overlaid onto the Standard Single Subject MNI template using methods described in Chapter 2.

8.3 RESULTS

8.3.1 Main Effect of HTN as a Binary Variable on rCBF

The Main Effect of HTN as a binary variable, controlling for comorbid MCI and dementia, is shown in Figure 59. This figure shows areas of lower rCBF in HTN persons compared to non-HTN persons in frontal lobes, including the orbital frontal cortex, and the temporal lobes.

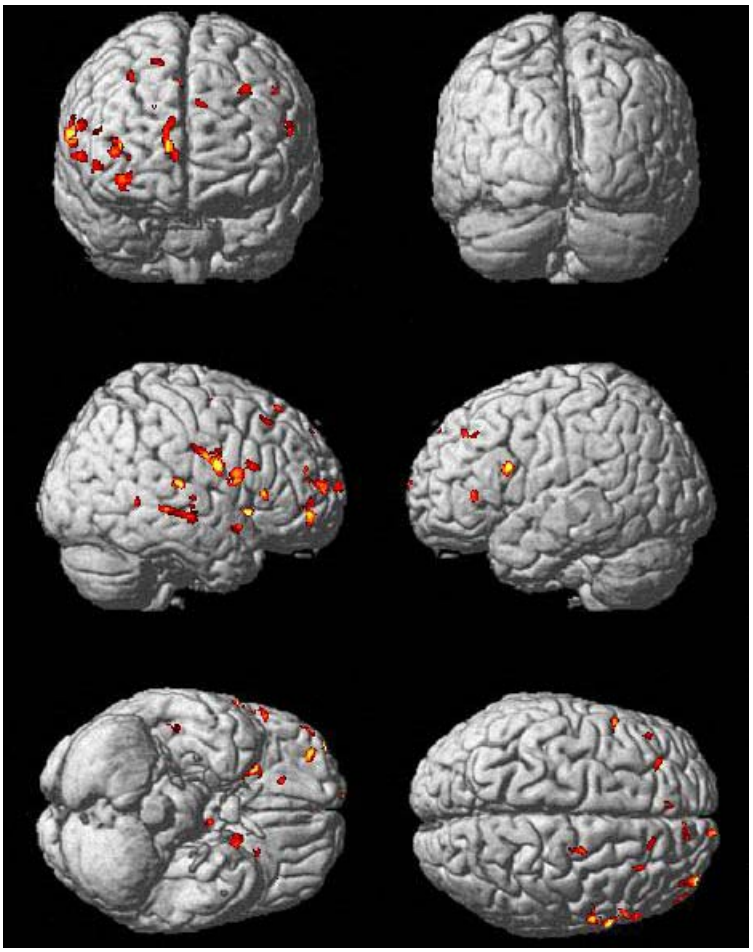

Figure 59: This figure shows the Main Effect of HTN on rCBF in 74 CHS-CS subjects projected onto the Standard Single Subject MNI template ($p_{uncorrected}$ = .001, FDR < .15, k = 30). Persons with HTN have lower perfusion in the frontal and temporal lobes as visible from this surface rendering.

Figure 60 shows the Main Effect of HTN projected onto the Standard Single Subject MNI template ($p_{uncorrected} < .001$, FDR < .15, k = 30). Part a shows that HTN is associated with lower rCBF, even when controlling for comorbid MCI and dementia, in such key strategic brain areas as the left posterior cingulate. Part b shows a similar effect in the left anterior cingulate. Part c shows three areas of HTN associated reduction in rCBF relative to the non-HTN group. The crosshairs show lower rCBF in association with HTN in the right anterior cingulate gyrus. The red arrow points to a Main Effect of HTN on rCBF in the right posterior cingulate and the green arrow points to a similar effect in the right precuneus. All related statistics are provided in Table 31.

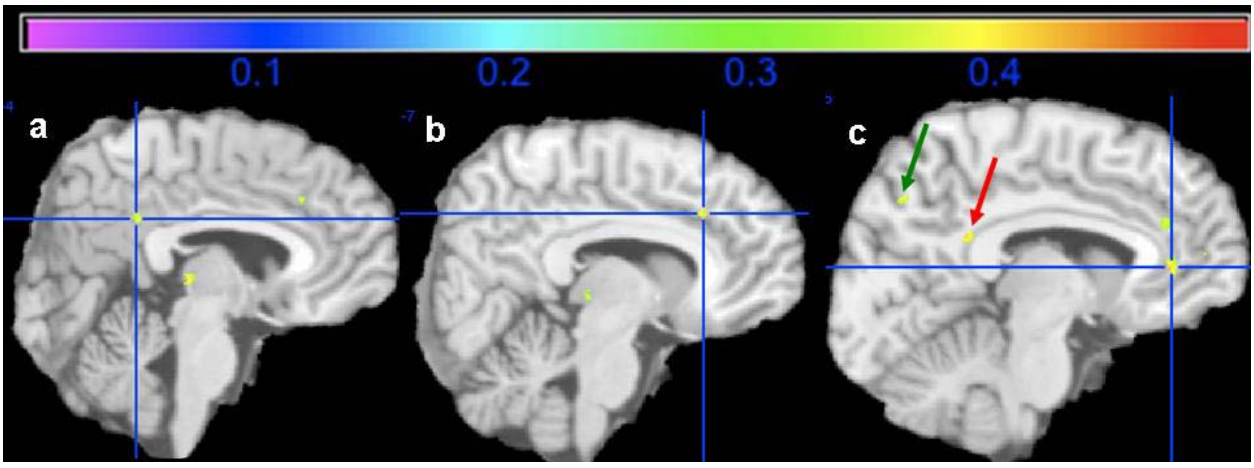

Figure 60: This figure shows lower rCBF in the HTN group compared to non-HTN subjects. All related statistics are provided in Table 31. Key strategic brain areas have lower rCBF in relation to HTN, as fully described in text.

Table 31 shows peak maxima of the HTN Main Effect in rCBF. Eleven of these peak maxima are located in key strategic brain regions. These include the putamen, orbital frontal cortex, anterior cingulate, posterior cingulate, precuneus and the thalamus.

Table 31: Peak Maxima of HTN Main Effects on rCBF. Key strategic brain regions are highlighted in bold.

Structure	Peak MNI Coordinates (x, y, z)	Cluster Volume (mm^3)	t/z scores	r^p value	$P_{uncorrected}$
R_Precentral	62, 10, 17	394	4.87/4.50	-.50	< .001
R_Rolandic_Operculum	58, 5, 12	394	3.64/3.47	-.40	< .001
R_Putamen	31, 6, -9	1880	4.81/4.46	-.50	< .001
R_Insula	27, 18, -16	1880	4.34/4.07	-.46	< .001
R_Sup_Temporal	47, -16, 3	147	4.66/4.34	-.48	< .001
R_Mid_Temporal	47, -28, -4	1084	4.51/4.22	-.47	< .001
R_Postcentral	60, -1, 22	800	4.52/4.23	-.47	< .001
L_Inf_Frontal_Operculum	-54, 12, 31	275	4.43/4.15	-.46	< .001
R_Mid_Frontal	37, 61, 11	479	4.40/4.13	-.46	< .001
L_Sup_Orbital_Frontal	-14, 9, -20	209	4.40/4.12	-.46	< .001
R_Medial_Sup_Frontal	12, 69, 11	108	4.15/3.91	-.44	< .001
R_Mid_Orbital_Frontal	35, 52, -7	269	4.06/3.84	-.43	< .001
R_Inf_Frontal_Trigone	57, 26, 6	135	4.04/3.82	-.43	< .001
L_Insula	-35, 11, 8	133	4.03/3.81	-.43	< .001

L_Inferior_Frontal_Trigone	-37, 31, 5	191	3.91/3.71	-.42	< .001
R_Sup_Temporal_Pole	46, 10, -14	95	3.85/3.66	-.42	< .001
R_Post_Cingulate	9, -30, 20	107	3.81/3.62	-.41	< .001
L_Sup_Frontal	-12, 72, 37	68	3.78/3.59	-.41	< .001
R_Ant_Cingulate	8, 55, 6	418	3.76/3.57	-.41	< .001
L_Putamen	-23, 21, -7	80	3.74/3.56	-.40	< .001
L_Mid_Frontal	-46, 31, 41	41	3.73/3.55	-.40	< .001
L_Thalamus	-4, -7, 0	79	3.71/3.53	-.40	< .001
R_Sup_Frontal	14, 34, 56	72	3.63/3.46	-.40	< .001
L_Ant_Cingulate	-7, 43, 34	66	3.63/3.46	-.40	< .001
R_Mid_Occipital	36, -54, 33	98	3.62/3.46	-.39	< .001
R_Sup_Orbital_Frontal	19, 35, -14	68	3.60/3.43	-.39	< .001
R_Sup_Motor_Area	5, 14, 47	30	3.57/3.41	-.39	< .001
L_Post_Cingulate	-5, -29, 27	38	3.54/3.39	-.39	< .001
R_Precuneus	8, -56, 36	30	3.52/3.47	-.39	< .001

8.3.2 Main Effect of Baseline Systolic Blood Pressure on rCBF 12-14 Years Later

The Main Effect of baseline CHS-CS systolic blood pressure taken in 1989 on rCBF as assessed with ASL MRI 12-14 years later is shown in Figure 61. As with the categorical variable of HTN, co-morbid MCI and dementia in 2002 were controlled for in the analysis. The figure shows that baseline SBP is correlated with lower rCBF measured 12-14 years later in the frontal and temporal lobes.

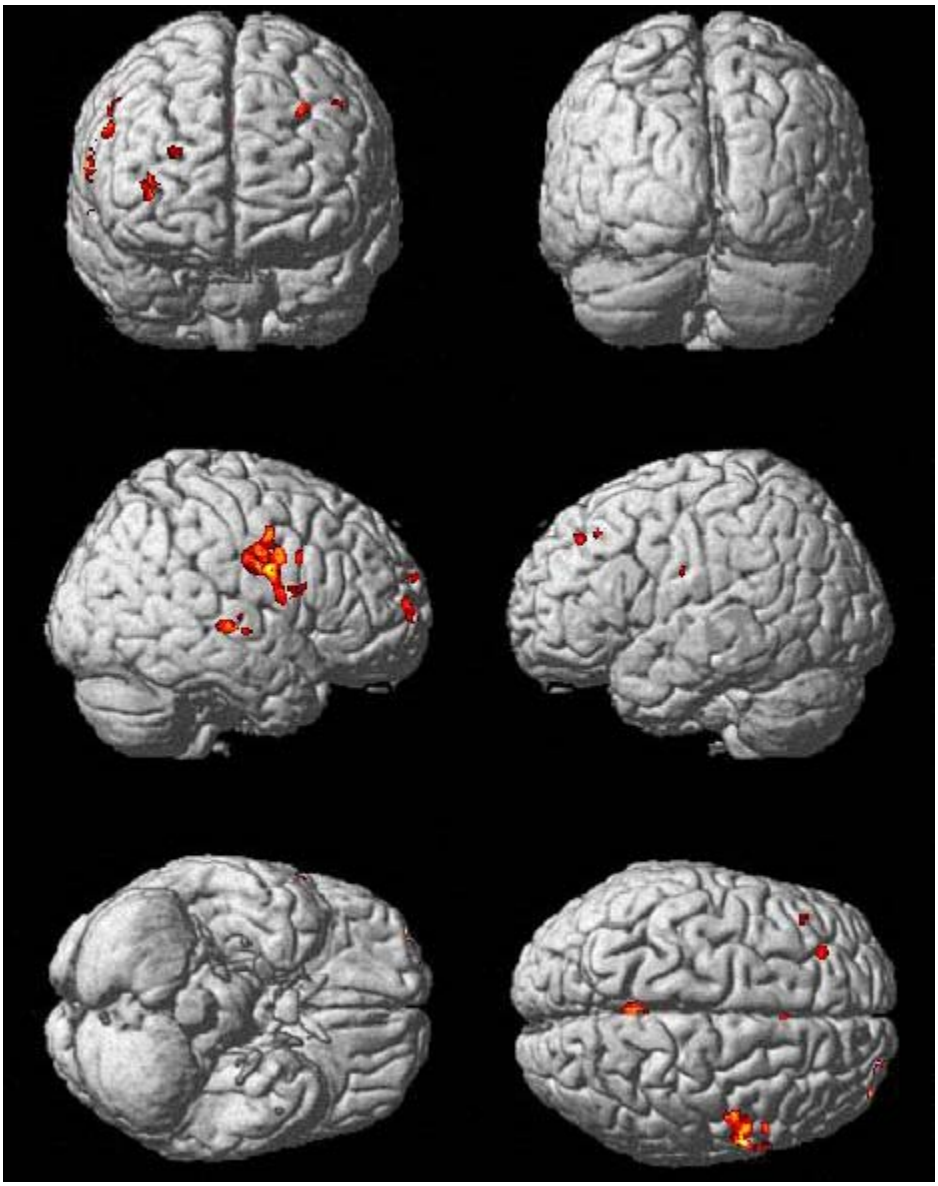

Figure 61: Main Effect of baseline systolic blood pressure on rCBF is observed in frontal, temporal, and parietal lobes.

The section rendered Main Effect of SBP is shown in Figure 62. This figure shows the section rendered Main Effect of baseline SBP on rCBF 12-14 years later. Part a shows that higher SBP at CHS-CS baseline evaluation correlated with lower rCBF in the left precuneus (crosshairs), even when accounting comorbid MCI and dementia at time of scan. Part b shows a similar Main Effect in the right precuneus (crosshairs). Finally, part c shows that higher SBP is

correlated with lower rCBF in the right posterior cingulate gyrus (crosshairs). There was no corresponding Main Effect on the left posterior cingulate. Correlation effect sizes and cluster volumes are provided in Table 28.

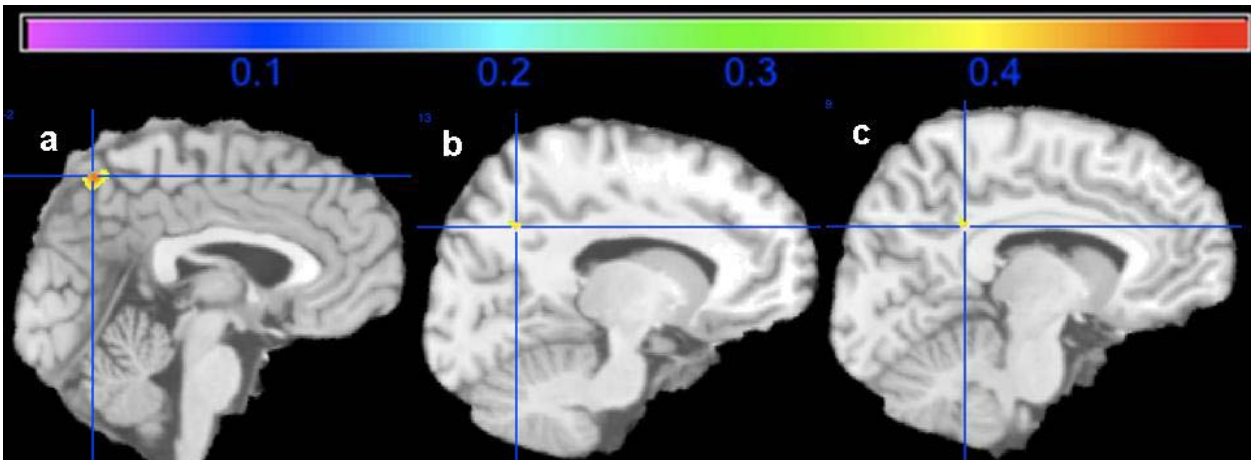

Figure 62: This figure that systolic blood pressure in 1989 is correlated with lower rCBF in 2002-2003 ASL MRI perfusion scans in the following key strategic brain regions: left precuneus (part a, crosshairs), right precuneus (part b, crosshairs), and the left posterior cingulate gyrus (part c, crosshairs). Table 32 has information on corresponding statistical effect sizes.

Table 32: Peak Maxima of Baseline SBP with rCBF. Key Strategic Brain areas are in bold.

Structure	Peak MNI Coordinates (x, y, z)	Cluster Volume (mm^3)	t/z scores	r^p value	$P_{uncorrected}$
R_Mid_Temporal	51, -21, 1	416	4.73/4.40	-.49	< .001
R_Mid_Frontal	35, 64, 6	463	4.59/4.28	-.48	< .001
R_Postcentral	58, -1, 24	1812	4.56/4.25	-.48	< .001
R_Precentral	49, -2, 41	1812	4.32/4.05	-.46	< .001
L_Precuneus	-2, -51, 51	266	4.11/3.88	-.44	< .001

L_Mid_Frontal	-44, 29, 43	33	3.87/3.67	-.42	< .001
R_Post_Cingulate	9, -30, 25	62	3.74/3.56	-.41	< .001
R_Precuneus	13, -47, 30	48	3.69/3.52	-.40	< .001
L_Mid_Cingulate	1, 20, 38	79	3.68/3.51	-.40	< .001
R_Sup_Temporal	60, -13, 12	49	3.63/3.46	-.40	< .001

8.3.3 Main Effect of Baseline Diastolic Blood Pressure on rCBF 12-14 Years Later

The Main Effect of baseline DBP on rCBF 12-14 years later is shown in the surface rendered image in Figure 63. Higher DBP is correlated with lower rCBF in largely the right frontal and temporal lobes, controlling for co-morbid MCI and dementia.

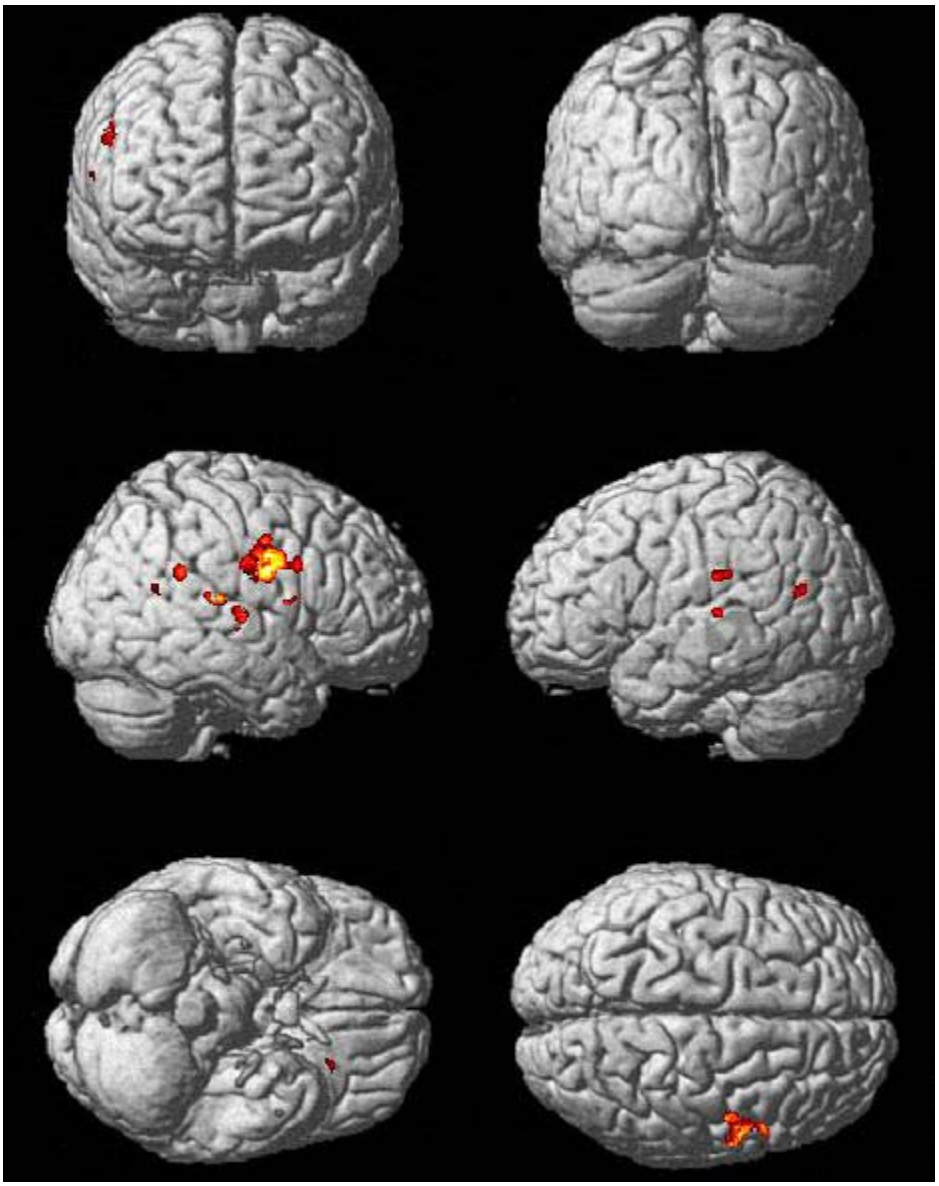

Figure 63: This figure shows the Main Effect of baseline DBP on rCBF and can be seen largely in the right frontal and temporal lobes.

The section rendered Main Effect of DBP on rCBF is shown in Figure 64. This figure shows the Main Effect of baseline DBP on rCBF projected onto the Standard Single Subject MNI template ($p_{uncorrected} < .001$, FDR < .15, k = 30). Part a shows the Main Effect in the left

precuneus (crosshairs) and the most posterior aspect of the left posterior cingulate (black arrow). Part b shows another Main Effect of baseline DBP on the left posterior cingulate (crosshair).

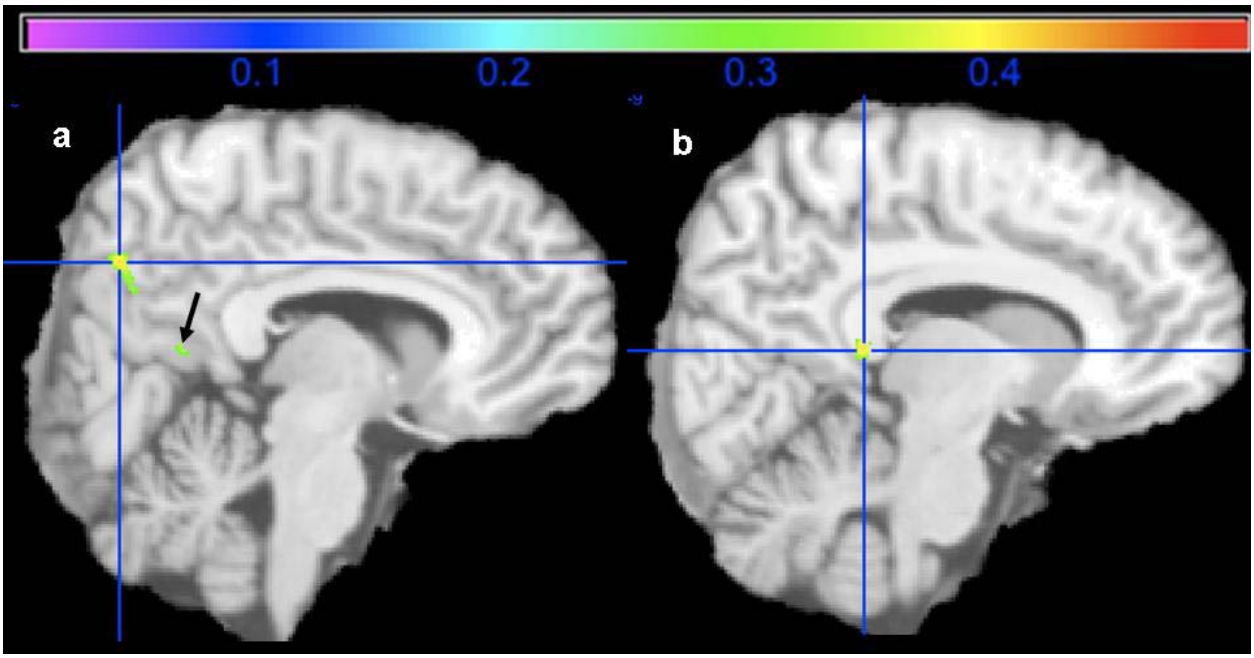

Figure 64: Main Effect of baseline DBP on rCBF projected onto the Standard Single Subject MNI template ($p_{uncorrected} < .001$, FDR < .15, k = 30).

Table 33 shows that peak local maxima for the baseline DBP Main Effect can be found in key strategic brain regions as the posterior cingulate gyrus, precuneus, and orbital frontal cortex.

Table 33: Peak Local Maxima for the Main Effect of Baseline DBP on rCBF.

Structure	Peak MNI Coordinates (x, y, z)	Cluster Volume (mm^3)	t/z scores	r^p value	$P_{uncorrected}$
R_Postcentral	57, -4, 27	2009	5.41/4.93	-.54	< .001
R_Precentral	45, -6, 31	2009	4.30/4.04	-.45	< .001
R_Mid_Temporal	49, -16, 4	268	4.39/4.11	-.46	< .001
R_Calcarine	15, -71, 3	84	4.16/3.93	-.44	< .001
L_Precuneus	-6, -57, 31	220	4.10/3.87	-.44	< .001
L_Post_Cingulate	-9, -22, 6	70	4.01/3.80	-.43	< .001
L_Mid_Temporal	-60, -26, 7	71	4.00/3.78	-.43	< .001
R_Supramarginal	51, -43, 26	196	3.81/3.62	-.41	< .001
R_Inf_Frontal_Operculum	34, 9, 33	58	3.69/3.52	-.40	< .001
L_Supramarginal	-52, -31, 25	154	3.65/3.48	-.40	< .001
L_Post_Cingulate	-6, -38, 5	33	3.55/3.40	-.39	< .001
L_Inf_Orbital_Frontal	-23, 26, -12	48	3.36/3.23	-.37	.001

A separate SPM analysis did not show any statistically significant interaction between SBP and DBP on rCBF. Additionally, when both variables were entered into the same model in SPM, there were no alterations in the Main Effects of either baseline SBP or DBP on rCBF. These analyses suggest that systolic and diastolic blood pressures neither mediate nor moderate the effect of one another on rCBF.

In broader terms, the data in this chapter shows that i) HTN is correlated with lower rCBF in the same areas known to be affected by MCI and dementia even controlling for those two conditions ii) Baseline SBP and DBP are also correlated with lower rCBF in key strategic brain regions. That baseline SBP and DBP showed this relationship but pressures taken during the year of the scan did not suggests that the effects of HTN on cerebral perfusion may have to be chronic in order for their effects to be detected. Since HTN is also associated with WMHL it his likely that HTN results in deleterious reductions in rCBF which may in turn lead to WMHL and cerebral atrophy. It important to note that no increased rCBF was detected with any of the HTN measures used; that is there was no positive correlation between categorical HTN, baseline SBP, and baseline DBP and rCBF.

The main contributions of this chapter to the overall model are documented in Figure 65 and this figure represents the completed model asserted by this dissertation. This figure summarizes the overall model asserted by this thesis. The specific chapter 8 contributions highlight how long standing HTN can lead to reduced cerebral perfusion, as shown by the green arrow drawn from hypertension to the reduced cerebral perfusion box. To summarize the entire model, age and hypertension pressure are correlated with white matter hyperintense lesions. These lesions affect the same areas of gray matter volume loss that are also predicted by aging and most importantly moderate the effects of age on gray matter volume loss (red arrow). White matter hyperintense lesion atrophy also overlaps with brain areas that are larger in volume in correlation with better performance on tests of cognitive function, as represented by the cognition box. MCI and dementia also affect many of the same brain regions that are lower in volume with higher burden of white matter hyperintense lesions. In groups containing only MCI or dementia subjects, white matter hyperintense lesions are themselves predictive of lower gray

matter volume and in the case of MCI, there is synergy between that clinical proxy for early neurodgeneration and WMHL (blue arrow). Finally, long standing hypertension is correlated with lower regional cerebral blood (green arrow) which can conceivably lead to WMHL and brain atrophy. Thus, this dissertation has shown hypertensive vascular disease can underlie the structural and function brain changes observed in normal aging, cognition, and neurodegeneration and that this convergence occurs in key strategic brain regions. These data consequently provide a powerful impetus for the control of HTN as an approach for improving brain aging, cognition, and reducing the vulnerability of the brain to neurodegenerative disease.

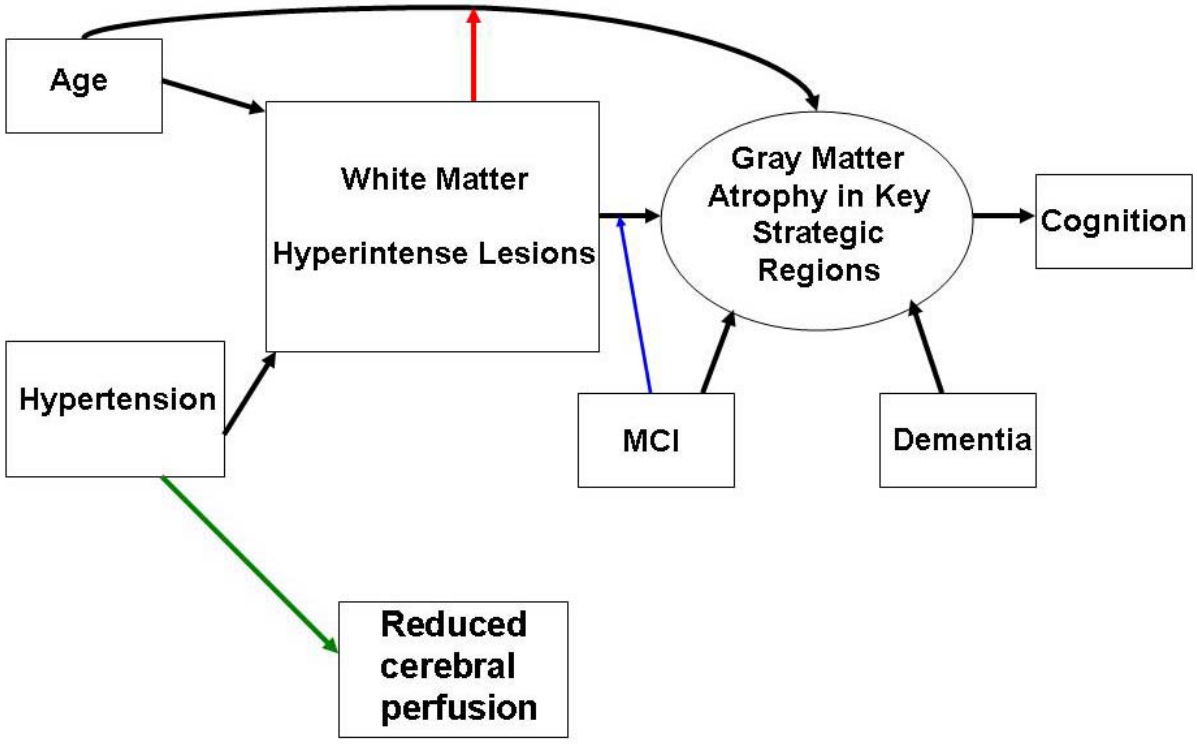

Figure 65: This figure summarizes the overall model derived from the data presented in Chapters 3-8. A full description is provided in the text.

9.0 CONCLUSIONS AND FUTURE DIRECTIONS

9.1.1 Conclusions

The main conclusion of this dissertation is that hypertensive vascular disease overlaps and interacts with structural and functional imaging measures of brain aging, cognition, early neurodegeneration as reflected by MCI and late neurodegeneration as represented by dementia. This dissertation has presented data strongly suggesting that hypertensive vascular disease affects many of the same areas of the brain known to be involved in cognitive function and neurodegenerative disease. These key strategic brain regions are the orbital frontal cortex, anterior cingulate gyrus, the posterior cingulate gyrus, the precuneus, hippocampal formation, thalamus, caudate, putamen, globus pallidus, and basal forebrain.

These effects have been shown with a multiple imaging modalities, namely structural and perfusion MRI, in a large population based community cohort with sample sizes ranging from 74 for the perfusion studies to almost 400 for the structural imaging work. This has maximized the probability that all analyses were done with optimal statistical power. The use of VBM has ensured unbiased examinations of every portion of GM in the human brain while the use of the AAL atlas has ensured that all statistical results obtained can be described in regional terms. Additionally, covariates in the majority of statistical analyses have included age, gender, race,

head size, education, and MRI identified infarcts. Such a multivariate approach minimizes the possibility that the results observed are due to confounding from any one of these variables.

While many of the models and results of this dissertation have been described in terms of statistical language, it is important for the reader to remember that all of my thinking has remained grounded in biologically plausible mechanisms. For example, I have shown that statistical Main Effects of age, hypertensive vascular disease, and neurodegeneration target similar brain areas such as the hippocampus, posterior cingulate gyrus, and precuneus. One biologically feasible reason for this is because all three of these phenomena could have a final common pathway with respect to affecting the neurovascular unit of the brain. The neurovascular unit is a fairly recent term (106) designed to describe all of the major cellular components of the brain including neurons, astrocytes, brain endothelium, pericytes, vascular smooth muscle cells (VSMC), microglia and perivascular macrophages. The emphasis, however, is on the vascular cellular components – that majority of which comprise the neurovascular unit.

Aging affects the neurovascular unit in ways that are difficult to mechanistically ascribe purely to the passage of chronological time. As such, there is overlap between arterial changes known to be due to vascular disease, which itself is tightly associated with aging. Consequently, age associated changes in the neurovascular unit are commonly described in terms of physiological mechanisms that, with the passage of time, result in the histopathological alterations that I will ascribe to vascular disease. To understand such physiological changes it is necessary to reiterate the unique aspects of cerebrovasculature, particularly the microvasculature.

Microvasculature in the brain is defined as blood vessels with lumen diameters smaller than 300 microns in diameter (22). They are responsible for achieving a compromise between providing enough blood for parenchyma metabolic needs while minimizing blood pressures that

fragile capillaries are exposed to. Consequences of exposing such capillaries to excessively high blood pressures include hyperfiltration, protein leakage, edema formation, and damage to the capillaries and tissue (22). Alterations in myogenic tone of blood vessels are a key determinant in achieving this balance. Myogenic tone refers to an intrinsic level of vascular smooth muscle cell tension, in the absence of specific vasoactive mediators such as nitric oxide, which is enhanced when vascular smooth muscle cells are mechanically stretched. Myogenic contraction is influenced in part by tensile strain of integrins attached to the extracellular matrix. It involves activation of calcium channels, subsequent changes in cellular calcium concentrations, and consequential alterations in the sensitivity of contractile proteins. Thus, myogenic tone plays an increasingly important role in modulating resistance to blood flow in progressively smaller vessels and controls short-term regulation of local blood flow, particularly in autoregulated organs such as the brain and kidneys. These organs have particularly small and intricate networks of blood vessels branching off from larger arteries.

With aging, persistent elevation of myogenic tone is replaced by remodeling of blood vessel wall components, which restores wall stress and tone to nominal levels while maintaining a new, elevated level of microvascular resistance. Proximal small arteries, which exhibit relatively less myogenic tone, undergo a combination of hypertrophy and rearrangement to a smaller relaxed lumen diameter. This process is known as hypertrophic remodeling. The microvasculature, which exert comparatively more vigorous myogenic tone, tends to remodel its wall components around a smaller lumen with no change in myocyte mass and this is known as eutrophic remodeling. Transduction of physical forces through interactions between the extracellular matrix, integrins, and the cytoskeleton of vascular smooth muscle cells activates the RhoA pathway. This activation, in turn, promotes migration and potentially hypertrophy or

hyperplasia of microvascular smooth muscle cells, resulting in a remodeled vascular wall and increased tunica media to lumen ratios (16). Therefore, microvascular remodeling may interfere with steady-state and dynamic control of local blood flow and may contribute to or complicate the pathogenesis of some forms of hypertension.

The alterations in the neurovascular unit described with aging are considered pathologic when they result in a series of alterations well known to neuropathologists. Macrosopically, the distribution of small vessel pathologies in the brain are best reflected by small lacunar infarcts found most commonly in the basal ganglia, thalamus, pons, and internal capsule (228-231). Microscopically, arteriosclerosis is the most common manifestation of vascular pathology and involves concentric thickening of the small arteries and arterioles of approximately 40 – 150 microns in diameter. The severity of arteriosclerosis is most commonly measured in terms the vessel wall thickness to lumen ratio and correlates closely with increasing age and HTN. In arteriosclerosis, there is a initial proliferation medial smooth muscles followed by degeneration and replacement by collagen. Arteriosclerosis is not collagenous thickening of small pervientricular veins, which is more common with WMHL. However, the severity of arteriosclerosis can correspond with the severity of WMHL, especially in the frontal and parietal lobes (27, 45, 232). Fibrinoid necrosis can also be seen as an end organ pathological consequence of malignant HTN and is distinct from arteriosclerosis. It is also known as lypohyalinosis and entails loss of normal vessel wall architecture, asymmetric hyaline/collagenous sclerosis, and mural foam cells (233, 234).

Alzheimer's pathology affects the cerebral vasculature in several ways. AD specific changes in brain blood vessels include atrophy and irregularities of arterioles and capillaries, swelling and increased number of pinocytic vesicles in endothelial cells, higher levels of

collagen IV, increased heparan sulfate proteoglycans and laminin deposition in the basement membrane, disruption of the basement membrane, lower total microvascular density and astrocytic end feet swelling (99). There is also considerable degeneration of the endothelium itself during disease progression as suggested by reduced staining of endothelial markers CD34 and CD31 observed in AD brains (235) . Neurovascular unit pathology in AD is also characterized by cerebral amyloid angiopathy (CAA) with Aβ deposits in the VSMC layer of small cerebral arteries. Aβ plaques also accumulate onto and around cerebral capillaries and impaired clearance of Aβ across the blood brain barrier and by cells of the neurovascular unit may contribute to CAA and parenchymal Aβ deposits. The prevalence of CAA in AD individuals and in the elderly population without AD is >80% and 10–40%, respectively (235). Such vascular alterations can also be observed in MCI, though typically to a lesser extent (236).

Although it is clear that age, vascular disease, and neurodgeneration employ different mechanisms, all target cerebral blood vessels as part of a final common pathway. Having therefore established that these states share a common pathological target, the findings of this dissertation are put into context. In age, vascular disease, and neurodgeneration there were repeated findings of the same key strategic brain regions being affected by these processes: the orbital frontal cortex, cingulate gyrus, hippocampus, posterior cingulate, and precuneus to name a few. Often, the Main Effects of all three phenomena were widespread – often encompassing large portions of all major lobes of the brain. This generalized nature of the effects is logical when one asserts that since age, vascular disease, and neurodegeneration all affect cerebrovasculature, which supplies the entire brain. Thus, if all three entities affect cerebral blood vessels it would be expected for their effects to be seen jointly in large areas of the brain and particularly in areas that perform cognitive function as these areas generally require

considerable energy and nutrients for optimal function (128). This is further supported by the fact that the strongest effects of age, vascular disease, and neurodegeneration were seen in such areas as the orbital frontal cortex and the hippocampus. Consequently, I posit that a critical synergy occurs between these three factors to promote hypoperfusion and brain atrophy in regions that have strategic importance with respect to cognitive function and thus risk for dementia. This concept extends the established notion that with brain infarcts it is not only the volume of brain involved but the location with respect to risk of cognitive impairment.

Tomlinson and colleagues compared postmortem 50 demented to 28 cognitively normal brains and suggested that 100 mL was the amount of brain tissue that had to be destroyed for dementia to be clinically expressed. However, this relationship was not direct: two subjects in their control group had lesions destroying more 50 mL of brain (91 mL in one case) (237). Thus, the authors qualified their results by stating that location of tissue destruction can determine of course of whether or not an individual remains cognitively normal or demented. This concept of strategic zones was further articulated by Mesulam (128) and refined by Zekry and colleagues (129). These same strategic areas have appeared in this dissertation and from this an emphasis on 10 key strategic brain areas has been expressed. The key strategic brain areas are orbital frontal cortex, anterior cingulate gyrus, the posterior cingulate gyrus, the precuneus, hippocampal formation, thalamus, caudate, putamen, globus pallidus, and basal forebrain. What I have shown in this dissertation is that all of these areas sustain multiple "hits" in terms of having lower GM volumes in association with age, hypertensive vascular disease, and neurodegeneration. These associations are independent of each other; that is the hypertension Main Effects held even after controlling for age, dementia and other potential confounders. The concept of these brain regions sustaining multiple hits from different sources, namely age, HTN, and neurodegeneration, is

summarized by Figure 66. This figure shows the strategic areas figure from the Zekry paper and Figure 1 and it also shows the volume rendered main effects of age, hypertensive vascular disease (i.e. WMHL), and neurodegeneration (as proxy indicated by a clinical classification of dementia). This figure shows that all three entities are associated with lower GM volumes in the frontal, temporal, and parietal lobes – all locations that are strategic areas of the brain with respect to cognitive function. This figure therefore summarizes a fundamental message: that there are common brain areas that are jointly affected by age, vascular disease, and neurodegeneration.

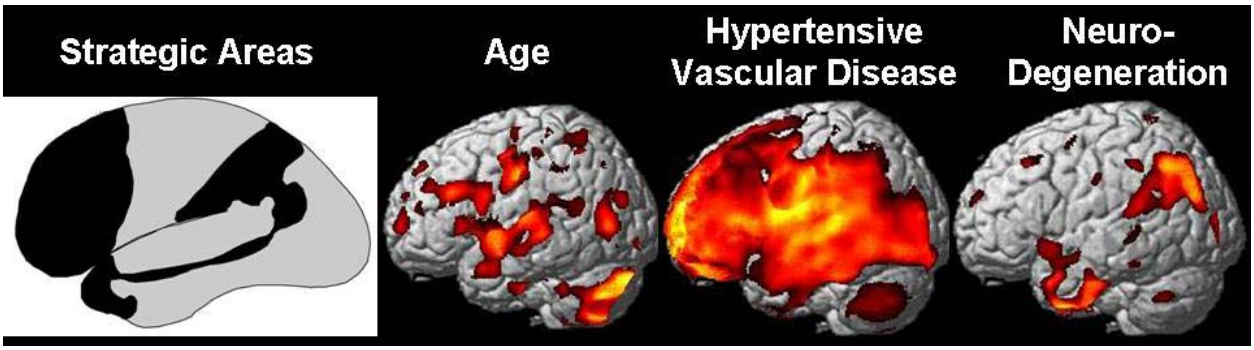

Figure 66: This figure shows the Zekry figure that was utilized in Figure 1 (with strategic areas with respect to cognitive function shaded in black) along with the Main Effects of age, hypertensive vascular disease, and neurodegeneration. All three of these entities independently effect strategic areas, particularly in the frontal, temporal, and parietal lobes.

Thus, a critical synergy exists between age, vascular disease, and neurodgeneration for the promotion of dementia and this is facilitated by the convergence of these phenomena in strategic cognitive zones of the human brain. Of these three, vascular disease is emerging as a key component because unlike aging and neurodegeneration, vascular disease such as hypertension is currently more effectively treated and can be prevented. Indeed, this dissertation has shown that vascular disease can moderate both age and early neurodegeneration in the gray

matter. Consequently, better prevention/treatment of vascular disease may have a beneficial effect of attenuating the effects of age and neurodegenerative effects on brain atrophy.

A growing body of literature provides support of this potentially powerful concept. The Rotterdam study followed 6992 cognitively normal individuals aged 55 or older at baseline who were participating in the Rotterdam Study and compared the risk for AD in participants with any prior use of cholesterol-lowering drugs and those with no prior use, adjusting for differences in demographics, vascular risk factors, duration of medication use, and APOE4 (238). A total of 582 participants developed AD. Even after accounting for these potential confounders, the use of statin cholesterol-lowering drugs (but not nonstatin cholesterol-lowering drugs) was associated with a lower AD risk compared with no cholesterol-lowering drug use (HR 0.57; 95% CI 0.37 to 0.90). Moreover, both lipophilic and hydrophilic statins were associated with reduced risks for AD, with no significant difference between the two. This was the largest prospective study to date specifically designed to assess cognitive function in elders that addresses the relation between statin use and development of AD. It suggests that statins, which lower cholesterol and thus reduce risk of cardiovascular disease, could be a viable option for prevention of cognitive decline and AD. Another study with results in support of this conclusion was done in 1,674 persons from the Sacramento Area Latino Study on Aging (SALSA) followed up over 5 years, with 27% of the cohort on statins. This study, done only on Mexican-American aged 60 and older, found that use of statins conferred a reduction in dementia risk compared to those who did not use statins (HR = 0.52; 95% CI 0.34, 0.80) (239). On the other hand the CHS did not find any statistically significant benefit of statins either in improving cognitive function longitudinally or reducing the risk of dementia (240, 241). Consequently, the investigation of

cardiovascular medicines as a pharmacological approach to improving brain vascular health in aging and neurodegeneration will continue to remain a research area in need of additional work.

Non-pharmacological methods for preventing vascular disease have also shown benefit with respect to brain health, cognition, and Alzheimer's pathology. Several studies suggest how brain atrophy and dementia risk may be attenuated using caloric restriction and physical exercise. Caloric restriction attenuates AD amyloid neuropathology in mouse models (242) and promotes brain longevity through several molecular mechanisms. These minimize oxidative damage to neurons by upregulation of brain derived neurotrophic growth factor, glial cell-line derived neurotrophic growth factor, heat-shock protein 70 and glucose regulated protein 78 (243).

Physical exercise is another intervention than can improve brain health with aging. Prior work comparing structural MRI brain volumes of groups with low and high aerobic fitness activity found larger volumes in pre-frontal GM, temporal lobe GM, and anterior WM in the higher fitness group (244). Physical exercise promotes increased functional activation on fMRI in the anterior cingulate gyrus, which relates to improved cognitive test performance (245). Both caloric restriction and physical exercise appear to promote higher brain volumes, better metabolic activation, and enhanced cognition. Most importantly, they share a common effect on the body by reducing body tissue adiposity. Physical activity was also evaluated in the context of a randomized clinical trial in which 170 individuals with subjective memory complaints were randomized to either physical activity program (typically aerobic in nature and most commonly walking) or a usual care group in which no physical activity intervention was implemented (246). Subjects were followed up for a subsequent 18 months and the main outcome was change in Alzheimer Disease Assessment Scale–Cognitive Subscale (ADAS-Cog) scores (possible range, 0-70). In the physical activity intervention group, participants improved 0.73 points (95%

confidence interval, –1.27 to 0.03) on the ADAS-Cog, and those in the usual care group improved 0.04 points (95% confidence interval, –0.46 to 0.88), a statistically significant difference ($p < .05$). Finally, a study found that wheel running in rodents increased levels of brain derived neurotrophic factor in the brain and improved performance on the Morris Water Maze (247). These results of these studies collectively suggest that physical activity can be implemented as a viable strategy for improving cognitive function in elderly persons who may be at risk for AD.

In conclusion, this dissertation shows that hypertensive vascular disease, as represented by categorical HTH, baseline SBP, baseline DBP, and WMHL, induced functional and structural changes in elderly brains that most impressively affect key strategic brain areas that are also targeted by aging and neurodegeneration. The main strength of this work is that is utilized large numbers of perfusion and structural imaging data from a well characterized clinical cohort. The primary disadvantage of this work is that it did not have serial structural and perfusion scans from different time points as that would have permitted for meaningful longitudinal analysis. Overall, the main message of this dissertation is that vascular disease underlies patterns of brain alterations seen in aging and neurodegeneration. This work has potentially broad public health implications for the treatment and prevention of vascular disease as a feasible approach for attenuating the deleterious effects of brain aging and reducing the risk for dementia.

9.1.2 Future Directions

The data presented in this dissertation opens possibilities for additional future studies. Broadly, these future studies could be designed in terms of multiple image sequences acquired at different time points for the purposes of better evaluating the natural history of vascular disease effects on

the human brain. For example, while the work presented in this dissertation suggests that perfusion alterations may precede structural brain changes, a longitudinal study would allow for a more rigorous examination of this question. Another question that would be very important to examine is the extent to which amyloid deposition in the brain is moderated by co-morbid vascular disease. This question is possible to answer due to the innovation of Pittsburgh Compound B (PiB), a thioflavin-T derivative the selectively binds and labels the amyloid plaques seen in Alzheimer's disease (131). If HTN or other forms of vascular disease to be shown to longitudinally modify PiB retention in the brain, it would provide considerable insight into the intersection between AD and vascular pathology.

Thus, one example of a powerful multimodal imaging study I would consider working on in the future is scanning elderly subjects longitudinally with 3-D volumetric structural MRI, T2 scans for WMHL rating, perfusion ASL MRI, PiB scans with PET, and white matter tract imaging using diffusion tensor imaging (248). Scanning subjects longitudinally and obtaining clinical data on their cardiovascular and cognitive status would not only allow for a truly multifaceted picture of how the brain changes with aging, vascular disease, and onset of neurodegeneration but it would also allow for interactions and synergy between these factors to be investigated. This work would also allow some of the earliest structural changes of AD and MCI to be identified, potentially prior to expression of clinical symptoms.

Such investigations could also involve studies on molecular markers of cellular aging itself. Telomere shortening, for example, is a powerful molecular marker for evaluating cellular age (249). Examining the relationship between that marker and image derived measures of structure, perfusion, and amyloid could also give additional insights into how vascular disease can moderate aging at the cellular level. Another molecular study of that type that could be

performed is on BDNF levels in the context of an outcomes study of physical activity intervention in the elderly. So, for instance, I could conceivably investigate if BDNF levels are higher in elderly persons who engage in physical activity and whether or not these levels are correlated with higher GM volumes, higher rCBF, and lower PiB levels.

While SPM will no doubt remain a key component for analyzing such neuroimaging data, other types of image analysis will be applied to compliment this software. There are a variety of methods for analyzing brain images. By far the most common methods (as above) utilize t-tests (and associated methods) that are useful for determining regional signal (atrophy, hypoperfusion) that occurs above a given threshold (*functional specialization*). However, another group of methods has focused on identifying functionally associated regions that may exist within a dataset and that can be revealed by analyses that emphasize *functional integration*. One example of such multivariate methods is *Partial Least Squares* (PLS). PLS, which was originally applied to neuroimaging data by McIntosh and colleagues (250, 251), is similar to a Principal Components Analysis, except that the solutions are constrained to the part of the covariance structure that is attributable to the experimental manipulations. PLS can therefore be used as a robust method for extracting distributed differences related to alterations in tissue compartments (i.e. GM, WM, CSF) and/or perfusion measures in diseased (ex. HTN, MCI, AD) and non-diseased states. Another advantage of PLS is that it allows one to express these differences in terms of "Brain scores" which indicate how strongly each subject expresses the observed differences. Such scores can be subsequently used to differentiate groups of subjects and potentially even single subjects. The main drawback to PLS is the considerable computational power required to compute non-parametric statistics, making it difficult to analyze large numbers of scans.

All of these future directions are investigations that will require new skills, methods of analysis and knowledge that will hopefully extend and enrich my life in academic medicine. They are efforts that will require participation with an interdisciplinary team of clinicians and scientists over multiple departments and institutions. I believe my PhD training and the work presented in this dissertation has provided me with a sound foundation with which to pursue these endeavors.

BIBLIOGRAPHY

1. Berrios GE, Freeman HL. Alzheimer and the dementias (Eponymists in Medicine). London: Royal Society of Medicine Services, Ltd., 1991.

2. Amaducci LA, Fratiglioni L, Rocca WA, et al. Risk factors for clinically diagnosed Alzheimer's disease: A case-control study of an Italian population. Neurology 1986; 36:922-931.

3. van Duijn CM, Hofman A. Risk factors for Alzheimer's disease: the EURODERM collaborative re-analysis of case-control studies. Neuroepidemiology 1992; 11:106-113.

4. van Duijn CM, Stijnen T, Hofman A. Risk factors for Alzheimer's disease: overview of the EURODERM collaborative re-analysis of case-control studies. EURODERM Risk Factors Research Group. Int J Epidemiol 1991; 20:S4-S12.

5. Lindsay J, Laurin D, Verreault R, et al. Risk factors for Alzheimer's disease: a prosepctive analysis from the Canadian Study of Health and Aging. Am J Epidemiol 2002; 156:445-453.

6. Klunk W, Price JC, Mathis CA, et al. Amyloid deposition begins in the striatum of presenilin-1 mutation carriers from two unrelated pedigrees. J Neurosci 2007; 27:6174-6184.

7. Lopez OL, Kuller LH, Becker JT, et al. Classification of vascular dementia in the Cardiovascular Health Study Cognition Study. Neurology 2005; 64:1538-1547.

8. Raz N. Cognitive Neuroscience of Aging: Linking Cognitive and Cerebral Aging: Oxford University Press, 2005.

9. Fredericks JAM. The neurology of aging and dementia. In: Fredericks JAM, ed. Handbook of clinical neurology. Amsterdam: Elsevier, 1985; 373-393.

10. Pakkenberg B, Gundersen HJ. Neocortical neuron number in humans: effect of sex and age. Journal of Comparative Neurology 1997; 384:312-320.

11. Simić G, Kostović I, Winblad B, Bogdanović N. Volume and number of neurons of the human hippocampal formation in normal aging and Alzheimer's disease. Journal of Comparative Neurology 1997; 379:482-494.

12. Haugh H. Are neurons of the human cerebral cortex really lost during aging? A morphometric examination. Berlin: Springer, 1985.

13. Rutten BP, Schmitz C, Gerlach OH, et al. The aging brain: accumulation of DNA damage or neuron loss? Neurobiology of Aging 2007; 1:91-98.

14. Cardenas VA, Du AT, Hardin D, et al. Comparison of methods for measuring longitudinal brain change in cognitive impairment and dementia. Neurobiol Aging 2003; 24:537-544.

15. Kannel WB. Blood pressure as a cardiovascular risk factor: prevention and treatment. JAMA 1996; 275:1571-1576.

16. Girouard H, Iadecola C. Neurovascular coupling in the normal brain and in hypertension, stroke, and Alzheimer disease. J Appl Physiol 2006; 100:328-335.

17. Wolf-Maier K, cooper RS, Banegas J, et al. Hypertension prevalence and blood pressure levels in 6 European countries, Canada, and the United States. JAMA 2003; 289:2362-2369.

18. Gianaros PJ, Greer PJ, Ryan CM, Jennings JR. Higher blood pressure predicts lower regional grey matter volume: Consequences on short-term information processing. Neuroimage 2006; 31:754-765.

19. Salerno J, Murphy DG, Horwitz B, et al. Brain atrophy in hypertension. A volumetric magnetic resonance imaging study. Hypertension 1992; 20:340-348.

20. Elias PK, Elias MF, Robbins MA, Budge MM. Blood pressure-related cognitive decline: Does age make a difference? Hypertension 2004; 44:631-636.

21. Strassburger TL, Lee HC, Daly EM, et al. Interactive effects of age and hypertension on volume of brain structures. Stroke 1997; 28:1410-1417.

22. Mitchell GF. Effects of central arterial aging on the structure and function of the peripheral vasculature: implications for end-organ damage. J Appl Physiol 2008; 105:1652-1660.

23. Manolio TA, Olson J, Longstreth WT. Hypertension and cognitive function: pathophysiologic effects of hypertension on the brain. Curr Hypertens Rep 2003; 5:255-261.

24. Jeerakathil T, Wolf PA, Beiser A, et al. Cerebral Microbleeds. Prevalence and associations with cardiovascular risk factors in the Framingham Study. Stroke 2004; 35:1831-1835.

25. Saczynski JS, Sigurdsson S, Jonsdottir MK, et al. Cerebral Infarcts and Cognitive Performance. Importance of Location and Number of Infarcts. Stroke 2009.

26. Murray AD, Staff RT, Shenkin SD, Deary IJ, Starr JM, Whalley LJ. Brain white matter hyperintensities: relative importance of vascular risk factors in nondemented elderly people. Radiology 2005; 237:251-257.

27. Liao D, Cooper L, Cai J, et al. Presence and severity of cerebral white matter lesions and hypertension, its treatment, and its control: The ARIC Study. Arteriosclerosis Risk in Communities Study. Stroke 1996; 27:2262-2270.

28. van Dijk EJ, Breteler MB, Schmidt R, et al. The association between blood pressure, hypertension, and cerebral white matter lesions. The Cardiovascular Determinants of Dementia Study. Hypertension 2004; 44:625-630.

29. de Leeuw F-E, dr Groot JC, Oudkerk M, et al. Hypertension and cerebral white matter lesions in a prospective cohort study. Brain 2002; 125:765-772.

30. Steingart A, Hachinski VC, Lau C, et al. Cognitive and neurologic findings in demented patients with diffuse white matter lucencies on computer tomographic scan (Leuko-Araiosis). Arch Neurol 1987; 44:36-39.

31. Pantoni L, Leys D, Fazekas F, et al. Role of white matter lesions in cognitive impairment of vascular origin. Alzheimer Dis Assoc Disord 1999; 13:S49-S54.

32. Diaz JF, Merskey H, Hachinski VC, et al. Improved recognition of leukoaraiosis and cognitive impairment in Alzheimer's disease. Arch Neurol 1991; 48:1022-1025.

33. Inzitari DI, Diaz F, Fox A, et al. Vascular risk factors and leuko-araiosis. Arch Neurol 1987; 44:42-47.

34. Janota I, Mirsen TR, Hachinski VC, Lee DH, Merskey H. Neuropathologic correlates of leuko-araiosis. Arch Neurol 1989; 46:1124-1128.

35. Kuller LH, Longstreth WT, Arnold AM, Bernick C, Bryan N, Beauchamp NJ. White matter hyperintensity on cranial magnetic resonance imaging. Stroke 2004; 35:1821-1825.

36. Longstreth WT, Manolio TA, Arnold A, et al. Clinical correlates of white matter findings on cranial magnetic resonance imaging of 3301 elderly people. Stroke 1996; 27:1274-1282.

37. Longstreth WT, Bernick C, Manolio TA, Bryan N, Jungreis CA, Price TR. Lacunar infarcts defined by magnetic resonance imaging of 3660 elderly people. Arch Neurol 1998; 55:1217-1225.

38. Longstreth WT, Bernick C, Fitzpatrick A, et al. Frequency and predictors of stroke death in 5,888 participants in the Cardiovascular Health Study. Neurology 2001; 56:368-375.

39. Young VG, Halliday GM, Kril JJ. Neuropathologic correlates of white matter hyperintensities. Neurology 2008; 71:804-811.

40. Marchal G, Rioux P, Petit-Taboue MC, et al. Regional cerebral oxygen consumption, blood flow, and blood volume in healthy human aging. Archives of Neurology. 1992; 49:1013-1020.

41. Fazekas F, Niederkorn K, Schmidt R, et al. White matter signal abnormalities in normal individuals: Correlation with carotid ultrasonography, cerebral blood flow measurements, and cerebrovascular risk factors. Stroke 1988; 19:1285-1288.

42. Schmidt R, Fazekas F, Offenbacher H, et al. Magnetic resonance imaging white matter lesions and cognitive impairment in hyperintensive individuals. Arch Neurol 1991; 48:417-420.

43. George AE, de Leon MJ, Gentes CI, Miller J, London E, Budzilovich GN. Leukoencephalopathy in normal and pathologic aging: 1. CT of brain lucencies. AJNR 1986; 7:561-566.

44. Fisher CM. Binswanger's encephalopathy: a review. J Neurol 1989; 236:65-79.

45. Manolio TA, Burke GL, O'Leary DH, et al. Relationships of cerebral MRI findings to ultrasonographic carotid atherosclerosis in older adults : the Cardiovascular Health Study. CHS Collaborative Research Group. Arterioscler Thromb Vasc Biol 1999; 19:356-365.

46. Sierra C. Cerebral white matter lesions in essential hypertension. Curr Hypertens Rep 2001; 3:429-433.

47. Jungreis CA, Kanal E, Hirsch WL, Martinez AJ, Moossy J. Normal perivascular spaces mimicking lacunar infarction: MR imaging. Radiology 1988; 169:101-104.

48. Reed BR, Eberling JL, Mungas D, Weiner M, Jagust WJ. Effects of white matter lesions and lacunes on cortical function. Arch Neurol 2004; 58:545-550.

49. Breteler MM, van Swieten JC, Bots ML, et al. Cerebral white matter lesions, vascular risk factors, and cognitive function in a population-based study: the Rotterdam Study. Neurology 1994; 44:1246-1252.

50. Petersen RC, Smith GE, Waring SC, Ivnik RJ, Tangalos EG, Kokmen E. Mild cognitive impairment: Clinical characterization and outcome. Arch Neurol 1999; 56:303-308.

51. Morris JC, Storandt M, Miller JP, et al. Mild cognitive impairment represents early-stage Alzheimer disease. Arch Neurol 2001; 58:397-405.

52. Elias MF, Beiser A, Wolf PA, Au R, White RF, R.B. DA. The preclinical phase of Alzheimer disease. A 22-year prosepctive study of the Framingham cohort. Arch Neurol 2000; 57:808-813.

53. Kilander L, Nyman H, Boberg M, Hansson L, Lithell H. Hypertension is related to cognitive impairment: a 20-year follow-up of 999 men. Hypertension 1998; 31:780-786.

54. Kivipelto M, Helkala E-L, Hanninen T, et al. Midlife vascular risk factors and late-life mild cognitive impairment. Neurology 2001; 56:1683-1689.

55. Reinprecht F, Elmstahl S, Janzon L, Andre-Petersson L. Hypertension and changes of cognitive function in 81-year-old men: a 13-year follow-up of the population study "Men born in 1914", Sweden. Journal of Hypertension 2003; 31:57-86.

56. Launer LJ, Masaki K, Petrovitch H, Foley D, Havlik R. The association between mid-life blood pressure levels and late life cognitive function: The Honolulu-Asia Aging Study. J Am Med Assoc 1995; 274:1846-1851.

57. Bennett DA, Schneider JA, Bienias JL, Evans DA, Wilson RS. Mild cognitive impairment is related to Alzheimer disease pathology and cerebral infarctions. Neurology 2005; 64:834-841.

58. Reitz C, Tang M-X, Manly J, Mayeux R, Luchsinger JA. Hypertension and the risk of mild cognitive impairment. Arch Neurol 2007; 64:1734-1740.

59. Solfrizzi V, Panza F, Colacicco AM, et al. Vascular risk factors, incidence of MCI, and rates of progression to dementia. Neurology 2004; 63:1882-1891.

60. Ma F, Wang T, Yin J, et al. [A case-control study on the influencing factors to mild cognitive impairment among the community-based elderly population]. Zhonghua Liu Xing Bing Xue Za Zhi 2008; 29:873-877.

61. Das SK, Bose P, Biswas A, et al. An epidemiologic study of mild cognitive impairment in Kolkata, India. Neurology 2007; 68:2019-2026.

62. Lopez OL, Jagust WJ, Dulberg C, et al. Risk factors for mild cognitive imapirment in the Cardiovascular Health Study Cognition Study: Part 2. Arch Neurol 2003; 60:1394-1399.

63. Schrader J, Luders S, Diener HC, et al. [Effects of long-term antihypertensive therapy with losartan on blood pressure and cognitive function in patients with essential hypertension and other cerebrovascular risk factors (AWARE observational study)]. Med Klin (Munich) 2008; 103:491-499.

64. Skoog I, Lithell H, Hansson L, et al. Effect of baseline cognitive function and antihypertensive treatment on cognitive and cardiovascular outcomes: Study on COgnition and Prognosis in the Elderly (SCOPE). Am J Hypertens 2005; 18:1052-1059.

65. Beckett NS, Peters R, Fletcher AE, et al. Treatment of Hypertension in Patients 80 Years of Age or Older. N Engl J Med 2008; 358:1887-1898.

66. Smith EE, Egorova S, Blacker D, et al. Magnetic resonance imaging white matter hyperintensities and brain volume in the prediction of mild cognitive impairment and dementia. Arch Neurol 2008; 65:94-100.

67. van Straaten EC, Harvey D, Scheltens P, et al. Periventricular white matter hyperintensities increase the likelihood of progression from amnestic mild cognitive impairment to dementia. J Neurol 2008; 255:1302-1308.

68. Moretti DV, Pievani M, Fracassi C, et al. Brain vascular damage of cholinergic pathways and EEG markers in mild cognitive impairment. J Alzheimers Dis 2008; 15:357-372.

69. Brayne C, Gill C, Huppert FA, et al. Vascular risks and incident dementia: results from a cohort study of the very old. Dement Geriatr Cogn Disord 1998; 9:175-180.

70. Corder EH, Lannfelt L, Bogdanovic N, Fratiglioni L, Mori H. The role of APOE polymorphisms in late-onset dementias. Cell Mol Life Sci 1998; 54:928-934.

71. Fratiglioni L, Viitanen M, von Strauss E, Tontodonati V, Herlitz A, Winblad B. Very old women at highest risk of dementia and Alzheimer's disease: incidence data from the Kungsholem Project, Stockholm. Neurology 1997; 48:132-138.

72. Hofman A, Ott A, Breteler MM, et al. Atherosclerosis, apolipoprotein E, and the prevalence of dementia and Alzheimer's disease in the Rotterdam study. Lancet 1997; 18:151-154.

73. Luchsinger JA, Reitz C, Honig LS, Tang M-X, Shea S, Mayeux R. Aggregation of vascular risk factors and risk of incident Alzheimer disease. Neurology 2005; 65:545-551.

74. Small BJ, Viitanen M, Winblad B, Backman L. Cognitive changes in very old persons with dementia: The influence of demographic, psychometric, and biological variables. J Clin Exp Neuropsychol 1997; 19:245-260.

75. Snowdon DA, Grainer LH, Mortimer JA, Riley KP, Grainer PA, Markesbery WR. Brain infarction and the clinical expression of Alzheimer disease: The nun study. JAMA 1997; 277:813-817.

76. van Duijn CM, de Knijff P, Cruts M, et al. Apolipoprotein E4 allele in a population-based study of early-onset Alzheimer's disease. Nat Genet 1994; 7:74-78.

77. Zhu L, Viitanen M, Guo Z, Winblad B, Fratiglioni L. Bloo dpressure reduction, cardiovascular diseases, and cognitive decline in the mini-mental state examination in a community population of normal very old people: a three-year follow-up. J Clin Epidemiol 1998; 51:385-391.

78. Starr JM, Whalley LJ, Inch S. Blood pressure and cognitive function in healthy old people. J Am Geriatr Soc 1993; 41:753-756.

79. Cacciatore F, Abete P, Ferrara N, et al. The role of blood pressure in cognitive impairment in an elderly population. Osservatorio Geriatrico Campano Group. J Hypertens 1997; 15:135-142.

80. Cerhan JR, Folsom AR, Mortimer JA, et al. Correlates of cognitive function in middle-aged adults. Atherosclerosis Risk in Communities (ARIC) Study Investigators. Gerontology 1998; 44:95-105.

81. Harrington F, Saxby BK, McKeith IG, Wesnes K, Ford GA. Cognitive performance in hypertensive and normotensive older subjects. Hypertension 2000; 36:1079-1082.

82. Haan MN, Shemanski L, Jagust WJ, Manolio TA, Kuller L. The role of APOE e4 in modulating effects of other risk factors for cognitive decline in elderly persons. JAMA 1999; 282:40-44.

83. Andre-Petersson L, Engstrom G, Hagberg B, Janzon L, Steen G. Adaptive behavior in stressful situations and stroke incidence in hypertensive men: results from prospective cohort study "men born in 1914" in Malmo, Sweden. Stroke 2001; 32:1712-1720.

84. Stewart R, Russ C, Richards M, Brayne C, Lovestone S, Mann A. Apolipoprotein E genotype, vascular risk and early cognitive impairment in an African Caribbean population. Dement Geriatr Cogn Disord 2001; 12:251-256.

85. Kuo HK, Sorond F, Iloputaife I, Gagnon M, Milberg W, Lipsitz LA. Effect of blood pressure on cognitive functions in elderly persons. J Gerontol A Biol Sci Med Sci 2004; 59:1191-1194.

86. Elias MF, Wolf PA, D'Agostino RB, Cobb J, White LR. Untreated blood pressure level is inversely related to cognitive functioning: the Framingham Study. Am J Epidemiol 1993; 138:353-364.

87. Swan GE, DeCarli C, Miller BL, et al. Association of midlife blood pressure to late-life cognitive decline and brain morphology. Neurology 1998; 51:986-993.

88. Swan GE, Carmelli D, Larue A. Systolic blood pressure tracking over 25 to 30 years and cognitive performance in older adults. Stroke 1998; 29:2334-2340.

89. McKhann G, Drachman DA, Folstein MF, Katzman R, Price DL, Stadlan E. Clinical diagnosis of Alzheimer's disease: Report of the NINCDS-ADRDA Work Group under the auspices of the Department of Health and Human Services Task Force on Alzheimer's disease. Neurology 1984; 34:939-944.

90. Launer LJ, Ross GW, Petrovitch H, et al. Midlife blood pressure and dementia: the Honolulu-Asia aging study. Neurobiol Aging 2000; 21:49-55.

91. Kivipelto M, Helkala E-L, Laakso MP, et al. Midlife vascular risk factors and Alzheimer's disease in later life: longitudinal, population based study. BMJ 2001; 322.

92. Wu C, Zhou D, Wen C, Zhang L, Como P, Qiao Y. Relationship between blood pressure and Alzheimer's disease in Linxian County, China. Life Sci 2003; 72:1125-1133.

93. Yamada M, Kasagi F, Sasaki H, Masunari N, Mimori Y, Suzuki G. Association between dementia and midlife risk factors: the Radiation Effects Research Foundation Adult Health Study. J Am Geriatr Soc 2003; 51:410-414.

94. Whitmer RA, Sidney S, Selby J, Johnston SC, Yaffe K. Midlife cardiovascular risk factors and risk factors and risk of dementia in late life. Neurology 2005; 64:277-281.

95. Forette F, Seux M-L, Staessen JA, et al. Prevention of dementia in randomised double-blind placebo-controlled systolic hypertension in Europe (Syst-Eur) trial. Lancet 1998; 352:1347-1351.

96. Forette F, Seux ML, Staessen JA, et al. The prevention of dementia with antihypertensive treatment: new evidence from the Systolic Hypertension in Europe (Syst-Eur) study. Arch Intern Med 2002; 162:2046-2052.

97. Mancia G, Ambrosioni E, Rosei EA, Leonetti G, Trimarco B, Volpe M. Blood pressure control and risk of stroke in untreated an dtreated hypertensive patients screened from clinical practice: results of the ForLife study. J Hypertension 2005; 23:1575-1581.

98. Struijs J, van Genugten LL, Evers SMAA, Ament AJHA, Baan CA, van den Bos GAM. Modeling the future burden of stroke in the Netherlands: Impact of aging, smoking, and hypertension. Stroke 2005; 36:1648-1655.

99. de la Torre JC. Alzheimer disease as a vascular disorder: Nosological evidence. Stroke 2002; 33:1152-1162.

100. Stern RA, Silva SG, Chaisson N, Evans DL. Influence of cognitive reserve on neuropsychological functioning in asymptomatic human immunodeficiency virus-1 infection. Arch Neurol 1996; 53:148-153.

101. Mortimer JA. Brain reserve and the clinical expression of Alzheimer's disease. Geriatrics 1997; 52:S50-S53.

102. Petrovitch H, Ross GW, Steinborn SC, et al. AD lesions and infarcts in demented and non-demented Japanese-American men. Ann Neurol 2005; 57:98-103.

103. Thomas T, McLendon C, Sutton ET, Thomas G. Cerebrovascular endothelial dysfunction mediated by beta-amyloid. NeuroReport 1997; 8:1387-1391.

104. Thomas T, Thomas G, McLendon C, Sutton T, Mullan M. beta-Amyloid-mediated vasoactivity and vascular endothelial damage. Nature 1996; 380:108-111.

105. Niwa K, Younkin L, Ebeling C, et al. ABeta1-40-related reduction in functional hyperemia in mouse neocortex during somatosensory activation. PNAS 2000; 97:9735-9740.

106. Iadecola C. Neurovascular regulation in the normal brain and in Alzheimer's disease. Neuroscience 2004; 5:347-360.

107. Arvanitakis Z, Lucas JA, Younkin LH, Younkin SG, Graff-Radford NR. Serum creatinine levels correlate with plasma amyloid beta protein. Alzheimer Disease and Associated Disorders 2002; 16:187-190.

108. Kalaria RN, Ince P, eds. Vascular factors in Alzheimer's disease: Ann NY Acad Sci, 2000.

109. Kalaria RN, Ballard C. Overlap between pathology of Alzheimer disease and vascular dementia. Alzheimer Dis and Assoc Disord 1999; 13:S115-S123.

110. Kalaria RN. Small vessel disease and Alzheimer's dementia: pathological considerations. Cerebrovasc Dis 2002; 12:48-52.

111. Wang J, Ho L, Chen L, et al. Valsartan lowers brain beta-amyloid protein levels and improves spatial learning in a mouse model of Alzheimer disease. J Clin Invest 2007; 117:3393-3402.

112. Korf ESC, White LR, Scheltens P, Launer LJ. Midlife blood pressure and the risk of hippocampal atrophy: The Honolulu Asia Aging Study. Hypertension 2004; 44:29-34.

113. Jennings JR, Muldoon MF, Ryan C, et al. Reduced cerebral blood flow response and compensation among patients with untreated hypertension. Neurology 2005; 64:1358-1365.

114. Jennings JR, Muldoon MF, Ryan CM, et al. Cerebral blood flow in hypertensive patients: an initial report of reduced and compensatory blood flow responses during performance of two cognitive tasks. Hypertension 1998; 31:1216-1222.

115. Gianaros PJ, Derbyshire SW, May JC, Siegle GJ, Gamalo MA, Jennings JR. Anterior cingulate activity correlates with blood pressure during stress. Psychophysiology 2005; 42:627-636.

116. Raz N, Rodrigue K. Hypertension and the Brain: Vulernability of the Prefrontal Regions and Executive Functions. Behavioral Neuroscience 2003; 117:1169-1180.

117. Braak H, Braak E. Neuropathological stageing of Alzheimer-related changes. Acta Neuropathol 1991; 82:239-259.

118. Pearson RCA, Esiri MM, Hiorns RW, Wilcock GK, Powell TPS. Anatomical correlates of the distribution of the pathological changes in the neocortex in Alzheimer's disease. Proceedings of the National Academy of Science, USA 1985; 82:4531-4534.

119. Moore T, Killiany R, Moss M, Rosene D, Somnath P, Hollander W. Impariment of Executive Function Induced by Hypertension in the Rhesus Monkey (Macaca mulatta). Behavioral Neuroscience 2002; 116:387-396.

120. Gunning-Dixon FM, Raz N. The cognitive correlates of white matter abnormalities in normal aging: a quantitative review. Neuropsychology 2000; 14:224-232.

121. Burns JM, Church JA, Johnson DK, et al. White matter lesions are prevalent but differentially related with cognition in aging and early Alzheimer disease. Arch Neurol 2005; 62:1870-1876.

122. Libon DJ, Price CC, Giovannetti T, et al. Linking MRI hyperintensities with patterns of neuropsychological impairment: evidence for a threshold effect. Stroke 2008; 39:806-813.

123. Staekenborg SS, Koedam EL, Henneman WJ, et al. Progression of mild cognitive impairment to dementia: contribution of cerebrovascular disease compared with medial temporal lobe atrophy. Stroke 2009; 40:1269-1274.

124. Bombois S, Debette S, Bruandet A, et al. Vascular subcortical hyperintensities predict conversion to vascular and mixed dementia in MCI patients. Stroke 2008; 39:2046-2051.

125. Kuller LH, Lopez OL, Jagust WJ, et al. Determinants of vascular dementia in the Cardiovascular Health Cognition Study. Neurology 2005; 64:1548-1552.

126. Corey-Bloom J, Galasko D, Hofstetter CR, Jackson JE, Thal L. Clinical features distinguishing large cohorts with possible AD, probable AD, and mixed dementia. J Am Geriatr Soc 1993; 41:31-37.

127. den Dunnen WF, Brouwer WH, Bijlard E, et al. No disease in the brain of a 115-year-old woman. Neurobiol Aging 2008; 29:1127-1132.

128. Mesulam M-M. Principles of behavioral and cognitive neurology. Oxford: Oxford University Press, 2000.

129. Zekry D, Duyckaerts C, Belmin J, et al. The vascular lesions in vascular and mixed dementia: the weight of functional neuroanatomy. Neurobiology of AGing 2003; 24:213-219.

130. Baddeley AD, Bressi S, Della Sala S, Logie R, Spinnler H. The decline of Working Memory in Alzheimer's Disease: A longitudinal study. Brain 1991; 114:2521-2542.

131. Klunk WE, Engler H, Nordberg A, et al. Imaging brain amyloid in Alzheimer's disease with Pittsburgh Compond-B. Ann Neurol 2004; 55:306-319.

132. Pardo JV, Lee JT, Sheikh SA, et al. Where the beain grows old: Decline in anterior cingulate and medial prefrontal function with normal aging. NeuroImage 2007; 35:1231-1237.

133. Raz N, Rodrigue KM. Differential aging of the brain patterns: cognitive correlates and modifiers. Neurosci Behav Rev 2006; 30:730-748.

134. Buckner RL, Snyder AZ, Shannon BJ, et al. Molecular, structural, and functional characterization of Alzheimer's disease: Evidence for a relationship between default activity, amyloid, and memory. J Neurosci 2005; 25:7709-7717.

135. Pardo JV, Pardo PJ, Janer KW, Raichle ME. The anterior cingulate cortex mediates processing selection in the Stroop attentional conflict paradigm. Proceedings of the National Academy of Sciences of the USA 1990; 87:256-259.

136. Cavanna AE, Trimble M. The precuneus: a review of its functional anatomy and behavioral correlates. Brain 2006; 129:564-583.

137. Bonte FJ, Harris TS, Roney CA, Hynan LS. Differential diagnosis between Alzheimer's and frontotemporal disease by the posterior cingulate sign. J Nucl Med 2004; 45:771-774.

138. Whitwell JL, Shiung MM, Przybelski SA, et al. MRI patterns of atrophy associated with progression to AD in amnestic mild cognitive impairment. Neurology 2008; 70:512-520.

139. Mesulam M-M. The patterns in behavioral neuroanatomy: Association areas, the limbic system, and hemispheric specialization. In: Mesulam M-M, ed. Principles of behavioral neurology. Philadelphia: F.A. Davis, 1985; 1-70.

140. Braak H, Alafuzoff I, Arzberger T, Kretzschmar H, Del Tredici K. Staging of Alzheimer disease-associated neurofibrillary pathology using paraffin sections and immunocytochemistry. Acta Neuropathol (Berl) 2006; 112:389-404.

141. Jack CR, Petersen RC, Xu YC, et al. Prediction of AD aith MRI-based hippocampal volume in mild cognitive impairment. Neurology 1999; 52:1397-1403.

142. Squire LR, Ojemann JG, Miezin FM, Petersen SE, Videen TO, Raichle ME. Activation of the hippocampus in normal humans: A functional anatomical study of memory. Proc Natl Acad Sci 1992; 89:1837-1841.

143. Douglas RJ. The hippocampus and behavior. Psychological Bulletin 1967; 67:416-442.

144. Olton DS, Becker JT, Handelman GE. Hippocampus, space, and memory. Behavioral and Brain Sciences 1979; 2:313-365.

145. Raz N, Gunning-Dixon FM, Head D, Dupuis JH, Acker JD. Neuroanatomical correlates of cognitive aging: evidence from structural magnetic resonance imaging. Neuropsychology 1998; 12:95-114.

146. Buckner RL. Memory and executive function in aging and AD: multiple factors that cause decline and reserve factors that compensate. Neuron 2004; 44:195-208.

147. Erkinjuntti T, Benavente O, Eliasiw M, et al. Diffuse vacuolization (spongiosis) and arteriolosclerosis in the frontal white matter occurs in vascular dementia. Arch Neurol 1996; 53:325-332.

148. Tekin S, Cummings JL. Frontal-subcortical neuronal circuits and clinical neuropsychiatry. An update. J Psychosomatic Research 2002; 53:647-654.

149. Mega MS, Cummings JL. Frontal-subcortical circuits and neuropsychiatric disorders. J Neuropsychiat Clin Neurosci 1994; 6:358-370.

150. Cummings JL. Frontal-subcortical circuits and human behavior. Arch Neurol 1993; 50:873-880.

151. Mesulam M-M. Structure and function of cholinergic pathways in the cerebral cortex, limbic system, basal ganglia, and thalamus of the human brain. In: Bloom FE, Kupfer DJ, eds. Psychopharmacology: The Fourth Generation of Progress. New York: Raven Press, 1995; 135-146.

152. Shintani EY, Uchida KM. Donepezil: an anticholinesterase inhibitor for Alzheimer's disease. Am J Health Syst Pharm 1997; 54:2805-2810.

153. Weiner MF, Martin-Cook K, Foster BM, Saine K, Fontaine CS, Svetlik DA. Effects of donepezil on emotional/behavioral symptoms in Alzheimer's disease patients. J Clin Psychiatry 2000; 61:487-492.

154. Fried LP, Borhani NO, Enright P, et al. The Cardiovascular Health Study: Design and Rationale. Ann Epidemiol 1991; 1:263-276.

155. Lopez OL, Kuller LH, Fitzpatrick A, Ives D, Becker JT, Beauchamp N. Evaluations of dementia in the cardiovascular health cognition study. Neuroepidemiology 2003; 22:1-12.

156. Lopez OL, Jagust WJ, DeKosky ST, et al. Prevalence and classification of mild cognitive impairment in the Cardiovascular Health Study Cognitive Study Part 1. Arch Neurology 2003; 60:1385-1389.

157. Brandt J, Spencer M, Folstein M. The Telephone Interview for Cognitive Status Neuropsychiat Neuropsychol Behav Neurol 1988; 1:111-117.

158. Jorm AF, Jacomb PA. The informant questionnaire on cognitive decline in the elderly (IQCODE): socio-demographic correlates, reliability, validity and some norms. Psychol Med 1989; 19:1015-1022.

159. Lopez OL, Becker JT, Jagust WJ, et al. Neuropsychological characteristics of mild cognitive impairment subgroups. Neurology 2003; 60:A243.

160. Andresen EM, Malmgren JA, Carter WB, Patrick DL. Screening for depression in well older adults: evaluation of a short form of the CES-D (Center for Epidemiologic Studies Depression Scale). Am J Prev Med 1994; 10:77-84.

161. Cummings JL, Mega M, Gray K, Rosenberg-Thompson S, Carusi DA, Gornbein J. The neuropsychiatric inventory: Comprehensive assessment of psychopathology in dementia. Neurology 1994; 44:2308-2314.

162. Fahn S, Elton RI. UPDRS Development Committee: Unified Parkinsons Rating Scale. In: Fahn S, Marsden CD, Caine D, Goldstein M, eds. Recent developments in Parkinson's disease. Florham Park: MacMillan Healthcare Information, 1987; 153-163.

163. Hachinski VC, Iliff LD, Zihka E, et al. Cerebral blood flow in dementia. Arch Neurol 1975; 32:632-637.

164. Burns A, Zaudig M. Mild cognitive impairment. Lancet 2002; 360:1963-1965.

165. Lopez OL, Becker JT, Klunk W, et al. Research evaluation and diagnosis of possible Alzheimer's disease over the last two decades: I. Neurology 2000; 55:1854-1862.

166. Bryan RN, Manolio TA, Scertz LD, et al. A method for using MR to evaluate the effects of cardiovascular disease on the brain: The cardiovascular health study. Am J Neuroradiol 1994; 15:1625-1633.

167. Yue NC, Arnold AM, Longstreth WT, et al. Sulcal, ventricular, and white matter changes at MR imaging in the aging brain: Data from the Cardiovascular Health Study. Radiology 1997; 202:33-39.

168. Bryan RN, Wells SW, Miller TJ, et al. Infarctlike lesions in the brain: prevalence and anatomic characteristics at MR imaging of the elderly - data from the Cardiovascular Health Study. Radiology 1997; 202:47-54.

169. Westbrook C, Roth CK, Talbot J. MRI in practice. Malden, MA: Blackwell Pub., 2005.

170. Bitar R, Leung G, Perng R, et al. MR pulse sequences: what every radiologist wants to know but is afraid to ask. Radiographics 2006; 26:513-537.

171. Jacobs MA, Ibrahim TS, Ouwerkerk R. AAPM/RSNA physics tutorials for residents: MR imaging: brief overview and emerging applications. Radiographics 2007; 27:1213-1229.

172. Detre JA, Alsop DC, Vives LR, Maccotta L, Teener JW, Raps EC. Noninvasive MRI evaluation of cerebral blood flow in cerebrovascular disease. Neurology 1998; 50:633-641.

173. Detre JA, Leigh JS, Williams DS, Koretsky AP. Perfusion imaging. Magn Reson Med 1992; 23:37-45.

174. Deibler AR, Pollock JM, Kraft RA, Tan H, Burdette JH, Maldjian JA. Arterial spin-labeling in routine clinical practice, part 1: technique and artifacts. AJNR Am J Neuroradiol 2008; 29:1228-1234.

175. Prince MR, Zhang H, Morris M, et al. Incidence of nephrogenic systemic fibrosis at two large medical centers. Radiology 2008; 248:807-816.

176. Wertman R, Altun E, Martin DR, et al. Risk of nephrogenic systemic fibrosis: evaluation of gadolinium chelate contrast agents at four American universities. Radiology 2008; 248:799-806.

177. Juluru K, Vogel-Claussen J, Macura KJ, Kamel IR, Steever A, Bluemke DA. MR Imaging in Patients at Risk for Developing Nephrogenic Systemic Fibrosis: Protocols, Practices, and Imaging Techniques to Maximize Patient Safety. Radiographics 2008.

178. Ye FQ, Berman KF. $H_2{}^{15}O$ PET validation of steady-state arterial spin tagging cerebral blood flow measurements in humans. Magnetic Resonance in Medicine 2000; 44:450-456.

179. Alsop DC, Detre JA, Grossman M. Assessment of cerebral blood flow in Alzheimer's disease by spin-labeled magnetic resonance imaging. Ann Neurol 2000; 47:93-100.

180. Du AT, Jahng GH, Hayasaka S, et al. Hypoperfusion in frontotemporal dementia and Alzheimer disease by arterial spin labelling MRI. Neurology 2006; 67:1215-1220.

181. Johnson NA, Jahng G-H, Weiner MW, et al. Pattern of cerebral hypoperfusion in Alzheimer disease and mild cognitive impairment measured with arterial spin-labeling MR imaging: Initial experience. Radiology 2005; 234:851-859.

182. Alsop DC, Casement M, de Bazelaire C, Fong T, Press DZ. Hippocampal hyperperfusion in Alzheimer's disease. Neuroimage 2008.

183. Deibler AR, Pollock JM, Kraft RA, Tan H, Burdette JH, Maldjian JA. Arterial spin-labeling in routine clinical practice, part 2: hypoperfusion patterns. AJNR Am J Neuroradiol 2008; 29:1235-1241.

184. Liu TT, Brown GG. Measurement of cerebral perfusion with arterial spin labeling: Part I. Methods. JINS 2007; 13:1-9.

185. Brown GG, Clark CM, Liu TT. Measurement of cerebral perfusion with arterial spin labeling: Part 2. Applications. JINS 2007; 13:1-13.

186. Silva AC, Kim S-G. Pseudo-continuous arterial spin labeling technique for measuring CBF dynamics with high temporal resolution. Magnetic Resonance in Medicine 1999; 42:425-429.

187. Manolio TA, Kronmal RA, Burke GL, et al. Magnetic resonance abnormalities and cardiovascular disease in older adults. The Cardiovascular Health Study. Stroke 1994; 25:318-327.

188. Chen M. 3-D deformable registration using a statistical atlas with applications in medicine. Doctoral dissertation. Pittsburgh, PA: Carnegie Mellon University, 1999.

189. Meltzer CC, Leal JP, Mayberg HS, Wagner HN, Frost JJ. Correction of PET data for partial volume effects in human cerebral cortex by magnetic resonance imaging. J Comput Assist Tomogr 1990; 14:561-570.

190. Ashburner J, Friston KJ. Voxel-based morphometry - the methods. Neurology 2000; 11:805-821.

191. Fein G, Landman B, Tran H, et al. Statistical parametric mapping of brain morphology: sensitivity is dramatically increased by using brain-extracted images as inputs. Neuroimage 2006; 30:1187-1195.

192. Spears JR, Greer PJ, Ziolko SK, et al. Evaluation of an age-specific neurological template. Presented at the Annual Meeting of the Organization of Human Brain Mapping. Toronto Ontario, Canada; June 2005 2005.

193. Hellier P, Ashburner J, Corouge I, Barillot C, Friston KJ. Inter Subject Registration of Functional and Anatomical Data Using SPM. Proceedings of the 5th International Conference on Medical Image Computing and Computer-Assisted Intervention- 2002; 2489:590-597.

194. Good CD, Johnsrude IS, Ashburner J, Henson RNA, Friston KJ, Frackowiak RSJ. A voxel-based morphometric study of aging in 465 normal adult human beings. NeuroImage 2001; 14:21-36.

195. Senjem MJ, Guner JL, Shiung MM, Petersen RC, Jack CR. Comparison of different methodological implementations of voxel-based morphometry in neurodegenerative disease. NeuroImage 2005; 26:600-608.

196. Shen S, Szameitat AJ, Sterr A. VBM lesion detection depends on the normalization template: a study using simulated atrophy. Magn Reson Imaging 2007; 25:1385-1396.

197. Ashburner J, Friston KJ. Unified segmentation. Neuroimage 2005; 26:839-851.

198. Klein A, Andersson J, Ardekani BA, et al. Evaluation of 14 nonlinear deformation algorithms applied to human brain MRI registration. Neuroimage 2009.

199. Fairchild AJ, Mackinnon DP. A General Model for Testing Mediation and Moderation Effects. Prev Sci 2008.

200. Friston KJ. Statistical parametric mapping : the analysis of funtional brain images. Amsterdam ; Boston: Elsevier/Academic Press, 2007.

201. Worsley KJ, Marrett S, Neelin P, Vandal AC, Friston JJ, Evans AC. A unified statistical approach for determining significant voxels in images of cerebral activation. Hum Brain Mapp 1996; 4:58-73.

202. Genovese CR, Lazar NA, Nichols TE. Thresholding of statistical maps in functional neuroimaging using the false discovery rate. Neuroimage 2002; 15:870-878.

203. Nichols T, Hayasaka S. Controlling the familywise error rate in functional neuroimaging: a comparative review. Stat Methods Med Res 2003; 12:419-446.

204. Holmes CJ, Hoge R, Collins L, Woods R, Toga AW, Evans AC. Enhancement of MR images using registration for signal averaging. J Comput Assist Tomogr 1998; 22:324-333.

205. Cohen J. Statistical Power Analysis for the Behavioral Sciences, 2nd Ed. Hillsdale, NJ: Lawrene Erlbaum Associates, 1988.

206. Cohen J, Cohen P, West SG, Aiken LS. Applied multiple regression/coorelation analysis for the behavioral sciences. Mahwah, NJ: Lawrence Erlbaum Associates, 2003.

207. Tzourio-Mazoyer N, Papathanassiou D, Crivello F, et al. Automated anatomical labeling of activations in SPM using a macroscopic anatomical parcellation of the MNI MRI single-subject brain. NeuroImage 2002; 15:273-289.

208. Rorden C, Karnath HO, Bonilha L. Improving lesion-symptom mapping. J Cogn Neurosci 2007; 19:1081-1088.

209. Devlin JT, Poldrack RA. In praise of tedious anatomy. Neuroimage 2007; 37:1033-1041; discussion 1050-1038.

210. Ohnishi T, Matsuda H, Tabira T, Asada T, Uno M. Changes in brain morphology in Alzheimer disease and normal aging: is Alzheimer disease an exaggerated aging process? AJNR Am J Neuroradiol 2001; 22:1680-1685.

211. Van Laere KJ, Dierckx RA. Brain perfusion SPECT: age- and sex-related effects correlated with voxel-based morphometric findings in healthy adults. Radiology 2001; 221:810-817.

212. Hall AM, Moore RY, Lopez OL, Kuller LH, Becker JT. Basal forebrain atrophy is a presymptomatic marker for Alzheimer's disease. Alzheimers Dement 2008; 4:271-279.

213. den Heijer T, Launer LJ, van Dijk EJ, et al. Association between blood pressure, white matter lesions, and atrophy of the medial temporal lobe. Neurology 2005; 64:263-267.

214. Lazarus R, Prettyman R, Cherryman G. White matter lesions on magnetic resonance imaging and their relationship with vascular risk factors in memory clinic attenders. Int J Geriatr Psychiatry 2005; 20:274-279.

215. Ryberg C, Rostrup E, Sjostrand K, et al. White matter changes contribute to corpus callosum atrophy in the elderly: the LADIS study. AJNR Am J Neuroradiol 2008; 29:1498-1504.

216. Enzinger C, Fazekas F, Ropele S, Schmidt R. Progression of cerebral white matter lesions -- clinical and radiological considerations. J Neurol Sci 2007; 257:5-10.

217. Dai W, Lopez OL, Carmichael OT, Becker JT, Kuller LH, Gach HM. Abnormal regional cerebral blood flow in cognitively normal elderly subjects with hypertension. Stroke 2008; 39:349-354.

218. Beason-Held LL, Moghekar A, Zonderman AB, Kraut MA, Resnick SM. Longitudinal changes in cerebral blood flow in the older hypertensive brain. Stroke 2007; 39:1766-1773.

219. Fujishima S, Imaizumi T, Abe I, Takeshita A, Fujishima M. Effects of intra-arterial infusion of insulin on forearm xasoreactivity in hypertensive humans. Hypertens Res 1995; 18:327-333.

220. Mentis MJ, Salerno J, Horwitz B, et al. Reduction of functional neuronal connectivity in long-term treated hypertension. Stroke 1994; 25:601-607.

221. Dai W, Lopez OL, Carmichael OT, Becker JT, Kuller L, Gach HM. Patterns of altered cerebral blood flow in mild cognitive impairment and early Alzhimer's disease. Radiology 2009; 250-57.

222. Buxton RB, Frank LR, Wong EC, Seiwert B, Warach S, Edelman RR. A general kinetic model for quantitative perfusion imaging with arterial spin labeling. Magnetic Resonance in Medicine 1998; 40:383-396.

223. Chen M. 3-D Deformable Registration Using a Statistical Atlas with Applications in Medicine. PhD thesis. Pittsburgh, PA: Robotics Institute, Carnegie Mellon University, 1999.

224. Dai WS, Davis SW, Meltzer C, et al. Segmentation comparison between the MNI and the University of Pittsburgh Elderly Template. Neurobiol of Aging 2004; 25:S301.

225. Dai W, University of Pittsburgh. School of Arts and Sciences. Advancements in Quantitative Perfusion Magnetic Resonance Imaging (Mri) of Dementia. In. Pittsburgh, PA: University of Pittsburgh, 2007.

226. Detre JA, Alsop DC. Perfusion magnetic resonance imaging with continuous arterial spin labeling: methods and clinical applications in the central nervous system. Eur J Radiol 1999; 30:115-124.

227. Kuller LH, Lopez OL, Newman A, et al. Risk factors for dementia in the cardiovascular health cognition study. Neuroepidemiology 2003; 22:13-22.

228. Pantoni L, Garcia JH, Brown GG. Vascular pathology in three cases of progressive cognitive deterioration. J Neurol Sci 1996; 135:131-139.

229. Aharon-Peretz J, Cummings JL, Hill MA. Vascular dementia and dementia of the Alzheimer type. Arch Neurol 1988; 45:719-721.

230. Claus JJ, Breteler MM, hasan D, et al. Vascular risk factors, atherosclerosis, cerebral white matter lesions and cerebral perfusion in a population-based study. Eur J Nucl Med 1996; 23:675-682.

231. Leys D, Erkinjuntti T, Desmond DW, et al. Vascular dementia: the role of cerebral infarcts. Alzheimer Dis Assoc Disord 1999; 13:S38-S48.

232. Tiehuis AM, van der Graaf Y, Visseren FL, et al. Diabetes increases atrophy and vascular lesions on brain MRI in patients with symptomatic arterial disease. Stroke 2008; 39:1600-1603.

233. Bennett DA, Schneider JA, Arvanitakis Z, et al. Neuropathology of older persons without cognitive impairment from two community-based studies. Neurology 2006; 66:1837-1844.

234. Knopman DS, Parisi JE, Salviati A, et al. Neuropathology of cognitively normal elderly. J Neuropathol Exp Neurol 2003; 62:1087-1095.

235. Bell RD, Zlokovic BV. Neurovascular mechanisms and blood-brain barrier disorder in Alzheimer's disease. Acta Neuropathol 2009.

236. Gauthier S, Reisberg B, M. Z, et al. Mild cognitive impairment. Lancet Neurol 2006; 367:1261-1270.

237. Tomlinson B, E., Blessed G, Roth M. Observations on the brain of demented old people. J Neurol Sci 1970; 11:205-242.

238. Haag MD, Hofman A, Koudstaal PJ, Stricker BH, Breteler MM. Statins are associated with a reduced risk of Alzheimer disease regardless of lipophilicity. The Rotterdam Study. J Neurol Neurosurg Psychiatry 2009; 80:13-17.

239. Cramer C, Haan MN, Galea S, Langa KM, Kalbfleisch JD. Use of statins and incidence of dementia and cognitive impairment without dementia in a cohort study. Neurology 2008; 71:344-350.

240. Rea TD, Breitner JC, Psaty BM, et al. Statins and the risk of incident dementia: The Cardiovascular Health Study. Arch Neurol In Press.

241. Bernick C, Katz R, Smith NL, et al. Statins and cognitive function in the elderly: the Cardiovascular Health Study. Neurology 2005; 65:1388-1394.

242. Wang J, Ho L, Qin W, et al. Caloric restriction attenuates beta-amyloid neuropathology in a mouse model of Alzheimer's disease. Faseb J 2005; 19:659-661.

243. Martin B, Golden E, Egan JM, Mattson MP, Maudsley S. Reduced energy intake: the secret to a long and healthy life? IBS J Sci 2007; 2:35-39.

244. Colcombe SJ, Erickson KI, Raz N, et al. Aerobic fitness reduces brain tissue loss in aging humans. J Gerontol A Biol Sci Med Sci 2003; 58:176-180.

245. Kramer AF, Colcombe SJ, McAuley E, Scalf PE, Erickson KJ. Fitness, aging, and neurocognitive function. Neurobiol Aging In Press.

246. Lautenschlager NT, Cox KL, Flicker L, et al. Effect of physical activity on cognitive function in older adults at risk for Azheimer disease. JAMA 2008; 300:1027-1037.

247. Berchtold NC, Chinn G, Chou M, Kesslak JP, Cotman CW. Exercise primes a molecular memory for brain-derived neurotrophic factor protein indiction in the rat hippocampus. Neuroscience 2005; 133:853-861.

248. Moseley M. Diffusion tensor imaging and aging - a review. NMR Biomed 2002; 15:553-560.

249. Fitzpatrick A, Kronmal R, Gardner JP, et al. Leukocyte Telomere length and cardiovascular disease in the Cardiovascular Health Study. Am J Epidemiology 2007; 165:14-21.

250. McIntosh AR, Grady CL, Ungerleider LG, Haxby JV, Rapoport SI, Horwitz B. Network analysis of cortical visual pathways mapped with PET. Journal of Neuroscience 1994; 14:655-666.

251. McIntosh AR, Bookstein FL, Haxby JV, Grady CL. Spatial pattern analysis of functional brain imaging using partial least squares. NeuroImage 1993; 3:143-157.